The Role of Vegetation Dynamics in the Climate of West Africa

by

Guiling Wang

B.E., Tsinghua University, 1992
M.S., Tsinghua University, 1995

Submitted to the Department of Civil and Environmental Engineering
in partial fulfillment of the requirements for the degree of

Doctor of Philosophy in Hydroclimatology

at the

Massachusetts Institute of Technology

February 2000

Author .....
Department of Civil and Environmental Engineering
November 10, 1999

Certified by .....
Elfatih A. B. Eltahir
Associate Professor of Civil and Environmental Engineering
Thesis Supervisor

Accepted by .....
Daniele Veneziano
Chairman, Department Committee on Graduate Students

The Role of Vegetation Dynamics in the Climate of West Africa

by

Guiling Wang

Submitted to the Department of Civil and Environmental Engineering
on November 10, 1999, in partial fulfillment of the
requirements for the degree of
Doctor of Philosophy in Hydroclimatology

Abstract

The climate of West Africa exhibits significant variability at the time scale of decades. The persistent drought of the past three decades is an example of such variability. This study investigates the role of vegetation dynamics in shaping the low-frequency variability of the climate over West Africa. A zonally symmetric, synchronously coupled biosphere-atmosphere model (ZonalBAM) which includes explicit representation of vegetation dynamics has been developed, and has been validated using observations on both the atmospheric and biospheric climate. The model is then used to study the dynamics of the coupled biosphere-atmosphere system over West Africa. Based on the model sensitivity to initial conditions and the resilience of the coupled system with respect to perturbations, we demonstrate that the coupled biosphere-atmosphere system over West Africa has multiple equilibrium states, with reversible transitions between different equilibria. The two-way biosphere-atmosphere feedback is a significant process in both climate persistence and climate transition.

Based on long-term climate simulations using ZonalBAM driven with the observed sea surface temperature (SST) variations, our study shows that vegetation dynamics is a significant process in shaping the climate variability of West Africa. The response of the regional climate system to large-scale forcings is significantly regulated by vegetation dynamics. The relatively slow response of vegetation to changes in the atmosphere is a significant mechanism that acts to enhance the low-frequency rainfall variability. Climate transitions between different equilibria act as another mechanism contributing to the low-frequency rainfall variability – multi-decadal fluctuations can take place as a collective reflection of climate persistence at one equilibrium and climate transition towards another.

Vegetation dynamics seems to play an important role in the development and persistence of the current Sahel drought. The most likely scenario for the triggering mechanism of the Sahel drought would involve a combination of several processes including regional changes in land cover as well as changes in the patterns of global and regional SST distributions. However, regardless of the nature of the triggering

mechanism, the response of the natural vegetation to the atmospheric changes is the critical process in the development and persistence of the observed drought.

Thesis Supervisor: Elfatih A. B. Eltahir
Title: Associate Professor of Civil and Environmental Engineering

Acknowledgments

I would like to first acknowledge the time and efforts of my thesis committee, including Professors Elfatih A. B. Eltahir, Rafael L. Bras, Raymond A. Plumb, and Jonathan A. Foley. Their comments and suggestions were extremely helpful to this study and significantly improved the quality of my thesis. I am very grateful to my advisor Professor Eltahir for his continuous and invaluable guidance, encouragement, and support during this research. His devotion for scientific excellence has always been inspiring, and his support for my professional development makes it possible for me to carry on.

Some components of the model developed in this study were provided courtesy of Dr. Xinyu Zheng who got his PhD degree from MIT, Professor Kerry A. Emanuel at MIT, and Professor Jonathan A. Foley and his group at the University of Wisconsin, Madison. Professor Emanuel kindly did several trouble shootings with me during the early stage of my model development. I am especially thankful to Professor Foley for bearing with me when I was a "layman" of IBIS, and for always being there whenever I needed his help.

My research also benefited tremendously from discussions and comments of many other people. Among them are Professor Ignacio Rodriguez-Iturbe (now at Princeton University), Dr. Jingfeng Wang, Julie Kiang, and Jeremy Pal, to name a few. Julie Kiang was also the "IBIS expert" whose sharing of knowledge significantly sped up my research. I am indebted to the "computer specialist" Jeremy Pal for his invaluable help in computer-related issues. I would also like to thank all members of the Eltahir group for creating a supportive environment and for the inspiring questions during numerous group meetings. My experience at MIT would have been far less enjoyable without the friendship of Nicole Gasparini, who has always been the source of joy and comfort.

It is with great appreciation that I acknowledge the help from my now parents-in-law, Furong Jia and Fengwu Cao, and sisters-in-law Xuemei and Xueqin. They encouraged me to pursue my Ph.D. in the states, and provided tremendous help during this process. I am also indebted to my sister Guirong and brothers Mingyi and Mingjun. At various stages of my education, they sacrificed their own comfort to create the best studying environment for me. I especially thank my husband and best friend Xuefeng Cao, for his unwavering love, support, and encouragement during my scientific thriving as well as personal development. Most important of all, my parents, Xiuqin Li and Zhaoen Wang, have always been the source of strength in my life. I owe who I am today and what I can achieve in the future to their constant emphasis on the importance of higher education. With love, respect, and appreciation, I dedicate this thesis to my parents and to my husband.

Contents

List of Figures

Chapter 1

Introduction

1.1 Physical Geography of West Africa

Geographically, West Africa consists of two different regions with different climates. Rainfall increases away from the Sahara both southward and northward. The region north of the Sahara, often referred to as North Africa, is influenced by the Mediterranean climate and mid-latitude cyclones. In this study, we focus on the region south of the Sahara, which is under the influence of the tropical climate and the West African monsoon circulation. In the following, the term "West Africa" is used to refer to the region between the Sahara desert (in the north) and the Atlantic coast (in the south).

West Africa is located within the tropics, where the atmospheric circulation features the meridional overturning known as the Hadley circulation. Driven by the differential heating in the atmospheric surface layer, the Hadley circulation occurs with the rising branch near the equator and descending branch over the subtropics. This sinking motion is the main cause for the formation of the Sahara desert over West Africa. Another important circulation in West Africa is the monsoon circulation, which is driven by the differential heating between the land and the ocean. During the summer, wind blows from the ocean to the land at the low levels, with the returning wind towards the ocean at the high levels. The rising branch of the monsoon circulation is located over land. The strong monsoon wind brings moist

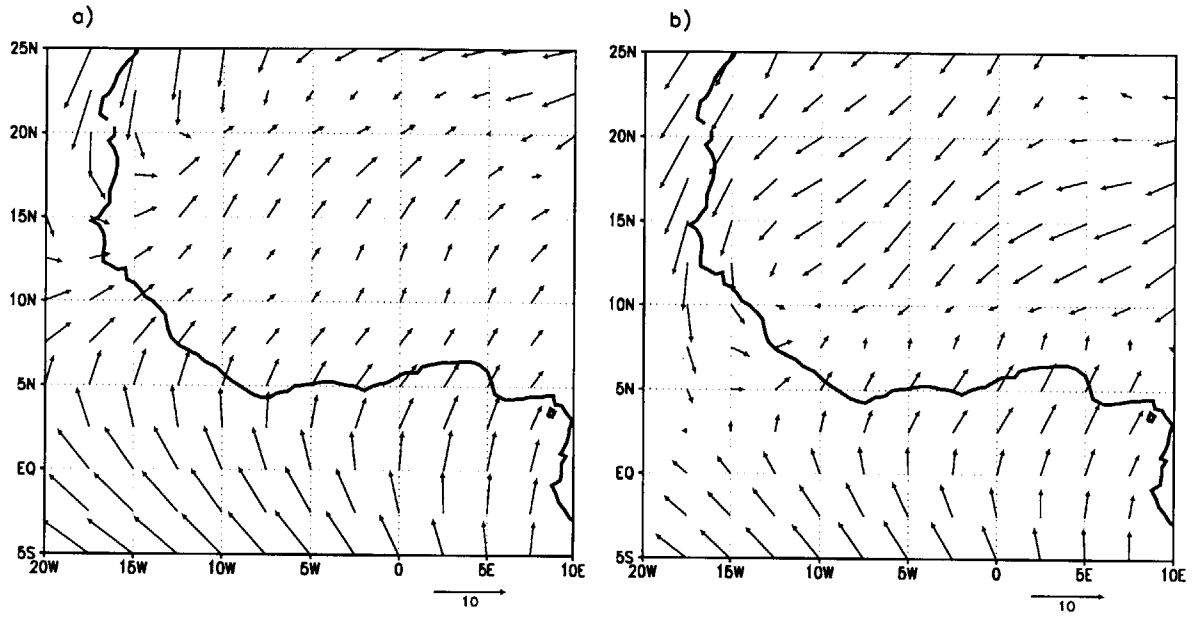

Figure 1-1: The horizontal wind (m/s) at 1000mb over West Africa: a) Summer (August); b) Winter (February). Based on the climatology (1982-1994) of the NCEP re-analysis data.

air from the ocean surface to the continent. The rising motion of the air over land generates summer rainfall in most of West Africa. During the winter, this circulation is reversed. Except along the coast where wind is towards the land all the time, the low-level wind in most of West Africa blows from the interior towards the ocean in winter, bringing with it the dry and dusty air from the desert. The subsiding branch of the winter circulation is over land, which suppresses rainfall. This seasonal pattern of the monsoon wind is shown in Figure 1-1, using August and February as examples. The seasonality of the monsoon circulation causes strong seasonality of climate over most of West Africa, marked by a wet summer and a dry winter. Moving away from the coast, the strength of the monsoon wind decreases, and so does the length of the rainy season. Figure 1-2 shows the rainfall seasonal cycle at 0° longitude. The length of the rainy season decreases from more than 10 months in the coastal area to 1-2 months on the desert margin.

Topography over West Africa is remarkably flat. Most of the region lies between the sea level and 400 meters. Therefore, the topography-induced modification to the

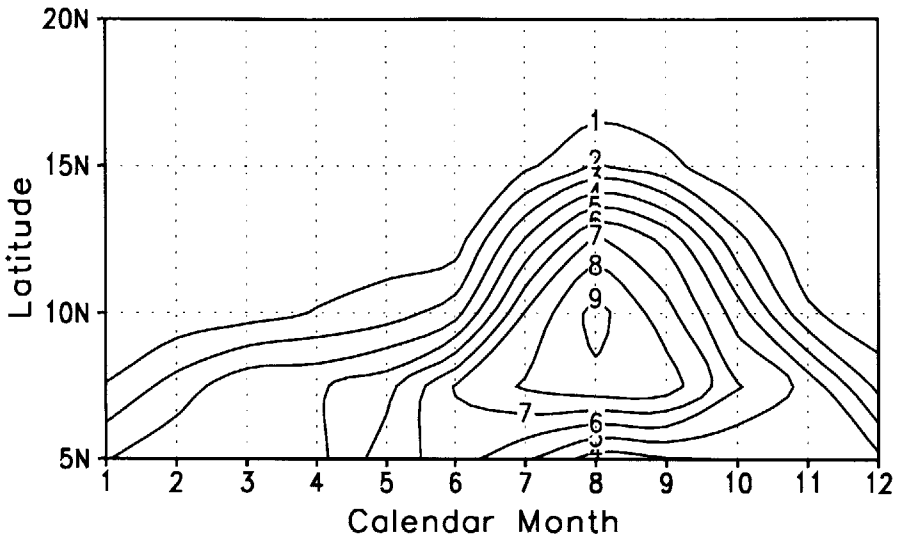

Figure 1-2: Rainfall seasonal cycle at 0° longitude, based on the climatology (1982-1994) of the NCEP re-analysis data. Unit: *mm/day*.

large-scale atmospheric circulation is negligible. Since the coast line in the south is almost parallel to the equator, the West African monsoon circulation is primarily a meridional phenomenon. Together with the meridional overturning associated with the Hadley circulation, this favors a high degree of zonal symmetry in the climate of West Africa. Figure 1-3 presents the spatial distribution of the annual precipitation, air temperature and specific humidity at the 1000-mb level, as well as the downward solar radiation at the surface. Clearly, the contour lines of these key climate variables are oriented parallel to the coast lines. Except for the coastal region in the west and southwest, the zonal variability of climate over West Africa is negligible. This justifies the use of zonally symmetric models (e.g., Zheng, 1997) and zonally averaged models (e.g., Xue and Liou, 1990) in simulating the climate of West Africa.

Climate plays the dominant role in determining the vegetation distribution in West Africa, as it does elsewhere. Due to the high degree of zonal symmetry in the atmospheric climate, the vegetation distribution also demonstrates significant zonal symmetry. The gradient of vegetation is mainly along the meridional direction. Moving away from the coast, annual rainfall decreases from over 2000 *mm* in the coastal region to less than 100 *mm* on the desert margins (Figure 1-3a). At the same

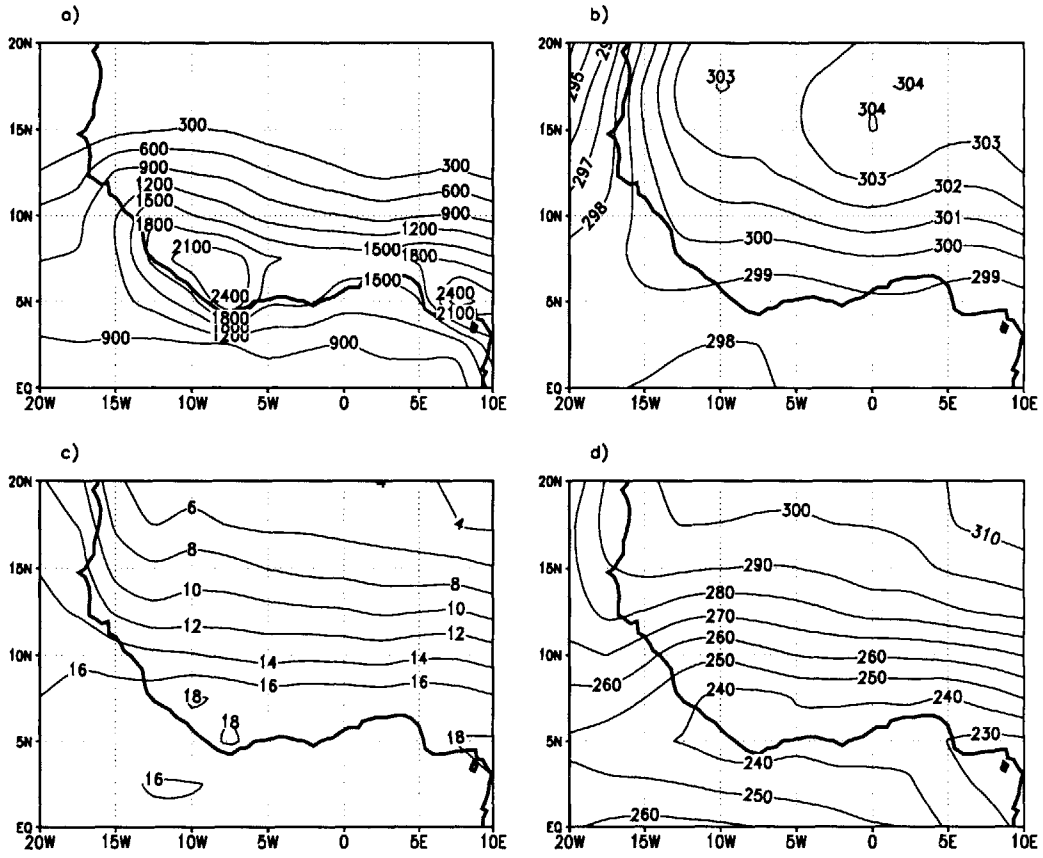

Figure 1-3: a) Annual accumulated precipitation; b) Annual average of the air temperature at $1000mb$; c) Annual average of the specific humidity at $1000mb$; d) Annual average of the downward solar radiation at the surface. Based on the climatology (1982-1994) of the NCEP re-analysis data.

time, the solar radiation increases northward (Figure 1-3d). In regions near the coast where there is abundant supply of water but sunlight availability is limited, forest is the dominant vegetation type, because trees have the advantage in the access to sunlight due to their tall woody structure. As water availability diminishes northward, trees would experience water stress and cannot produce enough biomass to develop a closed canopy. As a result, the sunlight can reach the ground, which provides an opportunity for herbaceous plants to survive. The shallow root system of grass has immediate access to water when the rain infiltrates into the soil. Therefore, grass becomes the dominant plant type in the north where rainfall is limited. Over all, in West Africa, from the coast northward, vegetation changes from forest to savannah to grassland and desert.

Within the forest region of West Africa, broad-leaf evergreen trees dominate along the coast where there is no well-defined dry season; more northward where the vegetation suffers from water stress during the short dry season, the dominant plant type is the broad-leaf drought-deciduous trees which can shed their leaves during the dry season to conserve water. Grass is the dominant plant type not only in grassland, but also in the savannah. As a transitional vegetation type between forest and grassland, savannah features a mixture of trees and grass, where the grass stratum is continuous but occasionally interrupted by trees and shrubs (Bourliere and Hadley, 1983). Perennial grass is the majority grass species in West Africa, while annual grass only constitutes a fleeting component of the ecosystem, filling the gaps when opportunity arises (Menaut, 1983). Although the aerial parts of the perennials die out in the dry season, their underground structures remain alive. In the beginning of the growing season, while the perennials start from the dense underground structure, the annuals have to start from seeds, which makes the annuals a competitively weak species. Over the desert region in the north, moisture becomes so scarce that little vegetation can survive. Species that survive are usually those which have developed various water conserving techniques during the long process of evolution.

1.2 Background and Motivation

Rainfall variability in West Africa shows remarkable spatial coherency. According to the patterns of rainfall fluctuations, Nicholson (1980) divided West Africa into five different zones: Guinea Coast (Nicholson and Palao, 1993), Soudano-Guinea, Soudan, Sahel, and Sahelo-Sahara. The main direction of the boundaries between different zones is along the latitudinal lines. Based on Nicholson's definition and using specific latitudinal lines as the boundaries, Rowell *et al.* (1995) divided West Africa into only three sub-regions: Guinea Coast (coast-10°N), Soudan (10°N-12.5°N), and Sahel (12.5°N-17.5°N). This coarser definition eliminates the transitional zones in Nicholson's (1980) study, and the use of latitudinal lines as the boundary makes it easier to apply in climate modeling studies which need grid data.

Based on the Hulme (1995) rainfall data, Rowell *et al.* (1995) showed that the rainfall fluctuations in the Soudan region are very similar to the Sahel region. The rainfall time series in both regions are dominated by low-frequency variations at the decadal time scale. The low-frequency variations in these two regions are almost perfectly correlated, and the two regions also share up to 50% of their high-frequency variations. In comparison, for the Guinea Coast region, rainfall variability is dominated by high-frequency components, and there is very little correlation between the rainfall fluctuations over Guinea Coast and the regions to the north. Therefore, for simplicity, Soudan and Sahel are treated as one homogeneous region in this study, and are jointly referred to as the Sahel region. Figure 1-4 shows the time series for the normalized anomaly of the annual rainfall averaged over the Sahel region (10°N-17.5°N) during the 20th century, which features two wet periods in the 1920s-1930s and the 1950s, and a long dry period from the late 1960s to present. The dominance of the low-frequent variability in the Sahel rainfall is rather unique. No similar phenomenon has been observed in its surrounding regions including East and South Africa (Nicholson, 1989).

The dominance of the low-frequency variability in the Sahel rainfall (Nicholson and Entekhabi, 1986; Nicholson and Palao, 1993; Rowell *et al*, 1995) is not a unique

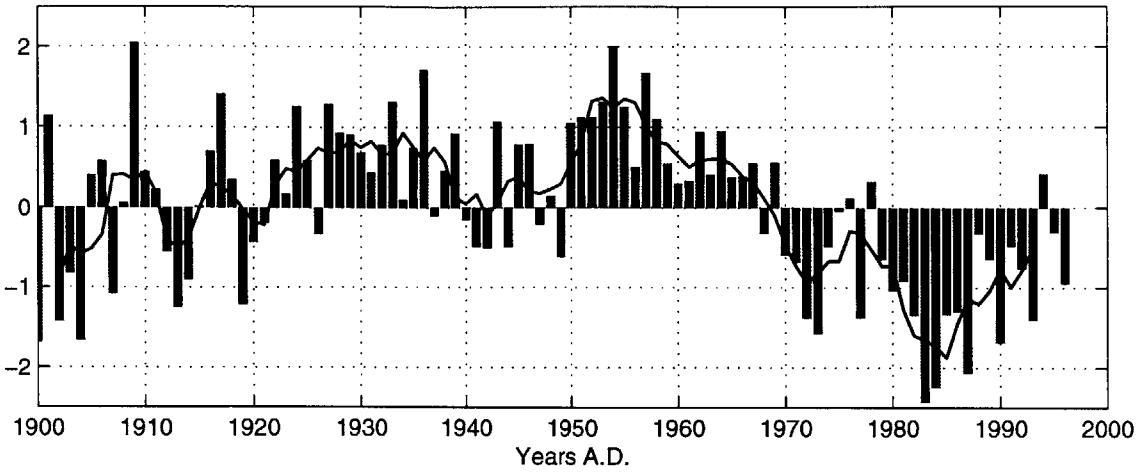

Figure 1-4: The normalized anomaly of the annual rainfall averaged over the entire Sahel region, based on the Hulme rainfall data.

feature of the 20th-century climate. It is also evident in the climate of the same region during the past several centuries (Malay, 1973,1981; Nicholson, 1981b; Farmer and Wigley, 1985). Figure 1-5 shows the level of the Lake Chad (located around 14°E, 13.5°N) in the past 6-7 centuries, reconstructed from the historical records presented by Malay (1973,1981), Nicholson (1981b), and Farmer and Wigley (1985). Changes of the lake level with time suggest that the Sahel climate tends to fluctuate between a humid regime and an arid regime, and that the period during which the climate persists in one specific regime is in the order of decades. This alternate occurrence of the dry and wet spells confirms the dominance of low-frequency variability found in the more recent rainfall data.

Another important feature of the recent climate in the Sahel region is the severe persistent drought in the second half of the 20th century, which can be seen in Figure 1-4. After a period of rainfall surplus during the 1950s and the early 1960s, the drought started around 1968, and has lasted for more than three decades. Compared with the wet period in the 1950s, the current drought caused a rainfall decrease of about 50% in the Sahel region. This severe drought caused the worst disaster in African history. Hundreds of thousands of individuals perished in the early 1970s alone, and millions have been displaced in order to survive (Druyan, 1989). Although

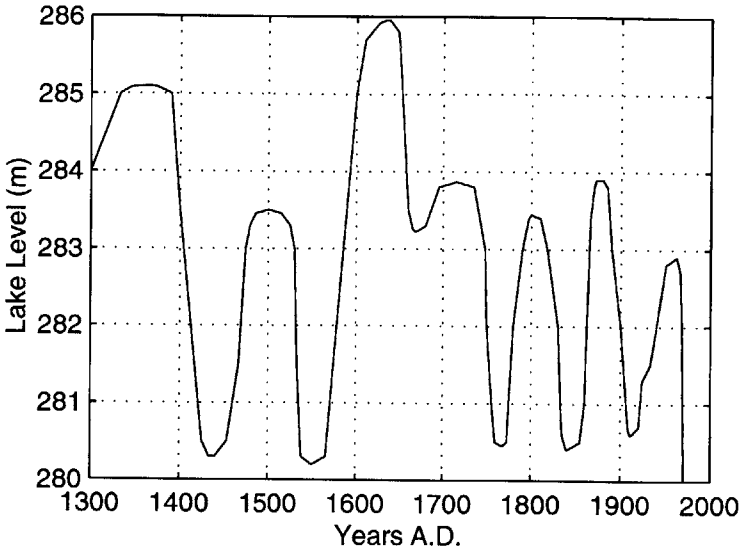

Figure 1-5: Historical fluctuations in the level of the Lake Chad.

West Africa had experienced several similar dry events in its recent history (Figure 1-5), the severity of the current drought is unprecedented.

Although numerous studies in the past two decades have focused on the Sahel droughts, the causes for the recurrent droughts in that region, including the current drought, are still unclear. Understanding the mechanisms of the triggering and persistence of the Sahel droughts is of great social and scientific importance. Motivated by this, this dissertation aims at studying the physical processes and mechanisms behind the observed rainfall variability over West Africa (the Sahel region in particular), including the decadal-scale fluctuations as well as the recent Sahel drought.

1.3 Literature Review

1.3.1 Current Sahel Drought

Studies on the mechanisms of the current Sahel drought can be divided into two general groups. One emphasizes the role of large-scale forcings; the other focuses on the land surface feedback mechanism, a more local factor.

Role of Large-Scale Forcings

There have been both empirical and modeling studies that emphasize the role of large-scale factors such as changes in the atmospheric circulation and changes in the global sea surface temperature in causing the current drought. Some of these studies investigate the mechanisms of rainfall inter-annual variability instead of directly focusing on the drought itself.

Early studies by Bryson (1973) and Winstanley (1973) linked the rainfall variability in West Africa with the position of the Inter-Tropical Convergence Zone (ITCZ), and suggested that the Sahel drought may have been caused by a southward shift of the ITCZ. However, further studies (e.g., Newell and Kidson, 1984; Nicholson, 1981a) showed that there is no systematic southward displacement of ITCZ over West Africa. As a distant forcing, the role of El Niño Southern Oscillation (ENSO) in the variability of the Sahel rainfall was also investigated (Nicholson and Entekhabi, 1986; Ropelewski and Halpert, 1987; Folland *et al.*, 1991; Janicot, 1992, 1996), but the correlation between ENSO and rainfall in most of West Africa is relatively weak.

Lamb (1978a,b) found that the surface circulation pattern in the tropical Atlantic can impact the rainfall over the Sahel region, and the spring SST pattern may play an important role in determining the summer rainfall over the Sahel. This was later confirmed by numerous other studies. For example, Hastenrath (1984) found that rainfall anomalies in the Sahel region tend to be associated with changes in the large-scale atmospheric and oceanic fields over the tropical Atlantic; Lough (1986) presented a strong correlation between the Atlantic SST and the Sahel rainfall during the period 1948-1972. The importance of regional SST forcings were also indicated by modeling studies which simulated the contrast of the Sahel rainfall between individual years based on only the regional SST forcings in those years (e.g., Druyan and Hastenrath, 1991; Druyan, 1991). Recently, a modeling study by Zheng *et al.* (1999) documented that a spring warming and/or a summer cooling in the tropical Atlantic favors a positive anomaly of the summer rainfall over the Sahel, which may have implications regarding the predictability of the Sahel rainfall.

Other studies extend the region of focus beyond the Atlantic ocean. Folland *et al.* (1986) found that the persistent wet and dry periods in the Sahel region are strongly related to contrasting patterns of SST anomalies at the global scale. Using an atmospheric general circulation model (AGCM), they showed that worldwide SST anomalies can influence the summer rainfall over the Sahel through changes in the tropical atmospheric circulation. Using the same AGCM, Palmer (1986) showed that the SST patterns in the Pacific and Atlantic oceans are equally important in reducing the rainfall over the western Sahel while the Indian ocean plays the dominant role in the rainfall reduction over the eastern Sahel. The importance of global-scale SST forcing found by Folland *et al.* (1986) and Palmer (1986) was confirmed by studies that forced general circulation models with observed SST data for individual years and successfully reproduced the observed anomalies of the seasonal Sahel rainfall for those years (Folland *et al*, 1991; Palmer *et al.*, 1992; Rowell *et al*, 1992, 1995).

Studies on large-scale forcings identified several important factors that can influence the variability of the Sahel rainfall and are therefore potentially important for the drought occurrence. However, few systematic changes in large-scale forcings have been documented, and no adequate explanation for the current drought has been established.

Role of Land Cover Changes

Studies on the role of land surface feedback in the development of the Sahel drought were motivated by the observation that West Africa has experienced intense and extensive land cover changes during the past several decades, including desertification and deforestation. In 1975, Charney proposed his pioneering biogeophysical feedback hypothesis: the cooling effect due to the albedo increase caused by desertification enhances local subsidence, thus reducing precipitation, which further limits the vegetation growth and makes the drought self-sustaining. Following this hypothesis, numerous modeling studies have investigated the impact of vegetation degradation at the desert border (e.g., Charney *et al.*, 1977; Sud and Smith, 1985; Cunnington and Rowntree, 1986; Sud and Molod, 1988; Xue *et al.*, 1990; Xue and Shukla, 1993;

Xue, 1997; Zheng and Eltahir 1997, 1998). Some of the studies focus on one or two aspects of the land surface changes associated with vegetation degradation, including the increase in surface albedo and decrease in soil moisture and surface roughness, while others considered the full impact of vegetation degradation. These studies support a common conclusion that desertification causes a significantly drier climate over the sahel region. It has also been found that desertification tends to cause a di-pole pattern of changes in the summer precipitation: a southward shift of the rain belt takes place which causes rainfall to decrease in the Sahel region but to increase in the south over the Guinea Coast (e.g., Xue and Shukla, 1993; Zheng and Eltahir, 1997, 1998).

In addition to the severe desertification, West Africa has also experienced intense deforestation. Although deforestation in Amazon Basin has attracted broad attention (Dickinson and Henderson-Sellers, 1988; Henderson-Sellers *et al*, 1993; Lean and Rowntree, 1993; Shukla *et al*, 1990; Sud *et al*, 1996; Zhang and Henderson-Sellers, 1996) in the past 10 years, very few studies have looked at the deforestation in tropical Africa. Using NCAR CCM1 coupled with BATS, Zhang and Henderson-Sellers (1996) showed that the replacement of rain forest in tropical Africa by grassland reduces local rainfall by 4%, which is negligible. On the other hand, using a zonally symmetric model, Zheng and Eltahir (1997) showed that the West African monsoon circulation is very sensitive to deforestation, and suggested that the extensive and intense deforestation in West Africa might have significantly contributed to the current drought.

Based on the finding that vegetation degradation can cause a drier climate in the Sahel region, many previous studies suggested that the current Sahel drought may have been a result of intense human activities. However, due to the lack of reliable data on land surface conditions before the time of the drought onset, it is hard to ascertain whether the drought was indeed anthropogenically induced. Although it is possible that desertification might have caused the drought, it is also possible that the land surface degradation in that region might have been a result of the drought. In addition, West Africa had experienced several similar droughts in the past (Malay,

1973, 1981; Nicholson, 1981b; Farmer and Wigley, 1985), before the human activities became a significant process that impacts the regional climate. Simply attributing the current drought to human activities fails to look at the present climate in the context of the long-term climate variability.

According to a recent study by Nicholson *et al.* (1998), although the drought in the Sahel region still continues, there has been no progressive man-made desertification since 1980 (no data is available for earlier period). Any attempt to blame human activities for the current drought has to address the persistence mechanism in the Charney hypothesis, i.e., the reduced precipitation following man-made desertification further limits the vegetation growth and makes the drought self-sustaining. However, in previous studies on land surface feedback, the vegetation distribution and vegetation perturbations are prescribed. Lack of the representation of vegetation dynamics in previous models made it impossible to simulate the response of vegetation to the induced atmospheric climate changes. As a result, previous studies on land cover changes, including those focusing on the region of West Africa and those focusing the Amazon Basin, only consider a one-way feedback from vegetation to climate. This is equivalent to assuming that all vegetation changes are permanent. In reality, most of the anthropogenically induced vegetation changes are not fully maintained, or not maintained at all, which allows active vegetation succession and two-way biosphere-atmosphere interactions. For example, forest harvesting usually takes place with a rotation cycle of several decades; farms are reclaimed by grass or trees upon agricultural abandonment; livestocks tend to migrate when a region is overgrazed; dense ground vegetation colonizes the land surface even in the first year following a sweeping fire; etc. To more realistically simulate the climatic impact of vegetation changes, climate models should take into account the response of the post-perturbation vegetation to the induced atmospheric climate change. This requires a model that includes an explicit representation of vegetation dynamics.

1.3.2 Low-Frequency Rainfall Variability

Compared with the large number of studies devoted to the interannual variability of the Sahel rainfall, fewer studies have investigated the issue of low-frequency rainfall variability. Due to the nature of this topic, most of the previous studies relied on statistical analysis or stochastic modeling.

Based on extensive statistical analysis, Ward (1998) found that the decadal variability of the Sahel rainfall is correlated with the variability of the north-south interhemispheric gradient of the sea surface temperature and sea level pressure. However, the shortness of the available records precludes reliable estimation of the statistical significance of this correlation. To confirm such an association, further investigation using general circulation models is required.

Nicholson (1989) viewed the land surface feedback as the potential factor perpetuating the climate condition in Sahel, and proposed that the large scale circulation might be the trigger for the switch between the drought and wet periods: *"If we assumed that large scale factors initiate a drought and that the resultant land surface changes reinforce the initial atmospheric forcing, the character of a given rainy season represents the interplay of these two types of forcing. Presumably, then, a drought would continue until an atmospheric perturbation favoring rainfall occurs and is sufficiently strong to overcome the surface-imposed drought-promoting feedback"*. This provides a theoretical explanation for the long-term rainfall variability over West Africa. However, it remains to be proven whether the land surface does play such a role, and through what mechanism.

Using a statistical-dynamical method, several previous studies (Nicolis, 1982; Demaree and Nicolis, 1990; Rodriguez-Iturbe *et al.*, 1991; Entekhabi *et al.*, 1992) suggested that the dominance of low-frequency variability in some climate records may be explained if the climate system is considered as a stochastic process driven by external forcings. Among these studies, Demaree and Nicolis (1990) focused on the Sahel rainfall, and viewed the low-frequency rainfall variability as a series of transitions between two stable states. Based on statistical analyses of the rainfall data over

the Sahel region, they constructed a conceptual model using stochastic differential equations and used it to successfully reproduce the statistical characteristics of the rainfall time series. However, similar to other studies that are statistically based, the Demaree and Nicolis theory puts little emphasis on physical mechanisms. A more physically based study by Entekhabi *et al* (1992) argued that the prolonged dry or moist behavior in some climate record is due to the nonlinear interactions between the components of the hydrological cycle in both the land and the atmosphere. In their study, the interaction was expressed by the soil moisture feedback in the water balance equation, which is expressed in its nonlinear differential form. Their stochastic analysis suggested that the climate may attain a multiple number of preferred modes with noise-induced transitions between the modes. This study supports Nicholson's (1989) view that land surface feedback may have caused the persistence of the Sahel climate. However, the land surface property responsible for this feedback is the soil moisture, which dries out in arid regions during the dry season regardless of how dry or how wet the previous rainy season might be. Therefore, the physical feedback mechanism of Entekhabi *et al* (1992) only takes effect at the seasonal time scale, not the multiple-year time scale.

For the land surface feedback to act as an effective mechanism of climate persistence, the surface property responsible for the feedback must have a "memory" long enough to carry the rainfall information from one year to the next. While soil moisture in general only has seasonal "memory", vegetation may maintain multiple-year "memory". This is obvious over the forest region since the canopy of trees is supported by the "year-to-year" accumulated woody structure. Over grassland region, as discussed in section 1.1, perennial grass is the dominant plant species. Although the aerial part of perennial grass shows strong seasonality, it has perennating underground structure which accumulates from year to year. Therefore, vegetation may have played a significant role in causing the observed climate persistence. This role has not yet been addressed due to the lack of representation of vegetation dynamics in previous models.

1.3.3 Two-way Biosphere-Atmosphere Interactions

The literature reviews in the previous two sections suggest that two-way biosphere-atmosphere interactions and vegetation dynamics may be the key towards a better understanding on the recent climate variability over the Sahel region. The role of vegetation dynamics has also been highlighted in studies of paleo-climatology in West Africa. For example, Kutzbach *et al* (1996a) simulated the middle-Holocene (6000 years BP) "climate optimum" in West Africa, and found that changes in the orbital forcing ("R") alone can only account for 40% of the observed rainfall difference between the middle Holocene and the present. The incorporation of paleo-vegetation and the associated soil texture difference ("RVS") brings the model simulation and the observations of paleo-climate into closer agreement. Then, the rainfall simulations are used to force a biome model. The results show that the vegetation simulated with "RVS" is in a better agreement with paleo-vegetation than that simulated with "R", which means, the vegetation/soil changes during the middle Holocene have increased rainfall sufficiently to be self-maintaining. Kutzbach *et al.* (1996a) strongly suggested that climate models need to incorporate the two-way biosphere-atmosphere interactions, and to include the biospheric processes involving both vegetation and soils. A similar conclusion was reached by several other studies (e.g., Foley *et al.*, 1994; Kutzbach *et al.*, 1996).

Among early studies on the two-way biosphere-atmosphere interactions are those by Gutman (1984 a,b; 1986). Gutman (1984 a,b) used the dryness index D (which is a function of the net radiation and precipitation) to parameterize the vegetation condition, and defined the water availability (which determines the latent heat flux) as a function of D, thus coupling the geobotanic state with the atmospheric climate. Using the two-way interactions described above with a zonally averaged annual steady state climate model, Gutman (1984 a) produced a long-term climate and vegetation state which agreed well with observations. However, in the deforestation and desertification (Gutman, 1984 b) experiments, he assumed a prescribed perturbation over certain regions while allowing two-way feedback in the unperturbed region. The rea-

son for making that assumption is the fact that this simple scheme can not simulate the transient geo-botanic change. In a later study, Gutman (1986) suggested a possible way to simulate the transient geobotanic process, which assumes that the speed of geobotanic changes is equal to the difference between the current geobotanic state and the equilibrium geobotanic state normalized by the related time scale. However, "much work is needed on investigating these time scales" (Gutman, 1986). The transient changes of vegetation were also considered by Protopapas and Bras (1988) in their hydrological modeling of soil-crop-climate interactions, but at the seasonal time scale.

As biospheric modeling achieved greater sophistication, more studies focused on the two-way biosphere-atmosphere interactions. Claussen (1994) coupled the equilibrium vegetation model BIOME (Prentice *et al.*, 1992) with the global climate model of the Max-Planck-Institute for Meteorology, ECHAM. The coupling between these two models is asynchronous: the monthly means of atmospheric forcings are produced from several years of integration with ECHAM; based on these data, BIOME predicts the global distribution of biomes, which then provides a new set of surface parameters for the subsequent ECHAM integration. This iteration is repeated until an equilibrium between the two models is established. In an effort to address the Sahel drought and desert dynamics, Claussen (1997) examined the sensitivity of the asynchronously coupled ECHAM-BIOME model to initial land surface conditions, and found two equilibrium solutions in North Africa and Central East Asia depending on the initial conditions. The present-day solution is associated with the present-day distribution of vegetation, while the anomalous solution features a significant northward expansion of the savannah and grassland which results in a "green Sahara". Claussen questioned whether the existence of two solutions is realistic. This is because the ECHAM-BIOME merely predicts equilibrium vegetation and cannot deal with transient vegetation dynamics. Hence the model does not tell how the vegetation grows into desert. If such an "intrusion" is unlikely to happen under present-day conditions, the anomalous state will not occur in reality and therefore will be irrelevant to the climate variability in West Africa.

The asynchronous coupling approach was also taken by Texier *et al.* (1997) who coupled BIOME to the LMD AGCM in a paleo-climate study. They explored the role of vegetation-climate interactions in the model's response to the mid-Holocene (6000 years BP) orbital forcing, and found that the inclusion of two-way interactions improved the qualitative agreement between the model simulation and the 6000 yr BP observational data derived from pollen and macrofossil evidence. The mid-Holocene climate in North Africa was significantly wetter than today, and some moisture-demanding vegetation types once existed in the now-arid region. With the mid-Holocene orbital forcing alone, Texier *et al.*'s simulation for North Africa was wetter and greener than today's condition, but not wet enough compared with the Holocene climate. The two-way vegetation-climate feedback was found to enhance the orbitally induced precipitation increase in North Africa by more than 100% and bring the model closer to observations.

Compared to those with prescribed vegetation, studies such as Claussen's (1994, 1997) and Texier *et al.*'s (1997) are more realistic. However, due to the use of equilibrium vegetation model and the asynchronous coupling between the biosphere and the atmosphere, these studies still could not simulate the transient vegetation dynamics. In order to simulate the synchronous coupling between the biosphere and the atmosphere, there is a need for a special type of biospheric models. Such models must be detailed enough to include the key biospheric processes, but at the same time simple enough to only include large-scale descriptions. For example, vegetation should be described at the scale of the overall canopy structure instead of at the scale of a single tree. The Integrated BIosphere Simulator (IBIS) (Foley *et al.*, 1996) is the first of this new generation of models. IBIS integrates a wide range of terrestrial phenomena, including the biophysical, physiological, and ecosystem dynamical processes, into a single, physically consistent simulator that can be directly coupled to atmospheric models. Foley *et al.* (1998) coupled IBIS with the AGCM GENESIS, and tested the model's performance in simulating the current climate conditions. The synchronously coupled IBIS-GENESIS correctly simulated the basic zonal distribution of temperature and precipitation, and roughly captured the general distribution of forests and

grasslands. Recently, Levis *et al.* (1999) used the fully coupled IBIS-GENESIS to examine the potential effects of changes in vegetation cover on simulations of CO_2-induced climate change, and demonstrated that vegetation feedbacks are potentially significant and must be included in assessments of anthropogenic climate change.

1.4 Research Objectives

The main objective of this dissertation is to elucidate the mechanisms of the climate variability over the Sahel region, which include the dominance of low-frequency variability and the persistence of the Sahel drought in the second half of the 20th century.

The uniqueness of the low-frequency variability in the Sahel region suggests that the land surface feedback in that region, a local factor, instead of the large-scale forcings, may play a more important role in the persistence of the Sahel climate. As discussed in Section 1.3.2, vegetation cover can have a multi-year "memory", which provides a potential mechanism through which the land surface feedback may regulate the variability of the regional climate. The recent advances in modeling the synchronous coupling between the biosphere and the atmosphere makes it possible to thoroughly investigate the vegetation feedback mechanism, and to study the climatic impact of vegetation changes within the scope of a natural, dynamic ecosystem. In this study, the role of vegetation dynamics in the climate variability of West Africa will be investigated using the numerical modeling approach. First, a synchronously coupled biosphere-atmosphere model will be developed to simulate the climate system over West Africa. The coupled model will then be used to address the following topics:

1. The nature and stability of the regional climate equilibrium (equilibria) over West Africa.

2. The role of vegetation dynamics in shaping the natural variability, low-frequency variability in particular, of the regional climate over West Africa.

3. The role of vegetation dynamics in the triggering and persistence of the current Sahel drought.

1.5 Thesis Structure

The main body of this thesis has two parts. In Part I, a zonally symmetric, synchronously coupled biosphere-atmosphere model (ZonalBAM) is developed to simulate the climate system over West Africa, and extensive model testings are carried out; in Part II, the newly developed model is used to study the two-way biosphere-atmosphere interactions over West Africa and to interpret the observed climate variability in the Sahel region.

Part I includes three chapters. Chapter 2 focuses on the model development. A zonally symmetric atmospheric model on the West African climate is developed, and is synchronously coupled to the fully dynamic biospheric model IBIS. Each component of the atmospheric model and the biospheric model is described, and modifications made to IBIS are presented. Chapter 3 presents the model validation. First, the atmospheric model and the biospheric model are separately tested against observations. The performance of the fully coupled model (ZonalBAM) is then examined. In the model development, a canopy interception scheme has been incorporated into IBIS to account for the impact of rainfall sub-grid variability. The importance of incorporating this sub-grid variability is demonstrated in Chapter 4 using West Africa as a case study.

Part II includes four chapters. Chapter 5 focuses on the response of the coupled biosphere-atmosphere system in West Africa to non-permanent vegetation perturbations. Emphasizing the role of vegetation dynamics, theoretical analyses lead to a hypothesis that the coupled biosphere-atmosphere system may have multiple equilibria states, with reversible transitions between different equilibria. This hypothesis is tested using ZonalBAM based on both the model sensitivity to initial conditions and the resilience of the coupled system with respect to vegetation perturbations. Both the existence of multiple climate equilibria and the possibility of climate transition are demonstrated. Chapter 6 investigates the response of the coupled biosphere-atmosphere system to continuously varying large-scale forcings (SST variations), and examined the multiple-equilibrium behavior of the system in a more realistic scenario.

Based on these, mechanisms of low-frequency rainfall variability are then explored and the role of vegetation dynamics is addressed. Chapter 7 explores the possible mechanisms for the triggering and persistence of the current Sahel drought. Two triggering mechanisms, human activities and large-scale forcings, are considered, and vegetation dynamics is seen to play a dominant role in both. This chapter also demonstrates how the coupled system responds to man-maintained land cover changes, and the role of vegetation dynamics in the case of permanent vegetation changes. Finally, Chapter 8 summarizes the main results and conclusions of this dissertation.

Part I

Modeling the Coupled Biosphere-Atmosphere System

Part I focuses on the development and validation of a coupled biosphere-atmosphere model (ZonalBAM). A zonally symmetric atmospheric model is synchronously coupled with a biospheric model that includes explicit representation of vegetation dynamics. Therefore, the coupled model simulates not only the transient atmospheric climate but also the associated transient vegetation. Chapter 2 presents the development of the coupled model, and describes each component of the zonally symmetric atmospheric submodel as well as the fully dynamic biospheric submodel. Chapter 3 examines the model's performance in simulating the biospheric climate, the atmospheric climate, and the coupled biosphere-atmosphere system. In the model development, a canopy interception scheme has been incorporated into IBIS to account for the rainfall sub-grid variability. The importance of doing so is demonstrated in Chapter 4 using West Africa as a case study.

Chapter 2

Model Development

2.1 Introduction

As reviewed in Chapter 1, the recent advances in modeling the synchronous coupling between the biosphere and the atmosphere make it possible to pursue studies on the climatic impact of land cover changes within the scope of a natural, dynamic ecosystem. We are interested in how the biosphere and the atmosphere as a synchronously coupled system respond to non-permanent vegetation perturbations over West Africa, and what role the vegetation dynamics play in the climate variability over that region. Due to the slow nature of vegetation growth and decay, the time scale associated with ecosystem dynamics is at the order of decades or centuries. To better serve our research purpose, we develop a zonally symmetric biosphere-atmosphere model (ZonalBAM) to simulate the synchronously coupled biosphere-atmosphere system, which is computationally more efficient than a model of the same kind that accounts for the zonal asymmetry. As documented by Zheng and Eltahir (1998), the observed climatic conditions justify the assumption of zonal symmetry in West Africa.

The newly developed model simulates the coupled biosphere-atmosphere system over West Africa including ecosystem dynamics. It combines a zonally symmetric atmospheric model and a fully dynamic biospheric model, which will be described in the following.

2.2 The Atmospheric Model

The development of the atmospheric model started from the framework of the zonally symmetric atmospheric model of Zheng (1997) (hereafter, "the Zheng model"), which has been used in several previous studies (Zheng and Eltahir, 1997, 1998; Zheng, 1998; Zheng *et al.*, 1999).

For atmospheric dynamics, the Zheng (1997) model follows Plumb and Hou (1992). It uses $z = -Hln\frac{p}{p_s}$ (log-pressure) as the vertical coordinate and $y = asin\phi$ as the meridional coordinate. Here H is a reference scale height ($8km$ is used), p the pressure, p_s the reference pressure (usually taken as $1000mb$), a the earth radius, and ϕ the latitude. In the meridional direction, the model domain covers the whole globe, with a uniform resolution in y axis. The land-ocean boundary is set at $6°N$, with land in the north and ocean in the south. Sea surface temperature is prescribed according to observations. In the vertical direction, the Zheng (1997) model assumes uniform resolution with respect to height. We modified the numerical scheme for the atmospheric dynamics so that the model can have a non-uniform vertical resolution with respect to height (usually finer for low levels and coarser for upper levels), which adds to the computational efficiency of the model.

For atmospheric physics, the Zheng model used the radiation scheme by Chou (1992) and Chou *et al.* (1991), and the convection scheme by Emanuel (1991) (version 2.02). Our new model uses the same radiation scheme. We also use Emanuel's convection scheme, but a recently updated version CONVECT4.1 (personal communication). Here our model development focuses on the representation of additional physical processes, including atmospheric boundary layer processes and the cloud-radiation feedback, which were not simulated in the Zheng model.

The atmospheric boundary layer is defined as the portion of the atmosphere directly influenced by the land surface. The free atmosphere "feels" the existence of the surface through the growth and decay of the boundary layer. It is the boundary layer that directly responds to land surface forcings. Therefore, to correctly simulate the biosphere-atmosphere interactions, a boundary layer scheme which describes the

boundary layer processes is incorporated into the new model.

Clouds cover more than half of the global surface. The presence of clouds significantly impacts the radiation budget of the earth-atmosphere system, thus modifying the atmospheric profile which then feeds back to influence the cloud formation, i.e., cloud-radiation feedback. For the biosphere, clouds reflect the incoming solar radiation thus reducing the photosynthetically active radiation at the land surface, which retards the vegetation growth. To account for these mechanisms, a cloud parameterization scheme is developed and incorporated into the new model to predict the cloudiness.

The components of the atmospheric model will be described in the following, with more detail given to those new components that were not represented in the Zheng model.

2.2.1 Atmospheric Dynamics

The framework of the model dynamics is same as in the Zheng (1997) model, which is based on Plumb and Hou (1992). The momentum equations, the hydrostatic approximation, the air mass conservation equation, the thermodynamic energy equation, and the water conservation equation of the meridional circulation in the log-pressure system can be written as follows:

$$\frac{\partial U}{\partial t} - fV = AU + DU + FU \tag{2.1}$$

$$\frac{\partial V}{\partial t} + fU = AV + DV + FV - cos^2\phi \frac{\partial \Psi}{\partial y} \tag{2.2}$$

$$T = M_2(\Psi) = (\frac{\partial}{\partial z} + \frac{\Psi}{2H})\Psi \tag{2.3}$$

$$\frac{\partial V}{\partial y} = -M_1(W) = -(\frac{\partial}{\partial z} - \frac{1}{2H})W \tag{2.4}$$

$$\frac{\partial T}{\partial t} + N^2 W = AT + DT + e^{-\frac{z}{2H}} \frac{R}{H} Q_d + FT \tag{2.5}$$

$$\frac{\partial Q}{\partial t} = AQ + DQ + e^{-\frac{z}{2H}} S_q + FQ \tag{2.6}$$

where

$$(U, V, W, \Psi, T, Q) = (ucos\phi, vcos\phi, w, \Phi, \frac{RT^*}{H}, q)e^{-\frac{z}{2H}},$$

In the above, u, v, w are the three velocity components, Φ is the geopotential, T^* is the departure of temperature from a reference state, and q is the specific humidity. Parameters and constants include the Coriolis parameter f, latitude ϕ, the gas constant for dry air R, a reference height scale H, and a reference pressure p_s.

In Eqs. 2.1-2.6, AU, AV, AT, AQ are the advective terms of U, V, T, Q, which can be expressed as follows:

$$AU = -e^{-\frac{z}{2H}} \{\frac{\partial}{\partial y}(VU) + \frac{\partial}{\partial z}(WU)\}, \tag{2.7}$$

$$AV = -e^{-\frac{z}{2H}} \frac{U^2 y}{a^2 cos^2 \phi}, \tag{2.8}$$

$$AT = -e^{-\frac{z}{2H}} \{\frac{\partial}{\partial y}(VT) + \frac{\partial}{\partial z}(WT)\}, \tag{2.9}$$

$$AQ = -e^{-\frac{z}{2H}} \{\frac{\partial}{\partial y}(VQ) + \frac{\partial}{\partial z}(WQ)\}. \tag{2.10}$$

DU, DV, DT, DQ in Eqs. 2.1-2.6 are diffusive terms. Different from the Zheng model which included the diffusive terms to suppress the numerical instabilities, the diffusive terms in this model are associated with the physical diffusion process, which will be explicitly described in the boundary layer scheme. FU, FV designate the zonal and meridional components of drag owing to small-scale eddies and surface momentum flux. FT, FQ are the surface fluxes of sensible heat and water vapor, which will be

supplied by the biospheric model. Q_d is the total diabatic heating which includes the radiative cooling, heating due to moist convection, and heating due to large-scale condensation. S_q is the total water vapor source/sink caused by moist convection and large-scale condensation.

2.2.2 Radiation Scheme

The model uses the radiation parameterization scheme developed by Chou (1986) and Chou *et al.* (1990). It computes the infrared and solar radiation fluxes at different absorption bands (or spectral regions), and derives the overall solar heating and thermal cooling rates in the atmosphere. For the infra-red radiation, this scheme considers the radiative emission in different H_2O bands, CO_2 bands, and O_3 bands, as well as the impact of CH_4 and N_2O. Details about the infra-red radiation calculation within this scheme can be found in Chou *et al.* (1990), Chou and Kouvaris (1990), Chou (1984), and Chou and Peng (1983). Solar radiation is calculated in the near-infrared region and the UV+Visible region. Within the near-infrared region, the solar radiation is absorbed by H_2O, CO_2, and O_3, scattered and reflected by clouds and aerosols. Within the UV+Visible region, it takes into account the ozone absorption and the effect of clouds and aerosols. For details about the solar radiation, please refer to Chou (1991), Chou (1990), and Chou (1986). In this study, we do not include the effect of aerosols.

2.2.3 Convection Scheme

The moist convection processes are simulated using the convection scheme developed by Emanuel (1991). We are using the recently updated version CONVECT 4.1. In this scheme, the convection representation is mainly based on the dynamics and microphysics of the cloud processes, which is deduced from recent observations and theories of convective clouds. The fundamental entities of convective transport are the subcloud-scale drafts rather than the clouds themselves. The main closure parameters are the parcel precipitation efficiencies, θ and ψ. θ determines how much

of the condensed water is converted to precipitation. ψ determines how much of the precipitation falls through the unsaturated air thus leading to warming and drying, while the remaining fraction $(1 - \psi)$ of the precipitation re-evaporates, leading to cooling and moisturing. These parameters are specified as functions of altitude, temperature, and adiabatic water content, thus relating the large scale forcings to the microphysics of cloud processes. Given the vertical profile of temperature and humidity, the convection scheme computes the amount of convective precipitation and the tendencies of temperature and moisture. Further details can be found in Emanuel (1991). Large scale condensation is treated separately from convection. When the atmosphere reaches super-saturation, the excess water is condensed out of the system as large-scale precipitation, and no re-evaporation is considered. During both the convection and large-scale condensation processes, enthalpy is conserved.

2.2.4 Cloud Parameterization Scheme

Clouds play an important role in the biosphere-atmosphere system through their impact on the radiative transfer within the atmosphere. Clouds reduce the incoming solar radiation mainly by reflection and scattering. For the biosphere, this change of the solar radiation directly reduces light availability for vegetation. For the earth-atmosphere system, the short-wave cloud radiative forcing has a cooling effect. At the same time, clouds also causes warming by trapping the outgoing long-wave radiation. The net radiative forcing varies significantly with different types and spatial distributions of clouds. For example, for the stratiform clouds in the boundary layer, the cooling effect is dominant; for cirrus clouds near the tropopause, the warming effect is dominant. Therefore it is important to distinguish different types of clouds.

The presence of clouds modifies the vertical distributions of temperature and water vapor, which feeds back to impact the formation of clouds through a set of complex microphysical processes. Simulating this clouds feedback remains a challenge to climate modelers. In fact, previous studies (e.g., Cess *et al.*, 1996; Cess *et al.*, 1989; Spelman and Manabe, 1984) have shown that variations in the representation of clouds are largely responsible for the differences in the sensitivity of existing models

to external forcings. On the other hand, the microphysical processes associated with clouds are extremely complex, and are poorly understood. Most of these processes take place at spatial scales much smaller than the typical grid size of climate models. One common approach in modeling clouds is to parameterize smaller scale processes as functions of large scale variables, which is also used in our model.

In this study, clouds are divided into three groups: high-level clouds, medium-level clouds, and low-level clouds. They are described by their fractional coverage, height, vertical extent, and cloud density (optical depth). According to London (1952), the globally averaged vertical extent for the high-, medium-, and low-level clouds are 220mb-280mb, 460mb-640mb, and 640mb-940mb, and, the optical depths of each cloud type are about 2, 6, and 12, respectively. Here we fix both the cloud vertical extents and the cloud optical depths at their global means. Only the fractional cloud cover is predicted by the model.

The parameterization of the fractional cloud cover is developed based on Kvamsto (1991). Previous studies (e.g., Slingo, 1980, 1987; Sunquist, 1989; Kvamsto, 1991) have developed many fractional cloudiness parameterization schemes. Some of these are complex and consider the impact of several physical variables, while others predict the cloudiness based on one single variable, the relative humidity. The Kvamsto (1991) scheme belongs to the latter group. It features a linear relationship between the relative humidity and the fractional coverage of the low-level clouds, as described by the following:

$$FC = max(0.0, \frac{RH - RH_0}{1 - RH_0}). \tag{2.11}$$

where FC is the cloud fractional cover, RH is the relative humidity, and RH_0 is the relative humidity threshold at which clouds start to form. Despite of its simplicity, the performance of the Kvamsto scheme is one of the best among the seven schemes examined by Mocko and Cotton (1995). Here the linear scheme shown in Equation 2.11 for the low-level clouds is adopted and its application is expanded to the medium- and high-level clouds. For the relative humidity threshold RH_0, 0.8, 0.65, and 0.7 are used for high-, medium-, and low-level clouds, respectively. Because of the difference

in spatial resolution, these threshold values are slightly lower than those usually used in meso-scale models (e.g., Slingo, 1980, 1987; Kvamsto, 1991).

The cloud scheme is summarized by Figure 2-1.

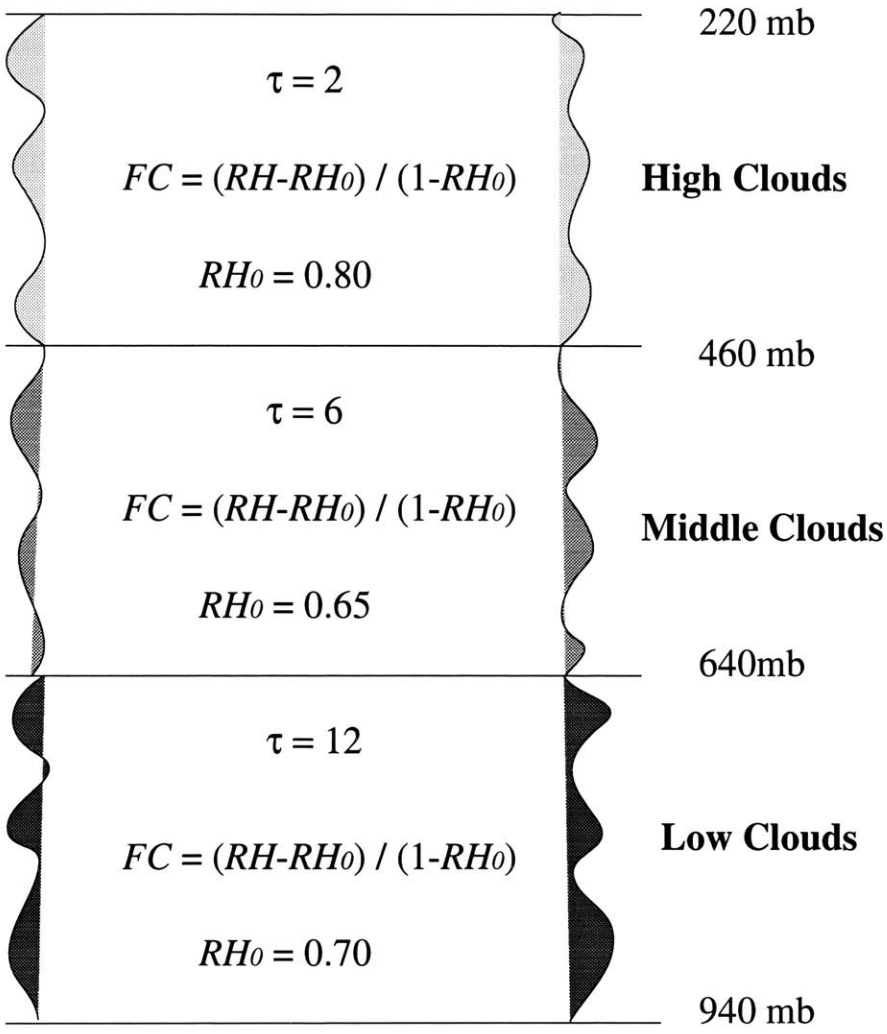

Figure 2-1: A summary of the cloud parameterization scheme. Here τ is the cloud optical depth, and the definition for RH and RH_0 is the same as in Eq. (2.11). FC is first calculated at each pressure level based on the relative humidity at the corresponding level. The average of FC within the vertical extent of each cloud type is then used as the fractional cover for that type of clouds.

2.2.5 Boundary Layer Scheme

The boundary layer responds to the land surface forcing through turbulence. It is the frequent occurrence of turbulence that distinguishes the atmospheric boundary layer from the free atmosphere above it. Heating from the warm ground and wind shear near the surface are the most important factors that contribute to the generation of turbulence. Within the boundary layer, the transport of quantities such as heat, moisture, and momentum in the vertical direction is dominated by turbulent transport, which is orders of magnitude more effective than the transport through molecular diffusion. Boundary layer models describe the turbulent transports of heat, moisture, and momentum within the atmospheric boundary layer.

Our boundary layer scheme is developed based on Hotslag and Boville's (1993) non-local scheme. This scheme is termed "non-local" relative to the usually used "local" schemes. In a "local" boundary layer scheme, the flux of a quantity is proportional to the local gradient of that quantity, and the eddy diffusivity depends typically on local gradients of the mean wind and mean virtual temperature. In contrast, for a "non-local" boundary layer scheme, the formulation of the eddy diffusivity depends on the bulk properties of the atmospheric boundary layer rather than local properties. It also incorporates nonlocal (vertical) transport effects for heat and moisture, the so called "counter-gradient transport". As shown by Holtslag and Boville (1993), simulations with a "non-local" scheme are in general more realistic than those with a "local" boundary layer scheme. Another advantage of using a "non-local" boundary layer scheme is that the effect of dry-adiabatic adjustment on the turbulent transport can be neglected.

The turbulent transport of heat, moisture, and momentum can be expressed by the following equations:

$$\frac{d\theta}{dt} = \frac{\partial}{\partial z} K_h \left(\frac{\partial \theta}{\partial z} - G_h \right) \tag{2.12}$$

$$\frac{dq}{dt} = \frac{\partial}{\partial z} K_q \left(\frac{\partial q}{\partial z} - G_q \right) \tag{2.13}$$

$$\frac{du}{dt} = \frac{\partial}{\partial z} K_m (\frac{\partial u}{\partial z}) \tag{2.14}$$

$$\frac{dv}{dt} = \frac{\partial}{\partial z} K_m (\frac{\partial v}{\partial z}) \tag{2.15}$$

In the above, Km, Kh, and Kq are the eddy diffusivities for momentum, heat and water vapor, and Gh, Gq represent the counter-gradient transport for heat and water vapor. The eddy diffusivity depends on the boundary layer height h, formulated as follows:

$$K = k\omega z(1 - \frac{z}{h})^2,$$

where k is the Von Karman constant, and ω is a characteristic turbulent velocity scale which differs between heat, water vapor and momentum. The boundary layer height h is a function of the bulk Richardson number R_i. The implicit relationship between the boundary layer height and the boundary layer Richardson number is used to determine h:

$$h = \frac{R_{i_{cr}}[u(h)^2 + v(h)^2]}{\frac{g}{\theta_s}(\theta_v(h) - \theta_s)},$$

where θ_s is the air temperature near the surface, θ_v is the virtual temperature, and $R_{i_{cr}}$ is the critical Richardson number.

2.3 The Biospheric Model

The dynamic biospheric model uses the Integrated BIosphere Simulator (IBIS), developed by Foley *et al.* (1996). IBIS integrates a wide range of terrestrial phenomena, including the biophysical, physiological, and ecosystem dynamical processes, into a single, physically consistent simulator that can be directly coupled to atmospheric models. IBIS takes the meteorological forcings provided by the atmospheric model as inputs, returns to the atmospheric model outputs that describe surface properties and surface fluxes, and updates the biospheric state including the vegetation structure. Here a brief description of IBIS is given, followed by a description of the modifications

we have made to IBIS including the incorporation of a canopy interception scheme.

2.3.1 IBIS Description

The vegetation cover in IBIS is a combination of different plant functional types (PFTs). PFTs are defined based on physiognomy (tree or grass), leaf form (broad-leaf or needle-leaf), leaf habit (evergreen or deciduous), and photosynthetic pathway (C_3 or C_4). For example, PFTs that grow well in the tropics include tropical broad-leaf evergreen trees, tropical broad-leaf drought-deciduous trees, and C4 grasses. Vegetation canopy in IBIS is divided into two layers, with woody plants in the upper canopy and herbaceous plants in the lower canopy. Soil texture is represented by the percentage of three different components: sand, silt, and clay. There are 6 soil layers in the root zone, which sum up to 4.0 m. The thickness of each soil layer, from the top to the bottom, is 0.10, 0.15, 0.25, 0.50, 1.00, and 2.00 m respectively. The rooting profile differs between different PFTs, and are based on published data (Jackson *et al.*, 1996). This land surface structure is schematized by Figure 2-2.

IBIS consists of four component modules: the land surface module, the vegetation phenology module, the carbon balance module, and the vegetation dynamics module. The hierarchical framework of IBIS is presented in Figure 2-3. Each of the sub-models are described in the following.

The land surface module represents the biophysical and physiological processes at the same time step as the atmospheric model (20 minutes in this study). It solves for the exchange of water vapor, energy, carbon dioxide, and momentum between the ground and vegetation, between different vegetation layers, and between vegetation and the atmosphere. Solar radiation is treated using two-stream approximations within each vegetation layer, with separate calculations for direct and diffuse radiation in two wavelength bands: 0.4-0.7 um and 0.7-4.0 um. For infrared radiation, each vegetation layer is treated as a semi-transparent plane with its emissivity dependent on the leaf and stem density. For the canopy hydrological processes, IBIS includes a detailed description for the cascade of precipitation. Formulations for interception, throughfall, evaporation from the intercepted water, and plant transpiration

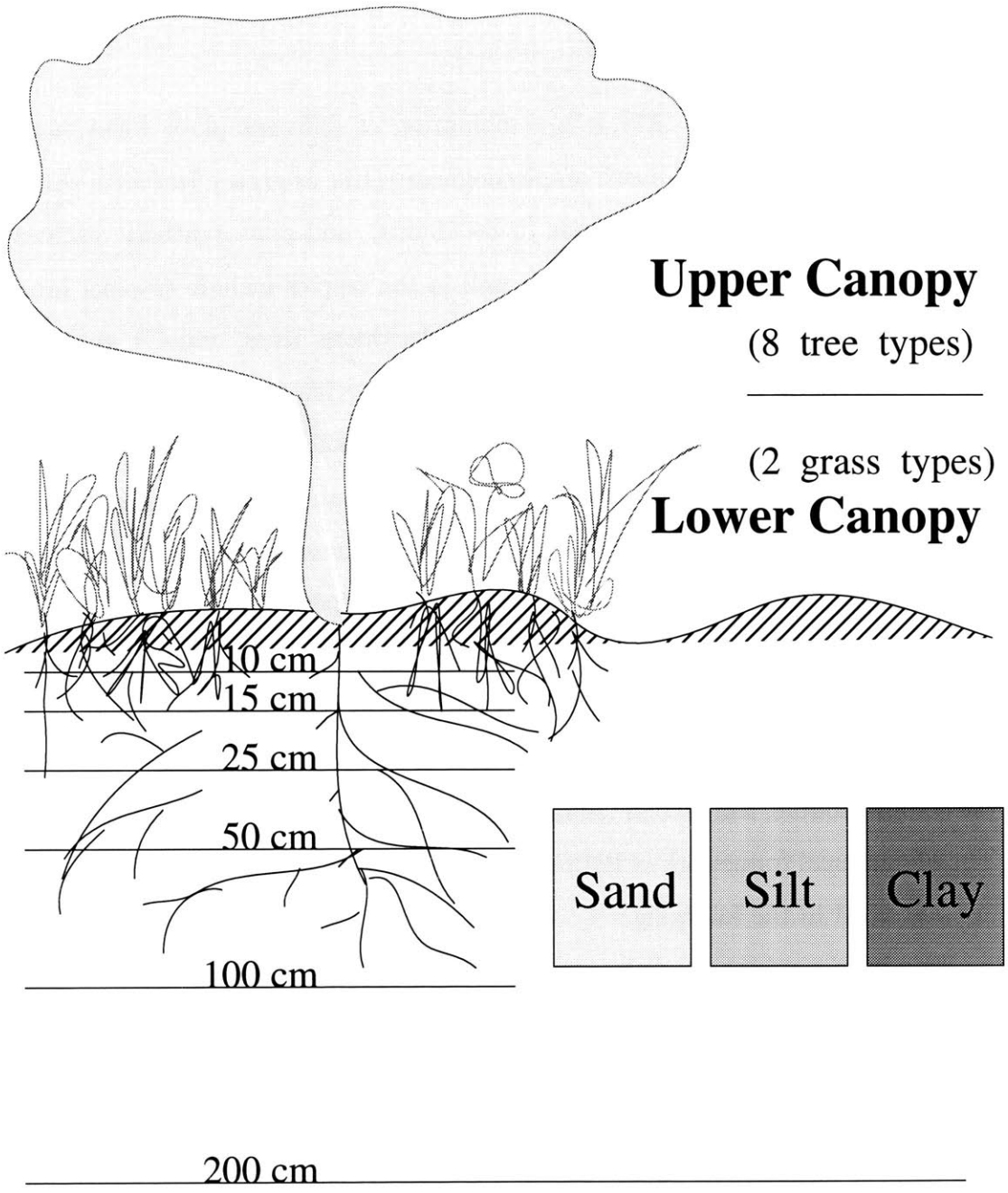

Figure 2-2: Structure of the land surface in IBIS. The numbers ($10cm$, $15cm$, ...) label the thickness of different soil layers.

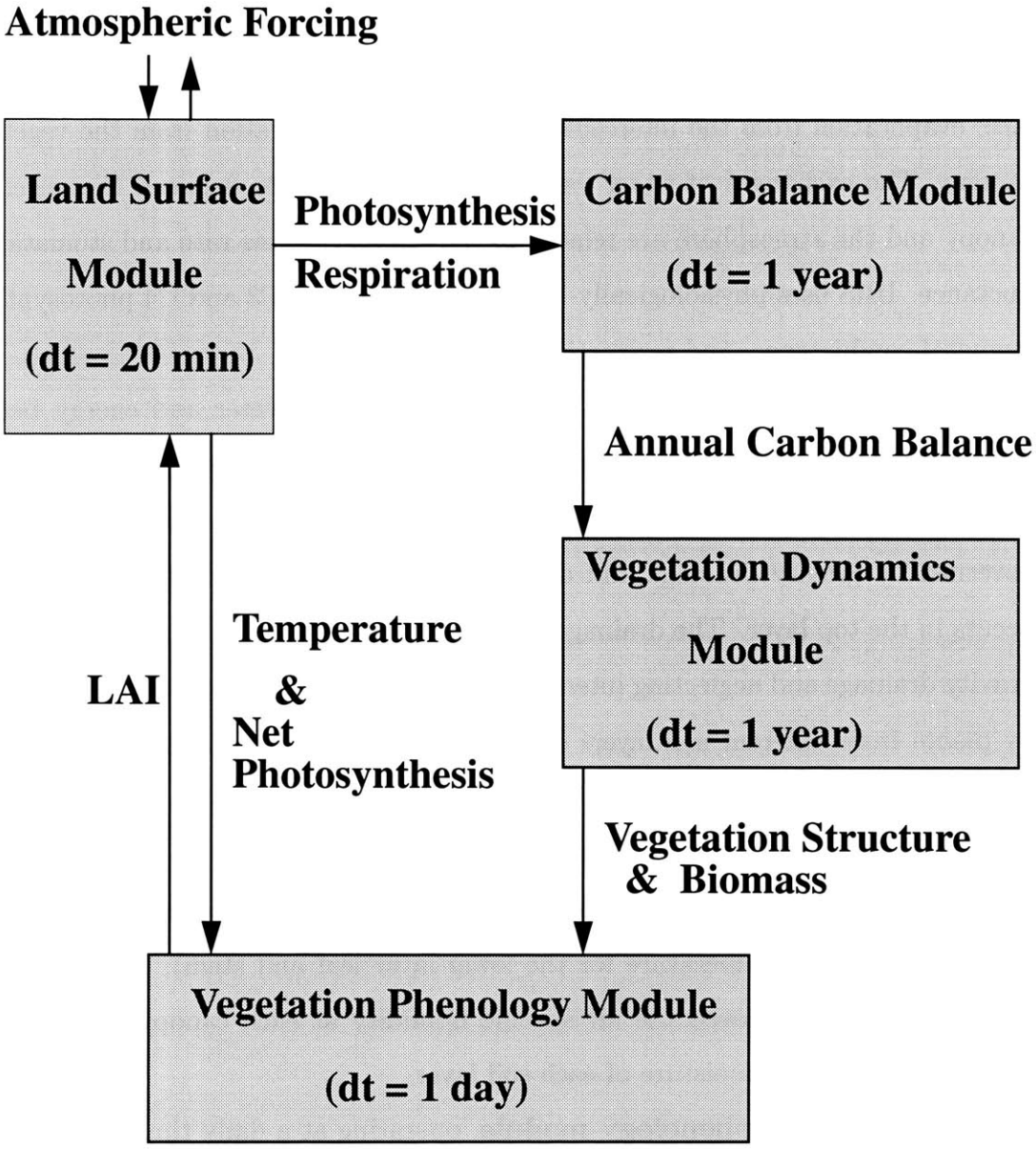

Figure 2-3: Hierarchical framework of IBIS, from Foley *et al.* (1996).

are all physically based. However, the sub-grid variability of rainfall is neglected. (The issue of sub-grid variability will be addressed in Section 2.3.2.). The overall evapotranspiration has three different components: evaporation from the ground surface, evaporation from the intercepted water, and transpiration from the vegetation canopy. The exchanges of water vapor and carbon dioxide between the vegetation canopy and the atmosphere are related to the photosynthesis rate and stomatal conductance. IBIS uses physiologically-based formulations of C3 and C4 photosynthesis, stomatal conductance, and respiration.

Also described in this module are the exchanges of water and energy between different soil layers. Relevant processes include heat diffusion, water transport within the soil, plant uptake of water, etc. Water transport between different soil layers is governed by gravity drainage and diffusion. Direct evaporation from the soil only occurs in the top layer. The drainage from the bottom soil layer is modeled assuming gravity drainage and neglecting interactions with groundwater aquifers. Water uptake by plants from different soil layers depends on the rooting profiles. Water stress is considered when the soil moisture is below the wilting point.

The main equations in the land surface module predict the temperature of different vegetation components (upper-layer leaf temperature, upper-layer stem temperature, and the combined temperature for the lower-layer leaf and stem), the air temperature at each canopy level, the air specific humidity at each canopy level, and, the temperature and soil moisture of each soil layer.

The vegetation phenology module, operating at a daily time step, describes the plant leaf display in response to seasonal climate conditions. For example, winter-deciduous plants shed their leaves when temperature drops below a threshold value; leaf-shedding for drought-deciduous plants takes place upon severe water stress.

The carbon balance module calculates the net primary productivity (NPP) for each PFT, and annually updates their carbon storages. The annual NPP is equal to the difference between photosynthesis and respiration, integrated through an entire year. NPP is allocated to three different carbon reservoir: leaves, stems, and roots. The change of carbon biomass in each reservoir depends on the NPP allocation and

the turnover rate. Parameters on allocation and turnover differ between different PFTs.

The vegetation dynamics module updates the vegetation structure for each PFT at an annual time step according to the carbon budget of that PFT. Whether a PFT can potentially exist at a specific location depends on the climatic constraints; whether it can actually survive depends on its competition with other PFTs for common resources. The transient change in vegetation structure, including the leaf area index (LAI) and living biomass, is a reflection of this competition. Common resources account for water and light. The effect of nutrient stress is not considered.

PFTs in different vegetation layers have different advantages in accessing light and water. The upper layer has easier access to sunlight, and shades the lower layer to a certain degree depending on its fractional coverage. Plants in the upper vegetation layer have deeper root structures than those in the lower layer. As a result, the lower-layer PFTs have the advantage of reaching water first in the process of infiltration, while the upper-layer PFTs have access to the water storage in the deeper soil. In terms of life form, herbaceous plants in the lower layer do not need to divert resources into the production and maintenance of the woody supporting structures as woody plants in the upper layer do.

Competition between PFTs within a same vegetation layer has to do with the difference in their ecological strategies. For example, under severe water stress, drought-deciduous plants shed their leaves to shut off the water consumption through transpiration. Needle leaf plants conserve water better than broad-leaf plants. C_4 plants use water more efficiently than C_3 plants. These factors cause the differences in carbon balance between different PFTs in the same layer.

For more details about IBIS, please refer to Foley *et al.* (1996).

2.3.2 Sub-grid Variability: Interception Scheme

In the past few decades, as land surface parameterization schemes developed towards greater physical realism, it has been widely recognized that the spatial variability in precipitation (e.g., vegetation type and soil texture) at the sub-grid scale significantly

affects the simulation of surface hydrological processes at the grid scale (Shuttleworth, 1988b; Entekhabi and Eagleson, 1989; Pitman *et al.*, 1990; Lloyd, 1990; Ghan *et al.*, 1997). The impact of sub-grid variability of rainfall is most pronounced in the tropics, where the vegetation canopy is dense and most of the precipitation takes place as convective rainfall. A typical convective rain cell has a spatial coverage at the order of $10^2 km^2$, while a typical grid cell in a climate model often covers an area of $10^3 - 10^6 km^2$. Modeled rainfall is actually the integrated rainfall over the entire grid element. Without considering the effect of this mismatch in scales, climate models will predict drizzle uniformly falling over the entire grid area instead of intense rainfall concentrated in a small portion of the grid cell. As a result, more rainfall will be intercepted by the vegetation canopy and subsequently re-evaporated (Lean and Warrilow, 1989; Dolman and Gregory, 1992; Eltahir and Bras, 1993a). Although IBIS includes detailed and sophisticated representation of canopy hydrological processes, it does not consider the effect of sub-grid variability in rainfall distribution. Here, we modify the representation of canopy hydrological processes in IBIS by including an interception scheme which accounts for the impact of rainfall sub-grid variability.

One commonly used approach in interception schemes is the "statistical approach", which combines the point description of canopy hydrology and the statistical treatment of rainfall sub-grid variability. This approach assumes that precipitation only covers a fraction μ of the grid cell, and assumes an idealized function for the precipitation probability distribution within the rain-covered region (Carson, 1986; Shuttleworth, 1988b; Eltahir and Bras, 1993a). The grid-averaged interception loss and throughfall are then computed based on these assumptions. The impact of sub-grid variability is therefore implicitly represented by modifying the grid-average values for variables of local relevance. Another commonly used approach is the "mosaic approach" (Koster and Suarez, 1992), which explicitly breaks each grid cell into certain number of smaller cells, and is frequently used when the heterogeneity of land surface properties (e.g., vegetation and soil) is also considered. In our model, for computational efficiency, we choose the statistical approach in representing the sub-grid variability of rainfall.

Our interception scheme is based on the Shuttleworth scheme (1988b). Precipitation is assumed to fall over a fraction μ of the grid cell. Within the rain-covered region, the probability density function for rainfall distribution takes the form:

$$f(P) = \frac{\mu}{P_0} exp(-\frac{\mu P}{P_0}), \tag{2.16}$$

where P_0 is the grid-averaged precipitation rate. Assuming that the canopy storage at the beginning of a time step is C, and that the canopy capacity is S, which is uniform over the entire grid cell. Within the time step, the maximum rate of infiltration into the canopy is $I_{max} = \frac{S-C}{\Delta t}$. Therefore, the canopy throughfall, which is defined here as the part of the canopy drainage contributed directly by rainfall (another component of the canopy drainage is the dripping from the canopy storage), can be expressed as:

$$T = P - I_{max} \quad (P > I_{max}); \qquad T = 0. \quad (P \leq I_{max}).$$

On average, the canopy throughfall within the precipitation-covered region due to the newly produced rainfall is:

$$R_\mu = \int_{I_{max}}^{\infty} (P - I_{max}) \frac{\mu}{P_0} exp(-\frac{\mu P}{P_0}) dP = \frac{\mu}{P_0} exp(-\frac{\mu I_{max}}{P_0}).$$

Consequently, the canopy throughfall averaged over the entire grid cell is:

$$R = P_0 exp(-\frac{\mu I_{max}}{P_0}). \tag{2.17}$$

Hence the grid-average rate of infiltration into the canopy will be:

$$I = P_0(1 - exp(-\frac{\mu I_{max}}{P_0})) \tag{2.18}$$

The parameter μ, as well as its spatial and temporal variation, may significantly affect the model's climatology. In fact, previous studies (Pitman *et al.*, 1990; Johnson *et al.*, 1991; Thomas and Henderson-Sellers, 1991) already showed that a model's climate is very sensitive to the choice of μ. Here the Eltahir and Bras (1993b) method

is used to estimate the fractional rainfall coverage:

$$\mu = \frac{P_{model}}{P_{obs}}, \tag{2.19}$$

where P_{model} is the modeled rainfall intensity, and P_{obs} is the climatology of observed rainfall intensity at the corresponding location and during the corresponding season. We estimate P_{obs} based on published data in Lebel *et al.* (1997) and Le Barbe and Lebel (1997). This method of estimating μ guarantees that the precipitation intensity in the model is always close to observations, and allows μ to change with time and location, therefore brings greater physical realism into the model.

2.3.3 Minor Modifications

In our model, several minor changes have been made to IBIS.

In IBIS, when there is vegetation patchiness, radiation and precipitation between and within patches are treated separately. For the fraction of bare soil, a very important factor is the soil albedo, which depends on both the soil texture and soil saturation. The current version of IBIS considers three different soil textures: sand, silt and clay. Different soil types have different percentage of these three textures. For example, silty loam has 20% of sand, 60% of silt, and 20% of clay. The albedo for saturated soil α_s follows Dickinson *et al.* (1993), i.e., 0.12 (sand), 0.085 (silt), and 0.05 (clay) for visible and UV solar radiation and is double those magnitudes for near-infrared solar radiation. Albedo for unsaturated soil α depends on both α_s and the soil saturation w:

$$\alpha = (1.0 + 1.0 * (1 - w)) * \alpha_s$$

However, according to the above formulation, the maximum possible albedo for a sandy desert is about 0.33, while albedo over the desert is observed to be around 0.35-0.45 (Ohmura *et al.*, 1998). For a better comparison with observed albedo over bare soil, the following formulation has been adapted in our model:

$$\alpha = (1.0 + 2.0 * (1 - w)) * \alpha_s$$

In the model, evaporation from the soil can only take place in the top soil layer. No water can directly evaporate from the lower soil layers. During the drying process of the top soil layer, moisture in the lower layers flows upward towards the top layer through diffusion and supplies the moisture for evaporation. This process is quite efficient and the whole soil can be dried out within a finite time if no precipitation takes place. This causes some over-drying in regions with little vegetation. In reality, especially over arid regions with sparse vegetation, after some time of drying, a dry crust forms at the surface, which limits the direct soil evaporation. Such soil crusting is an important mechanism for arid ecosystems (Walter, 1985). Crusted soil has a very low hydraulic conductivity compared with the normal soil. It not only limits the soil evaporation, but also slows down the infiltration at the beginning of wetting. However, the thickness of the dry crust is much smaller than the depth of the top soil layer in the model, which makes it difficult to simulate the exact physical processes associated with soil crusting. Instead, here we represent the overall effect in the model by setting a threshold for the soil saturation in the top layer, below which moisture diffusion from the second layer to the top layer ceases. This constraint slows down the top layer evaporation, which resembles the effect of soil crusting on evaporation. In the context of a climate model which does not simulate the horizontal movement of the surface water (in the form of surface runoff) within one grid cell, the effect of soil crusting on infiltration is significant only within a short duration at the beginning of the wet season. Therefore, the overall effect on infiltration is relatively small and can be neglected.

2.4 Summary

To summarize the model development, Figure 2-4 shows all the components of the zonally symmetric, synchronously coupled biosphere-atmosphere model (ZonalBAM).

Figure 2-4: Components of the coupled biosphere-atmosphere model.

Chapter 3

Model Validation

In the model validation, the biospheric model and the atmospheric model are first separately tested against observations: the modified IBIS is run in off-line mode to simulate the potential vegetation, with the atmospheric forcings fixed at today's condition; the model's performance in simulating the atmospheric climate is tested, with the vegetation fixed at today's condition and IBIS functioning as a land surface scheme. The full model is then used in a synchronous mode to simulate the coupled biosphere-atmosphere system.

3.1 Modeling the Biospheric Climate

Foley *et al.* (1996) used the stand-alone IBIS driven with the climatological atmospheric forcings to reproduce the global vegetation distribution. A similar study is performed here, but with the newly modified representation of canopy hydrology and with different atmospheric forcing. We use the daily climatology of the atmospheric forcings from the NCEP/NCAR re-analysis data, which is derived based on the data for the period 1958-1997, and averaged between $15°W$ and $15°E$. The temperature and specific humidity are interpolated into a finer temporal resolution by assuming a sinusoidal diurnal cycle. Following Foley *et al.* (1996), the daily precipitation is assumed to occur within a certain time period, and the length of precipitation events as well as the starting time is determined by sampling randomly from suitable statis-

tical distributions. In contrast to the simulations involving the atmospheric model, the incoming solar radiation and the incoming long-wave radiation in the off-line IBIS are calculated based on empirical formulas.

With a spatial resolution of 2°, the model domain spans from $5°N$ to $25°N$. The time step for the land surface processes is 30 minutes. The simulation starts with minimal amount of vegetation cover everywhere. At the beginning, each of the PFTs have an equal opportunity to survive – all of them exist at every grid point, with the same LAI of 0.1 in order for the physiological processes to get started. The stem and root biomass are initialized to be zero. The vegetation distribution at a later time depends on the competition between different PFTs for light and water under the corresponding atmospheric conditions. In this simulation, the soil texture is fixed with time, but varies from silty loam (20% sand, 60% silt, 20% clay) near the coast to loamy sand (80% sand, 10% silt, 10% clay) in the north, according to the Zobler (1986) data.

After 80 years of simulation, the model evolves to near equilibrium. The competition between grass and trees comes to an end, and the net primary productivity remains stable (Figure 3-1a). The only process that has not reached equilibrium state is the slow accumulation of the woody biomass (Figure 3-1b), which has a time scale in the order of centuries. Details of this "close-to-equilibrium" vegetation distribution are presented in Figure 3-2. Trees exist between the coast and $10°N$, while grass occupies the region between $10°N$ and $16°N$. North of that, the land surface is desertic. This vegetation distribution is in reasonable agreement with observations over West Africa. The simulated total NPP at the equilibrium state is also in a reasonable range. In Figure 3-3, the solid line shows the simulated NPP, while the two asterisks mark the mean of point measurements (Murphy, 1975) from humid and arid regions in West Africa. The error bars span the range $\mu \pm \sigma$, where μ is the mean and σ the standard deviation. The statistics for each region are based on five site measurements. The model simulation compares well with the site measurements.

Over locations that are eventually occupied by trees, competition between trees and grass takes place before the tree establishment. As an example, Figure 3-4

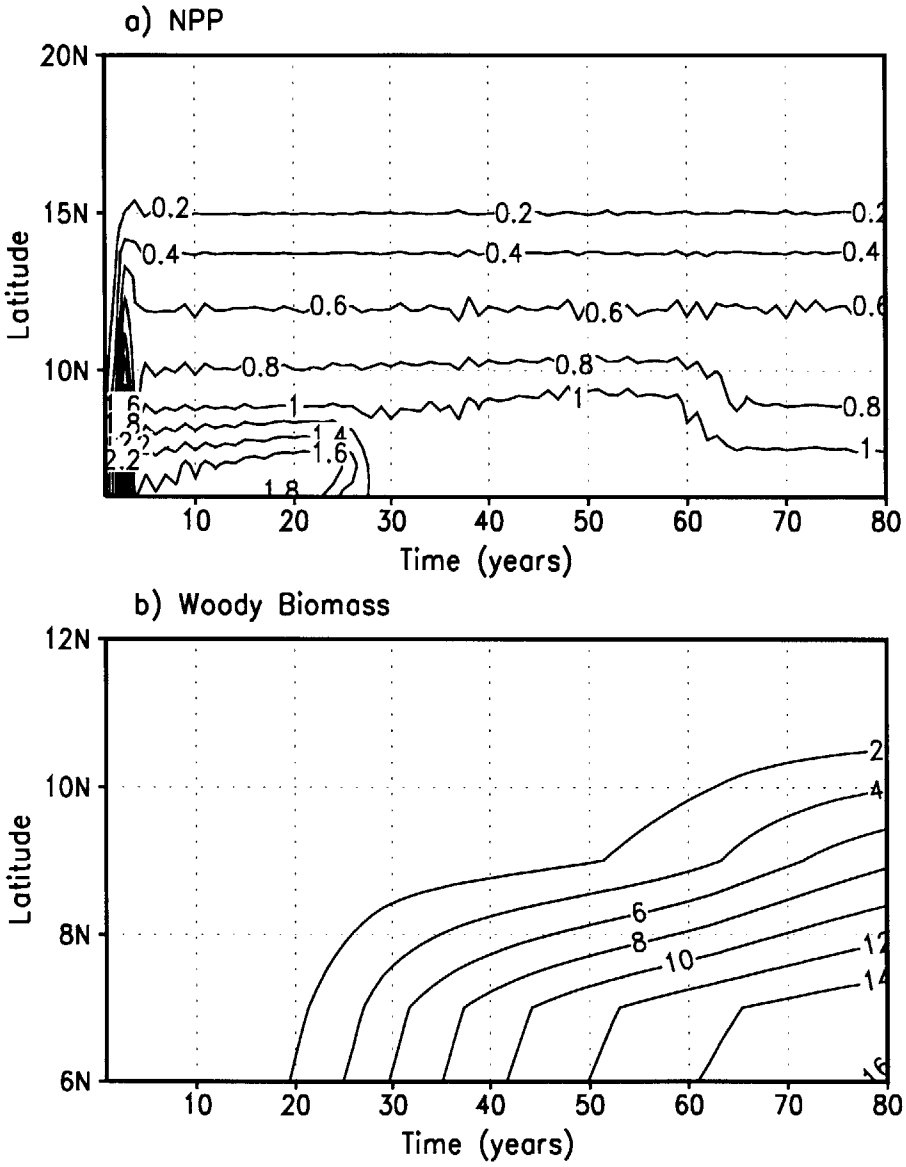

Figure 3-1: Vegetation growth process: a) Total net primary productivity ($kgC/m^2/year$); b) Wood biomass (kgC/m^2).

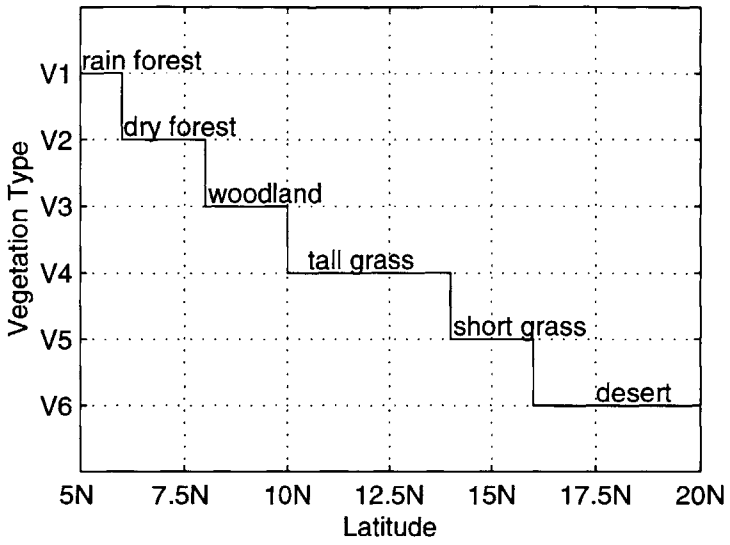

Figure 3-2: Vegetation distribution after the biosphere reaches equilibrium. V1: forest dominated by tropical broad-leaf evergreen trees; V2: forest dominated by tropical broad-leaf drought-deciduous trees; V3: woodland dominated by tropical broad-leaf drought-deciduous trees, but not as dense as V2; V4: dense tall C4 grass; V5: short C4 grass; V6: desert condition.

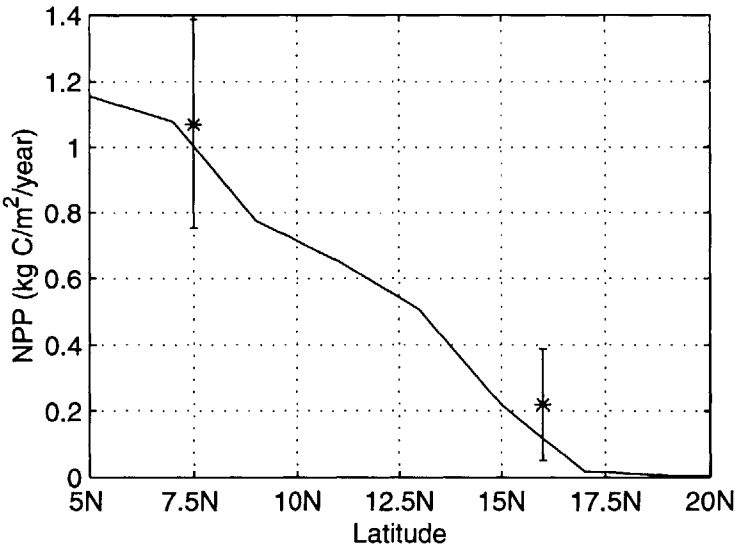

Figure 3-3: The total net primary productivity (in $kgC/m^2/year$) at the biospheric equilibrium.

presents the NPP of woody plants (solid line) and herbaceous plants (dashed line) at $7°N$. The early stage of vegetation development is dominated by dense grass, which has a very high NPP due to the large amount of precipitation and high LAI. Trees gradually take over and grass dies out within three decades. After that the tree NPP stays stable.

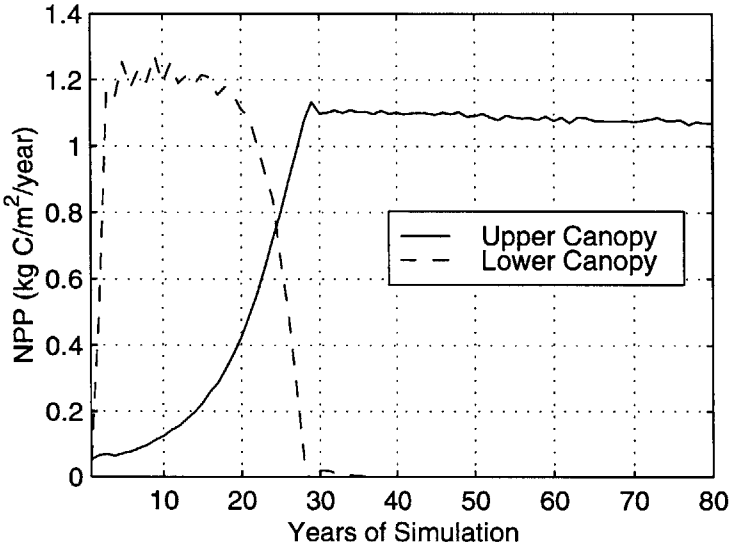

Figure 3-4: The net primary productivity (in $kgC/m^2/year$) of the upper and lower canopy at 7°N.

In general, the model captures the main features of the vegetation distribution in West Africa. As Foley *et al.* (1996) already found, due to the lack of disturbance mechanisms and climate variability, the model does not do well in simulating the savannah-type vegetation (i.e., a mixture between trees and grass). For example, at equilibrium (Figure 3-2), tall grass exists right next to the dense woodland, without a transitional vegetation type (e.g., savannah) located between the two. This issue will be further discussed in Section 3.3.

3.2 Modeling the Atmospheric Climate

3.2.1 Model Details

With the ecosystem dynamics turned off and the vegetation distribution fixed at a state close to today's condition, the biosphere-atmosphere model is used to simulate the current atmospheric climate over West Africa. Under this condition, IBIS functions as a sophisticated land surface model with static vegetation. Here static vegetation only implies that the vegetation structure does not change from one year to the next. The diurnal cycle and seasonal cycle for the biophysical, physiological, and phenological processes are still simulated.

According to observations (e.g., the USGS Global Land Cover Characterization data; Foley *et al.*, 1996; Gornitz and NASA, 1985) over West Africa, there is evergreen rain forest in the coastal region, and drought-deciduous forest and woodland extend from the coast to about $10°N$, from where the vegetation gradually changes from savannah northward to short grass. This vegetation distribution (Figure 3-5) is used as the model's boundary condition over land. Similar to the simulation in section 3.1,

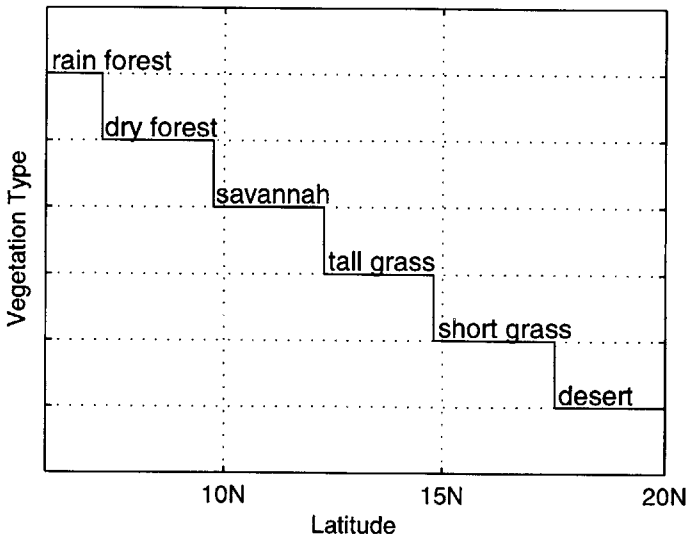

Figure 3-5: Vegetation distribution close to what has been observed.

the soil texture ranges from silty loam (20% sand, 60% silt, and 20% clay) near the coast to loamy sand (80% sand, 10% silt, and 10% clay) in the north. South of the coast (set at $6°N$), sea surface temperature is fixed at the zonal average ($10°E-10°W$) of its climatology (Reynolds and Smith, 1995). For the simulation in this section as well as in section 3.3, a vertical resolution corresponding to about 40 mb is used in the atmospheric model. The biospheric model and the atmospheric model use the same horizontal resolution, which corresponds to $\sim 2.5°$ within the tropics. The time step is 20 minutes.

A zonally symmetric model cannot correctly simulate the interaction between mid-latitudes and the tropics. To reduce the associated bias, surface conditions (including the albedo, temperature, sensible and latent heat fluxes) outside the tropics are fixed at their climatology from the NCEP re-analysis data, averaged between $15°W$ and $15°E$. Here the tropics are defined as $27°N$-$27°S$.

3.2.2 Results

Three years of integration are needed before the atmospheric model reaches equilibrium, after which no significant trend is found in the atmospheric simulation. Since the SST climatology is used as the driving forcing, the simulated climate features negligible interannual variability after three years from the beginning of the simulation. In the following the results from the fourth year of the simulation are presented.

The zonally symmetric model successfully reproduces the zonal mean of precipitation and surface temperature in West Africa. The seasonal cycle of the simulated surface temperature is plotted in Figure 3-6a, which compares well with the NCEP re-analysis data in Figure 3-6b. An identifiable difference is that the warm summer over the Sahara desert in the model lasts until October, which is more than one month longer than that in the NCEP re-analysis data. Over West Africa, credible and inclusive rainfall measurements are limited. A significant discrepancy between different rainfall data sets is frequently observed, which highlights the difficulty in comparing rainfall simulations with observations. Here the model rainfall seasonal cycle (Figure 3-7a) is compared with both the NCEP re-analysis data (Figure 3-7b)

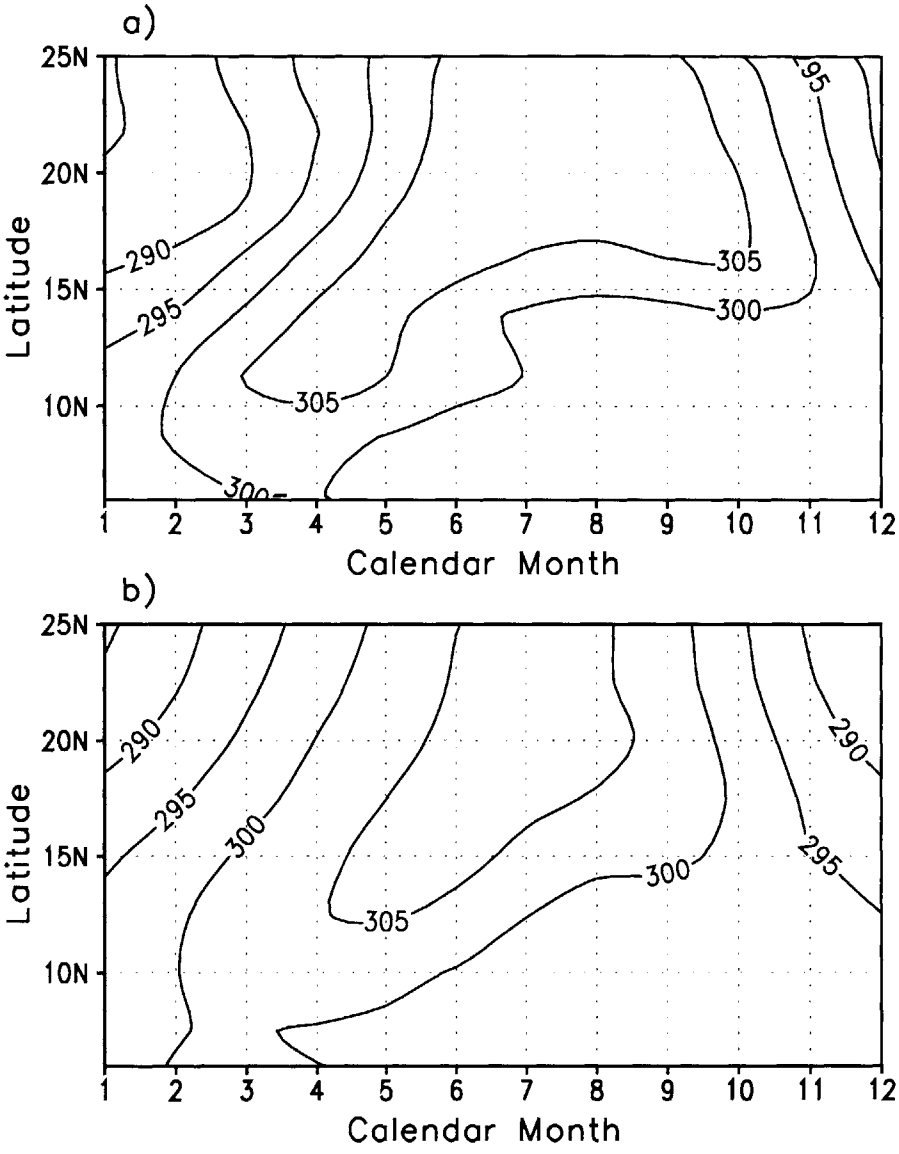

Figure 3-6: The seasonal cycle of the surface temperature (K): a) model simulation; b) climatology of the NCEP re-analysis data.

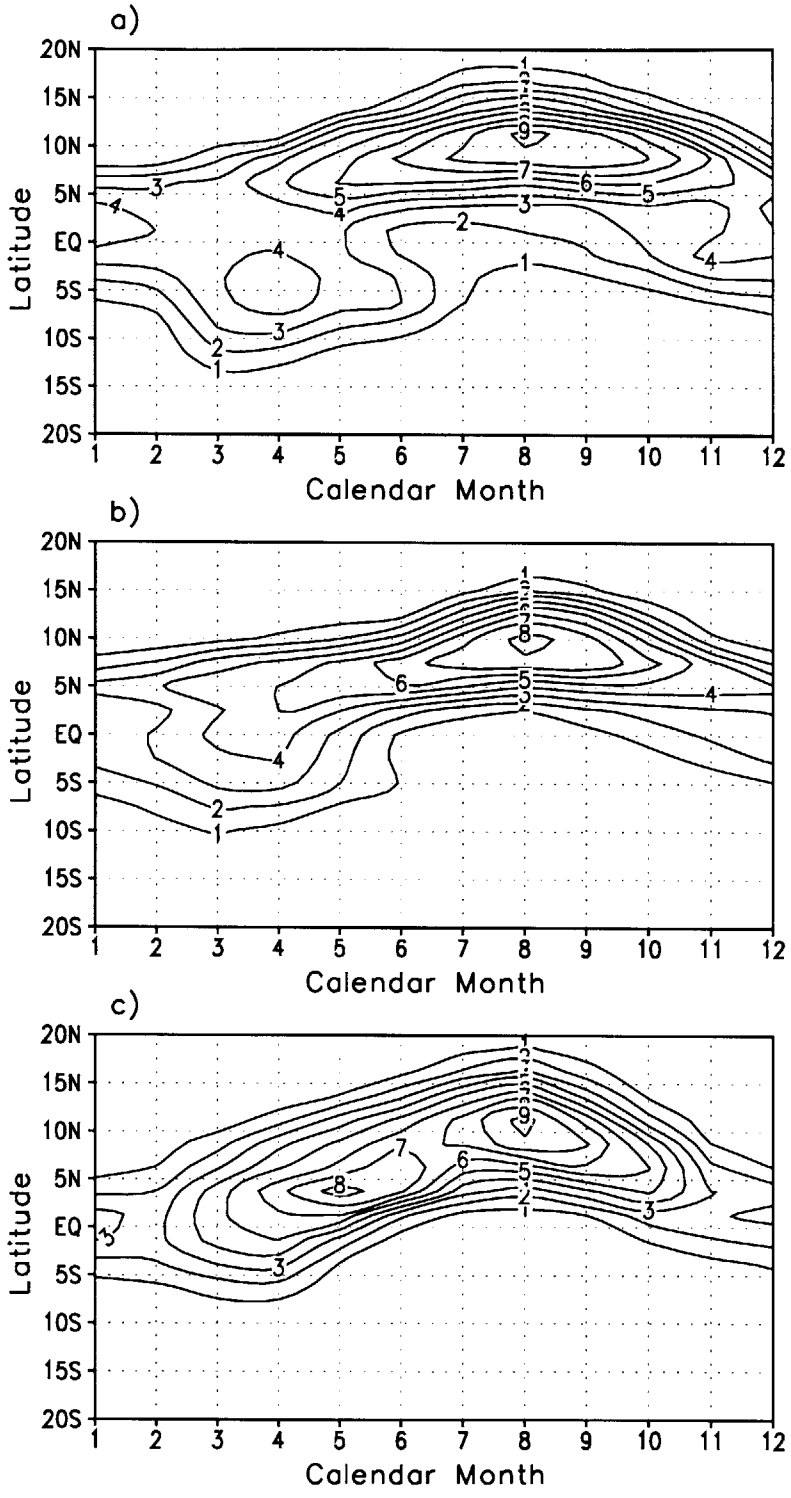

Figure 3-7: The rainfall seasonal cycle (mm/day): a) model simulation; b) climatology of the NCEP re-analysis data (1958-1997); and c) climatology of the GPCP data (1987-1997).

and the GPCP data (Figure 3-7c). The difference between the modeled rainfall seasonal cycle and either of the rainfall data sets is comparable to the difference between the GPCP data and the NCEP re-analysis data. This is especially true over land, where biosphere-atmosphere interactions take place. The comparison for the annual rainfall over land is presented in Figure 3-8, which shows a fair agreement between the model simulation and observations.

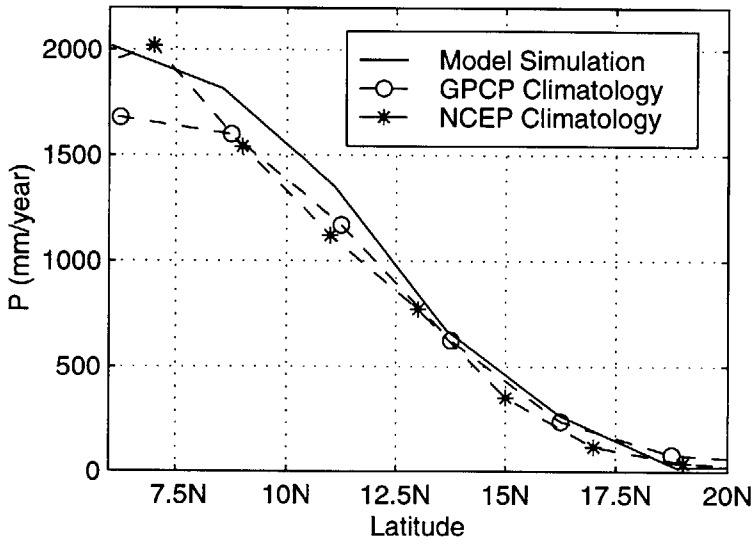

Figure 3-8: Comparison of the annual rainfall (in *mm/year*) between the model simulation (solid line), the GPCP climatology ($-\circ-$), and the NCEP climatology ($-*-$).

The model also reproduces the atmospheric circulation with reasonable accuracy. Taking the peak monsoon season (August) as an example, Figure 3-9 compares the simulated meridional wind field with the NCEP re-analysis data, and Figure 3-10 presents the comparison for the vertical velocity. The model captures the overall pattern of the meridional circulation. During the rainy season, wind blows from the ocean to the land at low levels, with the returning wind from the land to the ocean at high levels. Correspondingly, the rising branch of the monsoon cell is mainly

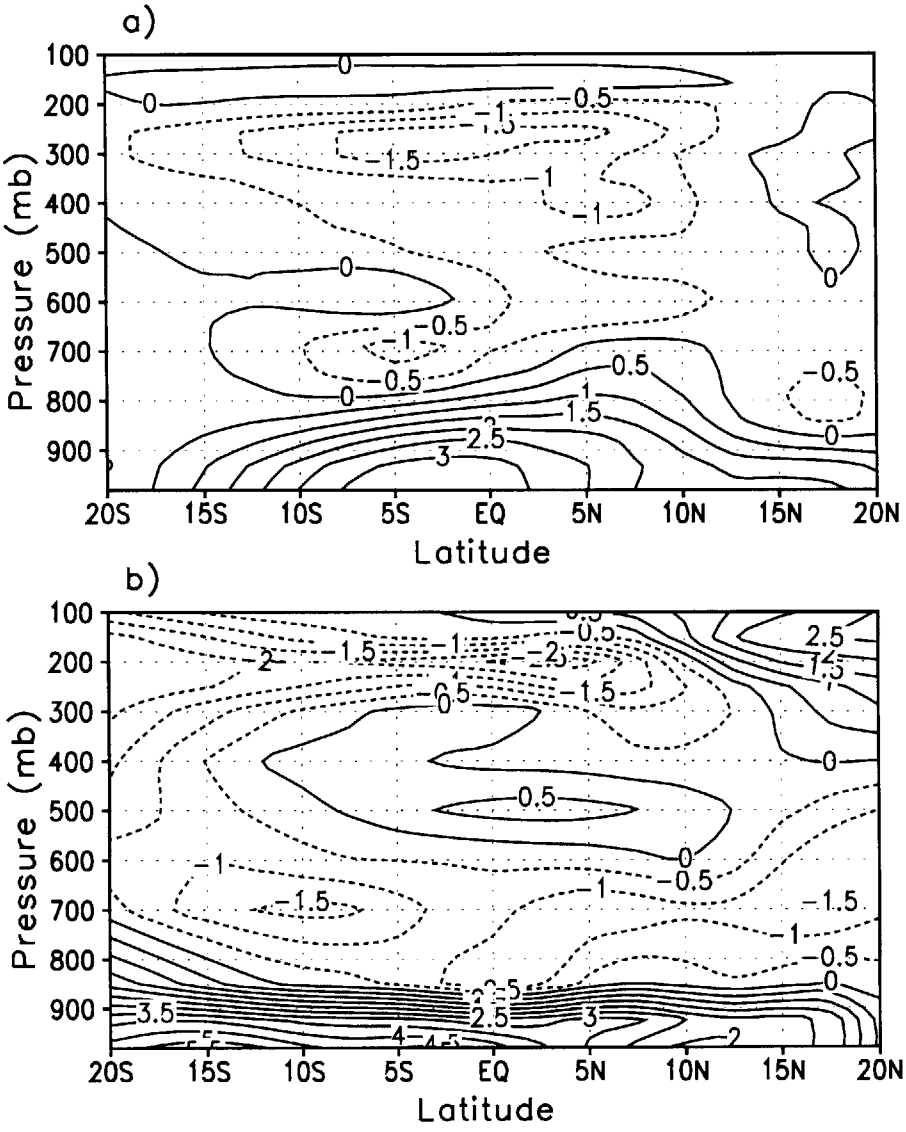

Figure 3-9: Comparison of the meridional wind in August between (a) the model simulation and (b) the NCEP re-analysis data. Unit: m/s.

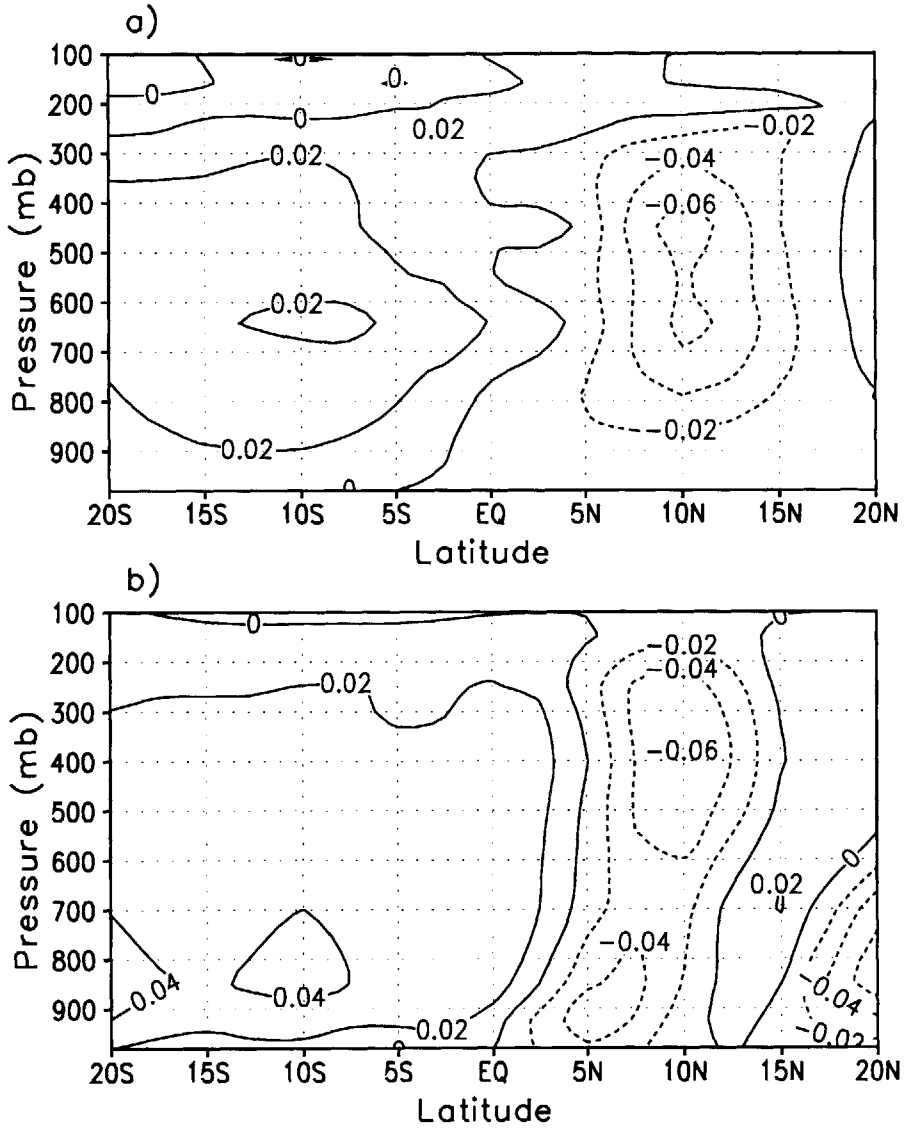

Figure 3-10: Comparison of the vertical velocity in August between (a) the model simulation and (b) the NCEP re-analysis data. Unit: Pa/s.

located over land, and the descending branch over the ocean. Compared to the NCEP re-analysis data, the model underestimates the magnitude and overestimates the vertical span of the northward wind. These two factors compensate for each other, which brings the total northward mass transport at low levels across the coast closer to the NCEP re-analysis data. A similar comparison for the zonal wind is shown in Figure 3-11. In the zonal wind field, an identifiable difference exists around the Sahara region at the level of 100mb-400 mb, where a westerly jet results from a local cooling (see Figure 3-12a) through the thermal wind mechanism. For example, at the 400-mb level over 20°N, temperature decreases northward at a rate of 0.7 $°C/km$ or so (at 20°N, this can cause an upward increase of westerly wind by about 7 $m/s/km$). Such a cooling is not observed in the NCEP re-analysis data (Figure 3-12b). This unrealistic cooling effect may have to do with the lack of easterly waves and zonal asymmetry in the model. According to Rodwell and Hoskins (1996), the diabatic heating associated with the Asian monsoon can induce a Rossby wave pattern to the west and causes descent over the eastern Sahara and Mediterranean. The adiabatic warming associated with this induced descent would have offset the unrealistic cooling in Figure 3-12a, eliminating the unrealistic westerly jet at high levels over the Sahara-Sahel region in Figure 3-11a.

Comparison of radiation fluxes with observations is complicated by both the limitation of the current understanding on the atmospheric radiative transfer (Cess *et al*, 1995; Pilewskie and Valero, 1995; Ramanathan *et al*, 1995; Li *et al.*, 1995; Arking, 1996; Stephens, 1996) and the large uncertainty in radiation measurements (Bishop *et al.*, 1997). Here the simulated radiation fluxes are compared with both the NCEP re-analysis data and the International Satellite Cloud Climatology Project (ISCCP) data (Gupta *et al.*, 1997), as shown in Figures 3-13 and 3-14. Note that the NCEP re-analysis data is a product based on both observations and model simulations. In Figure 3-13, the spatial and seasonal pattern of the incoming solar radiation in the model agrees well with both the NCEP re-analysis and ISCCP data. In terms of the magnitude, the model simulation is closer to the NCEP re-analysis data during the season of high radiation, and closer to the ISCCP data for the rest of the year. Note

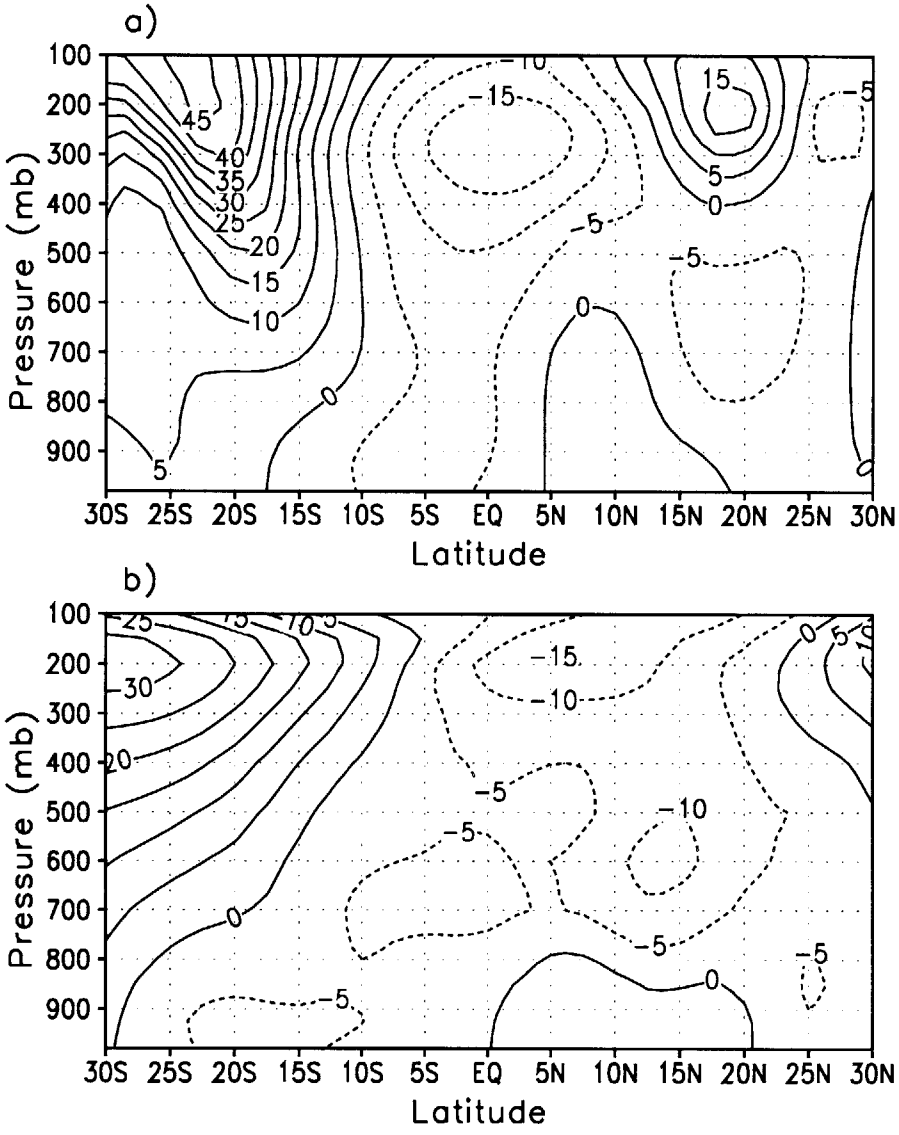

Figure 3-11: Comparison of the zonal wind in August between (a) the model simulation and (b) the NCEP re-analysis data. Unit: m/s.

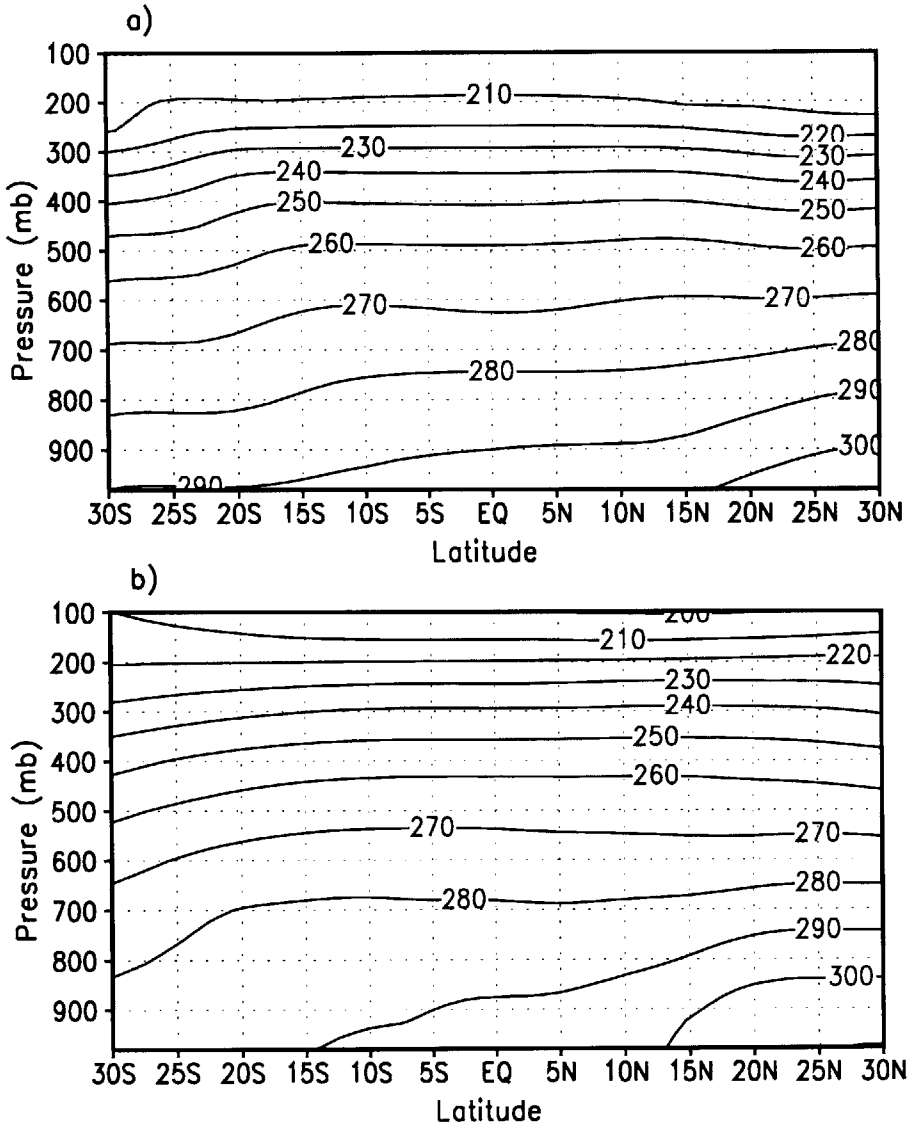

Figure 3-12: Comparison of the air temperature in August between (a) the model simulation and (b) the NCEP re-analysis data. Unit: K.

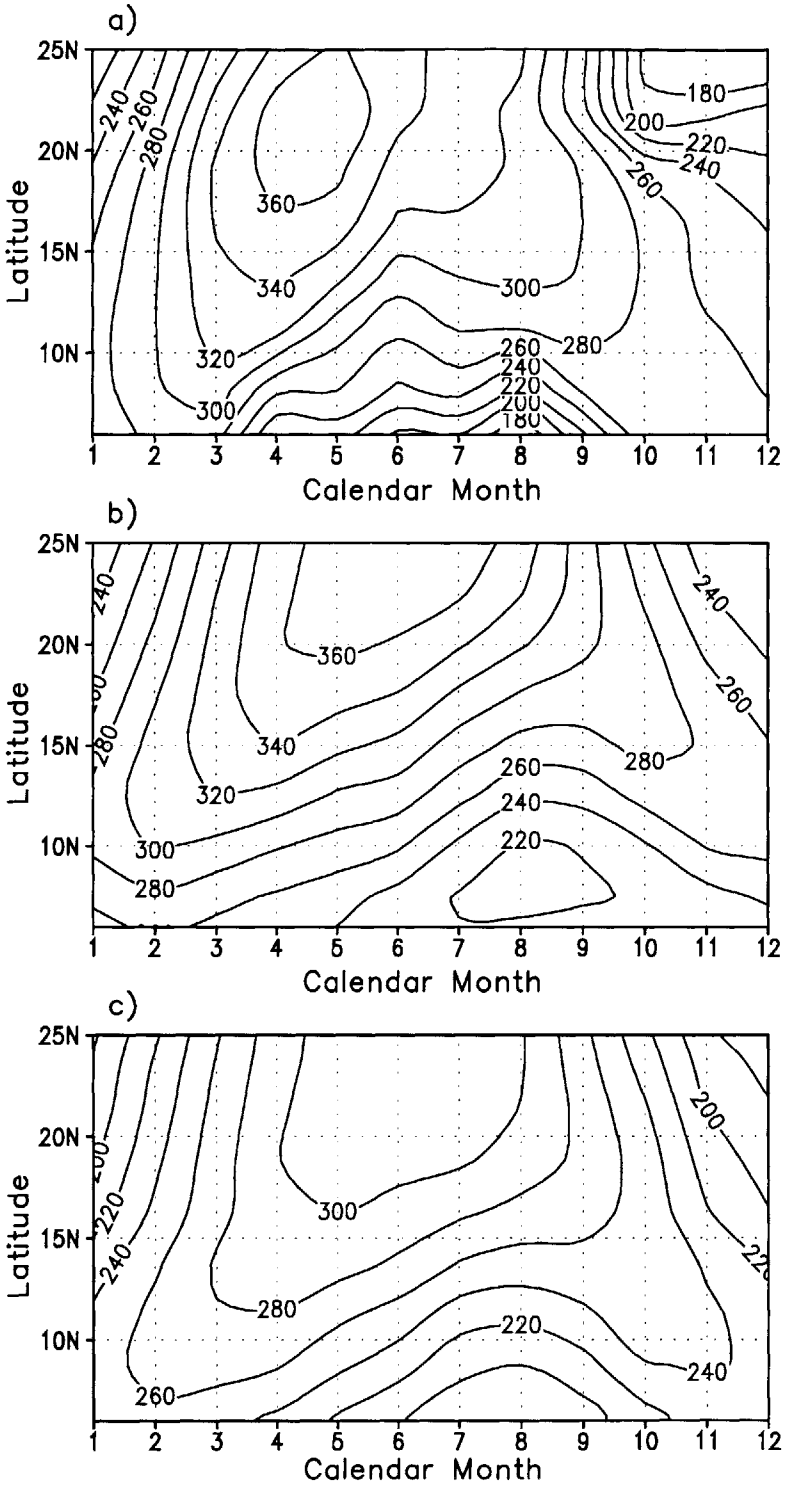

Figure 3-13: Seasonal cycle of the incoming solar radiation at surface, in W/m^2: a) model simulation; b) NCEP re-analysis data; c) ISCCP data.

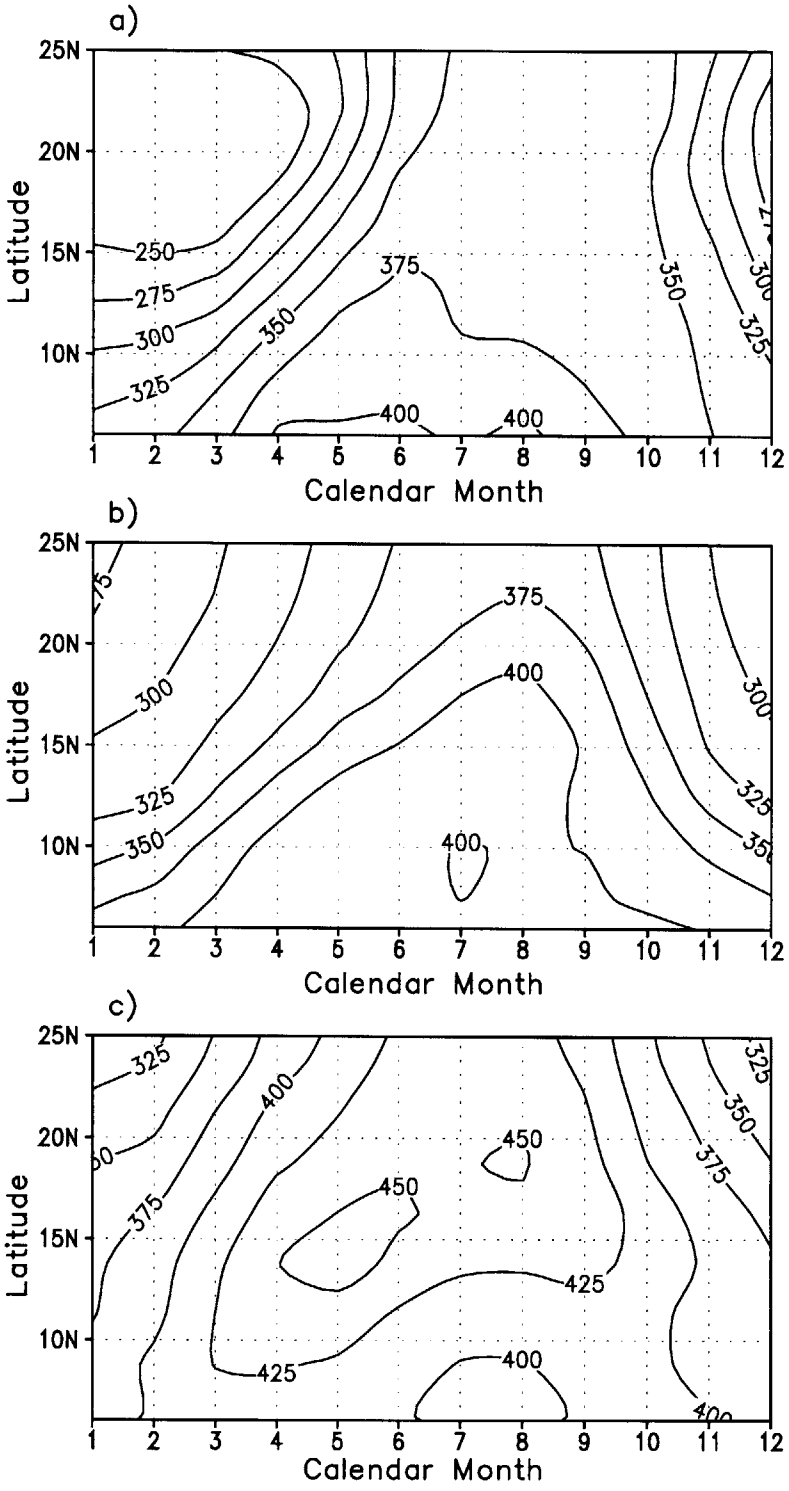

Figure 3-14: Seasonal cycle of the incoming long-wave radiation at surface, in W/m^2: a) model simulation; b) NCEP re-analysis data; c) ISCCP data.

that the season of high radiation varies with latitude. A general trend is observed that the solar radiation of both the model and the NCEP re-analysis data is higher than that of the ISCCP data, which may have to do with the underestimation of the atmospheric solar absorption by the current generation of radiation schemes (e.g., Cess *et al*, 1995; Li *et al.*, 1995; Arking, 1996). As shown in Figure 3-14, the spatial distribution of the incoming long-wave radiation in the model agrees well with the NCEP re-analysis data, while the ISCCP data shows a significantly different spatial pattern. Compared with the NCEP re-analysis data, the model tends to underestimate the long-wave radiation. This under-estimation becomes very significant when compared with the ISCCP data. It is worth noting that the difference between the model and NCEP re-analysis data is smaller than the difference between the NCEP re-analysis and ISCCP data.

The underestimation of the long-wave radiation may result from the underestimation of the atmospheric water vapor content in the model. Figure 3-15a presents the simulated seasonal cycle of specific humidity near the surface, compared with the NCEP re-analysis data (Figure 3-15b). Although the overall patterns agree well, the model underestimates the specific humidity by 1-4 g/kg. Although to a less degree, this underestimation also exists away from the land surface. For example, Figure 3-16 presents the comparison of the specific humidity distribution during the peak monsoon season in August, which shows that the specific humidity over land in the model is in general lower than the NCEP re-analysis data. The moisture maximum in the model occurs over the ocean near the coast, while in the NCEP re-analysis data, it is located inland over the savannah region. In the model, the humidity level of the atmosphere decreases from the forest region northward, while the NCEP re-analysis data suggests that the specific humidity over the arid savannah/grassland region is at the same level as the forest region.

The surface net radiation, which determines the total energy exchange between the biosphere and the atmosphere, is an important variable for the biosphere-atmosphere interactions. Also important is the land surface albedo which directly affects the net radiation. As shown in Figure 3-17, the model surface albedo agrees well with the

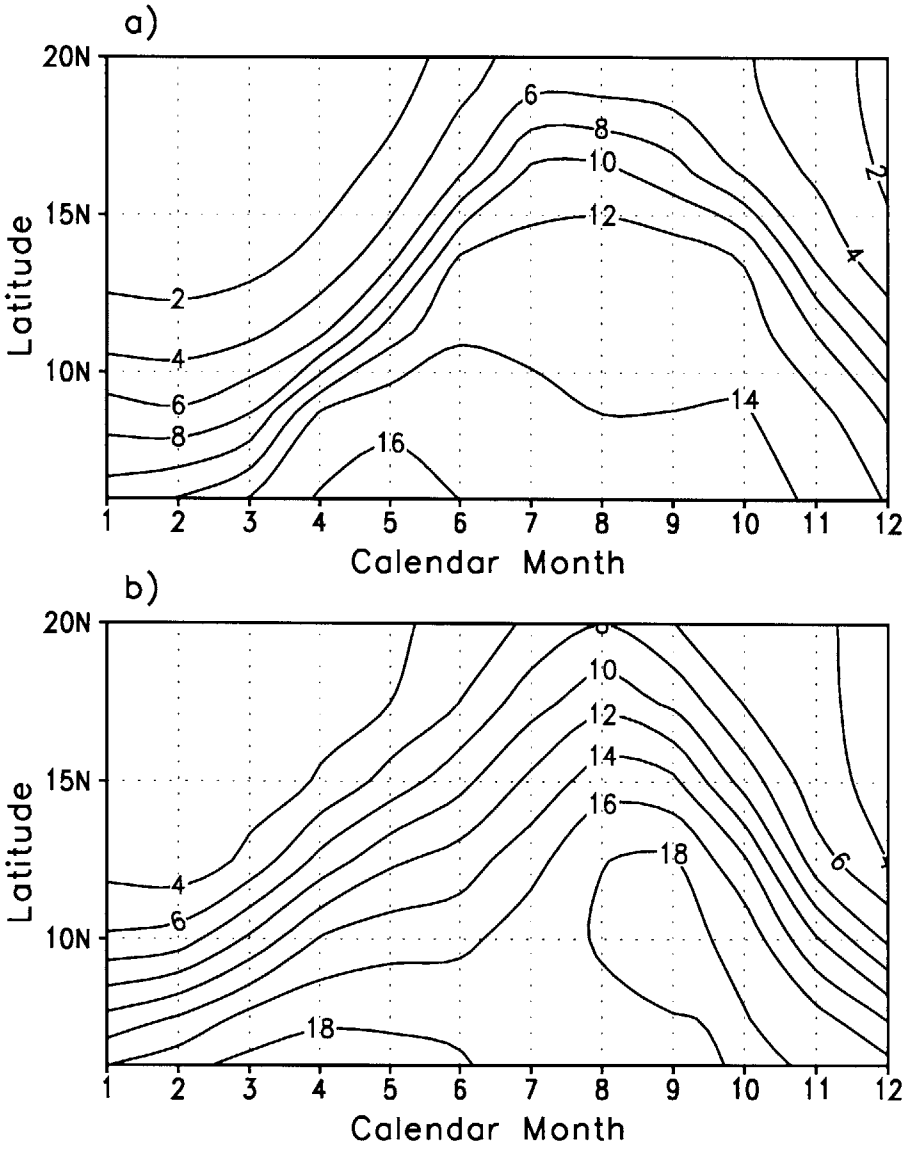

Figure 3-15: Seasonal cycle of the specific humidity near surface, in g/kg: a) model simulation; b) NCEP re-analysis data.

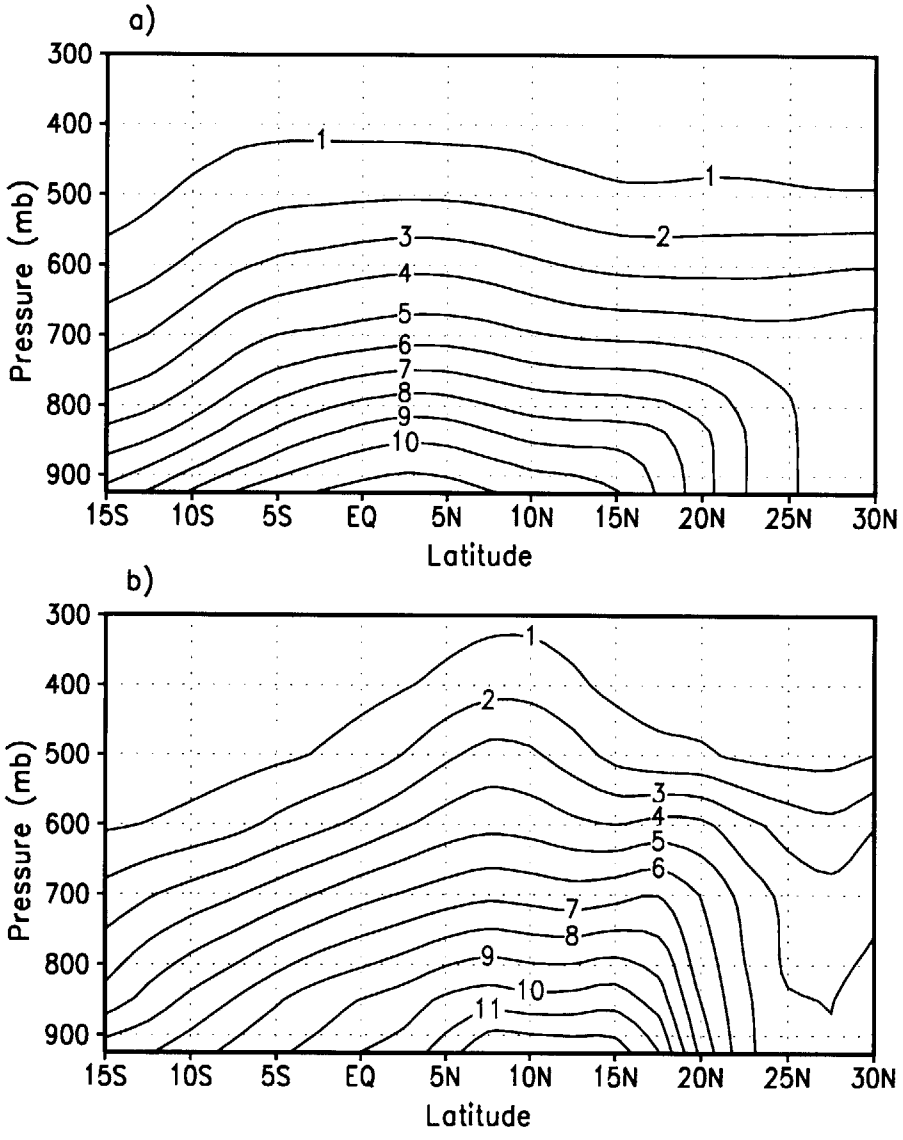

Figure 3-16: Specific humidity during August, in g/kg: a) model simulation; b) NCEP re-analysis data.

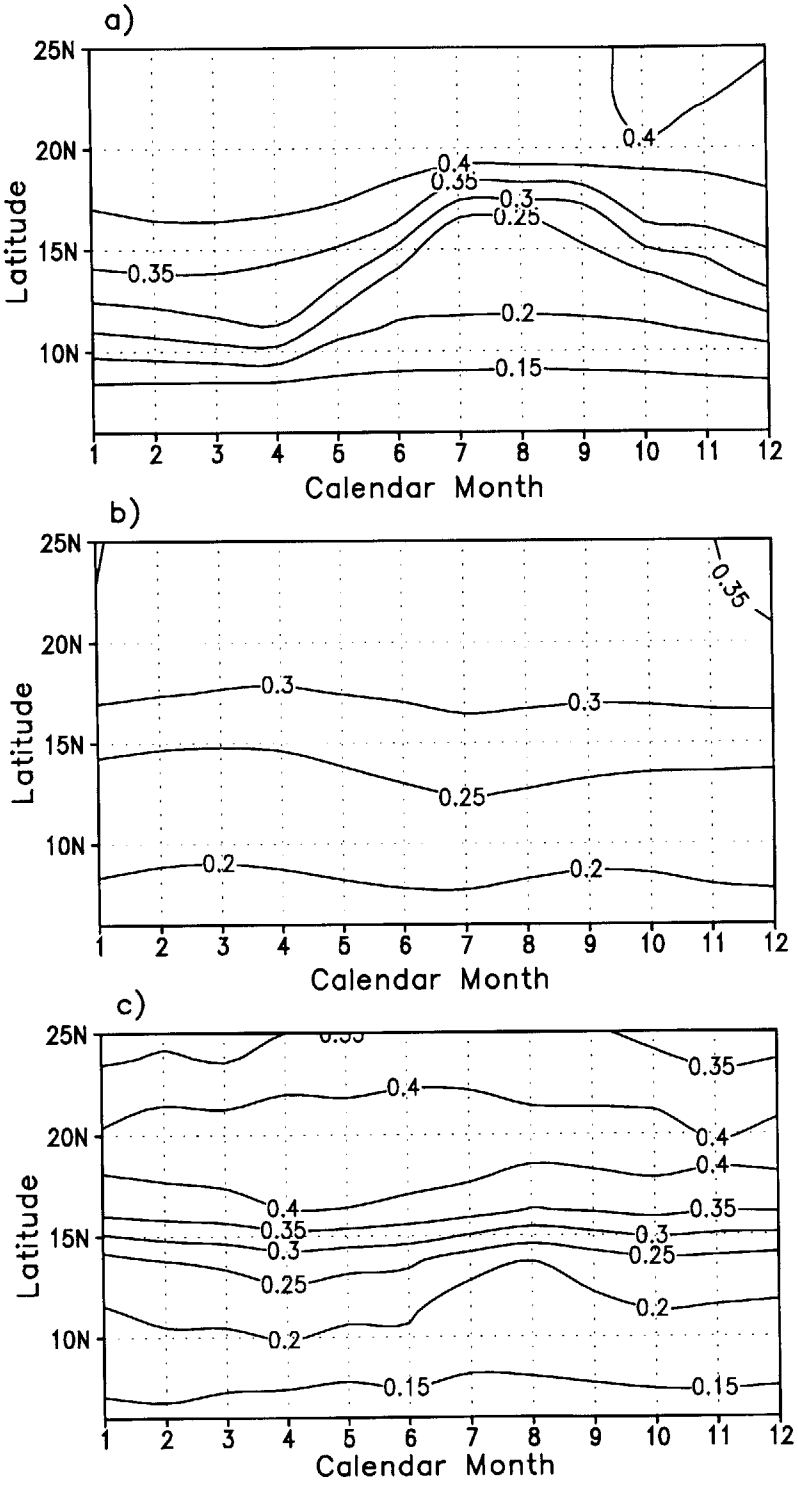

Figure 3-17: Seasonal cycle of the land surface albedo: a) model simulation; b) NCEP re-analysis data; c) ISCCP data.

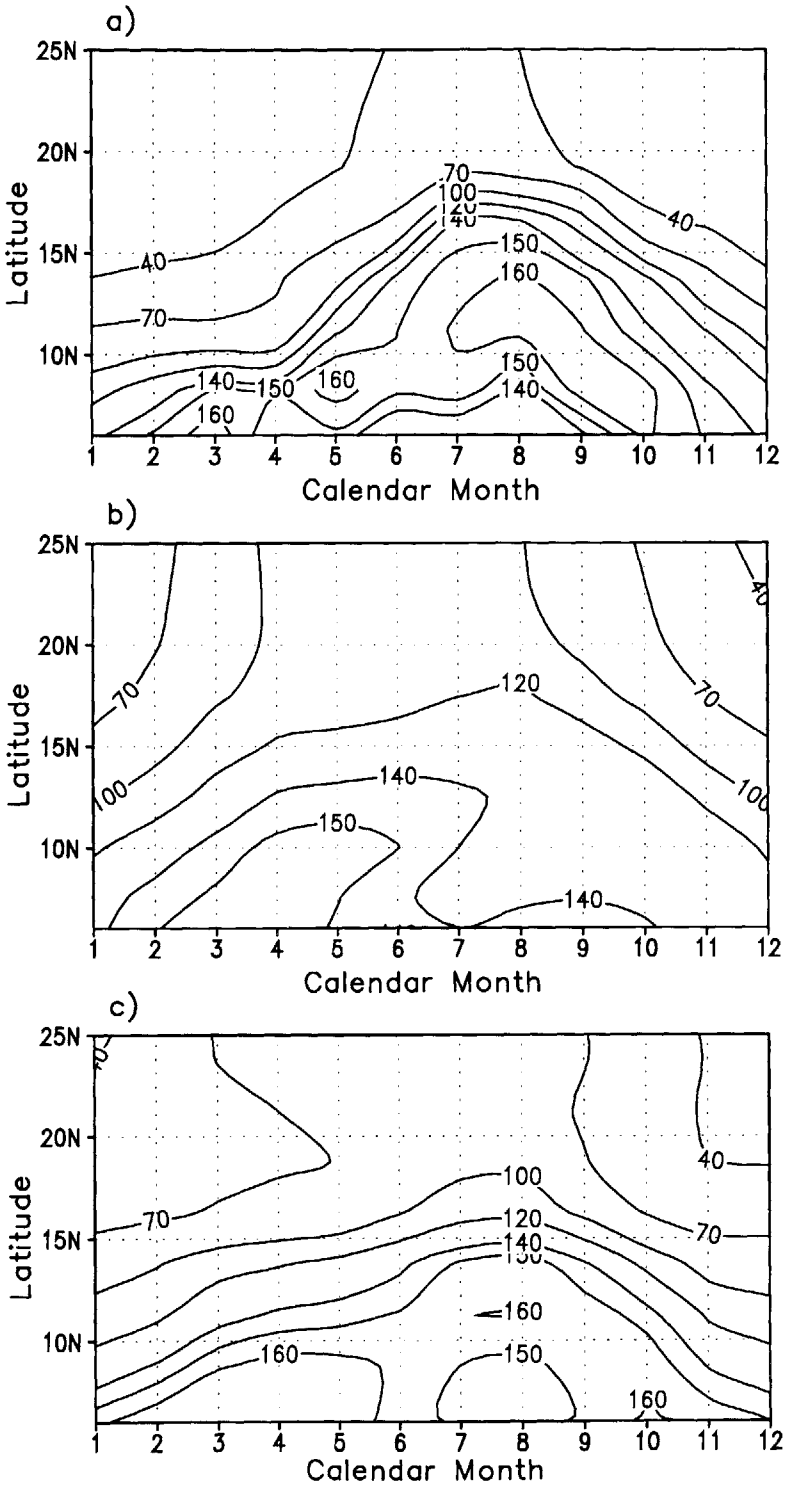

Figure 3-18: Seasonal cycle of the surface net radiation, in W/m^2: a) model simulation; b) NCEP re-analysis data; c) ISCCP data.

ISCCP observations. For both the model and the ISCCP data, the albedo magnitude increases from lower than 0.15 near the coast to above 0.40 over the desert, and decreases northward from the desert. In the NCEP re-analysis data, the albedo contrast between the forest and the desert is much smaller, and the desert albedo is significantly lower. In addition, the NCEP re-analysis data shows an unrealistic seasonal cycle of albedo: a maximum occurs during summer when the ground is wet. Similarly, the model net radiation compares better with the ISCCP data than with the NCEP re-analysis data (Figure 3-18). Over the forest region in all seasons, and over the grassland during the rainy season, the difference between the simulation and the ISCCP data is within $20W/m^2$. Larger discrepancy exists over the grassland in the dry season and over the desert region throughout the year. This difference is mainly a reflection of the differences in the incoming radiation fluxes (see Figures 3-13 and 3-14), which might be attributed to both the model deficiency and the data uncertainty. According to Bishop *et al.* (1997), inaccuracy in the ISCCP data is associated with the spatially and temporally varying aerosol distribution. On the other hand, our model does not account for the impact of aerosols. It is worth noting that the largest discrepancy between the model and ISCCP data takes place where and when the ground is dry and unprotected, which tends to cause a high aerosol loading in the atmosphere. For the NCEP re-analysis data, consistent with the small forest-desert contrast in albedo, there is no dramatic contrast in net radiation between the coast region and the desert. This is unlikely to be the case considering the well-known role of the Sahara desert as an energy sink.

As presented in Chapter 2, we incorporated into the model a canopy interception scheme to account for the impact of the rainfall sub-grid variability. Here the representation of canopy hydrology is evaluated using the fractional interception loss, as shown in Figure 3-19. The fractional interception loss is defined as the fraction of the evapotranspiration that is contributed by the direct evaporation of the intercepted water on the canopy. According to Shuttleworth (1988a), the fractional interception loss is approximately 25% at a forest site in the Amazon. Our model estimation over the forest region is also around 25%. As expected, interception loss over savannah

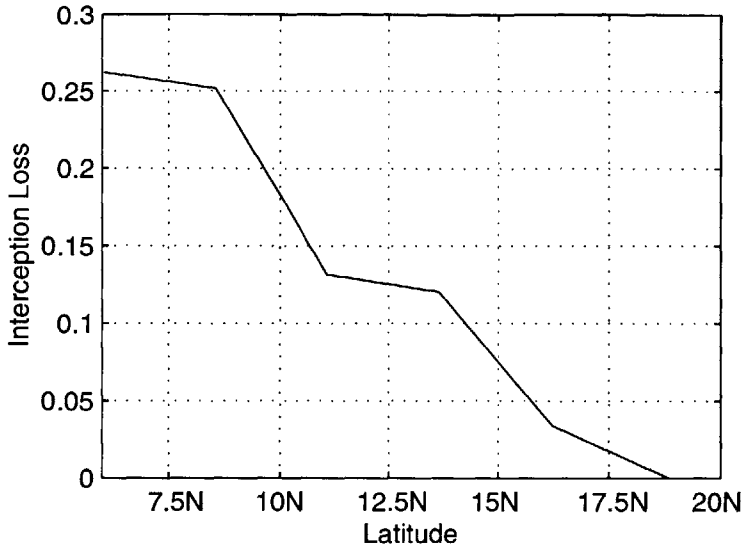

Figure 3-19: Interception loss as a fraction of the overall evapotranspiration.

and grassland is much smaller, at a magnitude of 10% or even smaller.

In summary, the zonally symmetric model reproduces the current atmospheric climate with reasonable accuracy. However, because the model is designed to carry out long integrations or simulations, its complexity is limited, and some of the physical processes are over simplified (e.g., the cloudiness) or not represented (e.g., aerosols effect). Moreover, the real world is not zonally symmetric. Therefore, some differences between the model and observations are expected, as have been shown above.

3.3 Modeling the Coupled Biosphere-Atmosphere System

After testing each of the two model components against observations, the synchronously coupled model including ecosystem dynamics is run to simulate the biosphere-atmosphere system of West Africa. The model starts with an initial vegetation distribution close to today's condition (Figure 3-5), with vegetation dynamics simulated in the region between $6°N$ (the coast) and $27°N$. Similar to the simulation of Section 3.2, surface properties and fluxes outside the tropics are fixed at their climatological values from

the NCEP re-analysis data, and SST is also fixed at the climatology allowing for seasonal variability (Reynolds and Smith, 1995).

For the atmospheric model to spin up, vegetation in the first three years remains static. Ecosystem dynamics start to take place in the fourth year of the simulation. The modeled system evolves into an equilibrium state within 25 years. An additional 15 years of simulation reveals no noticeable trend, as shown by the evolution of the annual precipitation and the total net primary productivity (NPP) in Figure 3-20. Similar to today's environment in West Africa, this equilibrium state features forest in the south and grassland in the north, as shown in Figure 3-21. However, in the region between the forest and the grassland, at a grid point near $11°N$, the initialized savannah vegetation gives way to dense woodland. As demonstrated by the evolution of the growing-season leaf area index (LAI) for the upper and lower canopy (Figure 3-22), grass at this savannah site becomes overwhelmingly dense immediately after the introduction of vegetation dynamics, probably due to the lack of disturbances under a relatively wet climate; trees gradually develop and eventually shade grass out. The annual rainfall at the model equilibrium is presented in Figure 3-23 (solid line). For comparison, also presented in Figure 3-23 is the annual rainfall simulated in Section 3.2 with fixed current vegetation (dashed line), which is comparable to the current climate (see Figure 3-8). In general, the climate of the equilibrium state is slightly wetter and greener than the current climate in West Africa.

Strictly speaking, the climate of the model equilibrium is not comparable to the observed current climate since the current biosphere-atmosphere system may not be at its natural equilibrium. First, it is uncertain whether the current system is at equilibrium at all; secondly, any equilibrium in the real world is expected to be different from the modeled natural equilibrium due to the recurrence of human disturbances.

Similar to the equilibrium biosphere in Section 3.1, a very noticeable feature of the simulated biosphere-atmosphere equilibrium is the absence of savannah. As shown in Figure 3-22, trees eventually take over in the region that is initialized with the observed savannah-type vegetation. Although several studies (e.g., Eagleson and Segarra, 1985; Rodriguez-Iturbe *et al.*, 1999) argued that the savannah vegetation

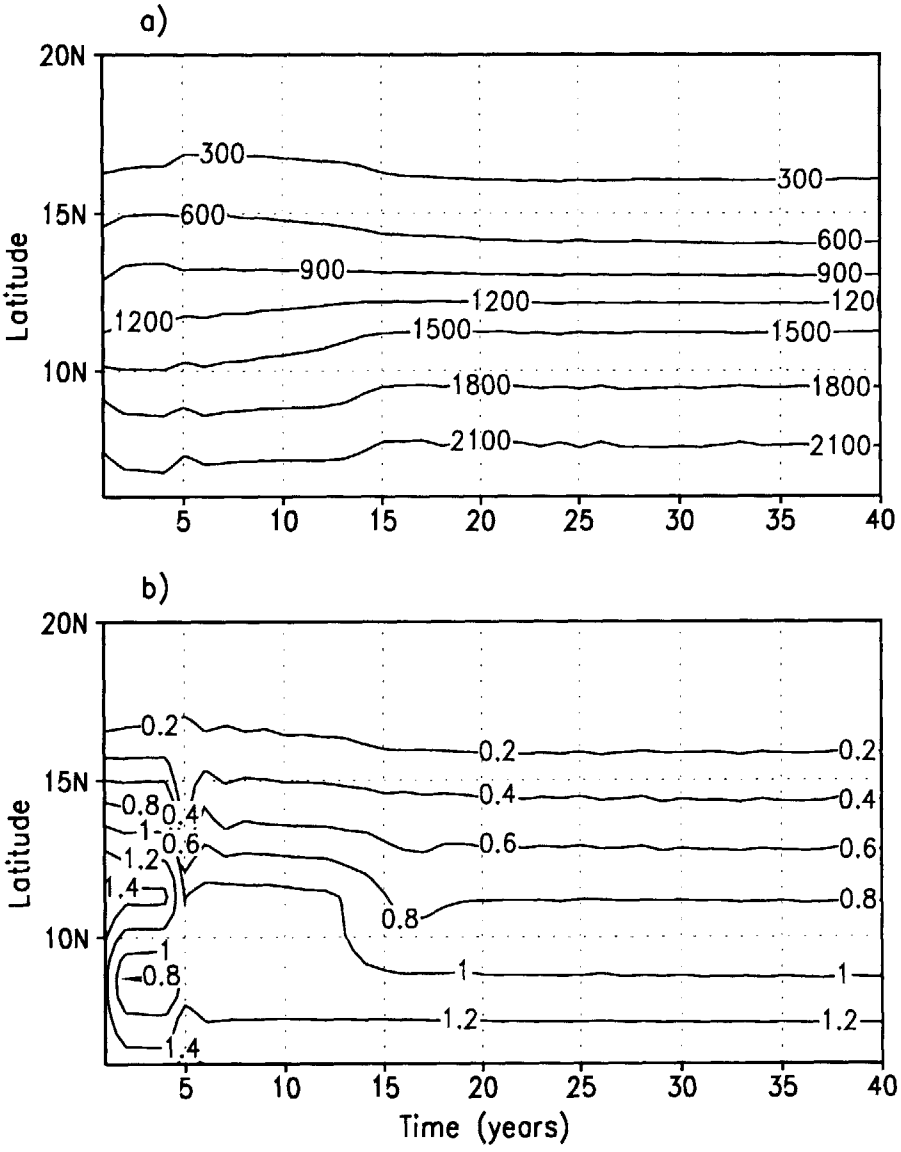

Figure 3-20: Evolution of the simulated biosphere-atmosphere system: a) Annual precipitation ($mm/year$); b) Total net primary productivity ($kgC/m^2/year$).

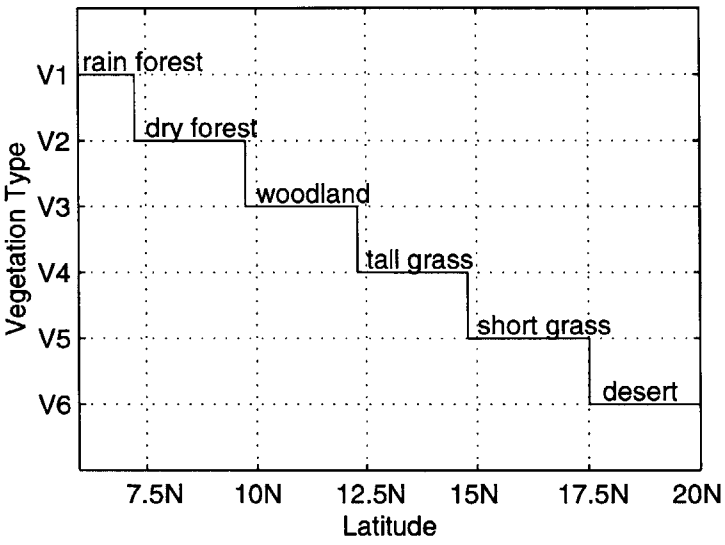

Figure 3-21: Vegetation distribution at the attained biosphere-atmosphere equilibrium. The definition of vegetation type is the same as in Figure 3-2.

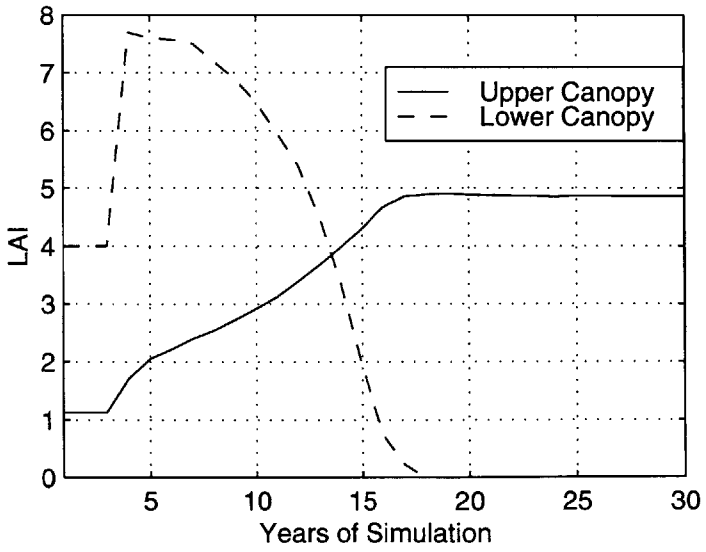

Figure 3-22: The evolutionary process of the growing-season leaf area index for the upper canopy (solid line) and for the lower canopy (dashed line) at $11°N$, where vegetation was initialized as savannah (a mixture of trees and grass).

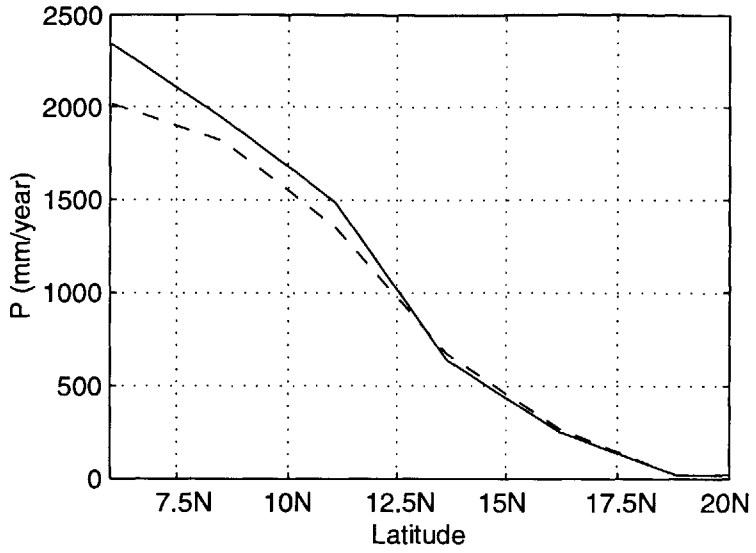

Figure 3-23: The meridional distribution of the annual rainfall (in *mm/year*), at the attained biosphere-atmosphere equilibrium (solid line). As a comparison, the dashed line plots the rainfall distribution modeled with fixed, "close-to-current" vegetation.

system is naturally stable, various ecological evidence suggests that the stability of savannah in some regions may depend on external disturbances. These disturbances can be of natural origin or anthropogenically induced. In many parts of West Africa, the savannah landscapes were originally created and are still maintained by recurrent burning for various human purposes (Bourliere and Hadley, 1983). According to Bourliere and Hadley (1983), *"when plots of such man-maintained savannas are protected from bush fires for a number of years, they very quickly turn into deciduous woodland"*. Grazing also plays an important role in maintaining the current savannah landscape in Africa (Sprugal, 1991). For example, tree establishment over the current savannah region started around 1895 when the cattle disease "rinderpest" was introduced into Africa (Sinclair, 1979), and was suppressed again when vaccines were developed later on to protect domestic livestock. Various human disturbances of this kind left the current landscape as a mixture of grass and trees. The transient nature of the savannah-type vegetation in the model may have to do with the lack of representation of these disturbances.

To qualitatively validate the above argument on the simulation of the savannah-

type vegetation, we perform one experiment with a certain degree of fire and grazing effect imposed over the savannah and grassland region. Fire is assumed to take place every year in the dry season and consumes a fraction f of the above-ground live biomass, where f varies from one year to the next and is a random number uniformly distributed between 0 and 10%. We assume that grazing consumes 50% of the grass NPP every year. Figure 3-24 shows the evolution of peak LAI for the upper and

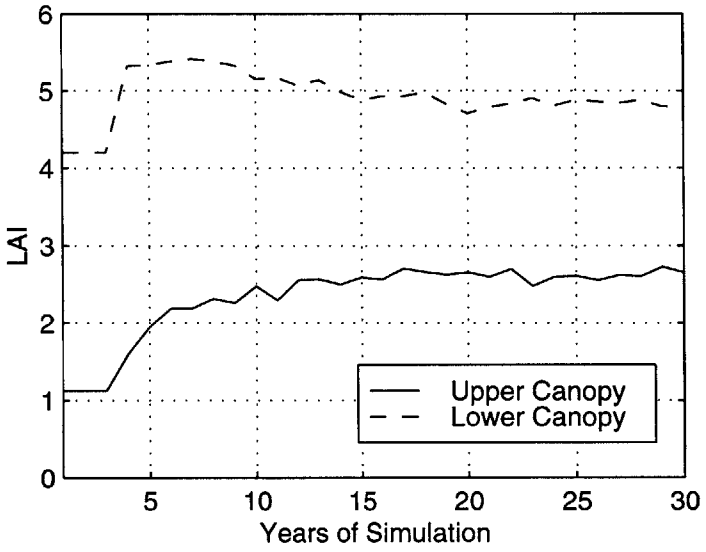

Figure 3-24: Same as Figure 3-22, but with the impact of fire and grazing over the savannah and grassland region.

lower canopy at the grid point near $11°N$, where initial vegetation is a mixture of trees and grass. Under the impact of disturbances, the savannah-type vegetation survives into the model equilibrium. Comparison between Figures 3-22 and 3-24 confirms that disturbances could indeed play an important role in the survival of the savannah-type vegetation. This experiment is designed to investigate the qualitative impact of disturbances on the model's equilibrium state, therefore we made no effort to reproduce the historical occurrence of fire and grazing.

3.4 Summary

The newly developed zonally symmetric biosphere-atmosphere model ZonalBAM is applied to the region of West Africa, where climate conditions show high degree of zonal symmetry. Experiments are carried out to separately test the model's performance in simulating the biospheric climate and the atmospheric climate. The results suggest that the model can reproduce the observed climate in West Africa with reasonable accuracy. Since the real world is not zonally symmetric, it is expected that there would be some differences between the model and observations, as shown in previous sections.

After separately validating the biospheric model and the atmospheric model, we simulate the natural climate system of West Africa using the synchronously coupled biosphere-atmosphere model. At the equilibrium derived in this chapter, the climate of the natural biosphere-atmosphere system is close to, but slightly wetter and greener than, the current climate. Focusing on the natural interactions between the biosphere and the atmosphere, at this stage we have not accounted for the impact of various human activities. At the same time, it is impossible to identify whether the current observed climate system is at equilibrium. Therefore, the comparison between the model equilibrium and the current climate may not be justifiable. Nevertheless, the "close-to-current" equilibrium of the model provides an ideal control state for further studies.

Chapter 4

Impact of Rainfall Sub-Grid Variability – a Case Study

4.1 Introduction

To account for the impact of rainfall sub-grid variability, a canopy interception scheme was incorporated into the coupled biosphere-atmosphere model ZonalBAM which was validated in Chapter 3. However, it is unclear what impact the rainfall sub-grid variability has on the performance of a coupled biosphere-atmosphere model. In this chapter, using ZonalBAM and taking West Africa as an example, we demonstrate the importance of including rainfall sub-grid variability in modeling the biosphere-atmosphere system.

The impact of rainfall sub-grid variability on surface processes has been investigated by many studies (Pitman *et al.*, 1990; Eltahir and Bras, 1993a; Seth *et al.*, 1994; Ghan *et al.*, 1997) using the land surface model BATS (Dickinson *et al.*, 1993). While Eltahir and Bras (1993a) focused on the estimation of canopy interception, other studies paid more attention to the energy and water balance of the overall land surface. According to Pitman *et al.* (1990), changing the areal distribution of precipitation alters the balance between runoff and evaporation. In their study, modifying the rain-covered area can change the surface climatology from an evaporation-dominated regime into a runoff-dominated regime. Consistently, Seth *et al.* (1994) showed that

considering the rainfall sub-grid variability affects the surface energy partitioning and modifies the Bowen ratio. A study by Ghan *et al.* (1997) showed that neglecting the sub-grid variability in summer precipitation causes a decrease of runoff by 48% and increase of evapotranspiration by 15%. A common conclusion can be drawn from these studies that the sub-grid variability of rainfall or the lack of it significantly affects the water partitioning between evapotranspiration and runoff as well as the energy partitioning between the sensible heat and latent heat fluxes at the land surface.

In most of the previous studies, off-line land surface models were used. The atmospheric forcings were prescribed. It is not obvious how the land surface-atmosphere feedback would modify the sensitivity of surface processes to the representation of rainfall interception (Kim and Entekhabi, 1998). Dolman and Gregory (1992) investigated this issue using a 1-D version of the UKMO's 11-layer GCM with a simple land surface scheme, and found that total evapotranspiration in their model is strongly controlled by the radiation input and is rather insensitive to the representation of rainfall interception. In their study, when the rain-covered fraction changes from 0.1 to 0.3, the total amount of evapotranspiration differs by only 1%. It appears that the parameterization of rainfall sub-grid variability only affects the partitioning between direct evaporation from the canopy storage and plant transpiration, but not the total evapotranspiration.

In addition to the contradiction between the studies using off-line models and those using coupled models, previous studies have been limited to the impact of sub-grid variability on the surface hydrological processes. Its broader effects have not been evaluated. Even if the total evapotranspiration remains the same, the incorrect partitioning between the evaporation and plant transpiration may still have a significant impact on the atmosphere as well as the biosphere due to various feedback mechanisms. In addition, no previous study has looked at the issue of sub-grid variability in the context of a dynamic biosphere. Here, using the coupled biosphere-atmosphere model ZonalBAM, we investigate the impact of rainfall sub-grid variability on modeling the biosphere-atmosphere system over West Africa. We will demonstrate how, despite the accurate simulation of total evapotranspiration, the errors in the repre-

sentation of land surface hydrology propagate into the atmospheric and biospheric simulations, and how it influences the biosphere-atmosphere equilibrium state when vegetation dynamics is considered.

4.2 Relevant Model Details

Surface hydrological processes are the starting point for the broad impact of the rainfall sub-grid variability on the simulated climate system. To help understand the results of this study, here we describe how the surface hydrology is treated in the model, adding more details to the description in Chapter 2.

The land surface module in IBIS includes a detailed description for the precipitation cascade. Rain falls over the upper vegetation canopy and part of it gets intercepted, which contributes to the upper canopy storage. The throughfall from the upper canopy, including the instantaneous throughfall and the slow canopy dripping, falls over the lower canopy. After the canopy interception at the lower layer, what reaches the ground is the drainage from the lower canopy. The intercepted rainfall stays as free water on the vegetation canopy. Dripping and re-evaporation reduce the water storage at both canopy layers.

The amount of water that reaches the ground is partitioned into three parts: direct evaporation from surface puddles; surface runoff that discharges out of the system; infiltration that recharges the water storage in the soil. Within the soil, water movement between different layers is governed by gravity drainage and diffusion, with three moisture sinks: direct evaporation, plant uptake (transpiration), and drainage out of the bottom. Direct evaporation from the soil only occurs in the top soil layer. Water uptake by plants from different soil layers depends on the rooting profiles. The drainage from the bottom soil layer is modeled assuming gravity drainage and neglecting interactions with groundwater aquifers.

Within the vegetation canopy, the major component of water vapor exchange is the plant transpiration, which is strongly related to photosynthesis and stomatal conductance. Plant stomata opens during photosynthesis to let CO_2 in. As a result,

the stomata loses water to the ambient environment in the form of transpiration. When part of the canopy becomes wet, sunlight can only reach part of the leaf surface. As a result, photosynthesis is suppressed, which would correspondingly reduce the stomatal conductance therefore the transpiration. The water supply for transpiration is the plant uptake from the soil. Upon water stress, stomatal conductance decreases, therefore the transpiration rate also decreases. When water stress becomes severe enough, drought-deciduous plants shed their leaves to preserve water.

Although the land surface module in IBIS has detailed description of surface hydrology, it does not consider the impact of rainfall sub-grid variability. For example, canopy interception (I) is estimated as a function of the vegetation density (represented by the single-sided leaf area index LAI) and does not depend on the sub-grid distribution of rainfall:

$$I = P_0(1 - exp(-LAI))$$

where P_0 is the precipitation rate predicted by the atmospheric model, which represents the rainfall average over each grid cell. For greater physical realism, as described in Chapter 2, we modified the representation of canopy hydrology by incorporating into the model an interception scheme (Section 2.3.2) which accounts for the spatial variability in rainfall interception.

When incorporating the interception scheme, an approximation is made regarding the representation of canopy hydrology in the presence of two vegetation layers. The "rain" falling over the lower layer canopy is actually the drainage from the upper layer. The "routing" effect of the upper-layer canopy will significantly modify the "rain" distribution for the lower canopy. However, in the model, it is assumed that both the parameter μ and the form of probability distribution function for the lower-layer canopy are the same as the upper-layer canopy. This assumption may cause inaccuracy in regions with savannah-type vegetation (i.e., mixture of trees and grass), but makes no difference over regions with tree-only or grass-only vegetation.

4.3 Design of Experiments

Our study on the impact of rainfall sub-grid variability is based on two main experiments, one labeled as variable and one uniform. In the variable case, the interception scheme presented in section 2.3.2 is used; in the uniform case, the interception calculation of original IBIS described in Section 4.2 is used, which assumes uniform rainfall distribution over each grid cell.

The model setup is the same as in Section 3.2, with the land-ocean boundary at 6°N and SST fixed at its climatology. We first look at the case with static vegetation – the role of vegetation dynamics will be addressed later. For the static vegetation distribution, forest occupies the region between the coast and 12.5N, with rain forest near the coast and drought-deciduous forest to the north; grassland extends from 12.5N to the desert border near 17.5N, with dense tall grass near the forest and short grass near the desert. This vegetation condition is similar to, but slightly different from, the observations in West Africa (Foley *et al.*, 1996; Gornitz and NASA, 1985). Reaching as far north as 12.5N, the drought-deciduous forest in the model covers both the dry forest region and the savannah region of today's West Africa. As a result, vegetation specified in the model is either forest or grassland, without the mixture of trees and grasses. Therefore, the assumption that the "rainfall" sub-grid distribution for the lower canopy is the same as the upper canopy does not affect our experiments. Moreover, the larger forest-covered region makes the effect of rainfall sub-grid variability more distinguishable since trees have a higher canopy capacity than other vegetation forms.

Three years of integration is needed before the model reaches equilibrium. Results from the fourth year of the simulation are presented in the following. Our interest in this chapter is not how well each of the experiments reproduces the observed climate. Instead, we focus on the simulation differences that result from the assumption of uniform rainfall distribution. For the purpose of this study, we only concentrate on the region of West Africa between 6°N (the coast) and 20°N (desert)

4.4 Analysis of Results

4.4.1 Main Results

Here the results are presented in the form of a comparison between the two experiments: the variable experiment which considers the rainfall sub-grid variability, and the uniform experiment which assumes uniform rainfall distribution within each grid cell.

Results on surface hydrology are presented in Figure 4-1 (a-d). Figure 4-1 (a, b) show the interception loss and transpiration respectively. The uniform case overestimates the interception loss by more than 100%, and significantly underestimates the plant transpiration over the forest region, which is qualitatively consistent with previous studies (e.g., Eltahir and Bras, 1993a,b). The difference over the grassland region is not as significant. Figure 4-1c and 4-1d present the evapotranspiration and runoff, respectively. Despite the dramatic difference in the partitioning between interception loss and transpiration, the overall evapotranspiration shows negligible difference over the forest region. Over the grassland region in the uniform case, an increase of evapotranspiration is observed. Although the total evapotranspiration is rather insensitive to the representation of rainfall interception, a significant difference is observed in runoff. Runoff, which is up to 725 $mm/year$ in the variable case, is almost non-existent in the uniform case. Our results over the forest region, including the overestimation of interception loss, underestimation of transpiration, and more importantly, the low sensitivity of the total evapotranspiration, are consistent with the findings of Dolman and Gregory (1992). It is important to note that the Dolman and Gregory (1992) study also used a coupled land-atmosphere model. This agreement suggests that the high sensitivity of total evapotranspiration to the representation of rainfall interception found in studies using off-line land surface models may have to do with the lack of atmospheric feedback.

The bias caused by neglecting the rainfall sub-grid variability is not limited to the surface hydrological processes. It also affects the simulation of biospheric and atmospheric processes to a great degree, as shown in Figure 4-1 (e,f). Figure 4-

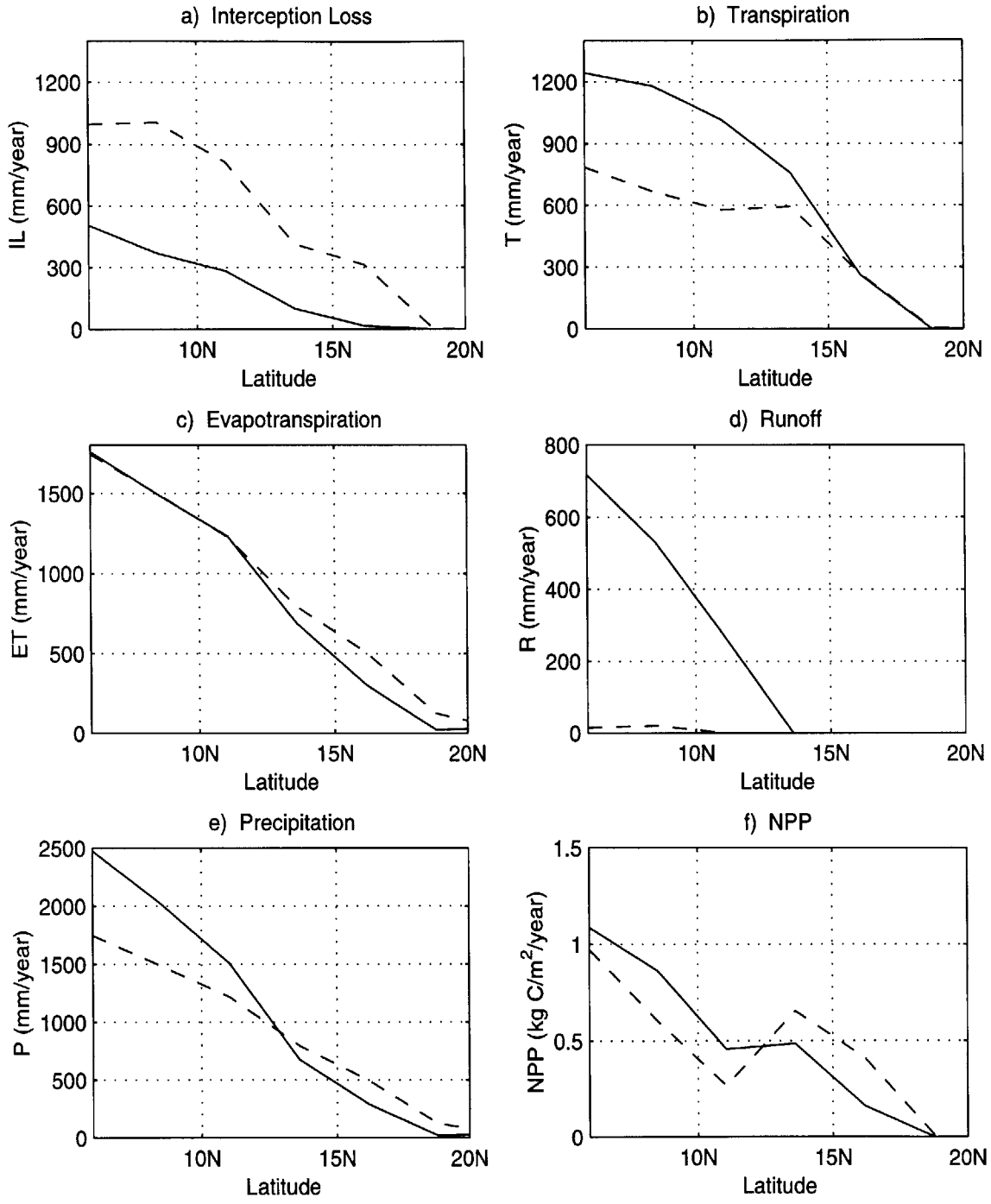

Figure 4-1: The comparison between the uniform case (dash line) and the variable case (solid line) for: a) Interception loss; b) Transpiration; c) Evapotranspiration; d) Total runoff; e) Precipitation; f) Net primary productivity.

1e presents precipitation as an example for the atmospheric climate, and Figure 4-1f presents the net primary productivity (NPP) as an example for the biospheric climate. Although the total evapotranspiration remains the same, comparison of the precipitation between the two experiments shows a striking difference. Precipitation is underestimated in the uniform case by up to 35% in the forest region, and significantly overestimated in the grassland region. Correspondingly, in the biosphere, NPP is underestimated in the forest region and overestimated in the grassland region.

In the following we focus on interpreting the results presented above, in particular, on understanding how errors in the representation of rainfall interception propagate into the atmosphere and the biosphere although the total evapotranspiration is correctly simulated. As shown by Figure 4-1 (e,f), the response of the biosphere-atmosphere system differs between the forest region and the grassland region. Therefore these two regions are analyzed separately in the following.

4.4.2 Interpretation of Results for the Forest Region

To understand the impact of rainfall sub-grid variability, we start from the micrometeorological processes within the vegetation canopy. When falling uniformly over the entire grid cell, rainfall occurs in the form of drizzle in climate models with coarse resolution. The fine rain drops tend to stay on the leaves. Therefore, the amount of free water on the canopy, as well as the wet canopy area, increases. Similar to the difference between land and ocean, the easily accessible canopy water favors a moister and cooler environment within the canopy. Consequently, humidity of the air within the canopy increases, and canopy temperatures, including the leaf temperature and stem temperature, decrease. As an example, Figure 4-2a shows the fraction of the wet leaf area on a typical day of August, which is larger in the uniform case due to the extra wetting effect; the corresponding leaf temperature and canopy air humidity on that same day are presented in Figure 4-2(b,c). Clearly, for the uniform case, the canopy is cooler and the air within the canopy is moister.

The rate of evaporation ("E") from the intercepted water over a unit wet leaf area is proportional to the moisture deficit $Q_s - Q_a$, where Q_s is the saturation specific

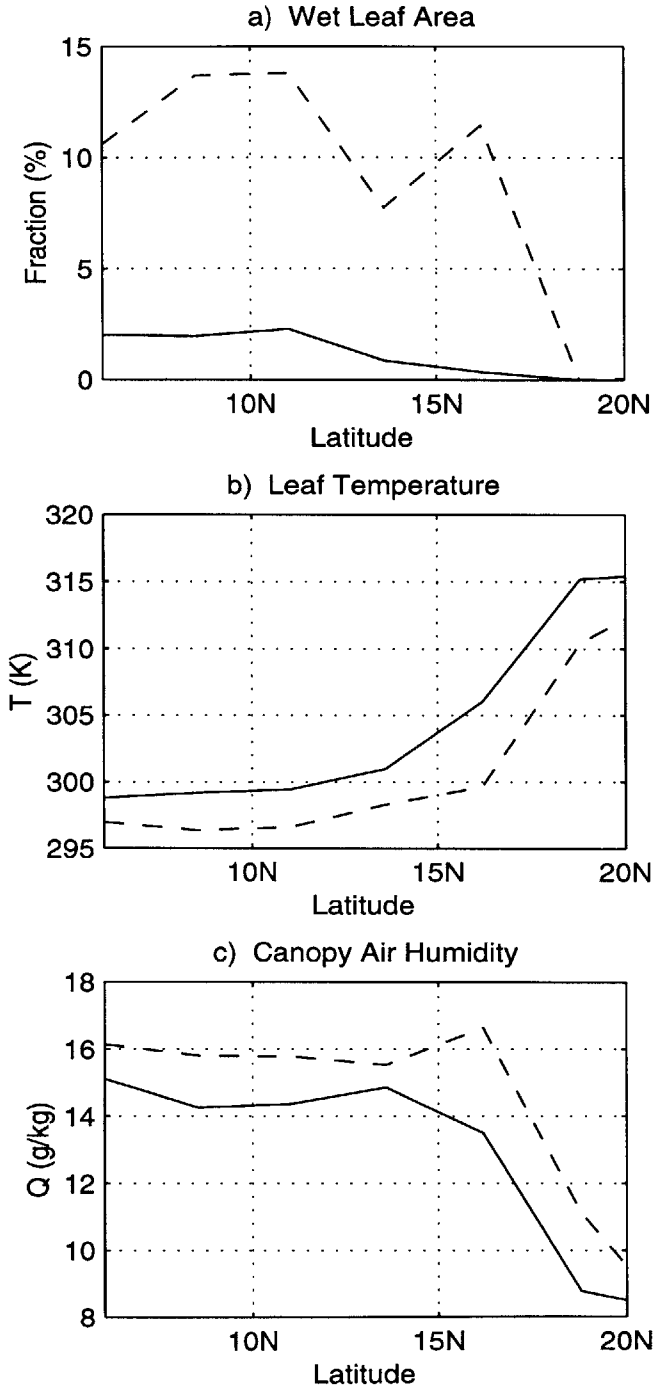

Figure 4-2: The comparison between the uniform case (dash line) and the variable case (solid line) for the canopy condition on a typical day of August (the rainy season): a) Fraction of the leaf area that is wet; b) Leaf temperature; c) Specific humidity of the canopy air.

humidity at the canopy temperature, and Q_a is the specific humidity of the canopy air. For the uniform case, both the lower temperature of the canopy and the moister air within the canopy favor a smaller moisture deficit. As a result, "E" over a unit wet leaf area is lower in the uniform case. However, in the uniform case, the wet leaf area is larger. For example, the wetting fraction of the forest at $6°N$ is about 2.5% for the variable case, but is more than 10% for the uniform case (Figure 4-2a). This significant increase of wetness (by a factor of more than 3) dominates over the impact of reduced moisture deficit, thus causing a higher interception loss in the uniform case (Figure 4-1a).

The rate of plant transpiration ("T") is proportional to the stomatal conductance K_s and the moisture deficit $Q_{sl} - Q_a$, where Q_{sl} is the saturation specific humidity at the leaf temperature, and Q_a is the specific humidity of the canopy air. Similar to the effect on "E", the canopy environment in the uniform case favors a smaller moisture deficit. At the same time, due to the excessive wetness in the uniform case, less leaf area is available for the absorption of photons. As a result, the photosynthesis rate decreases, which causes a decrease in plant stomatal conductance K_s. The reductions in both $Q_{sl} - Q_a$ and K_s contribute to the lower transpiration in the uniform case, as observed in Figure 4-1b.

The total evapotranspiration has three components: interception loss, transpiration, and soil evaporation. Over the forest region, soil evaporation is negligible. Interception loss and transpiration count for most of the evapotranspiration. The increase of interception loss and the decrease of transpiration compensate for each other, thus bringing the total evapotranspiration for the uniform case close to the variable case (Figure 4-2c). This mechanism is described by the flow chart in Figure 4-3. Here we would like to emphasize that it is physically possible for a climate model to have severe errors in the description of surface hydrology but still get accurate simulation of the total evapotranspiration. What makes this issue critical is the fact that these errors are not limited to the land surface. Instead, they propagate into the atmosphere and the biosphere through feedback mechanisms as analyzed in the following.

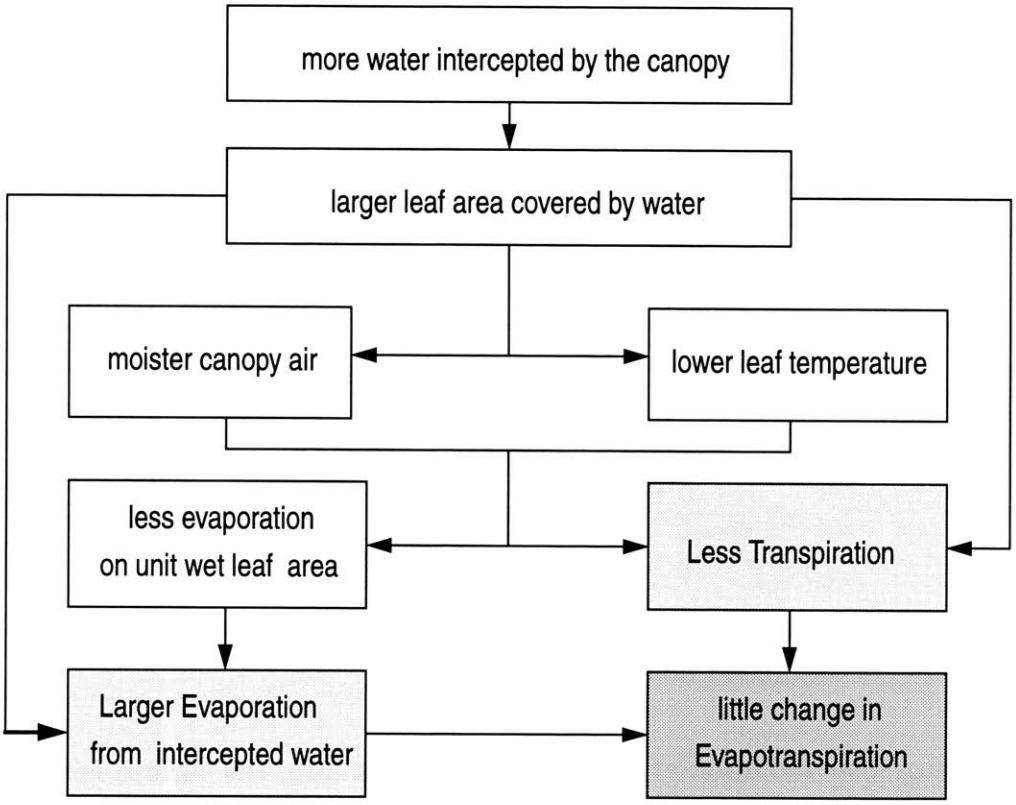

Figure 4-3: A mechanism through which the neglect of sub-grid variability influences the simulation of surface hydrology. The shortcut between the "larger leaf area covered by water" and the "less transpiration" is through the photosynthesis and stomatal conductance.

In the uniform case, the higher humidity of the canopy air tends to increase the rate of water vapor flux, thus having a moistening effect for the atmosphere above; the lower vegetation temperature tends to reduce the sensible heat flux, thus causing a cooling effect for the atmosphere above. As the low-level atmosphere gets moister and cooler, more low-level clouds will form. Figure 4-4 presents the fractional cover of low-level clouds during August. The increase of low-level clouds reduces not only

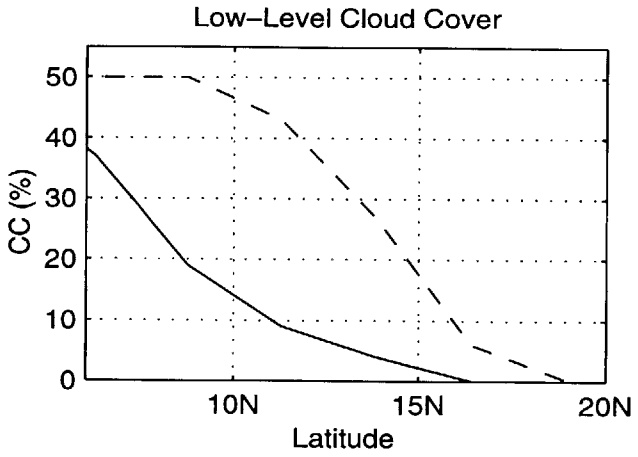

Figure 4-4: The fractional cover of low-level clouds in the uniform case (dash line) and the variable case (solid line).

the incoming solar radiation at the land surface, but also, the surface net radiation (Slingo, 1990; Klein and Hartmann, 1993; Baker, 1997), as shown in Figure 4-5(a,b). This cloud feedback further enhances the sensible heat flux reduction initiated by the reduced canopy temperature. It also tends to suppress the evapotranspiration, which may offset the increase initiated by the overestimated canopy air humidity. As a result, the sensible heat flux in the uniform case is lower, but very little difference in the latent heat flux is observed (Figure 4-5c). Therefore, the total energy flux from the land surface to the atmosphere is lower in the uniform case.

In the uniform case, the lower energy flux from the land surface to the atmospheric boundary layer tends to stabilize the atmosphere. As a result, the intensity of local atmospheric convection decreases, and so does the precipitation falling to the surface

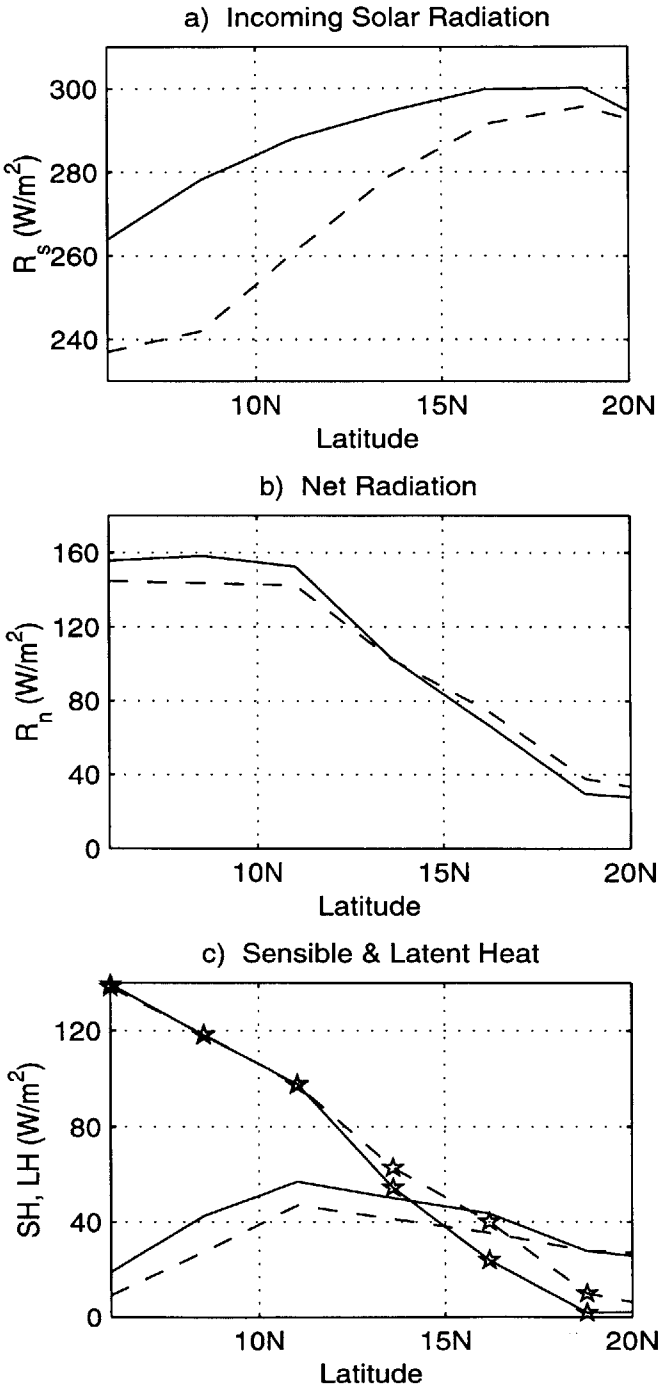

Figure 4-5: The comparison between the uniform case (dash line) and the variable case (solid line) for energy fluxes at the surface: a) Incoming solar radiation; b) Net radiation; c) Sensible heat flux (plain line) and latent heat flux (line with pentagram).

(Figure 4-1e). Since the evapotranspiration remains the same, the reduction of precipitation signals a decrease of moisture convergence due to changes in the large-scale circulation which is, in this case, the West African monsoon circulation. As demonstrated before, the assumption of uniform rainfall distribution causes underestimation of total surface energy flux, which is the energy supply for the atmospheric boundary layer. This would tent to reduce the moist static energy supplied to the atmospheric boundary layer. At the same time, the depth of the boundary layer over forest would be smaller in the uniform case due to the reduction in sensible heat flux (Figure 4-5). This effect would tend to increase the magnitude of the moist static energy per unit depth. It seems that the effect of the decrease in the total flux of energy is larger than the effect of the change in boundary layer depth. Therefore, the boundary layer moist static energy and entropy over the forest region are underestimated (Eltahir 1996). As a result, in the uniform case, the boundary layer entropy gradient from the ocean toward the land is smaller, and the peak of the boundary layer entropy moves northward (Figure 4-6). During the monsoon season, such differences favor a monsoon

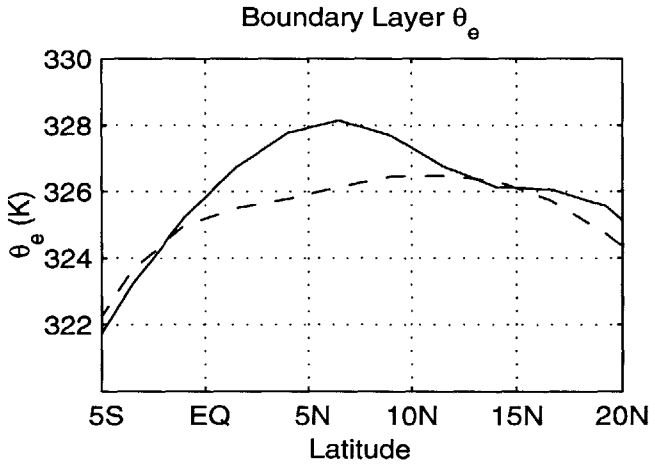

Figure 4-6: The equivalent potential temperature θ_e for the uniform case (dash line) and the variable case (solid line), averaged between 1000mb-800mb. θ_e can be viewed as an index of the boundary layer entropy Θ: $\Theta = C_p ln\theta_e + const.$

circulation that is weaker (Eltahir and Gong 1996) but penetrates further inland. This is clearly demonstrated by Figures 4-7 and 4-8. According to Figure 4-7(a,b),

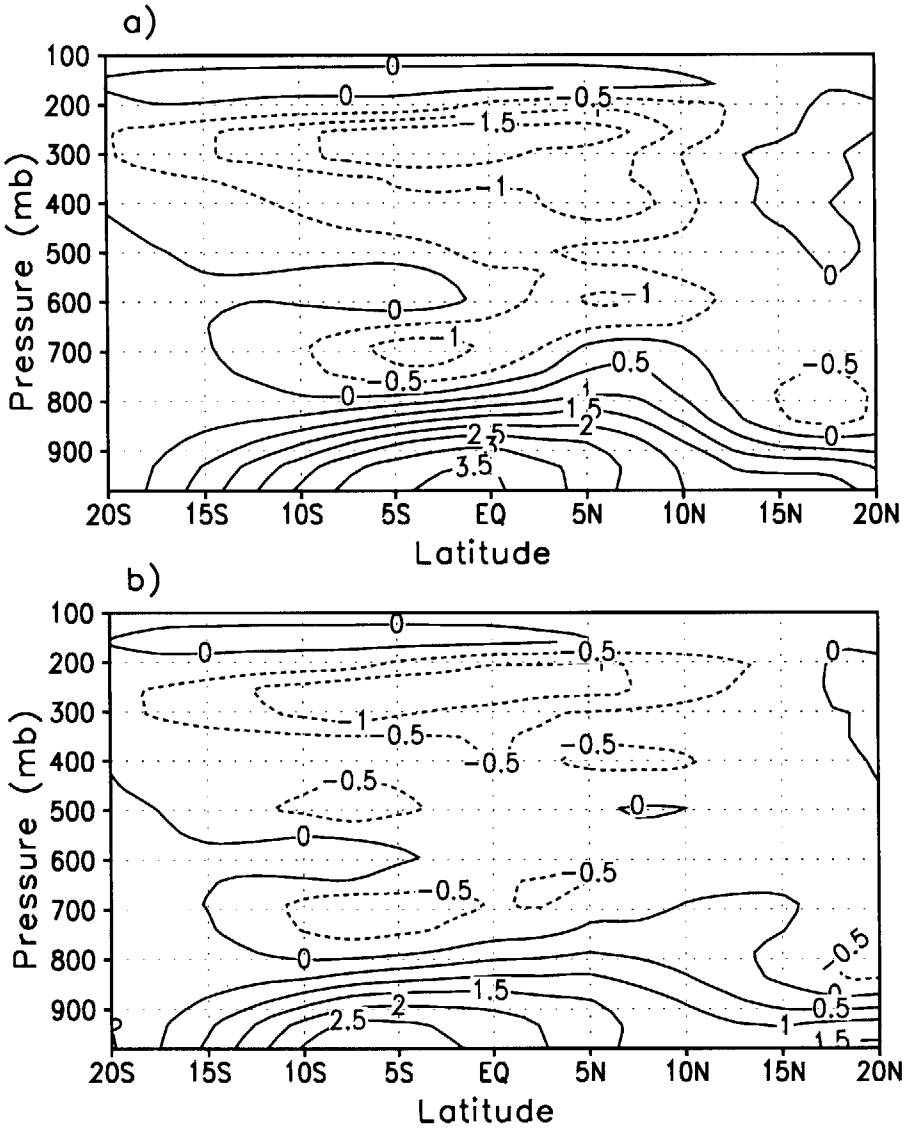

Figure 4-7: The meridional wind during August, in m/sec. a) for the variable case; b) for the uniform case.

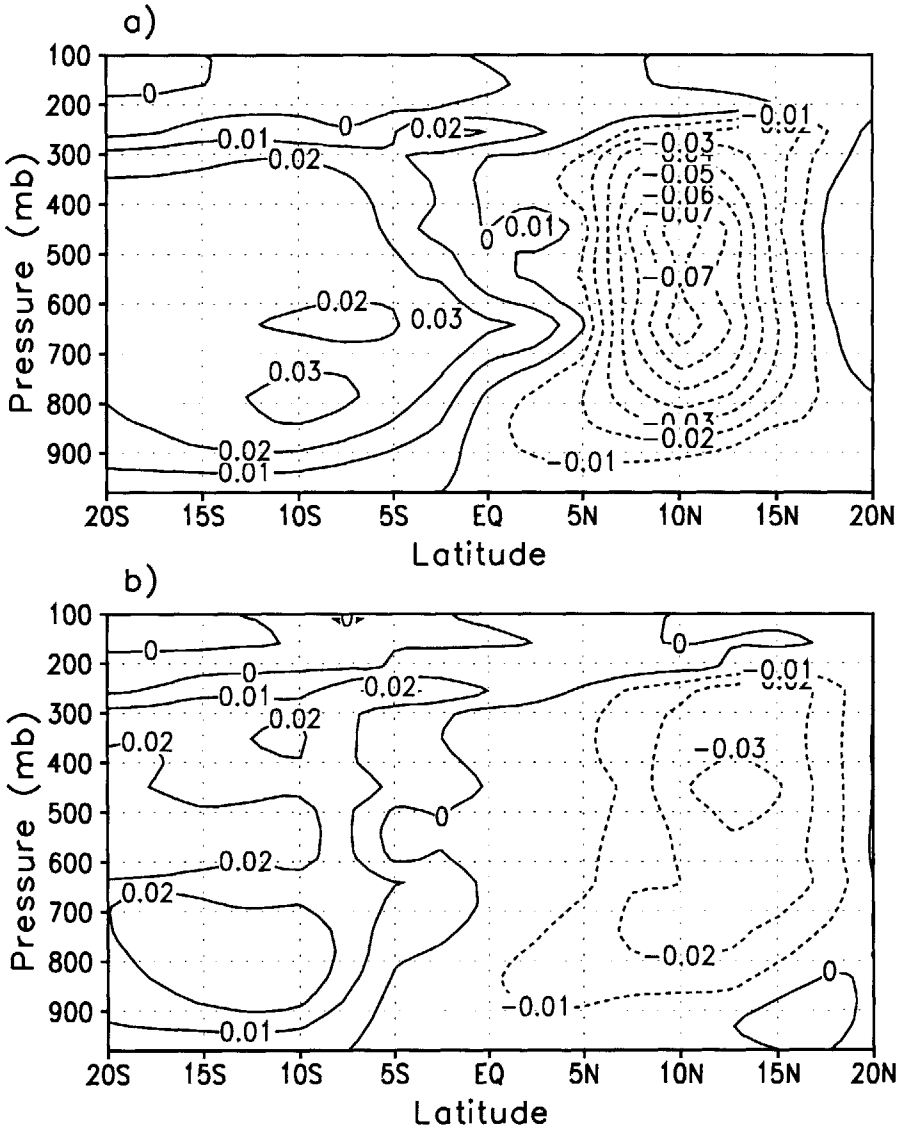

Figure 4-8: Vertical velocity during August, in Pa/sec. a) for the variable case; b) for the uniform case.

the low-level meridional wind across the coast is weaker in the uniform case than in the variable case; at the same time, as shown in Figure 4-8(a,b), the rising motion over the land is weaker in the uniform case, and its peak occurs further northward. These changes in the monsoon circulation cause a decrease of rainfall over the forest region in the south. In the land surface water budget, the precipitation reduction is balanced by the runoff decrease (Figure 4-1d).

The difference in NPP between the uniform case and the variable case (Figure 4-1f) is closely related to two factors: leaf wetting and clouds. As mentioned above, in the uniform case, the excessive canopy wetness leaves less area available for photosynthesis. At the same time, the increase of low-level clouds reduces the incoming solar radiation, therefore reduces the photosynthetically active radiation. Both of these two factors cause lower photosynthesis rate, thus lower NPP.

In addition to the above mentioned effects, another important mechanism has to do with the water availability in the root zone. Over the forest region in the uniform case, both the over-estimation of interception loss and the underestimation of precipitation reduce the water availability in the root zone. The resulting water stress will further suppress the plant photosynthesis and transpiration. However, this effect may not be significant since the plant growth over forest region is more frequently limited by light availability instead of water availability.

The main mechanisms involved in the above interpretation are summarized by Figure 4-9.

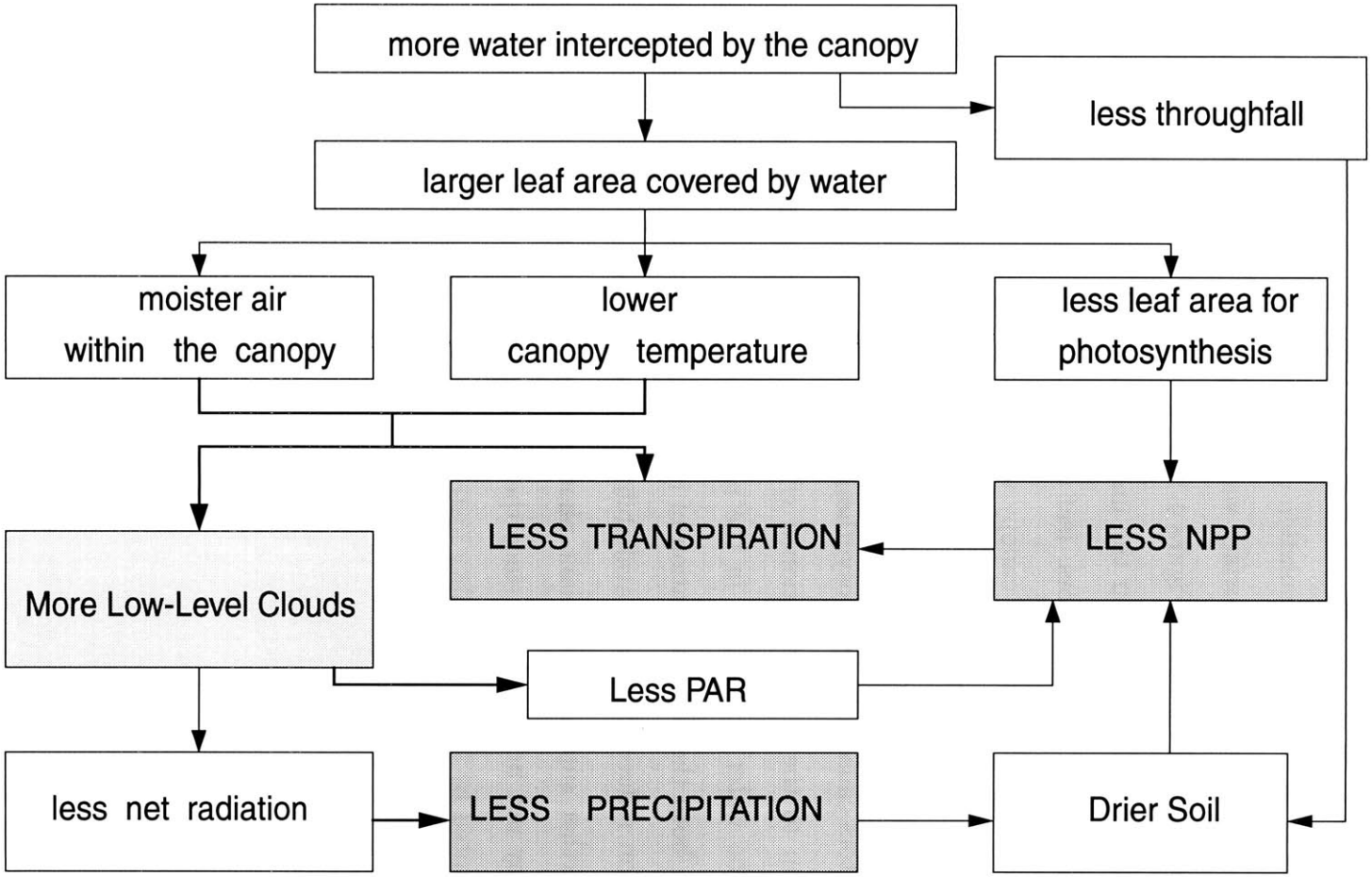

Figure 4-9: Mechanisms through which the neglect of the sub-grid rainfall variability impacts the broad aspects of the biosphere-atmosphere system.

4.4.3 Interpretation of Results for the Grassland Region

The physical mechanisms responsible for the error propagation over the forest region are also valid over the grassland region. However, these local factors may not play the dominant role in the grassland region, according to Figure 4-1(e,f). Climate over West Africa is under the influence of the West African monsoon circulation. As demonstrated in Figures 4-7 and 4-8, the assumption of uniform rainfall distribution causes a monsoon circulation that is weaker but penetrates further inland, which results in a northward expansion of the monsoon rain belt at the expense of a rainfall decrease in the south. Therefore, over the grassland in the north, rainfall is overestimated in the uniform case (Figure 4-1e). As a response to this excessive water availability, the total evapotranspiration and NPP are all overestimated (Figure 4-1).

4.5 Role of Cloud Feedback in Error Propagation

Analyses in section 4.4 suggest that the cloud feedback plays an important role in propagating the errors associated with the misrepresentation of rainfall interception. To further validate the above interpretation, here we investigate the sensitivity of the model results to cloud feedback by conducting two experiments, one uniform and one variable. These two experiments are the same as their counterparts described in Section 4.3 but without the cloud feedback, i.e., the cloud cover for the experiments of this section is prescribed, instead of predicted by the model. Here the fractional cloud cover in both experiments are fixed at the same value, which is derived from the seasonal cycle of the cloud cover predicted by the variable experiment in Section 4.3.

The role of cloud feedback in error propagation can be demonstrated from comparisons between experiments with prescribed clouds (in this section) and those with interactive clouds (in Section 4.3). Figure 4-10(a,b) presents the results for the interception loss and transpiration at the same scale as Figure 4-1(a,b); Figure 4-10(c,d) presents the results for the precipitation and NPP at the same scale as Figure 4-1(e,f). Although a significant difference between the uniform case and the variable

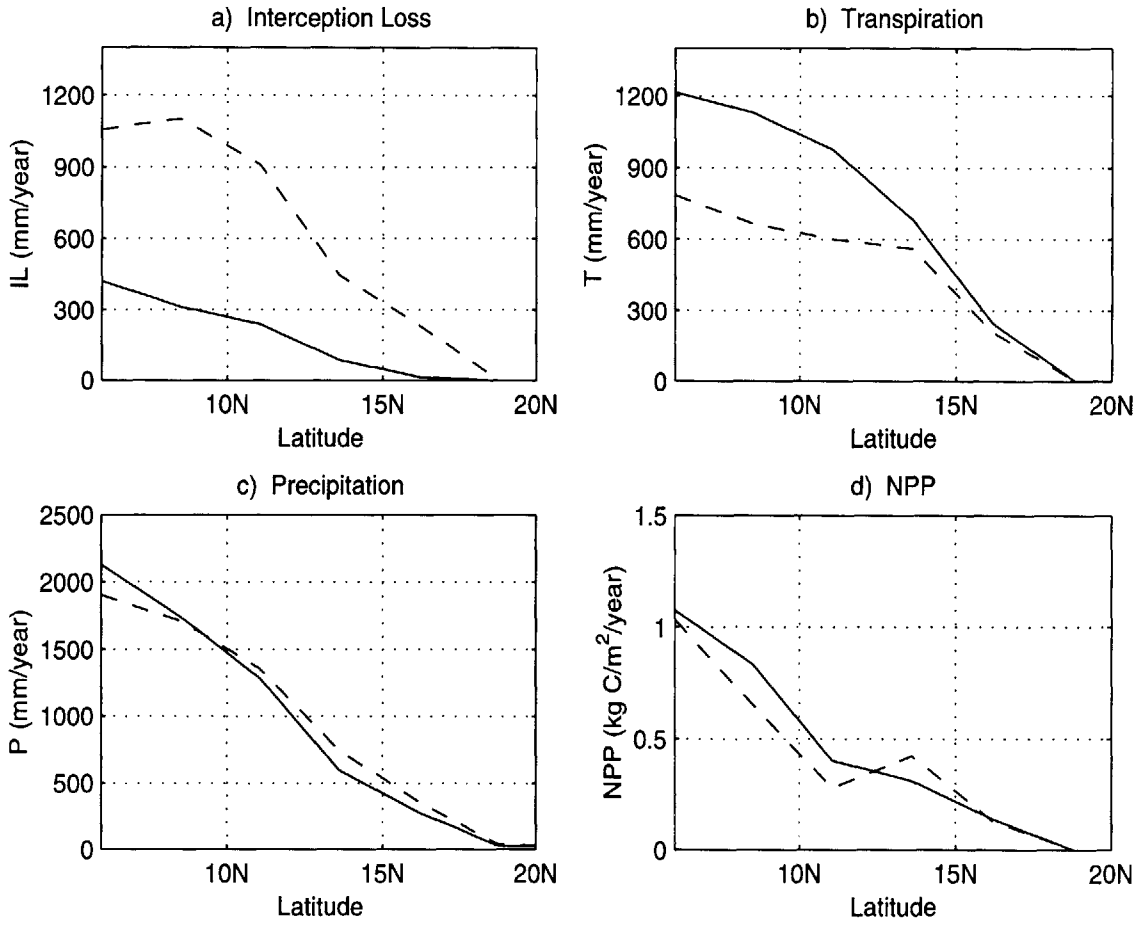

Figure 4-10: The comparison between the uniform case (dash line) and the variable case (solid line) for: a) Interception loss; b) Transpiration; c) Precipitation; d) Net primary productivity. Similar to Figure 4-1, but with prescribed cloud cover, and the cloud fractional cover in the uniform case is the same as in the variable case.

case still exists in the partition of evapotranspiration between interception loss and transpiration, the differences in precipitation as well as in NPP are much smaller when no cloud feedback is allowed (Figure 4-10(c,d), compared with Figure 4-1(e,f)). The cloud feedback is responsible for most of the precipitation difference between the uniform case and the variable case shown in Figure 4-1e. Of the difference in NPP in Figure 4-1f, about one half is attributed to the cloud feedback.

4.6 Error Propagation via Vegetation Dynamics

In the above simulations, a static vegetation distribution was used and the effect of vegetation dynamics was not considered. However, since the representation of rainfall sub-grid variability affects the estimation of the net primary productivity, further error propagation is expected when vegetation dynamics are included. To address this issue, two experiments are designed, one uniform and one variable, which are the same as the experiments described in Section 4.3 but with dynamic vegetation. The vegetation distribution described in Section 4.3 is used as the initial vegetation condition. The synchronously coupled biosphere-atmosphere system is then allowed to evolve towards its equilibrium state.

It takes 3-4 decades for the simulations in both experiments to reach an equilibrium. Here we use the leaf area index, precipitation, and NPP to represent the equilibrium state. Figure 4-11a presents the growing-season leaf area index (LAI) for trees at the equilibrium in both the uniform (dash line) and the variable (solid line) experiments, compared with the initial condition (dot line). A similar comparison is made for herbaceous plants in Figure 4-11b. In general, trees in the variable experiment grow denser, but become less dense in the uniform experiment. In contrast, the herbaceous plants in the uniform case are significantly denser than the initial condition. These vegetation changes are associated with other changes in the biosphere-atmosphere system. For example, Figure 4-11(c,d) show the precipitation and NPP at equilibrium in both the uniform and the variable experiments. Comparing Figure 4-11(c,d) with Figure 4-1(e,f) suggests that the differences in both the

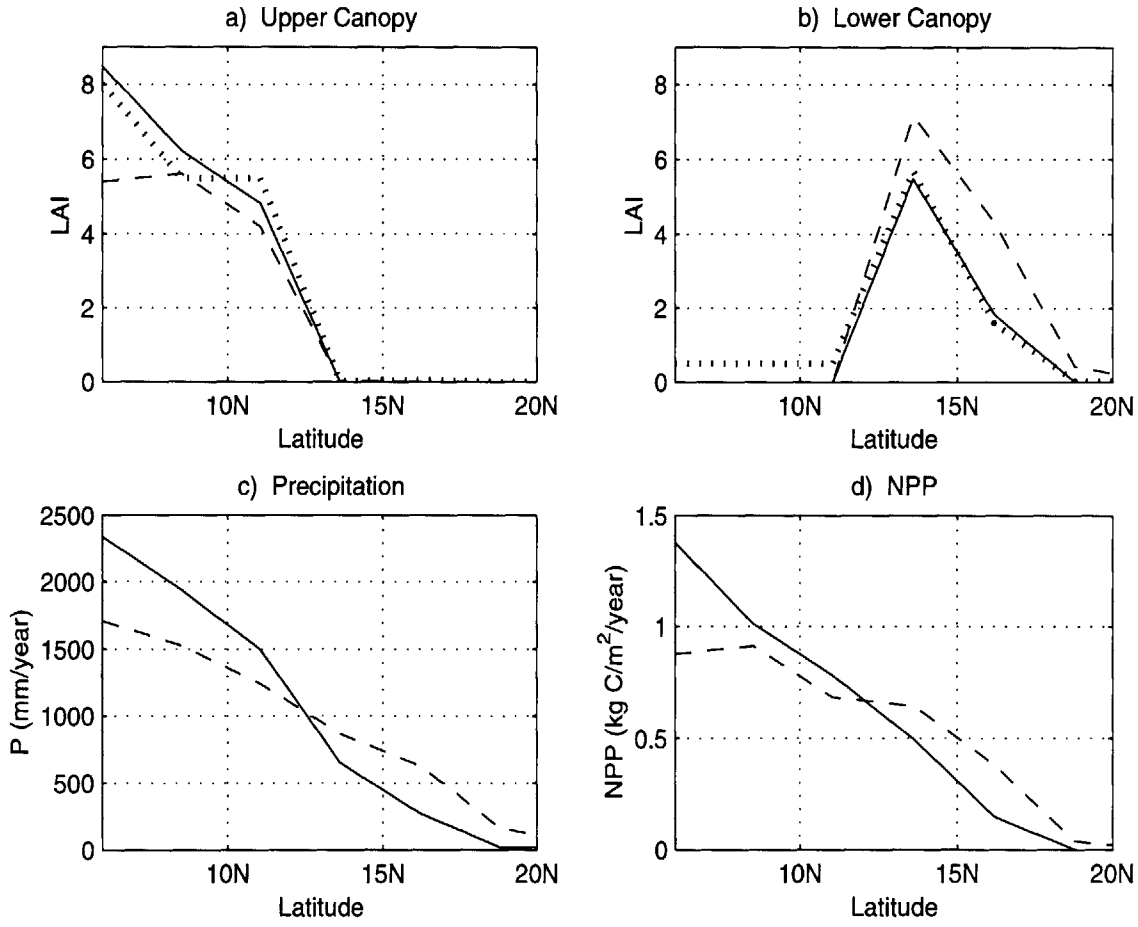

Figure 4-11: Comparison of the equilibrium state between the uniform case (dash line) and the variable case (solid line). a) Leaf area index for the upper canopy; b) Leaf area index for the lower canopy; c) Precipitation; d) Net primary productivity. The dot line in a) and b) represents the LAI at the initial condition.

precipitation and NPP between the uniform case and the variable case are enhanced by vegetation dynamics, especially over the grassland region. The bias caused by neglecting the rainfall sub-grid variability drives the biosphere-atmosphere system into a different equilibrium state.

4.7 Conclusions

This chapter carries out a case study on the impact of rainfall sub-grid variability on climate modeling using a coupled biosphere-atmosphere model. This study provides evidence for the need for great physical realism in modeling the coupled biosphere-atmosphere-ocean system. One important finding is that a climate model may succeed in accurately simulating the total evapotranspiration while misrepresenting the canopy hydrology, and the bias in the canopy hydrology would introduce significant errors in the broad aspects of the biosphere-atmosphere system. Several conclusions can be drawn from our results:

1) Neglecting the rainfall sub-grid variability may not cause noticeable bias in the simulation of total evapotranspiration. However, interception loss is significantly overestimated and transpiration is significantly underestimated. At the same time, runoff is significantly underestimated.

2) Even though the total evapotranspiration remains the same, the error in its partitioning between interception loss and transpiration causes significant differences in the atmospheric processes: moister atmosphere, more low-level clouds, smaller sensible heat flux, and weaker monsoon circulation. These errors result in an underestimation of precipitation over the forest region in West Africa. However, over the grassland region, an overestimation of precipitation results, because the local factors associated with the representation of sub-grid rainfall variability are dominated by large-scale factors involving gradient of the boundary layer entropy.

3) Among biospheric processes, NPP for the forest is significantly underestimated when the rainfall sub-grid variability is neglected. Over the grassland region where plant growth is limited by water availability, NPP is overestimated due to the over-

estimation of precipitation.

4) The low-level cloud feedback plays an important role in propagating the errors in surface hydrology to both atmospheric processes and biospheric processes.

5) Vegetation dynamics further propagate the resultant errors by changing the state of the biosphere, which then feeds back to the atmosphere and eventually leads to a different biosphere-atmosphere equilibrium. This resultant equilibrium features denser vegetation in the grassland region but less dense vegetation in the forest region.

While previous studies focused on the impact of the sub-grid variability on the simulation of land surface processes, the investigation of our study extends to the broad aspects of climate modeling including the simulation of the biosphere, the atmosphere, and the biosphere-atmosphere equilibrium. In addition, a considerable effort has been devoted to understanding the mechanisms of error propagation. However, at this stage we only focus on the sub-grid variability of rainfall interception and did not consider the importance of land surface heterogeneity (Koster and Suarez, 1992; Seth *et al.*, 1994; Giorgi and Avissar, 1997; Giorgi, 1997). Also, there has been no consideration for the impact of rainfall sub-grid variability on the infiltration and runoff generation. The lack of treatment for these sub-grid land surface processes and properties may have an impact on the general applicability of the results from this study. While a full study on the heterogeneity of land surface properties remains a topic of future research, a simple mosaic approach for the representation of land surface heterogeneity is adopted in Chapter 7 of this thesis.

Part II

Two-Way Biosphere-Atmosphere Interactions

This part of the study uses the coupled biosphere-atmosphere model developed in Part I, and focuses on interpreting the observed characteristics of the West African climate, including the dominance of low-frequency variability and the persistence of the current Sahel drought. Chapter 5 explores the multiple-equilibrium nature of the regional climate system over West Africa, which provides the theoretical basis for further studies in this part; Chapter 6 investigates the physical mechanisms for the observed low-frequency rainfall variability over West Africa; Chapter 7 studies the potential causes for the Sahel drought in the twentieth century. The most fundamental finding is that the two-way biosphere-atmosphere interactions involving ecosystem dynamics can act as an important physical mechanism for both the low-frequency variability of the Sahel rainfall and the persistence of the current drought.

Chapter 5

Multiple Climate Equilibria and Climate Transition

This chapter studies the behavior of the biosphere-atmosphere system which includes a natural dynamic ecosystem. We first develop a theoretical understanding of the two-way biosphere-atmosphere feedback by considering the role of ecosystem dynamics, and describe the conditions under which the climate system may have multiple equilibrium states coexisting under the same precessional forcing. We then demonstrate the multiple climate equilibria and climate transitions between different equilibria using the coupled biosphere-atmosphere model ZonalBAM which was introduced and tested in Part I. The multiple-equilibrium behavior of this regional climate system provides a theoretical basis for understanding the natural climate variability over West Africa.

5.1 Theory and Hypothesis

Vegetation plays a prominent role in the exchange of energy, moisture, momentum, and carbon between the land surface and the atmosphere. Removal of vegetation modifies the local energy balance and the local water cycle. According to Eltahir (1996), the deforestation-induced reduction in net radiation causes a decrease in the total heat flux from the surface, which is the source of energy and entropy for the

atmospheric boundary layer; on the other hand, the degradation of vegetation causes an increase of the surface temperature therefore an increase of the sensible heat flux, which is associated with a larger boundary layer depth. As a result, the moist static energy within a unit depth of the boundary layer decreases, so does the boundary layer entropy (BLE). The lower BLE over the land favors less local convective rainfall, a weaker monsoon circulation, and less monsoon rainfall over West Africa (Eltahir and Gong, 1996). Therefore, a drier climate results following vegetation degradation. However, this response does not necessarily point to a positive feedback that was frequently suggested by previous studies (see the review in Chapter 1). Whether a feedback is positive or negative depends not only on the response of the atmospheric climate to vegetation changes, but more importantly, on the response of vegetation to the induced change in the atmospheric climate. Here a feedback is defined as negative if it moderates the perturbation, and as positive if it enhances the perturbation.

In moist regions such as the tropical rain forest, it is often the energy availability, instead of the water availability, that limits the plant growth. Therefore, a rainfall decrease within a certain range has negligible effect in limiting the plant growth. Even in arid regions such as the Sahel where plant growth is limited by water availability, a rainfall reduction caused by desertification still does not necessarily trigger a positive feedback. With the degradation of vegetation, the water demand of the vegetation community would also decrease. Most likely, rainfall following the vegetation degradation may not fulfill the water requirement to maintain the pre-perturbation vegetation. However, it may still be enough for the maintenance and further growth of the post-perturbation vegetation. Under this circumstance, the biosphere-atmosphere feedback will be negative, and will drive the system towards its pre-perturbation state, although sometimes it may not fully recover. If the reduced rainfall cannot support the post-perturbation vegetation, the biosphere-atmosphere feedback will be positive, and the vegetation degradation will be enhanced therefore self-perpetuating.

Based on the above analysis, when a perturbation occurs to a biosphere-atmosphere system at equilibrium, the system may respond in three qualitatively different ways: a negative feedback leading to a full recovery; a positive feedback leading to a perturba-

tion enhancement; a negative feedback leading to a partial recovery. When a positive feedback takes place, or when a negative feedback only leads to a partial recovery, the biosphere-atmosphere system will develop into a different equilibrium state. Therefore, we propose that the biosphere-atmosphere system can have multiple equilibrium states coexisting under the same precessional forcing, with the two-way biosphere-atmosphere feedback acting as the mechanism for both the climate persistence at one equilibrium and the climate transition towards another.

A system with multiple equilibria can be described using the example of a ball moving on a simple landscape, as shown in Figure 5-1. Here the full circle represents an equilibrium climate system, and the shaded circle marks the extent of the perturbation imposed on the system. When a perturbation occurs, the response of the system depends on both the perturbation magnitude and the status of the post-perturbation system relative to its neighboring equilibria. With perturbation of increasing magnitude, the system falls into different response zones in sequence, as shown in case "a", "b", and "c" of Figure 5-1, where "a", "b", and "c" respectively represent the case of a full recovery, a perturbation enhancement, and a partial recovery. The climate system can remain around one equilibrium under the influence of small perturbations (i.e., climate persistence) until a large enough perturbation leads the system towards a different equilibrium (i.e., climate transition). It is worth emphasizing that, when the perturbation is large enough, the transition to a different equilibrium may take place via a negative feedback which leads to a partial recovery.

This hypothesis not only applies to anthropogenic vegetation perturbations, it also applies to natural variations in the large-scale atmospheric or oceanic processes. The biosphere-atmosphere system responds to both types of disturbances in similar ways. A large disturbance may develop into a persistent anomaly, while a small disturbance may be wiped out through the two-way feedback between the biosphere and the atmosphere.

The possibility of multiple equilibria has been suggested by several previous studies (e.g., Nicholson, 1989; Entekhabi *et al.*, 1992), but lacked a clear demonstration prior to this study. A series of studies on this topic were carried out by Claussen (1997,

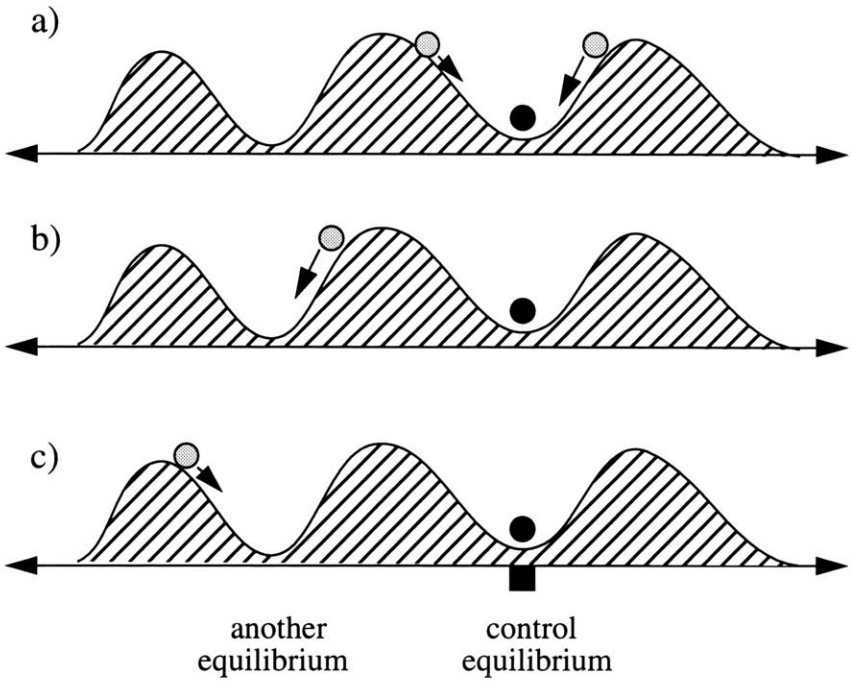

Figure 5-1: The movement of a ball on a simple landscape, as an analogy of the climate system with multiple equilibria. The three cases represent the system's responses to different perturbations: a) small perturbations: a negative feedback leads to a full recovery; b) larger perturbations: a positive feedback leads to a new equilibrium; c) perturbations even larger: a negative feedback leads to a new equilibrium.

1998), who used the asynchronously coupled ECHAM-BIOME model to investigate the sensitivity of the model's equilibrium to its initial vegetation conditions. The ECHAM-BIOME model found two equilibrium solutions in North Africa and Central East Asia. However, as pointed out in Chapter 1, BIOME is an equilibrium vegetation model which cannot simulate ecosystem dynamics, and the coupling between ECHAM and BIOME is asynchronous. These two limitations make it difficult for the Claussen (1997, 1998) study to address the issue of multiple equilibria which is closely related to the synchronous biosphere-atmosphere coupling as well as ecosystem dynamics. Moreover, using an equilibrium vegetation model such as BIOME, it is impossible to address whether and how the climate can actually make a transition between different equilibria. Here, we study the topic of multiple equilibria using the newly developed model ZonalBAM, which is a synchronously coupled biosphere-atmosphere model and includes explicit representation of ecosystem dynamics. Section 5.2 presents the sensitivity of the coupled biosphere-atmosphere system to initial conditions; Section 5.3 demonstrates the existence of multiple climate equilibria and the possibility of climate transitions by studying the resilience of the coupled biosphere-atmosphere system with respect to perturbations.

5.2 Sensitivity of the Biosphere-Atmosphere System to Initial Conditions

5.2.1 Experiments Design

One necessary condition for a system to have multiple equilibria is its sensitivity to initial conditions. Using ZonalBAM, experiments are carried out to test the sensitivity of the synchronously coupled biosphere-atmosphere system to its initial vegetation distribution. First, for the highest sensitivity, the two extremes of initial vegetation distributions are considered: a West Africa uniformly covered by rain forest and a West Africa uniformly covered by desert. Second, an initial vegetation distribution similar to today's condition is also considered.

In the sensitivity experiments, the land-ocean boundary is set at $6°N$, with land in the north and ocean in the south. The Atlantic sea surface temperature is fixed at its climatology (1950-1979) (Reynolds and Smith, 1994), averaged over $10°W - 10°E$. Since a zonally symmetric model cannot correctly simulate the atmospheric circulation in mid-latitudes and the related biosphere-atmosphere feedback as well, we only apply vegetation dynamics to the region of $6°N - 27°N$. Under the extreme initial vegetation distributions considered here, the simulated climate is expected to be very different from the current climate not only within but also beyond the tropics. Therefore, we choose not to fix the land surface fluxes and other properties beyond the tropics at their climatological values. Instead, here we fix the vegetation north of $27°N$ at short grass and let the model compute the surface fluxes and temperature.

5.2.2 Results Analysis

In each of the sensitivity experiments, initialized with different vegetation distributions, the coupled model ZonalBAM is run until it reaches equilibrium. For all the cases considered here, it takes several decades for the model to reach an equilibrium. Comparison between the final equilibrium states shows that the modeled biosphere-atmosphere system is indeed sensitive to its initial conditions.

Equilibria at the Extreme

When starting with forest everywhere, the coupled system evolves into an equilibrium (labeled as *F.I.C.*) with trees covering most of West Africa and grass covering a narrow band in the north (Figure 5-2a). When starting with desert everywhere, the coupled system develops into an equilibrium (labeled as *D.I.C.*) whose vegetation ranges from tall grass near the coast to short grass and desert in the north (Figure 5-2b). At equilibrium *F.I.C.*, woody plants reach as far north as 25°N, and no desert condition exists in West Africa; at equilibrium *D.I.C.*, the southern boundary of the desert is located south of 15°N, and no woody plants get established in West Africa. Consistent with the extreme difference in their vegetation distributions, equilibrium *F.I.C.* is

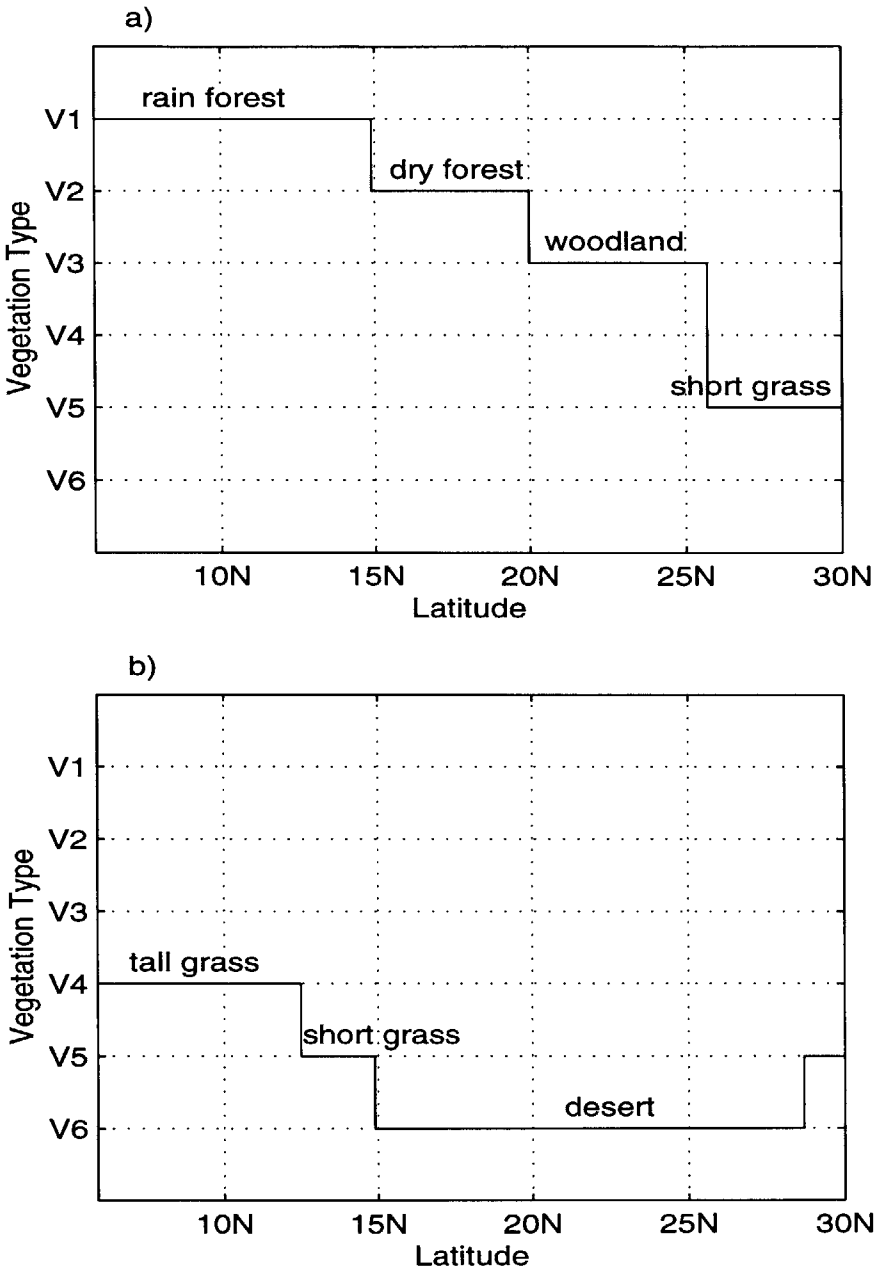

Figure 5-2: Vegetation distribution for a) Equilibrium *F.I.C.*; and b) Equilibrium *D.I.C.*. *F.I.C.* is the shortening of "Forest Initial Condition", and *D.I.C.* stands for "Desert Initial Condition". The vegetation types include V1 (rain forest), V2 (dry forest), V3 (woodland), V4 (tall grass), V5 (short grass), and V6 (desert).

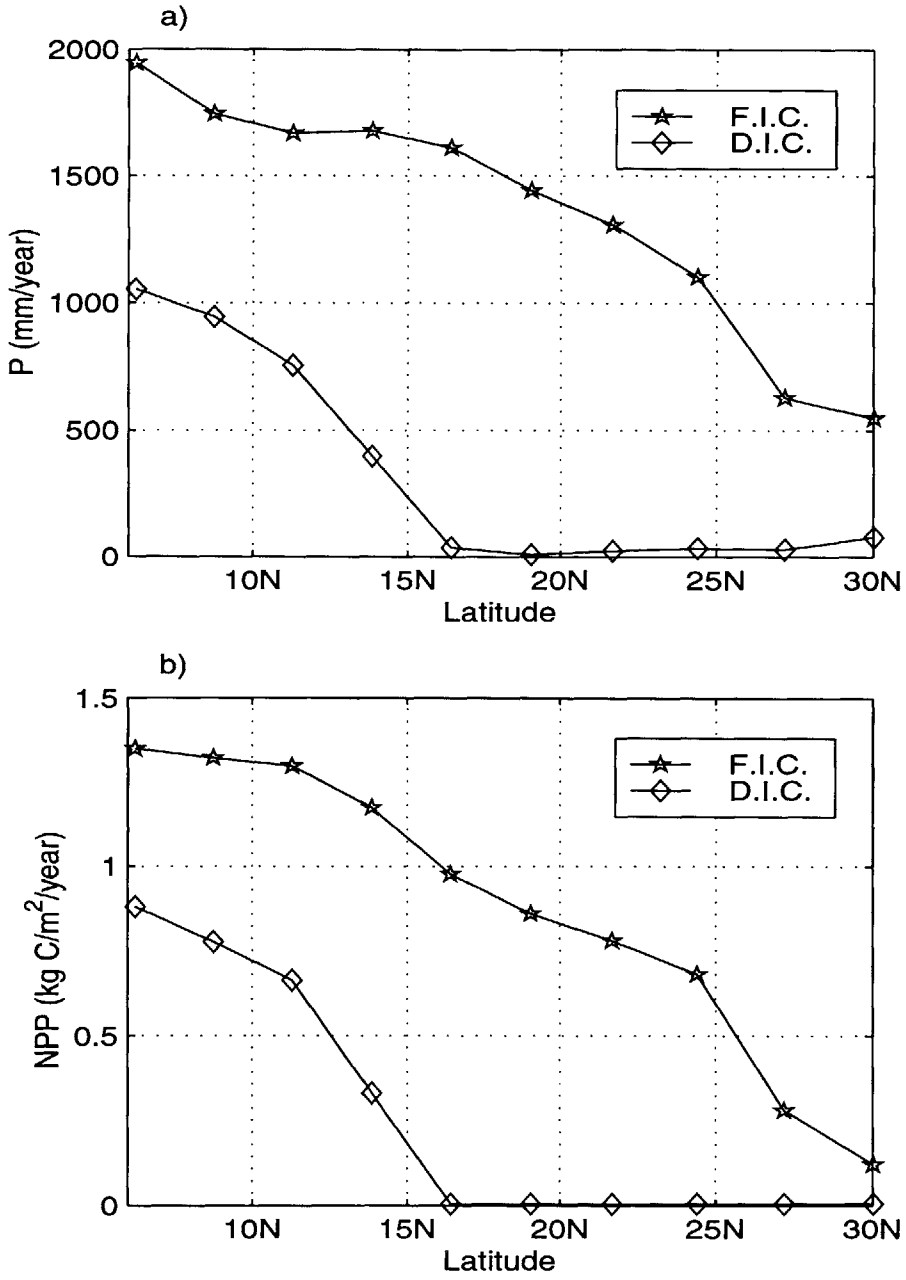

Figure 5-3: Comparison between equilibrium *F.I.C.* and equilibrium *D.I.C.*: a) Annual precipitation; b) NPP.

significantly wetter and more productive than equilibrium *D.I.C.*, as indicated by the distribution of the annual rainfall (Figure 5-3a) and NPP (Figure 5-3b). Due to the extreme nature of the two initial conditions, it is expected that equilibria *F.I.C.* and *D.I.C.* respectively represent the wettest (the most productive) and driest (the least productive) equilibria of the natural biosphere-atmosphere system under the current precessional forcing.

In the following we look in more detail at the differences between the two extreme equilibria. As shown by the rainfall seasonal cycle in Figure 5-4, the south-north extent of the rain belt of equilibrium *F.I.C.* is about twice as wide as that of equilibrium *D.I.C.*, which occurs mainly in the form of a northward expansion of the rain belt. During the dry season, the isohyet of 1-mm/day rainfall at equilibrium *D.I.C* is located at 6°N, while the 1-mm/day rainfall reaches as far north as 16°N at equilibrium *F.I.C.* However, no significant difference is observed in the magnitude of the peak rainfall. During the rainy season when the monsoon circulation develops, the magnitude of the peak rainfall increases from 5.5mm/day at equilibrium *D.I.C.* to about 9.0mm/day at equilibrium *F.I.C.*, and the location of the peak rainfall moves from 10°N to about 22°N. In addition, the 1-mm/day rainfall isohyet of equilibrium *F.I.C.* reaches as far north as 36°N, about 20° northward from that of the equilibrium *D.I.C.*. During the dry season, the differences in rainfall distribution mainly reflect the differences in evapotranspiration associated with the vegetation distribution (Figure 5-5). However, during the active monsoon season, the differences in rainfall distribution also reflect the differences in the intensity of the monsoon circulation between the two equilibria.

We compare the monsoon circulation between the two cases taking the peak monsoon season August as an example. As shown in Figure 5-6, the meridional wind (at both low levels and high levels) of equilibrium *F.I.C.* during August is more than twice as strong as that of equilibrium *D.I.C.*, which suggests that the monsoon circulation at equilibrium *F.I.C.* is much stronger (Figure 5-6). Correspondingly, for equilibrium *F.I.C.*, the rising branch of the monsoon circulation covers the whole West Africa and centers around 20°N; for equilibrium *D.I.C.*, this rising branch is

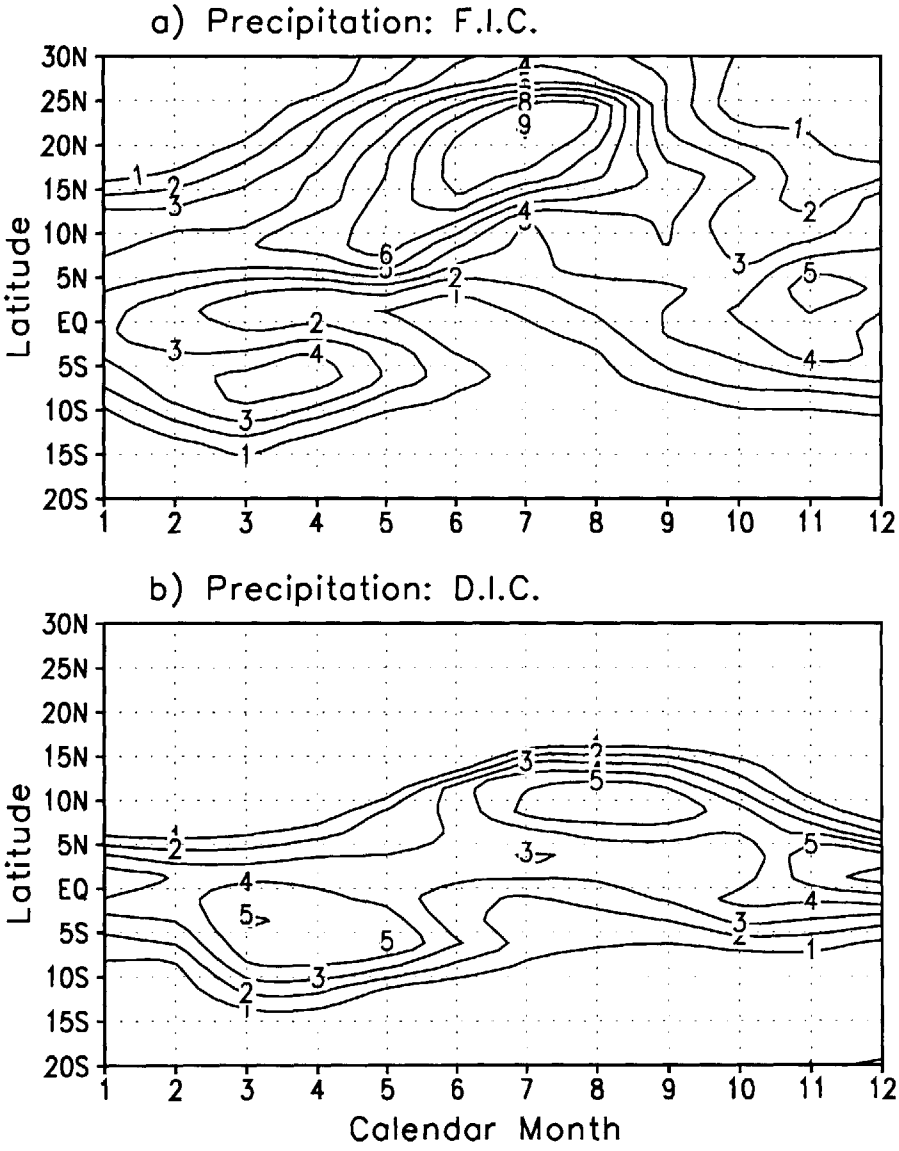

Figure 5-4: Seasonal cycle of rainfall, in *mm/day*: a) Equilibrium *F.I.C.*; b) Equilibrium *D.I.C.*.

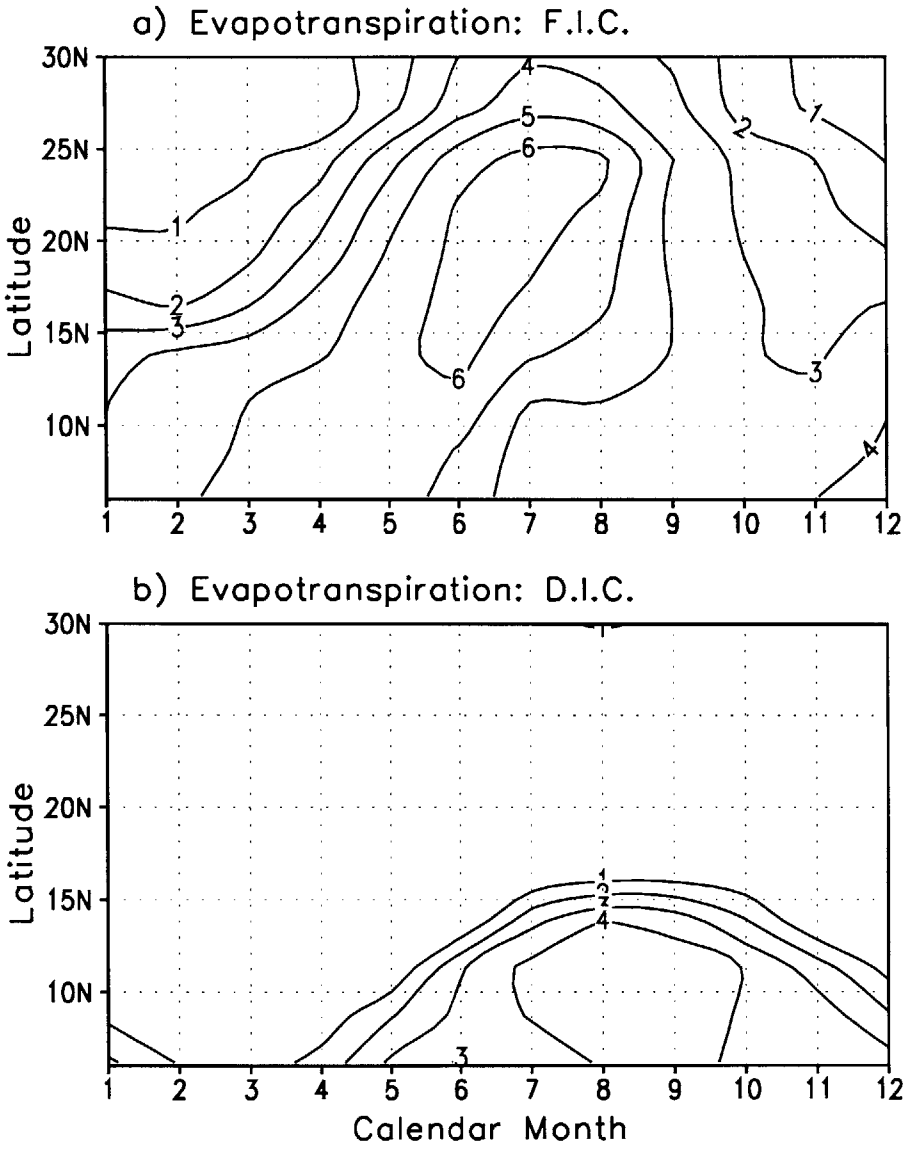

Figure 5-5: Seasonal cycle of the total evapotranspiration, in mm/day: a) Equilibrium *F.I.C.*; b) Equilibrium *D.I.C.*.

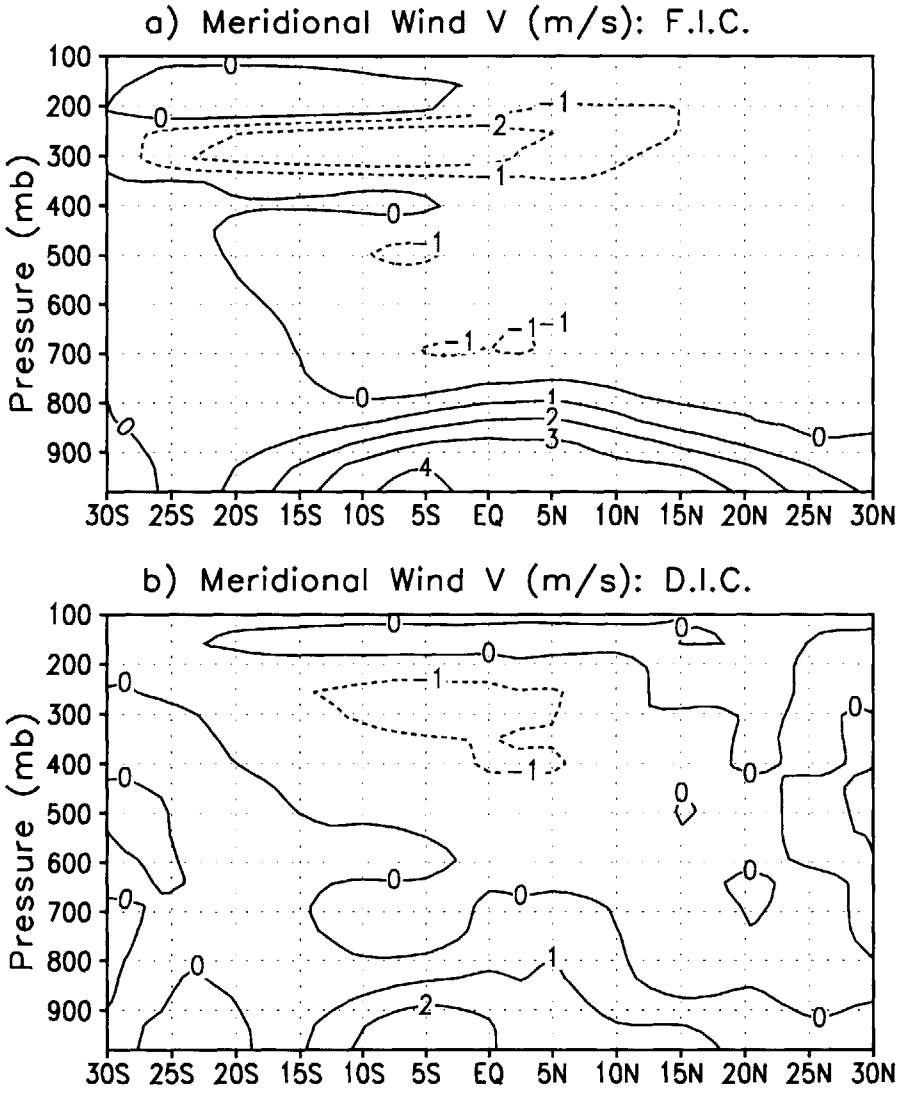

Figure 5-6: The meridional wind during the peak monsoon season August, in m/s: a) Equilibrium *F.I.C.*; b) Equilibrium *D.I.C.*.

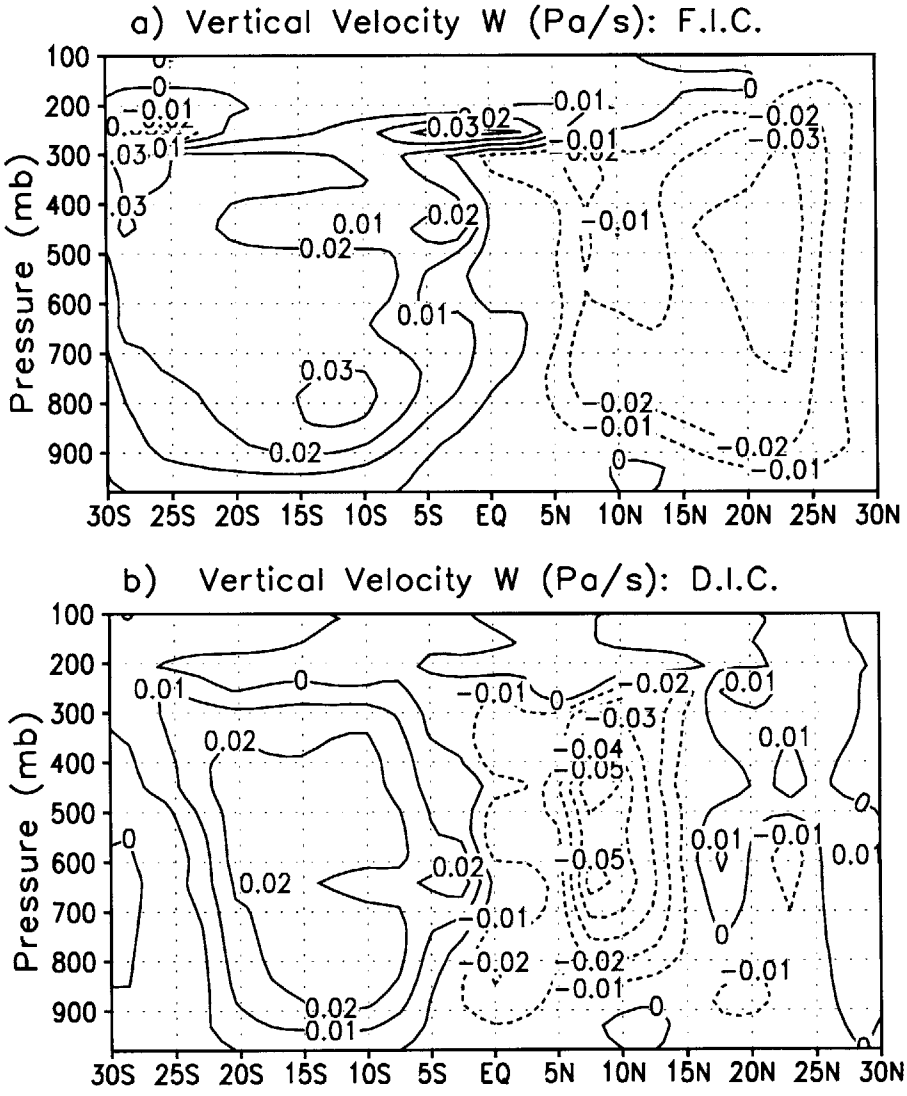

Figure 5-7: The vertical velocity during the peak monsoon season August, in Pa/s: a) Equilibrium $F.I.C.$; b) Equilibrium $D.I.C.$.

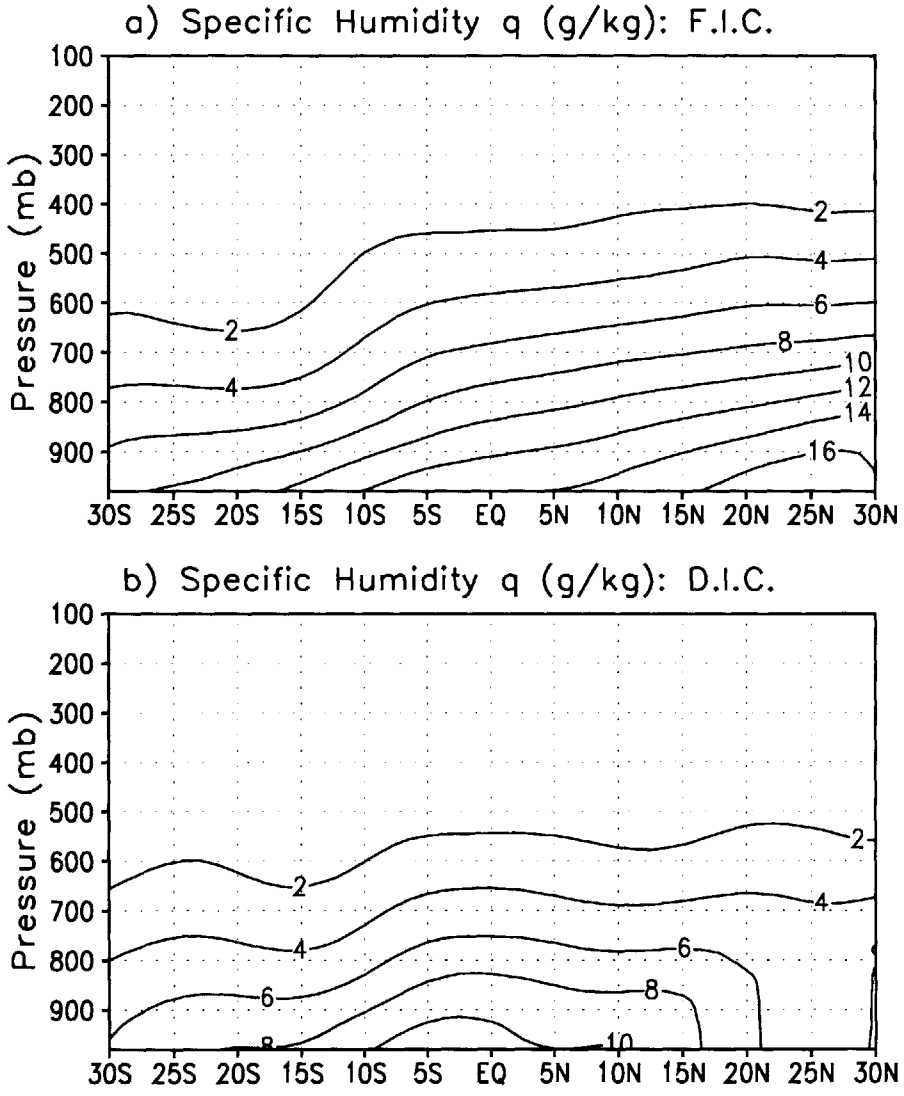

Figure 5-8: The specific humidity during the peak monsoon season August, in g/kg: a) Equilibrium *F.I.C.*; b) Equilibrium *D.I.C.*.

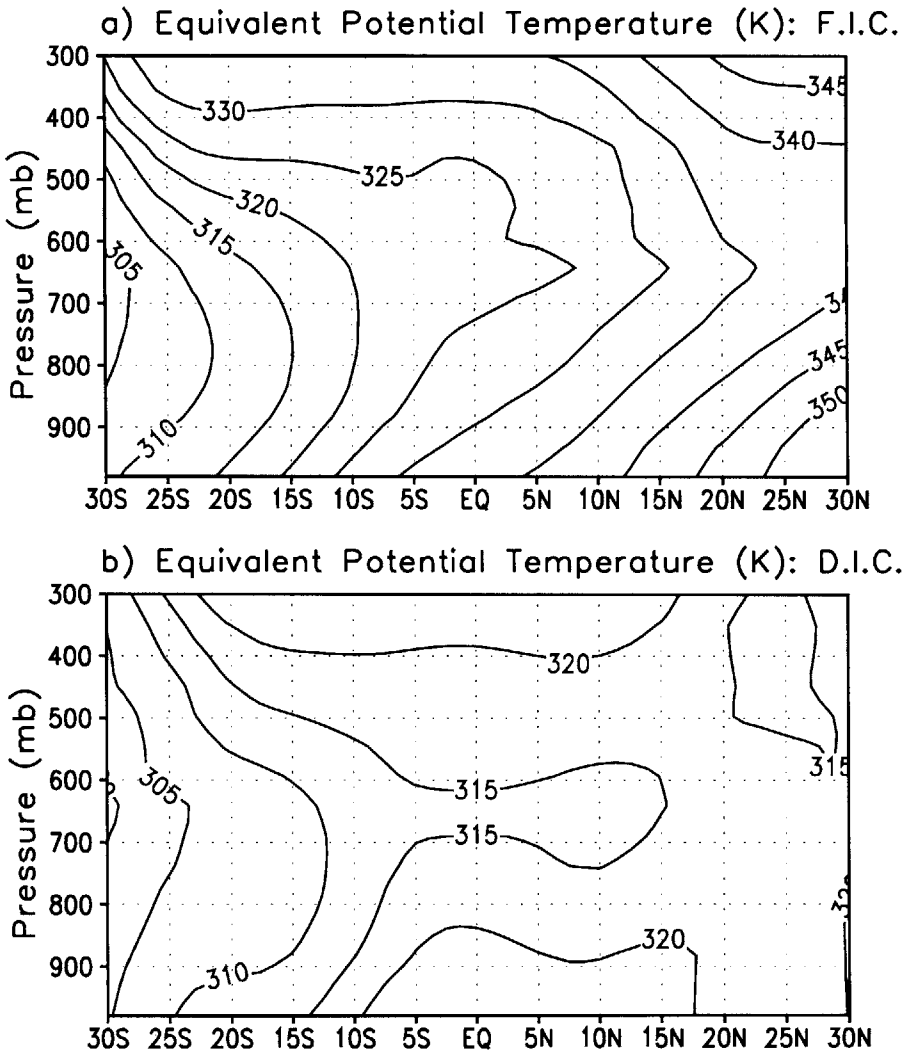

Figure 5-9: The equivalent potential temperature θ_e during the monsoon season August, in K. a) Equilibrium $F.I.C.$; b) Equilibrium $D.I.C.$. θ_e is an index for the moist entropy Θ: $\Theta = C_p\theta_e + const.$

located more southward, and only covers the region near the coast (Figure 5-7). Although the rising motion at the center of the rising branch is slower for equilibrium *F.I.C.*, it still generates more precipitation due to its higher content of atmospheric moisture (Figure 5-8). According to Eltahir and Gong (1996), the monsoon circulation in West Africa is driven by the gradient of the boundary layer entropy. The differences in monsoon intensity between the two equilibria presented in Figure 5-6 and 5-7 are consistent with their entropy distribution (Figure 5-9), which shows that the gradient of the boundary layer entropy from the ocean to the land for equilibrium *F.I.C.* is much larger.

For equilibrium *F.I.C.*, the dense vegetation all over West Africa provides the atmosphere with abundant water vapor supply in the form of evapotranspiration; at the same time, the strong monsoon circulation brings the moisture-abundant air from the ocean inland, which also increases the atmospheric humidity. While the latter is only effective during the monsoon season, the moistening effect due to evapotranspiration takes place throughout the year. As a result, as shown in Figure 5-10, the near-surface atmosphere at equilibrium *F.I.C.* is significantly moister than equilibrium *D.I.C.* all over West Africa and during the whole year.

Figure 5-11 presents the comparison of surface temperature between the two extreme equilibria. Equilibrium *F.I.C.* is generally warmer than equilibrium *D.I.C.*. However, a cooling of equilibrium *F.I.C.* is observed during the time and within the region of intense evapotranspiration, which moves gradually from the coast region northward from spring to summer. In general, denser vegetation favors higher net radiation at the surface, which tends to warm up the land surface; at the same time, the higher evapotranspiration associated with the denser vegetation has a cooling impact. The change of the surface temperature associated with vegetation changes depends on the balance between these two opposite effects. In a case of vegetation increase, the warming effect may be dominant during the dry season when there is no significant evapotranspiration, while the cooling effect may become dominant during the rainy season when the evapotranspiration is intense. The temperature comparison in Figure 5-11 shows this general trend. The response of surface temperature to

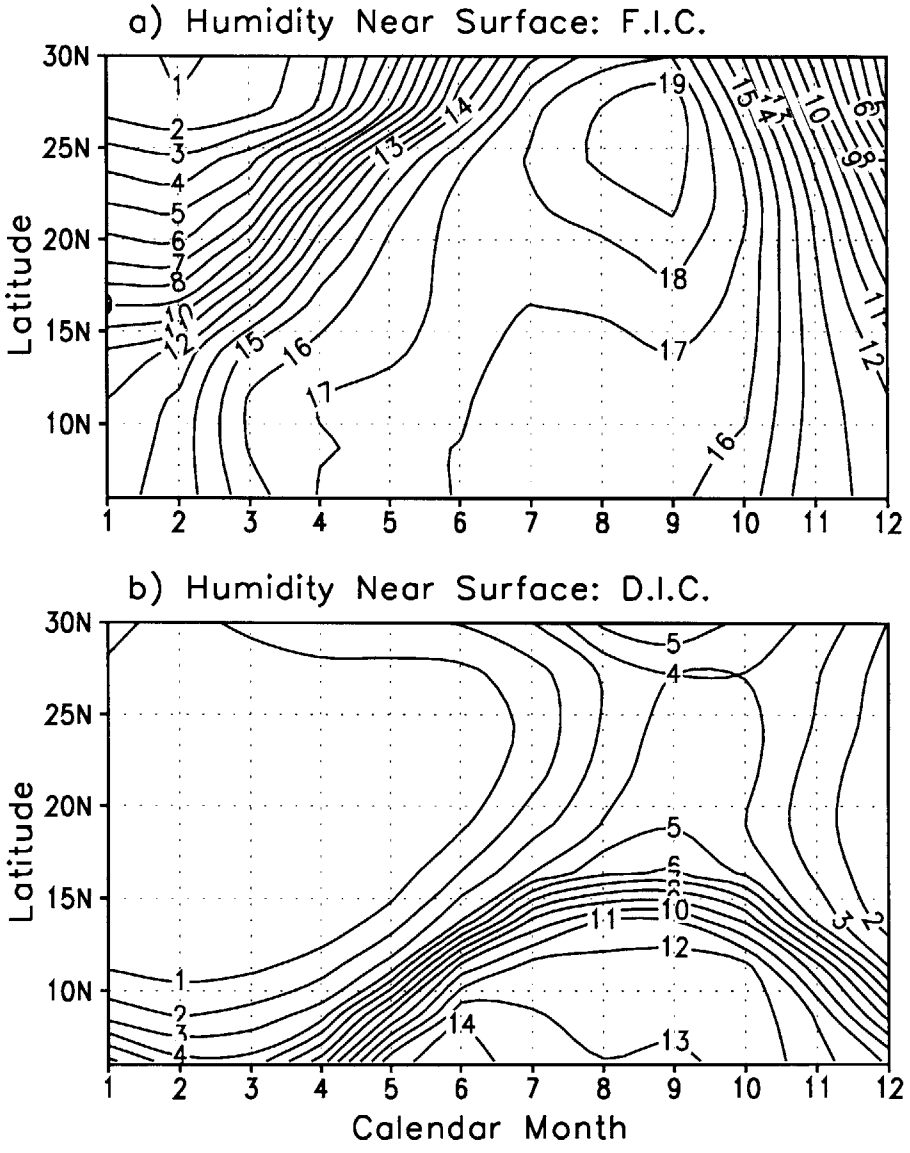

Figure 5-10: Seasonal cycle of the near-surface specific humidity, in g/kg: a) Equilibrium *F.I.C.*; b) Equilibrium *D.I.C.*.

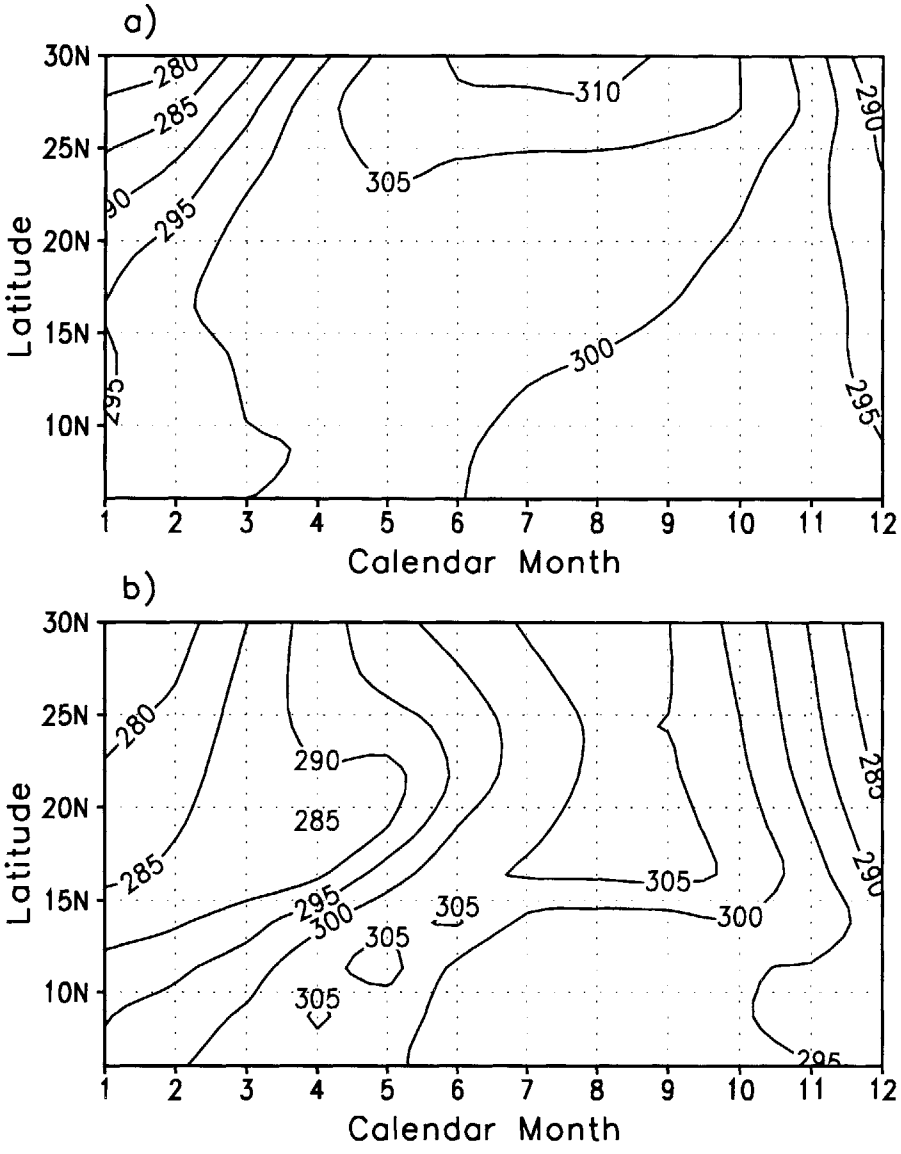

Figure 5-11: Seasonal cycle of the surface temperature, in K: a) Equilibrium *F.I.C.*; b) Equilibrium *D.I.C.*.

vegetation differences will be discussed in more detail in Section 5.3.

A Midway Equilibrium

Due to the extreme nature of their initial conditions, equilibria *F.I.C.* and *D.I.C.* respectively represent the wettest (the most productive) equilibrium and driest (the least productive) equilibrium of the natural biosphere-atmosphere system under the current precessional forcing. Other equilibria of the climate system will most likely fall in-between. To give an example for a midway equilibrium, we consider an initial vegetation distribution similar to today's observation: forest in the south, desert in the north, with savannah and grassland in between. Several experiments are carried out, with initial vegetation ranging from slightly thinner to slightly denser than the current condition.

Despite the differences in their initial vegetation distribution, within two to three decades, all the experiments converge into the same equilibrium state. The vegetation of this equilibrium (Figure 5-12), ranging from forest near the coast to grassland which borders the desert around 15°N, falls in between the two extremes *F.I.C.* and *D.I.C.* (Figure 5-2). This is also true for the precipitation and net primary productivity. Figure 5-13 shows that, in general, this midway equilibrium is wetter and more productive than equilibrium *D.I.C.*, but drier and less productive than equilibrium *F.I.C.*.

As shown in Figure 5-13, the statement that other equilibria would fall between the two extremes *F.I.C.* and *D.I.C.* only holds at the continental scale. The midway equilibrium presented here provides an example that this regional climate system can develop an equilibrium which is slightly wetter than equilibrium *F.I.C.* in a small sub-region but much drier in most of West Africa. However, at the continental scale, equilibrium *F.I.C.* is by far the wettest and the most productive.

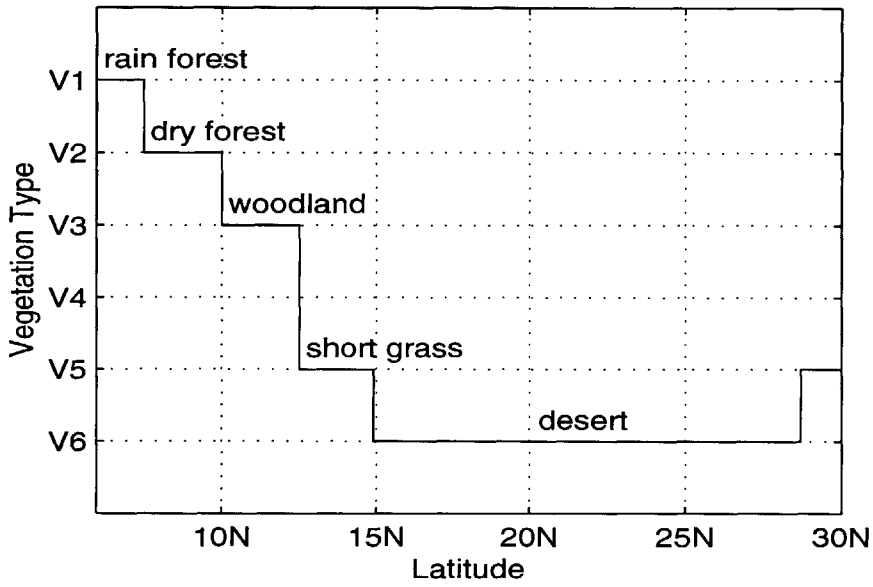

Figure 5-12: Vegetation distribution of a midway equilibrium. This equilibrium is derived by initializing the biosphere-atmosphere model with a vegetation distribution close to the current observation.

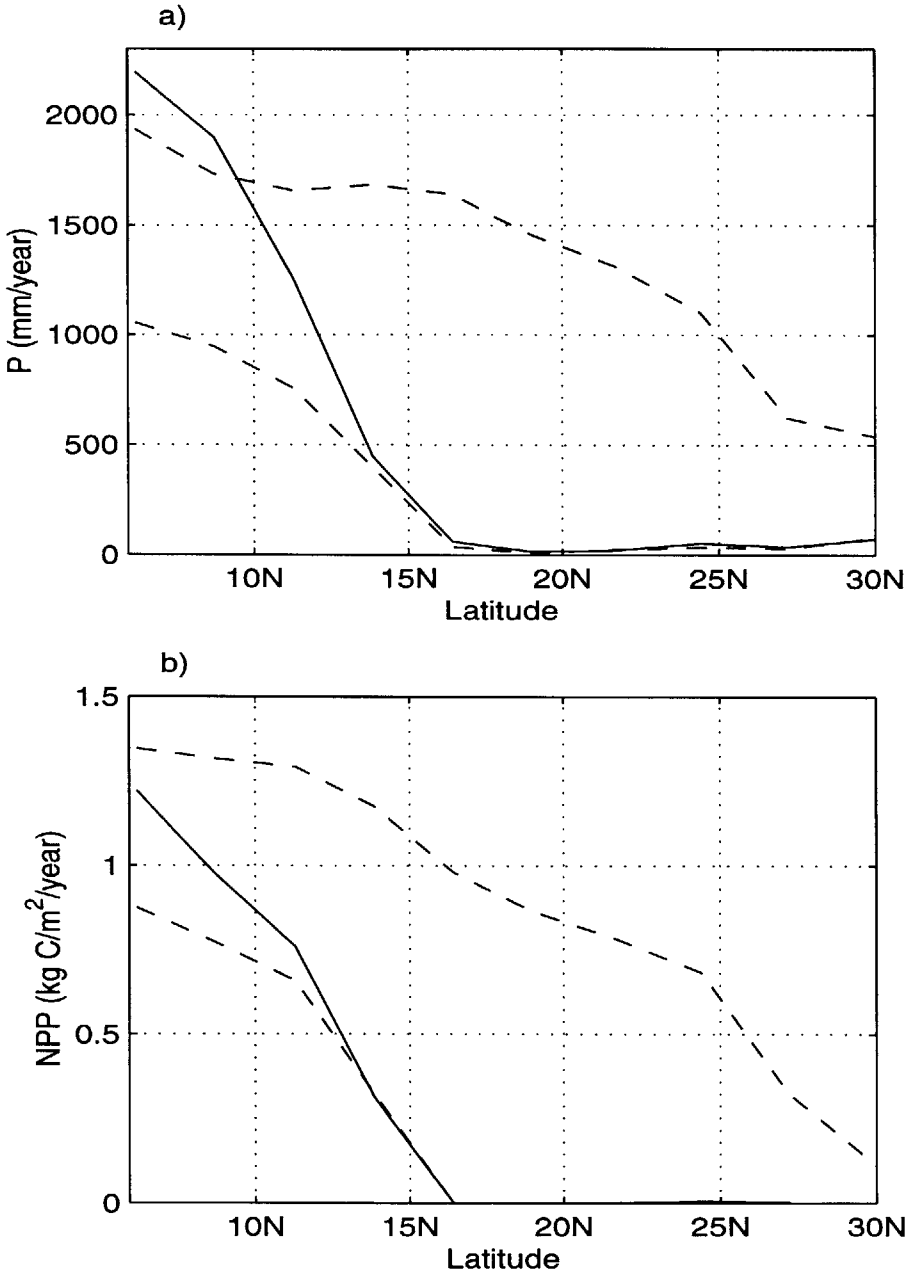

Figure 5-13: a) Precipitation and b) Net primary productivity of a midway equilibrium (solid line), whose vegetation distribution is shown in Figure 5-12. Dash lines present the results of the two extreme equilibria for comparison.

5.2.3 Summary

This section focuses on the sensitivity of the biosphere-atmosphere system to initial conditions. Our results support the conclusion that the coupled biosphere-atmosphere system is sensitive to its initial vegetation distribution. Depending on its initial condition, the coupled biosphere-atmosphere model has multiple equilibrium states coexisting under the same precessional forcing.

When initialized with an all-forest West Africa, the biosphere-atmosphere model evolves into an equilibrium with healthy vegetation cover all over West Africa; when initialized with an all-desert West Africa, an arid equilibrium results, which features grassland near the coast and desert condition over a large portion of West Africa. These two distinct equilibria represent the most productive (wettest) scenario and the least productive (driest) scenario of the biosphere-atmosphere equilibria over that region. Compared with the arid equilibrium, the equilibrium at the wet end features a northward expansion of the rain belt, more effective evapotranspiration, a stronger monsoon circulation, and a moister atmosphere. Both the biospheric climate and the atmospheric climate for other equilibria would most likely fall in between these two extremes.

More equilibria can be explored by dramatically changing the vegetation initial conditions. However, the purpose of this study is not to explore every single equilibrium of the coupled model. Instead, the objective here is to show that the coupled biosphere-atmosphere system is indeed sensitive to its initial conditions.

5.3 Resilience of the Biosphere-Atmosphere System

5.3.1 Introduction

Theoretically, the demonstrated sensitivity of the model equilibrium to initial vegetation distribution suggests the existence of multiple equilibria. However, it is not obvious whether the transition between different equilibria is physically possible. If the regional climate could not evolve from one equilibrium to another under the same precessional forcing within a reasonable time, the existence of multiple equilibria would be practically irrelevant to the observed climate variability over West Africa. To address the issue of climate transition between different equilibria, here we focus on the equilibria that are close to today's climate, and investigate the resilience of the biosphere-atmosphere system with respect to different types of perturbations using ZonalBAM. The model setup is the same as in Section 3.3, which is different from Section 5.2 in the assumption regarding the mid-latitudes. In particular, here the land surface fluxes and other properties beyond the tropics are fixed at their climatology based on NCEP re-analysis data so that the simulated climate system is close to its current state.

Used as the control equilibrium here is the "close-to-current" equilibrium found in Section 3.3, which is derived from 40 years of simulation using ZonalBAM initialized with today's land surface condition. Figure 5-14 shows the annual rainfall and net primary productivity (NPP) of this equilibrium. As shown in Section 3.3, this control equilibrium is close to, but slightly wetter and greener than, today's climate.

With respect to the control equilibrium, major land surface changes of different type and magnitude are added to the system in the 41st year of the simulation. Our study focuses on the impact of non-permanent perturbations – a perturbation takes place during the 41st year, then the landscape is allowed to evolve naturally through the two-way biosphere-atmosphere interactions. Three different types of perturbations are considered: deforestation, desertification, and irrigation. Here the

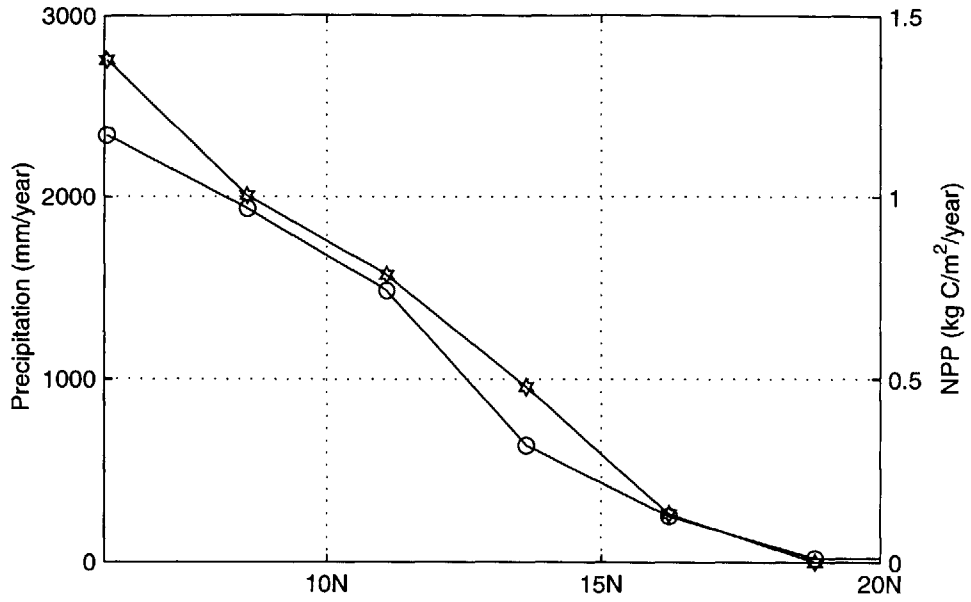

Figure 5-14: Precipitation (solid line with open circles) and NPP (solid line with hexagrams) at the control equilibrium state. This equilibrium is derived by starting the model with a vegetation distribution close to today's condition.

deforestation and desertification take place as a uniform thinning instead of a mosaic exposure of bare soil. Similarly, the effect of irrigation is simulated by a uniform increase of vegetation density.

According to the theoretical analysis in Section 5.1, climate transitions between different equilibria may take place as a response of the coupled biosphere-atmosphere system to perturbations. In the following, we demonstrate both the existence of multiple climate equilibria and the possibility of climate transitions using results of the perturbation experiments.

5.3.2 Deforestation

Deforestation is imposed to the forest and woodland region ($6°N - 12.5°N$) of the control equilibrium. A group of experiments have been performed, with deforestation ranging from mild selective logging (tree thinning) to forest clearing (the most severe form of deforestation). During the early stage of succession, in all these deforestation experiments, major precipitation reduction takes place. However, the biosphere-

atmosphere system can always fully recover from the deforestation perturbation. Here the case of forest clearing is presented as an example. In this experiment, a clear cut removes all the tree biomass over the whole forest and woodland region, leaving behind only the sparse ground vegetation that usually grows during the process of tree clearing.

Figure 5-15a shows the distribution of annual precipitation over West Africa before and after the clearing; Figure 5-15b and 5-15c present the growing season LAI for the upper and lower vegetation canopy, respectively. In the first year following the perturbation, rainfall over the perturbation zone decreases by 30-40% (Figure 5-15a). However, the post-perturbation rainfall is still as high as 1000-1500 $mm/year$, which is more than enough for the herbaceous ground vegetation to grow and prevail. As shown in Figure 5-15c, the sparse herbaceous vegetation becomes overwhelmingly dense within one year after the forest clearing. The quick colonization by herbaceous plants following a large-scale clear cut is consistent with ecological observations in the tropics. "*Succession in the wet tropical lowlands usually starts with rapid soil coverage by a mixture of weedy herbaceous plants and fast growing vines*" (Ewel, 1983). These dense herbaceous plants remain as the dominant vegetation for years to decades until trees eventually take over (Figure 5-15b,c). Interestingly, the grassland region north of the perturbation zone enjoyed a very wet period (Figure 5-15a) after the establishment of dense herbaceous plants in the deforested region and before the eventual take-over by woody plants. Correspondingly, the vegetation growth over the grassland region is enhanced during that period, as shown by the increase of growing season LAI in Figure 5-15c. After the recovery of the upper canopy over the perturbation zone, rainfall over the entire domain returns to its pre-perturbation level (Figure 5-15a).

The time it takes for the upper canopy to fully recover ranges from one decade near the coast to four decades at the northern boundary of the perturbation zone. Here the recovery of the upper canopy is measured using upper canopy LAI. To avoid confusion, it is worth pointing out that although the tree LAI and NPP reaches the pre-perturbation level within years after the selective logging and within decades after a clear cut, it takes much longer for the carbon storage to recover due to the slow

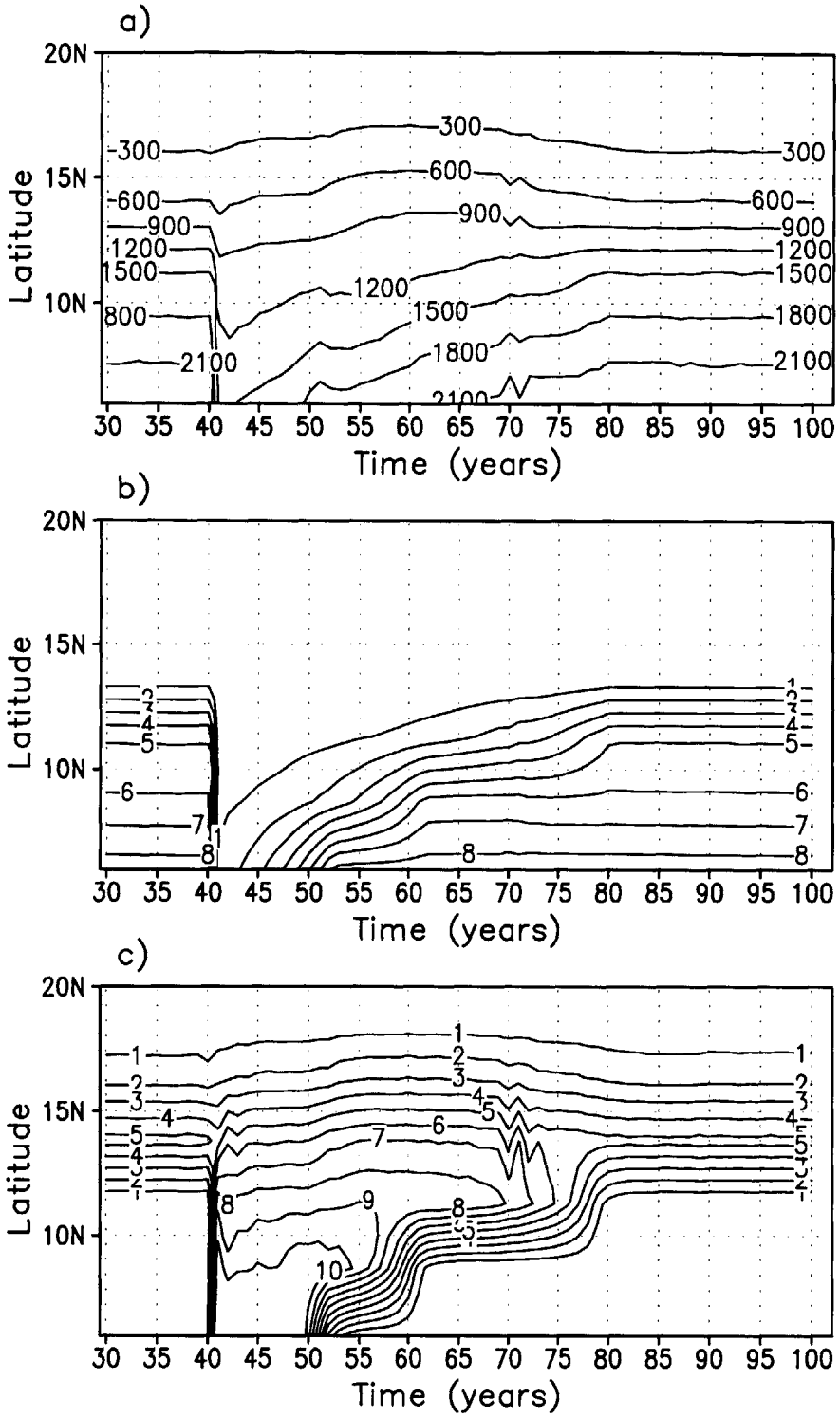

Figure 5-15: Evolution of the biosphere-atmosphere system before and after a forest clearing that takes place over the entire forest and woodland region in the 41st year of the simulation. a) Annual precipitation ($mm/year$); b) Growing-season LAI for the woody plants; c) Growing-season LAI for the herbaceous plants.

accumulation of woody biomass. According to Ewel (1971) and Golley (1975), leaf production is very high during the early stage of forest succession. The LAI for a secondary stand of six years old can be as large as the LAI for a well-stored mature forest (Golley *et al.*, 1975). It is the leaf area, not the woody biomass, that really matters for the biospheric production and the biosphere-atmosphere interactions. Therefore, in this study the biospheric state is defined based on the LAI instead of the carbon biomass.

As demonstrated in Figure 5-15, within the perturbation zone, the deforestation-induced biosphere-atmosphere feedback is negative, and this negative feedback leads to a full recovery. The biosphere-atmosphere system reaches its pre-perturbation equilibrium within four decades following the forest clearing. The recovery time is much shorter following selective logging. The event of rainfall enhancement in the grassland region during the process of forest succession is not observed in the selective logging experiments, when the deforestation is not severe enough to allow the development of a dense ground vegetation on the forest floor.

5.3.3 Desertification and Irrigation

The modeled desertification takes place at the grassland region of the control equilibrium, between $12.5°N$ and $17.5°N$. The vegetation is degraded in the form of a uniform grass thinning, which resembles the effect of grazing. A group of experiments have been carried out, with the severity of desertification increasing gradually. Compared with the system's response to deforestation, its response to desertification is more diverse – desertification of different magnitude can cause qualitatively different biosphere-atmosphere feedback. Here the results from four specific experiments (Exp1, Exp2, Exp3, and Exp4) are presented. In Exp1-Exp4, 50%, 60%, 75%, and 80% of the grass biomass are uniformly removed from the entire perturbation zone, and the induced exposures of bare soil are about 25%, 40%, 60%, and 75%, respectively. These four experiments are chosen because their induced biosphere-atmosphere feedbacks are close to the thresholds between different types of responses.

The impact of desertification on the biosphere-atmosphere system is rather local-

ized. In spite of the significant reduction in precipitation as well as NPP over the perturbed region immediately after desertification, the induced precipitation change over the forest and woodland region is relatively small compared to the large rainfall amount before the perturbation. Correspondingly, vegetation over the forest and woodland region show little detectable response. Therefore, the following analyses only focus on the response of the climate system over the grassland region, i.e., the perturbation zone, and take the grid point near $16°N$ as an example. For all the four experiments (and also Exp5 which is described later), the annual precipitation in each year before and after the perturbation is plotted in Figure 5-16a, and the growing-season LAI is plotted in Figure 5-16b. The evolutionary pattern is similar in other part of the perturbation zone as well as for other properties of the coupled biosphere-atmosphere system.

As shown by Figure 5-16(a,b), after removing 50% of the grass biomass (Exp1), the two-way biosphere-atmosphere interactions trigger a negative feedback, which drives the system back to its pre-perturbation equilibrium (labeled as equilibrium "A") within 10 years. However, when the fraction of grass removal increases to 60% (Exp2), a positive feedback takes place, which leads to a perturbation enhancement – both the precipitation and LAI further decrease with time after the perturbation. The biosphere-atmosphere system evolves into a different equilibrium state (referred to as equilibrium "B"). As the perturbation magnitude increases to 75% grass removal (Exp3), a negative feedback is encountered again, but only leads to a partial recovery – the system rebounds to a certain degree and evolves into the same equilibrium state as in Exp2. As the grass loss increases to 80% (Exp4), the biosphere-atmosphere feedback becomes positive again, which drives the system into a more arid equilibrium state (referred to as equilibrium "C"). The equilibrium "C" features desert condition at the grid point near $16°N$ where grassland exists at the control equilibrium. Induced by different degrees of desertification over the region $12.5°N - 17.5°N$, the biosphere-atmosphere system is able to evolve from the control equilibrium into two new equilibria.

To simulate the effect of irrigation, several experiments have been performed on

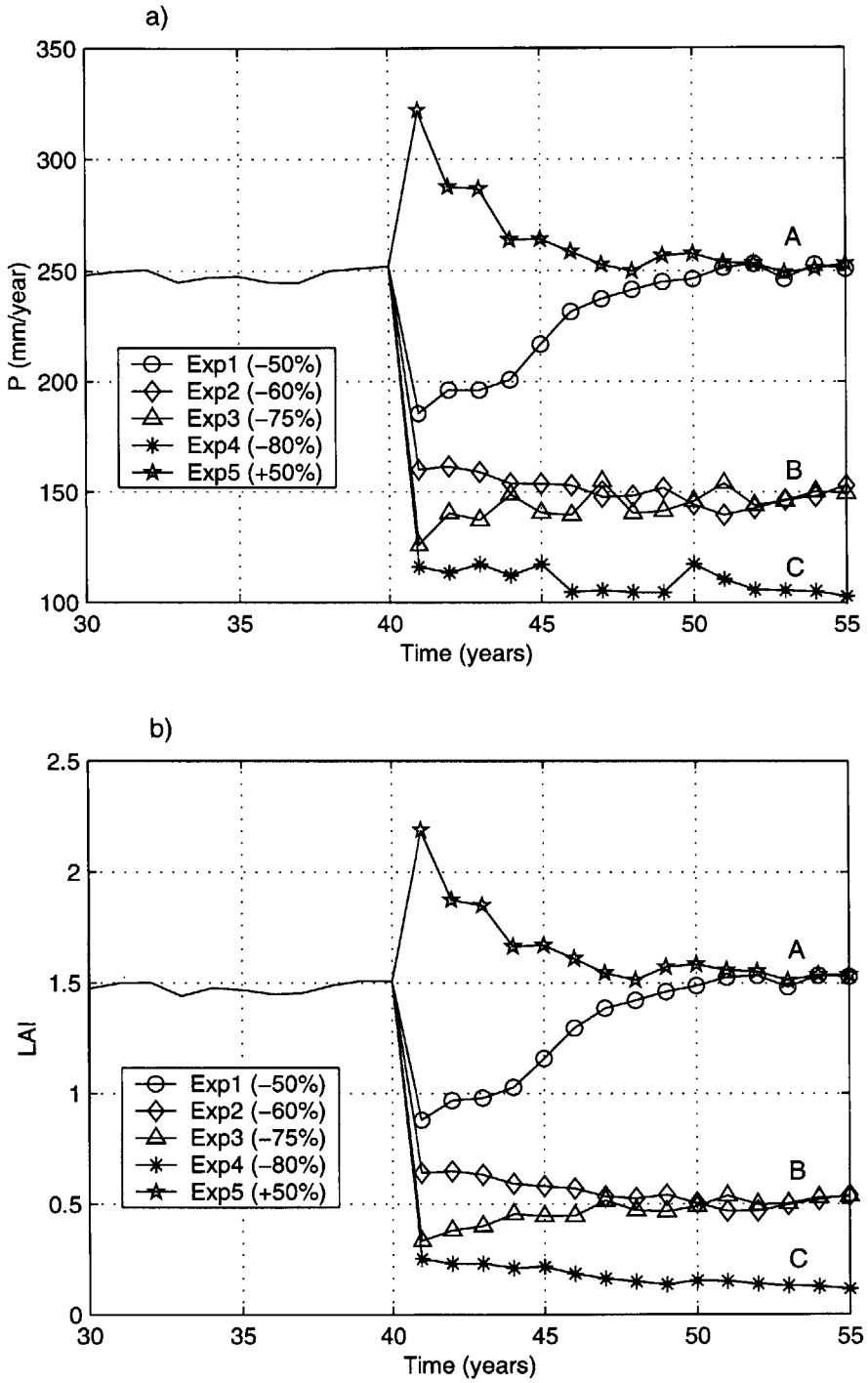

Figure 5-16: Evolution of the biosphere-atmosphere system before and after various perturbations that take place over the grassland region in the 41st year of the simulation. a) Precipitation at 16N; b) Growing-season LAI for grass at 16N.

the uniform increase of grass density over the grassland region $12.5°N - 17.5°N$. As an example, the LAI and annual precipitation near $16°N$ in experiment Exp5 are plotted in Figure 5-16a and b respectively. Exp5 features a 50% increase of the grass density over the entire grassland region. Although the climate in the year of irrigation is significantly wetter and greener, it gradually decays back to the control equilibrium. Interestingly, further increase of grass density fails to cause a transition of the biosphere-atmosphere system from the control equilibrium to a wetter one. The control climate presented in Figure 5-14 might be the most favorable equilibrium the climate system can maintain within the perturbation regime of this study, i.e., removal or enhancement of grass between $12.5°N$ and $17.5°N$.

As demonstrated clearly by Figure 5-16(a,b), experiments Exp1, Exp2, and Exp3 represent three different types of responses of the coupled biosphere-atmosphere system: a negative feedback leading to a full recovery (Exp1); a positive feedback leading to a perturbation enhancement (Exp2); and a negative feedback leading to a partial recovery (Exp3). The response of the climate system in experiment Exp4 is of the same type as Exp2, but within the attraction zone of a different equilibrium. Our modeling results support the theoretical hypothesis of Section 5.1 on the necessary conditions for the existence of multiple equilibria and on how the coupled biosphere-atmosphere system responds to non-permanent vegetation perturbations.

In the experiments presented above, vegetation degradation over the grassland region causes climate transitions from the control equilibrium to drier equilibria. These transitions are reversible. Further experiments demonstrate that, for the climate system at a drier equilibrium, favorable perturbations such as irrigation can trigger the system to develop into a wetter equilibrium. As an example, Figure 5-17 presents the change of the annual rainfall at 16°N after an irrigation effect is imposed to the biosphere-atmosphere system at the dry equilibrium "B". Here the irrigation features a 30% increase of grass density, which is a change of small magnitude given the low base value of the grass density at equilibrium "B". As shown in Figure 5-17, the irrigation perturbation induces a positive feedback which eventually leads the system to the wet equilibrium "A".

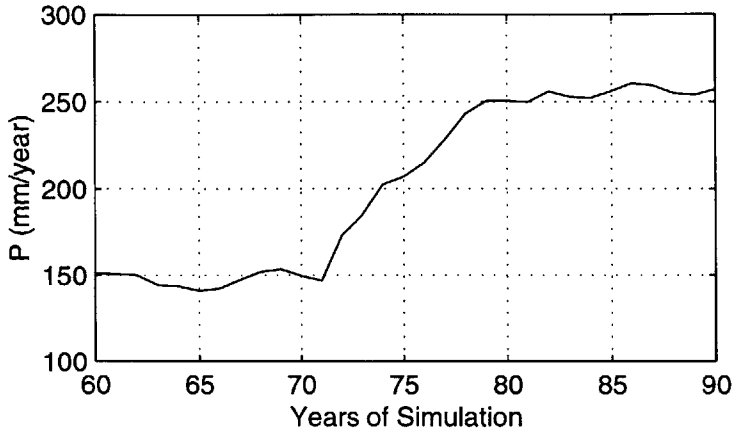

Figure 5-17: The evolutionary pattern for precipitation at 16N when an irrigation event occurs to the biosphere-atmosphere system at equilibrium "B" during the 72nd year of the simulation.

In summary, through desertification and irrigation experiments, it is demonstrated that the regional climate system over West Africa has multiple equilibrium states, and there are reversible transitions between the different equilibria.

5.3.4 Comparison Between Different Equilibria

Experiments on the resilience of the coupled biosphere-atmosphere system have explored three distinct climate equilibria over the region of West Africa: a wet equilibrium "A", a medium equilibrium "B", and a dry equilibrium "C". Figure 5-18(a,b) present the normalized differences between equilibrium "A" and the two drier equilibria, in annual rainfall and NPP, respectively. Although very little difference is observed over the forest region, both equilibria "B" and "C" are significantly drier and less productive than equilibrium "A" over the Sahel region. At the grid point near 16°N which is south of the desert border, the decrease of productivity from equilibrium "A" to "C" is up to 98%, which reflects a southward expansion of the Sahara desert. This is consistent with the significant vegetation loss as shown in Figure 5-16. In the following, using equilibrium "C" as an example, we present in more detail the characteristics of the arid climate equilibrium in comparison with the wetter and

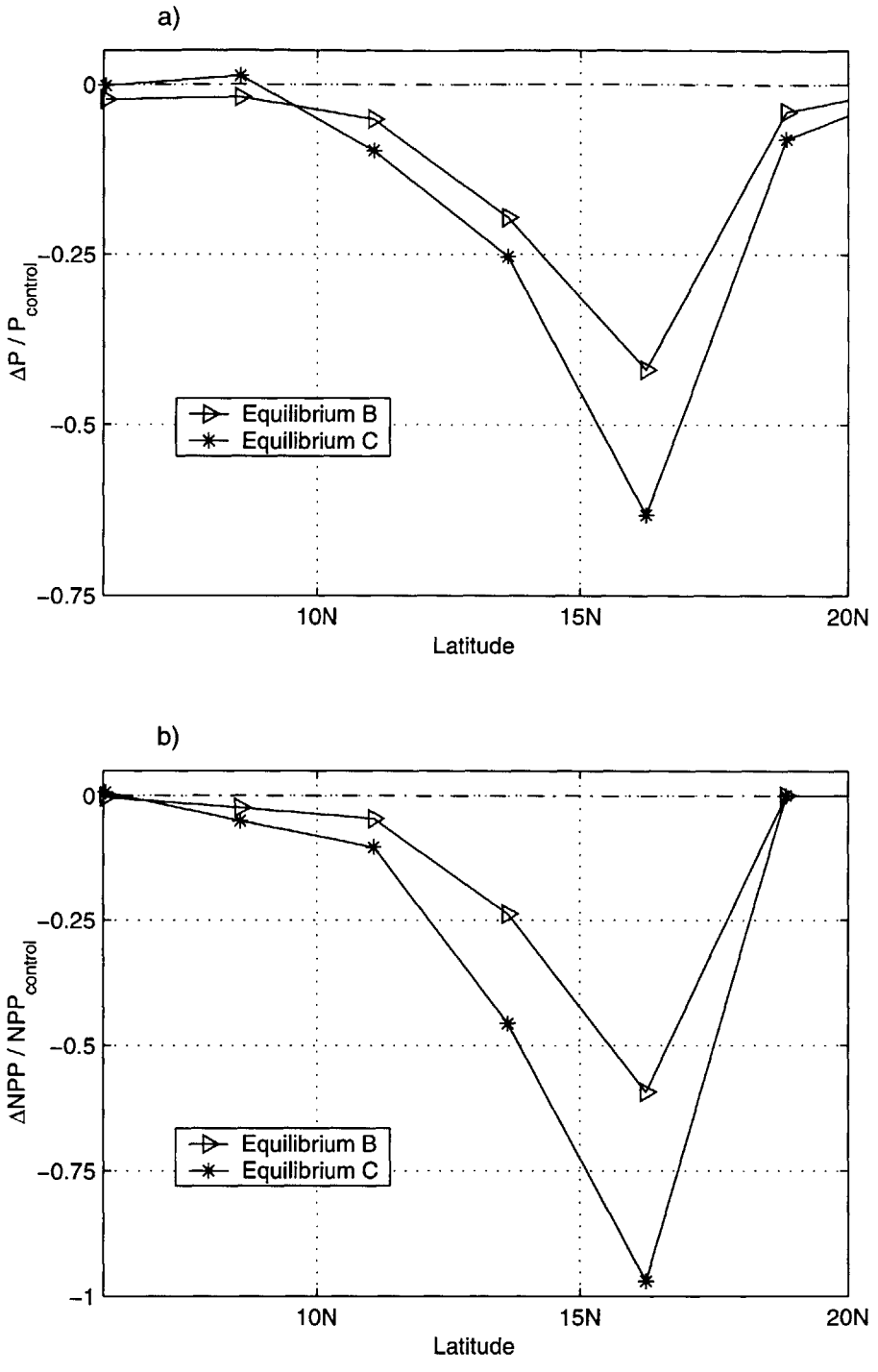

Figure 5-18: The normalized difference between the control equilibrium ("A") and the new equilibria ("B" & "C"): a) Precipitation; b) NPP.

greener equilibrium "A".

Figure 5-19 presents the comparison of rainfall seasonal cycle between equilibria "A" and "C". Over the Sahel region, the rainy season of equilibrium "C" is significantly drier than that of equilibrium "A"; at the same time, equilibrium "C" is slightly wetter near the coast region in the south, which signals a slight southward shift of the rain belt. Correspondingly, during the rainy season, the local ascending motion for equilibrium "C" over most part of the Sahel region is weaker, and this difference can be as much as 50% around $15°N$ in August (Figure 5-20). As already reflected by the slight rainfall increase, the ascending velocity in the south is slightly higher. Figure 5-21 presents the comparison of the meridional wind field in August between equilibria "A" and "C". At low levels, equilibrium "C" features a slightly weaker northward wind across the coast, which signals a slightly weaker monsoon circulation.

The differences in the Sahel rainfall between equilibria "A" and "C" also reflect the differences in the local atmospheric circulation. Vegetation degradation results in a reduction in the net surface radiation including both the short-wave and long-wave components (Eltahir, 1996). Therefore, the net radiation for equilibrium "C" is lower than equilibrium "A", as shown in Figure 5-22. This causes a reduction in the total heat flux from the surface (i.e., the sum of the sensible and latent heat fluxes), which is the energy supply for the atmospheric boundary layer. At the same time, as will be shown later, the sparse vegetation at equilibrium "C" favors higher surface temperature during the rainy season, which causes higher sensible heat flux. Therefore, the boundary layer depth of equilibrium "C" is larger than equilibrium "A". Together with the lower energy supply for the entire boundary layer, this results in a significantly lower moist static energy for equilibrium "C" (Figure 5-23). This decrease of energy reduces the likelihood of the local convection. At the same time, the thinner vegetation at equilibrium "C" provides the atmosphere with less water vapor supply in the form of evapotranspiration, thus causing drier atmospheric conditions (Figure 5-24). Both the weaker local convection and the lower atmospheric humidity reduce the local convective rainfall.

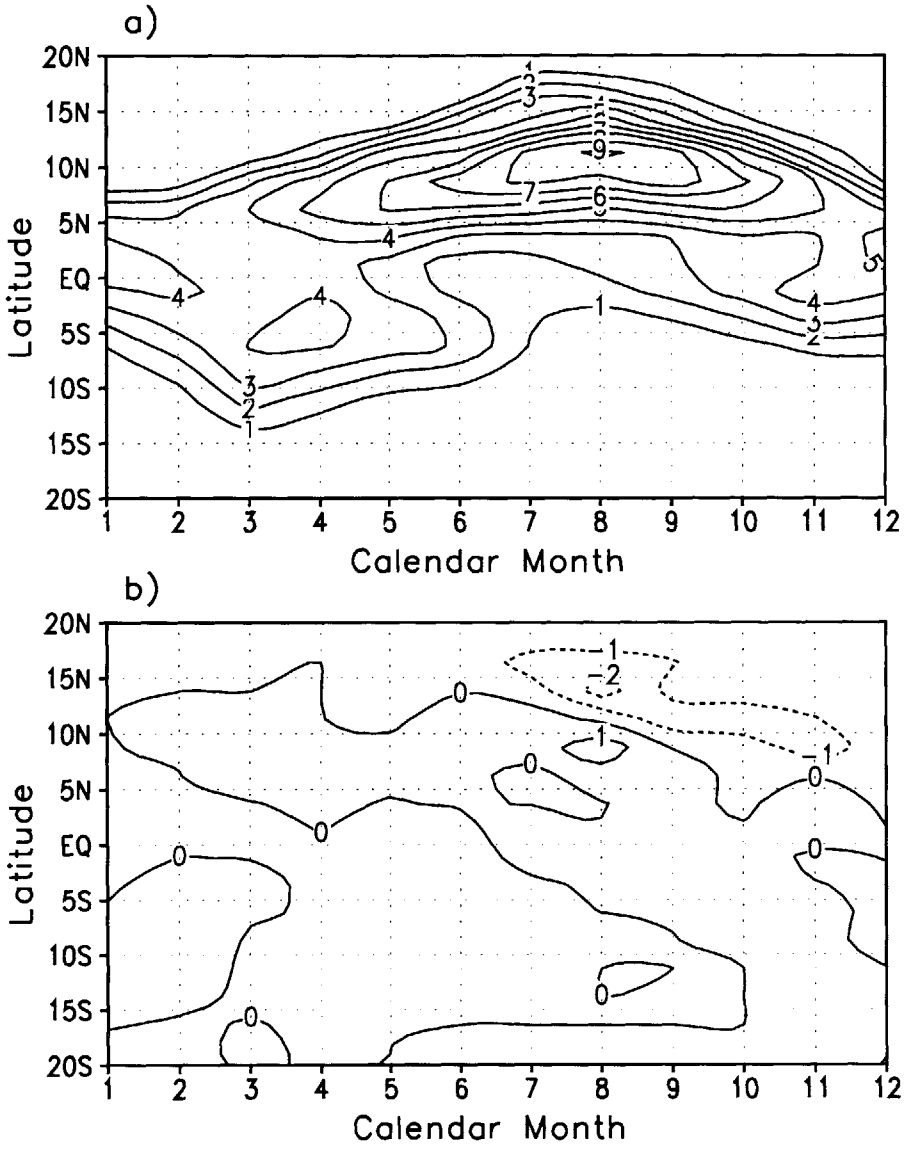

Figure 5-19: The rainfall seasonal cycle, in *mm/day*. a) Equilibrium "A"; b) The difference between equilibria "C" and "A": "C" - "A".

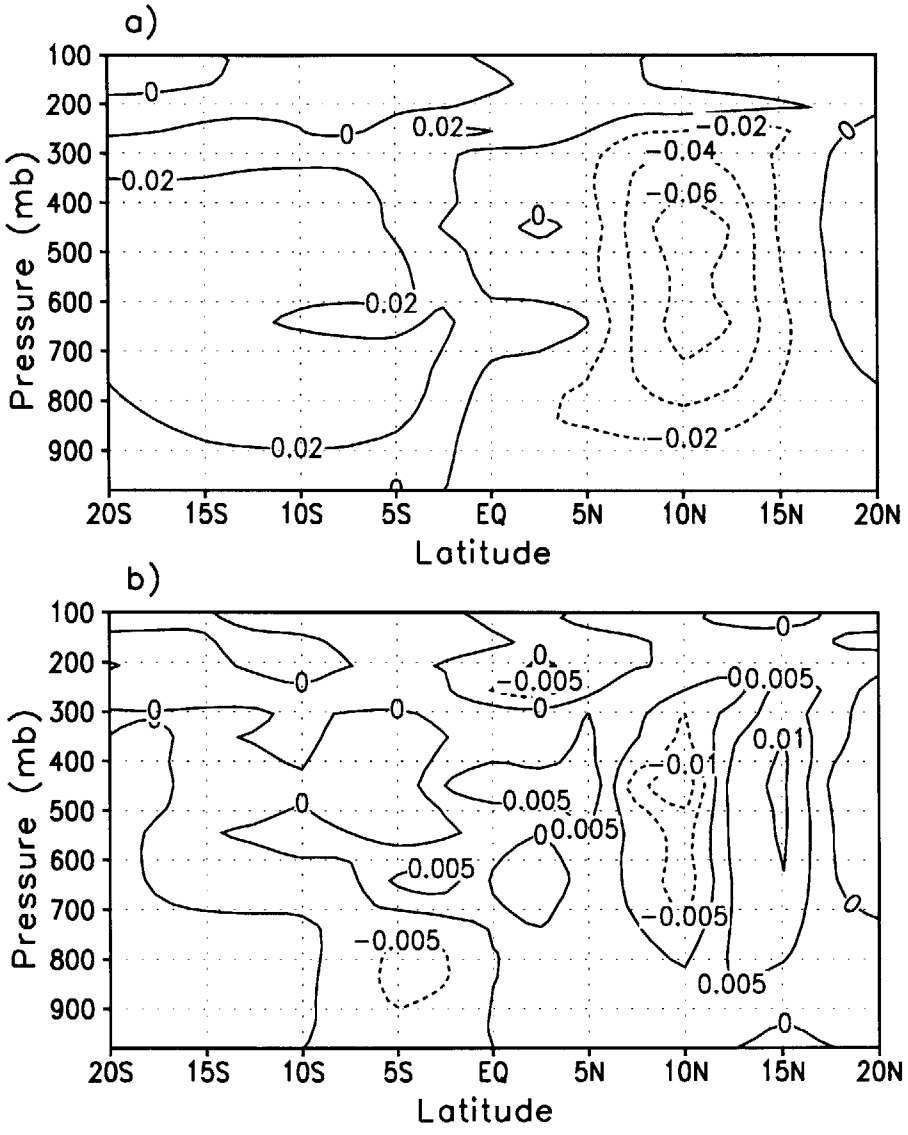

Figure 5-20: Vertical velocity (Pa/s) in August. a) Equilibrium "A"; b) The difference between equilibria "C" and "A": "C" - "A".

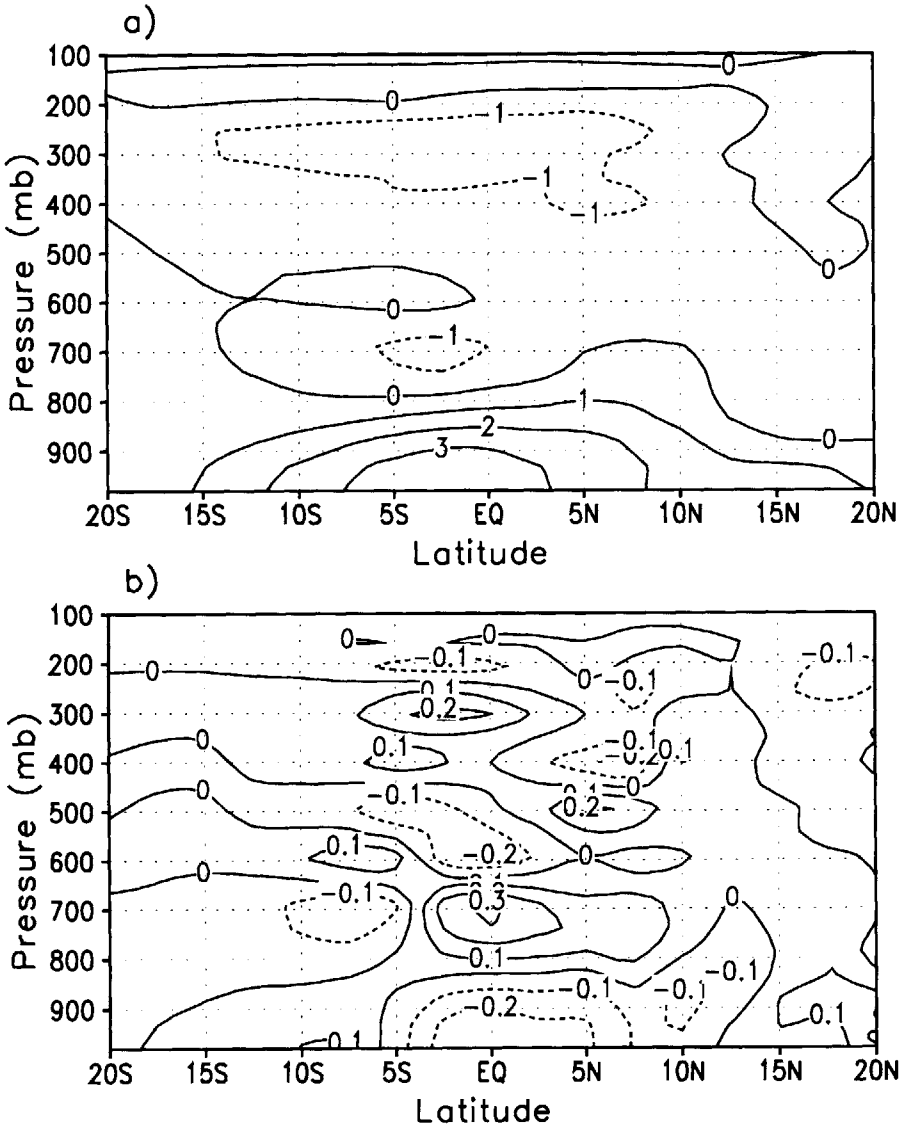

Figure 5-21: Meridional wind (m/s) in August. a) Equilibrium "A"; b) The difference between equilibria "C" and "A": "C" - "A".

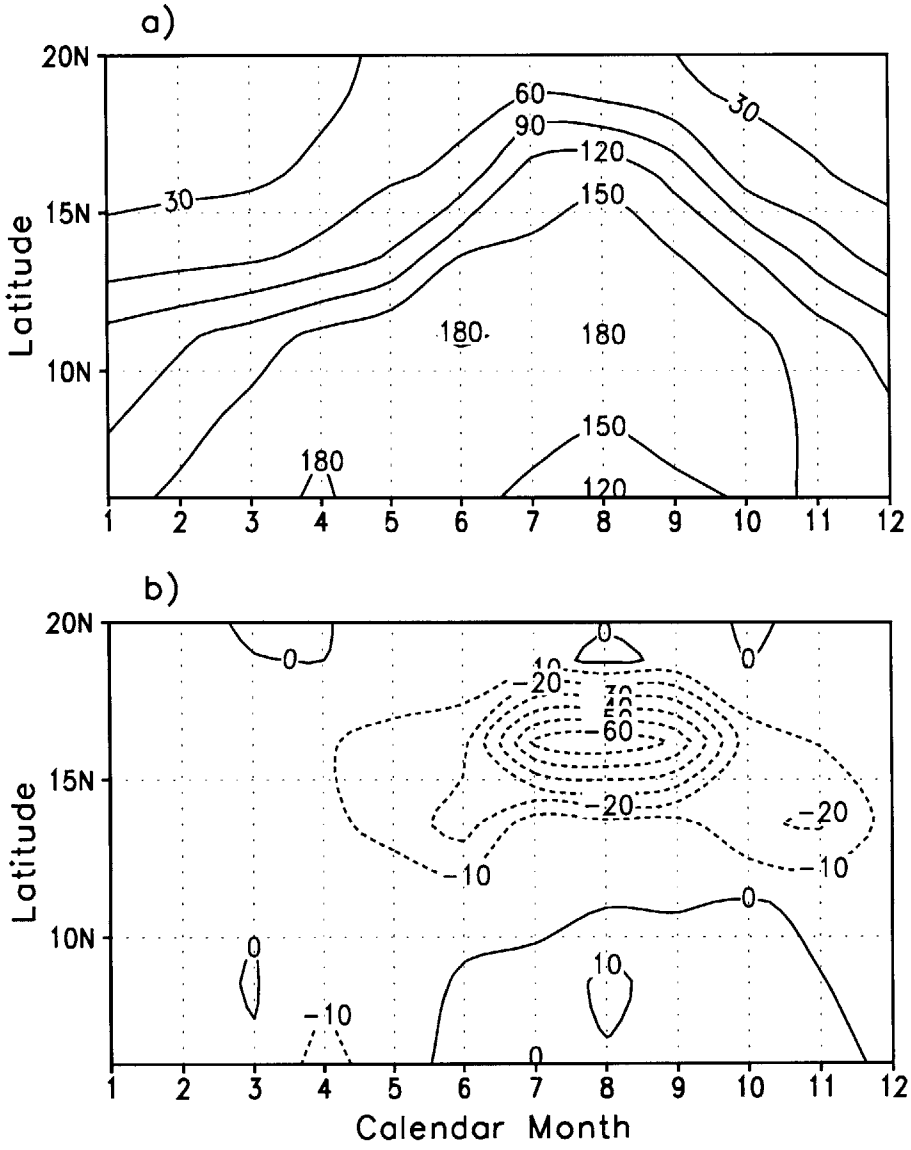

Figure 5-22: Seasonal cycle of the net radiation, in W/m^2. a) Equilibrium "A"; b) The difference between equilibria "C" and "A": "C" - "A".

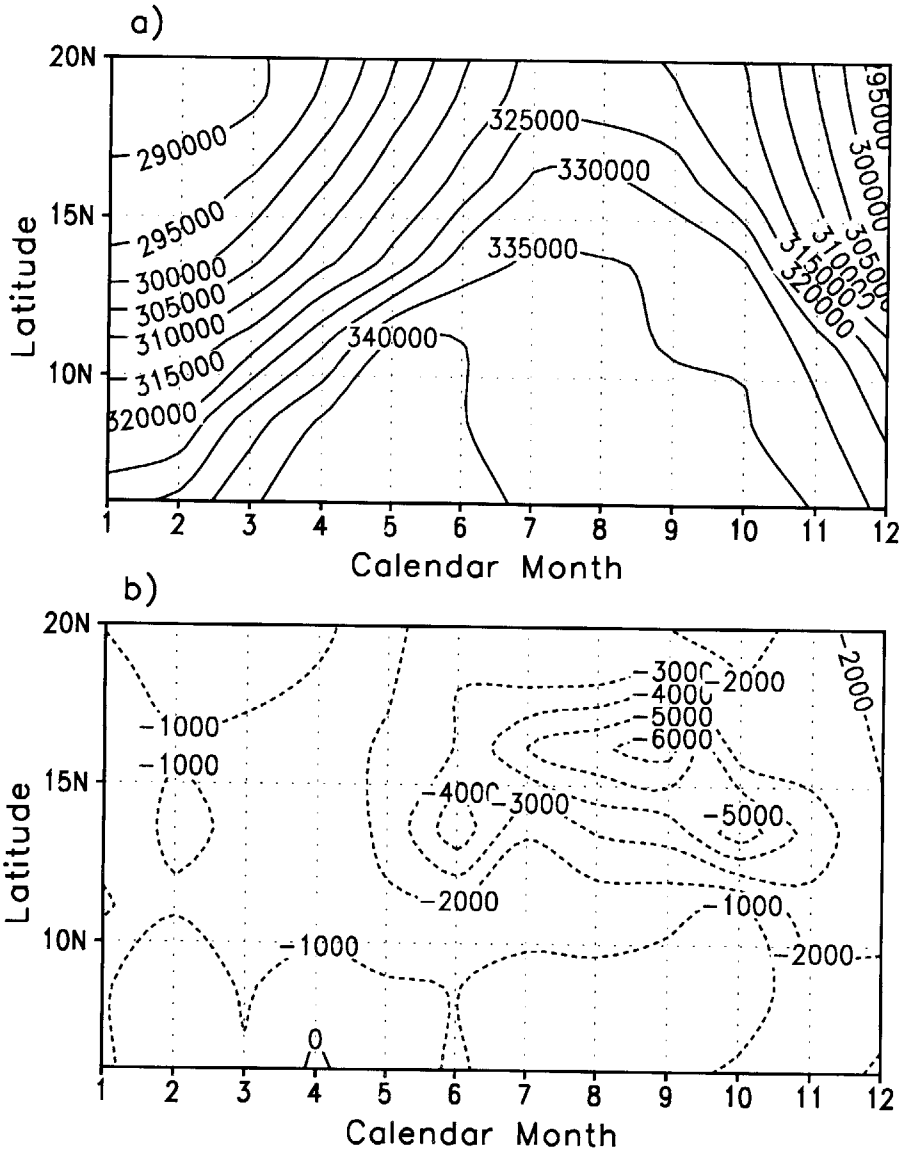

Figure 5-23: Seasonal cycle of the moist static energy near the surface, in J. a) Equilibrium "A"; b) The difference between equilibria "C" and "A": "C" - "A".

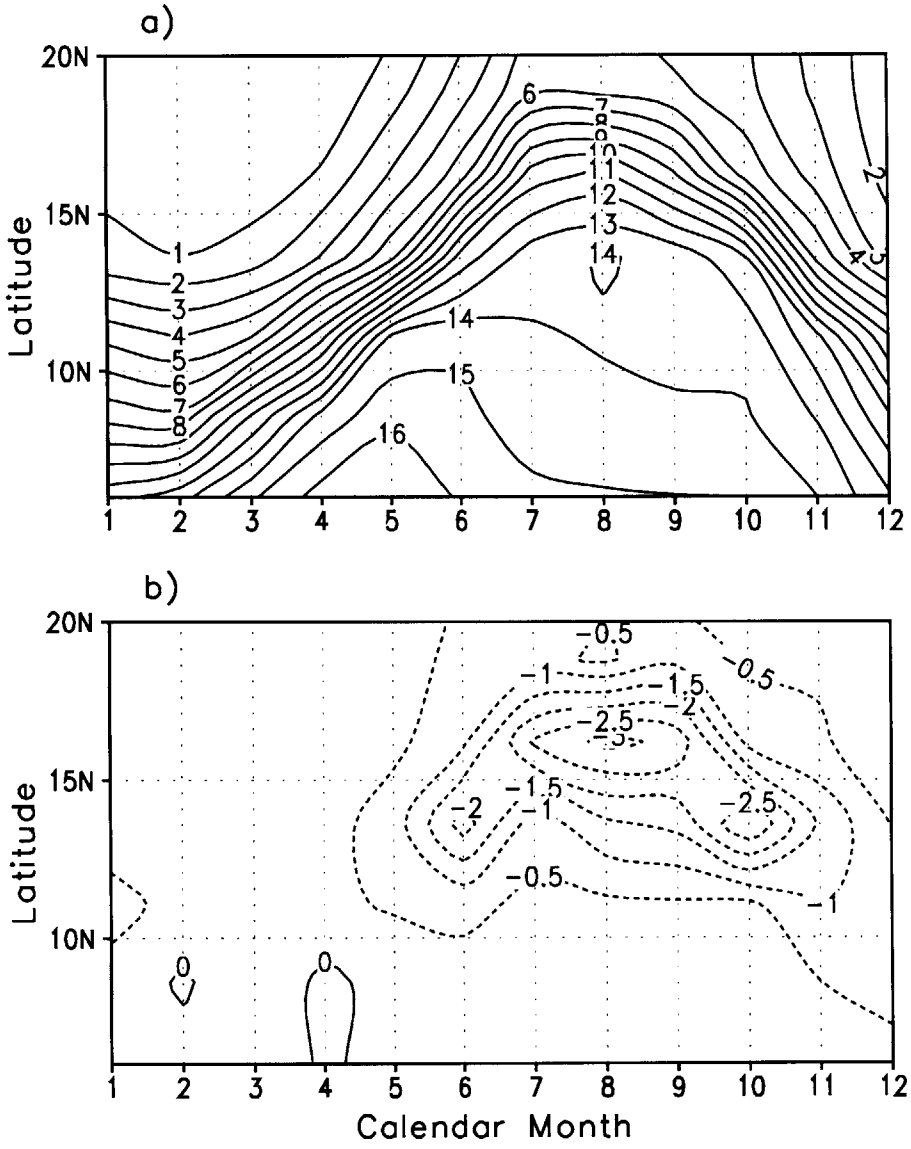

Figure 5-24: Seasonal cycle of the specific humidity near the surface, in g/kg. a) Equilibrium "A"; b) The difference between equilibria "C" and "A": "C" - "A".

A comparison of the surface temperature between the equilibria "A" and "C" reveals an interesting seasonal pattern: over most part of the Sahel region, equilibrium "C" is warmer by up to 1.5 K during the rainy season and cooler by more than 1.0 K during the dry season (Figure 5-25). The warming during the rainy season of equilibrium "C" takes place in spite of a decrease in the net radiation (Figure 5-22). Upon vegetation degradation, the increase of albedo (Figure 5-26) reduces the net solar radiation, which tends to cool the land surface (Charney, 1975); on the other hand, evapotranspiration decreases, which tends to warm up the land surface (Idso, 1977). The net impact on the surface temperature depends on which factor is dominant. Figure 5-27a presents the difference between equilibria "A" and "C" in the net solar radiation, which is mainly due to the albedo effect; Figure 5-27b presents the difference in the latent heat flux, which stands for the evapotranspiration effect. Clearly, over the Sahel region, the evapotranspiration effect is dominant during the rainy season when the water supply is adequate. During the dry season, the evapotranspiration process is constrained by the limited water supply, and the albedo effect becomes dominant. Therefore, a vegetation degradation such as the change from equilibrium "A" to "C" causes a summer warming and winter cooling in the Sahel region, as shown in Figure 5-25.

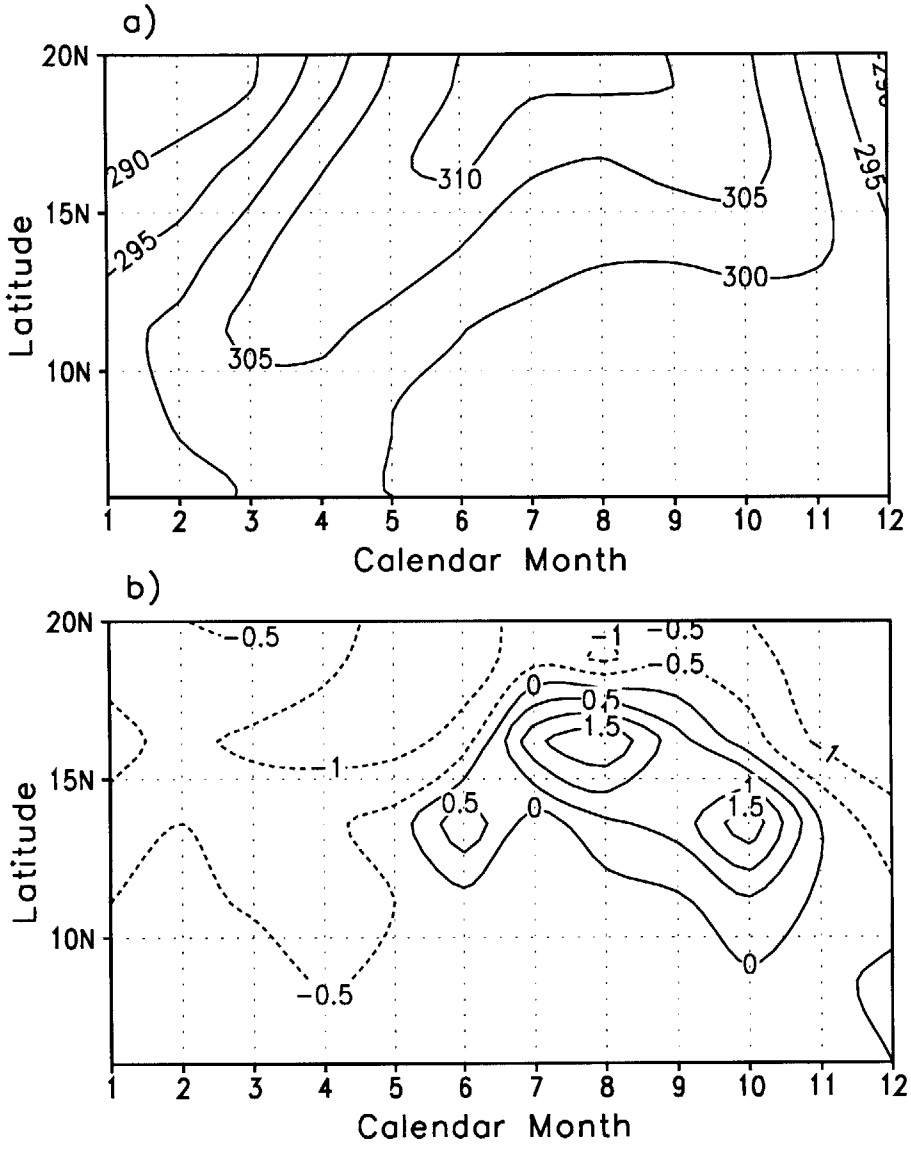

Figure 5-25: Seasonal cycle of the surface temperature, in K. a) Equilibrium "A"; b) The difference between equilibria "C" and "A": "C" - "A".

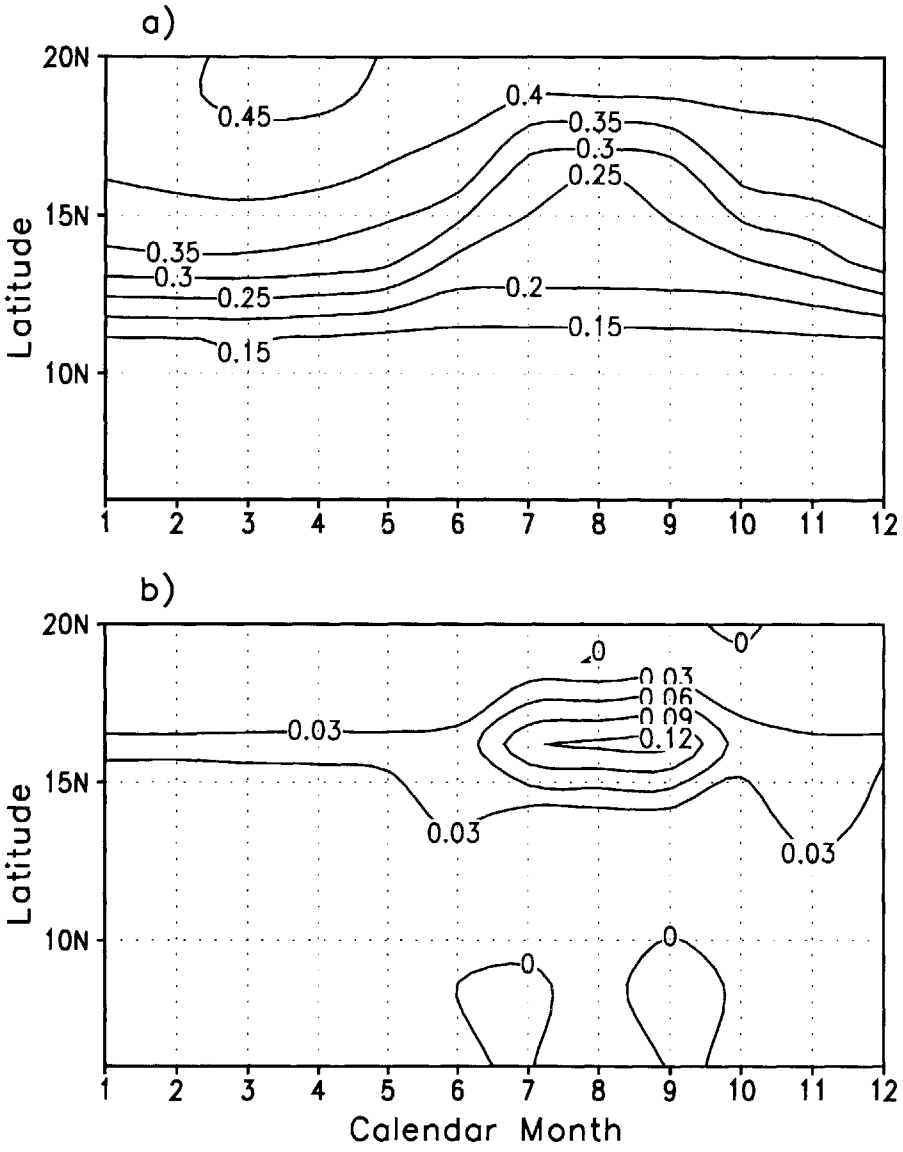

Figure 5-26: Seasonal cycle of the surface albedo. a) Equilibrium "A"; b) The difference between equilibria "C" and "A": "C" - "A".

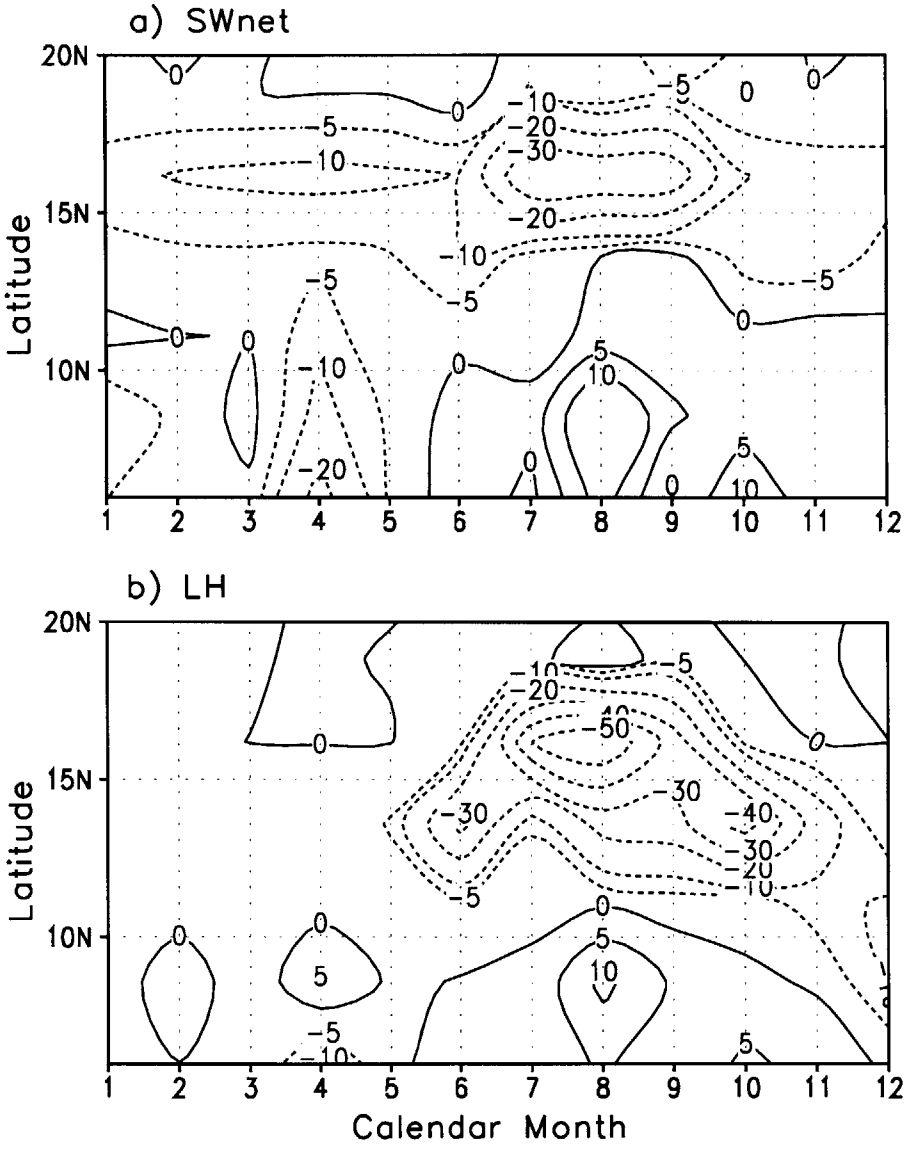

Figure 5-27: Differences between equilibria "C" and "A": "C" - "A". a) Seasonal cycle of the net solar radiation at the land surface (W/m^2); b) Seasonal cycle of the latent heat flux (W/m^2).

5.4 Discussion

Experiments on different types of vegetation perturbations showed that the simulated biosphere-atmosphere system is more resilient to perturbations over the forest region than to perturbations over the grassland region. If the ecosystem is saved from further human disturbances, the biosphere-atmosphere system can recover from a disturbance over the forest region, while it may not recover from a disturbance over the grassland. However, this does not imply that deforestation is less significant than desertification. In fact, as shown in Figure 5-15, the deforestation-induced decrease in precipitation is very significant during the early stage of the succession which lasts for decades.

Although the study on the resilience of the coupled biosphere-atmosphere system focuses on the anthropogenic vegetation perturbations, natural climate variations can cause similar effects in degrading or enhancing the vegetation, especially in the grassland region. An event of one extremely dry year or several dry years in a row could cause as much vegetation degradation as man-made desertification. Similarly, a naturally induced wet event can significantly enhance the grass growth. Therefore, transitions between different equilibria are not necessarily caused by human activities. Historically, and before the emergence of human activity as a significant process, the main forcing in triggering a climate transition would be the large-scale forcings such as the global SST variations, as well as natural local factors such as plant pathogens and diseases of grazing fauna.

The existence of multiple climate equilibria and equally important, the possibility of climate transitions between different equilibria, have significant implications regarding the past, present and future climate over West Africa. The alternate occurrences of dry and wet spells over West Africa (see Figure 1-5) can be viewed as a collective reflection of the climate persistence at one equilibrium and the climate transition to another. For the current drought, it is conceivable that the climate system before the drought might have been in a state similar to the wet equilibrium "A" of this study. A single dry year or several dry years in a row, or man-made desertification, might have triggered the climate system to evolve into a drier equilibrium

("B" or "C"). An event of one or more significantly wet years in the future, or man-made perturbations such as large-scale irrigation, may trigger the system towards a wetter equilibrium thus starting a wet period. The irrigation-induced recovery of the wet equilibrium brings up the possibility of mitigating the current drought by way of human perturbations. A 3-D model with a finer resolution is required for an accurate estimation on how much irrigation is needed to induce such a beneficial effect. Such a study may or may not be attainable due to the high computational expense involved.

The multiple-equilibrium nature of the climate system adds more uncertainty and challenge to climate studies using coupled biosphere-atmosphere models (e.g., Foley *et al.*, 1998). Discrepancies between model simulations and observations may not necessarily reflect a deficiency in the model, since observations and simulations may possibly describe two different equilibria. It is technically difficult and computationally expensive to identify all the relevant equilibria that a model might have, especially for 3-D models.

Finally, our results have important implications regarding the general topic of climate predictability. The perturbation-induced climate transition between different equilibria, as well as the sensitivity of the climate system to its initial conditions, implies that climate in West Africa should be considered as an initial value problem as well as a boundary value problem. The traditional notion of climate as exclusively a boundary value problem, which is used to justify most of the current approaches for predicting future climate, is seriously challenged (Pielke, 1998). Our finding necessitates a reevaluation of the current understanding regarding climate predictability, and calls for new approaches to climate prediction.

5.5 Conclusions

This chapter focuses on the multiple-equilibrium behavior of the coupled biosphere-atmosphere system over West Africa. After the hypothesis regarding the multiple climate equilibria is described, numerical experiments using ZonalBAM are performed to investigate the sensitivity of the coupled biosphere-atmosphere system to initial

conditions and the resilience of the coupled biosphere-atmosphere system with respect to various perturbations. The main conclusions include:

1) The regional climate system over West Africa has multiple equilibrium states coexisting under the same precessional forcing.

2) Triggered by external perturbations and governed by the two-way biosphere-atmosphere interactions, the climate system over West Africa can evolve from one equilibrium to another within a relatively short time (in the order of one decade). Such climate transitions are reversible.

3) Following a vegetation perturbation, the biosphere-atmosphere system has three different ways of responding: a negative feedback leading to a full recovery; a positive feedback leading to a perturbation enhancement (therefore a new equilibrium); a negative feedback leading to a partial recovery (therefore a new equilibrium).

The scope of this chapter is limited to the response of the natural biosphere-atmosphere system to a major non-permanent perturbation. In reality, the climate system is constantly subjected to continuous variations in the large-scale atmospheric and oceanic processes as well as recurrent local disturbances due to human activities. Based on the understanding developed up to this point, the following chapters will investigate how the coupled biosphere-atmosphere system responds to continuous forcings or disturbances.

Chapter 6

Mechanisms for the Low-Frequency Rainfall Variability

6.1 Introduction

Precipitation in the Sahel region of West Africa is dominated by low-frequency variability at the time scale of decades or longer, a characteristic not observed in the surrounding regions. While the time scale of the dominant rainfall variability is about 2-7 years for the Guinea coast region and for regions in East and South Africa, it is up to several decades over the Sahel region, according to analyses of observations collected during the past century (e.g., Nicholson and Entekhabi, 1986; Rowell *et al.*, 1995). Consistently, historical records for the level of Lake Chad (Figure 1-5) confirms the dominance of the low-frequency variability found in the more recent observations over the Sahel region. However, the physical mechanisms behind this well-documented low-frequency variability are still not well understood (see the review in Chapter 1).

Using the coupled biosphere-atmosphere model ZonalBAM, Chapter 5 documented the multiple-equilibrium behavior of the coupled biosphere-atmosphere system in West Africa, and suggested that the climate fluctuations at decadal time scale may be viewed as a collective reflection of climate persistence at one equilibrium and climate transition to another. However, Chapter 5 focused on the response of the climate system to single isolated perturbations, and assumed climatological SST sea-

sonal cycle over the ocean. In reality, the regional climate system is continuously subjected to small successive perturbations. Unavoidably, subsequent disturbances would modify or even override the system's response to any precedent event. For example, climate transitions from one equilibrium towards another may be interrupted or reversed by subsequent forcings. The goal of this chapter is to investigate how the coupled biosphere-atmosphere system in West Africa responds to successive forcings such as SST variations in the Atlantic Ocean, and to study the low-frequency rainfall variability over the Sahel region in a more realistic scenario. This study is based on long-term climate simulations using ZonalBAM driven with the observed SST variations over the Atlantic Ocean during the period 1898-1997. The monthly SST data from the UK Meteorological Office (Parker *et al.*, 1995; Rayner *et al.*, 1996) is used. We interpolate in time the monthly SST observations averaged between 10°W and 10°E. The diurnal cycle of SST is not considered.

6.2 Modeling the Rainfall Variability at Decadal Scale

6.2.1 Control Simulation

To study the long-term climate variability over the Sahel region, a simulation of 100 years (*Dyn-Control*) is carried out using ZonalBAM, with dynamic vegetation over land and SST varying from 1898 to 1997 over the ocean. In the first year of the simulation, the biosphere-atmosphere system is assumed to be at the equilibrium derived in Chapter 3, which is also the wettest of the three equilibria explored in Chapter 5 (see Figure 5-16). This equilibrium is close to the climate of the current century, with forest in the south, grassland in the north, and the desert border around 17.5°N (see Figure 3-21).

Figure 6-1 presents the annual rainfall distribution over West Africa during the period 1898-1997 in the *Dyn-Control* simulation. The rainfall climatology based on this 100-year simulation is shown in Figure 6-2, compared with the GPCP data and

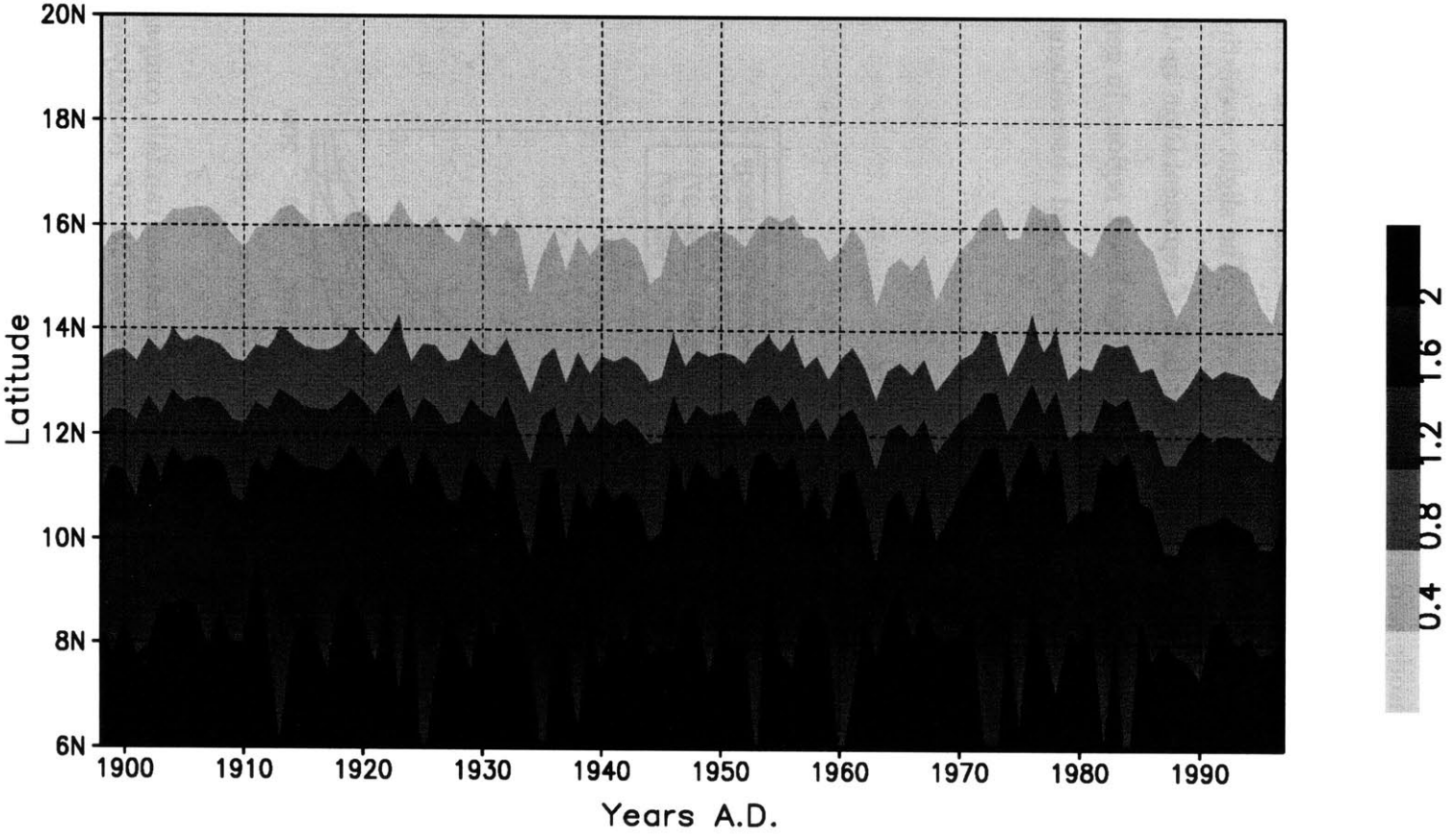

Figure 6-1: Rainfall distribution along latitude and time, simulated in *Dyn-Control*. The unit is $m/year$.

the NCEP re-analysis data. The GPCP data spans the period 1987-1997, amid the extended Sahel drought. The temporal coverage of the NCEP re-analysis data includes both a wet episode and the drought. For further comparison, the NCEP reanalysis data are presented for the wet period (1958-67) and the dry period (1968-1997). Over most of the domain, the climatology of the simulated rainfall falls between the observations for the dry period and the wet period. The slight overestimation of rainfall near the coast may have to do with the lack of representation in the model for detailed distribution of land use patterns within the forest region. In general, the comparison of rainfall climatology between the simulation and observations shows a fair agreement.

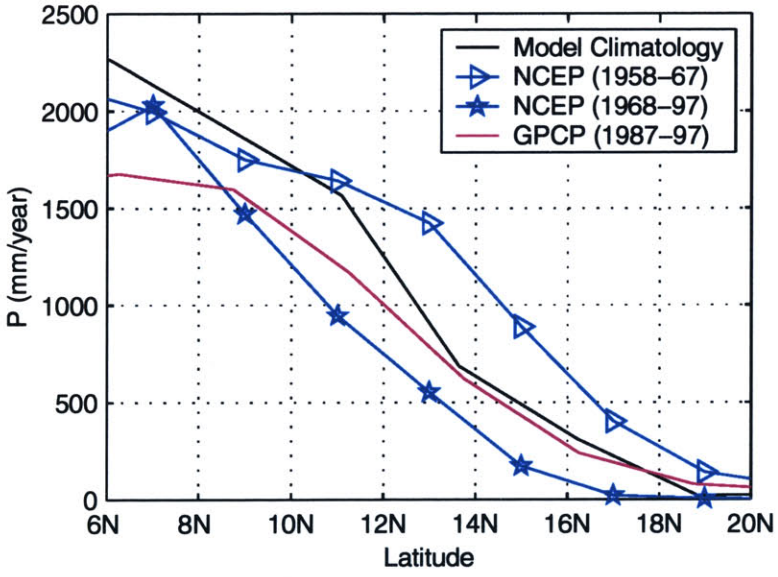

Figure 6-2: The model climatology (1898-1997) of the annual rainfall, compared with the climatology based on the GPCP data (1987-97), the NCEP re-analysis data in the wet period (1958-67), and the NCEP re-analysis data in the dry period (1968-97).

In Figure 6-1, the temporal variability of rainfall over the region north of 10°N exhibits a high degree of spatial coherency. The same statement also holds for the region south of 10°N, but with a different pattern of the rainfall temporal variability. There-

fore, we can study the rainfall variability of West Africa based on the time series of the rainfall average within the Sahel region (defined as the region 10°N-17.5°N in Chapter 1) and the rainfall average within the Guinea Coast region (defined as the region between the coast and 10°N in Chapter 1). Figure 6-3a and 6-3b present the normalized anomaly of the annual rainfall averaged over the two regions, respectively. Qualitatively, the model rainfall over the Sahel region contains more low-frequency variability than the Guinea Coast region, which is consistent with observations (Nicholson and Palao, 1993; Rowell *et al*, 1995). Analyses in the following focus on the Sahel region where the low-frequency rainfall variability is prominent.

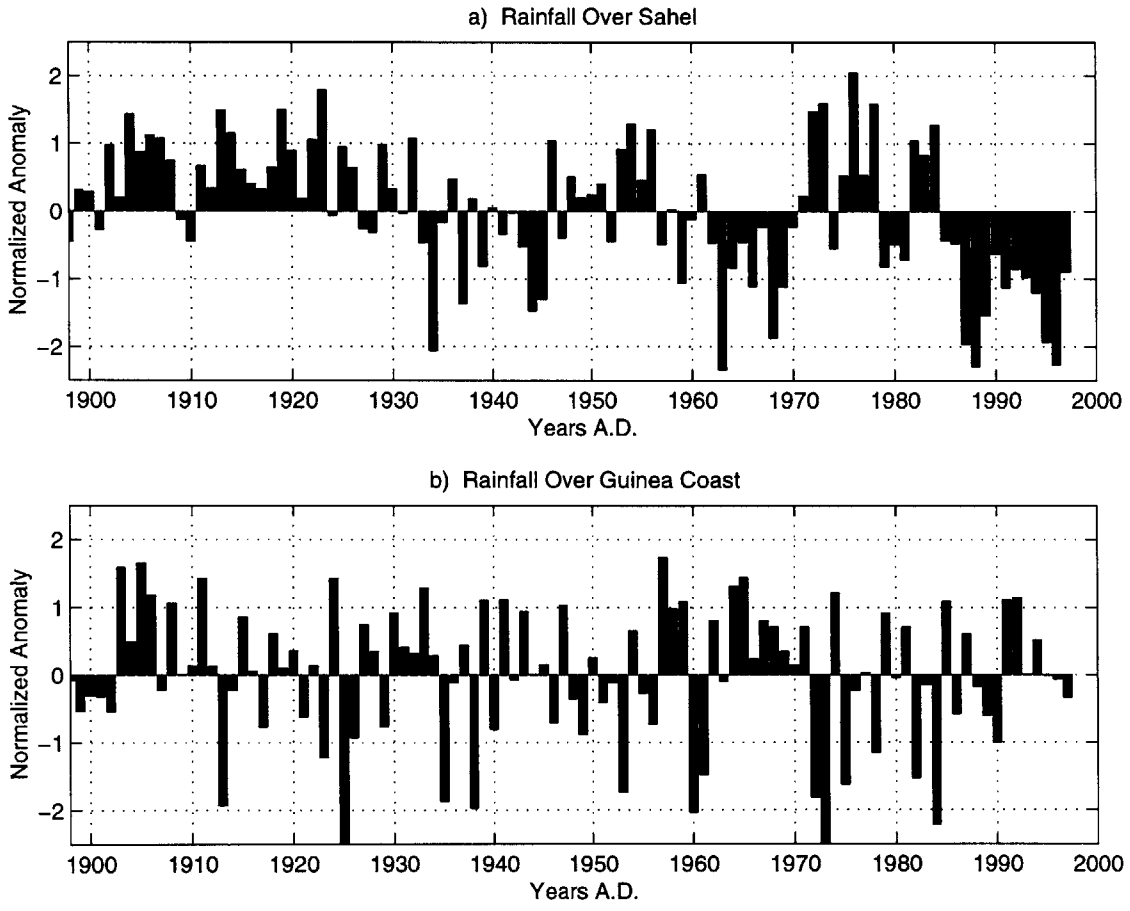

Figure 6-3: Time series of the normalized rainfall anomaly averaged over (a) the Sahel region and (b) the Guinea Coast region, based on the simulation shown in Figure 6-1. The climatology for each region is based on the whole time series (1898-1997).

Although the model captures both the rainfall climatology and the spatial contrast

in the time scale of the rainfall variability, it lacks representation of several climatically important factors, which include (but are not limited to) the large scale impact of the "Little Ice Age" that ended in the 1920s (Dansgaard *et al.*, 1975; Porter, 1986), the anthropogenically induced land cover changes since 1950s (Gornitz and NASA, 1985; Fairhead and Leach, 1998), changes in the level of CO_2 and industrial aerosols in the atmosphere, and the impact of global SST forcings (Palmer, 1986). Therefore, on a year-to-year basis, the model simulation may not be comparable with observations. For example, in the same scale as Figure 6-3a, Figure 6-4 presents the observed rainfall anomaly in the Sahel region for the period 1900-1996, based on the Hulme data (Hulme *et al.*, 1998). For the rainfall variability at decadal time scale, two

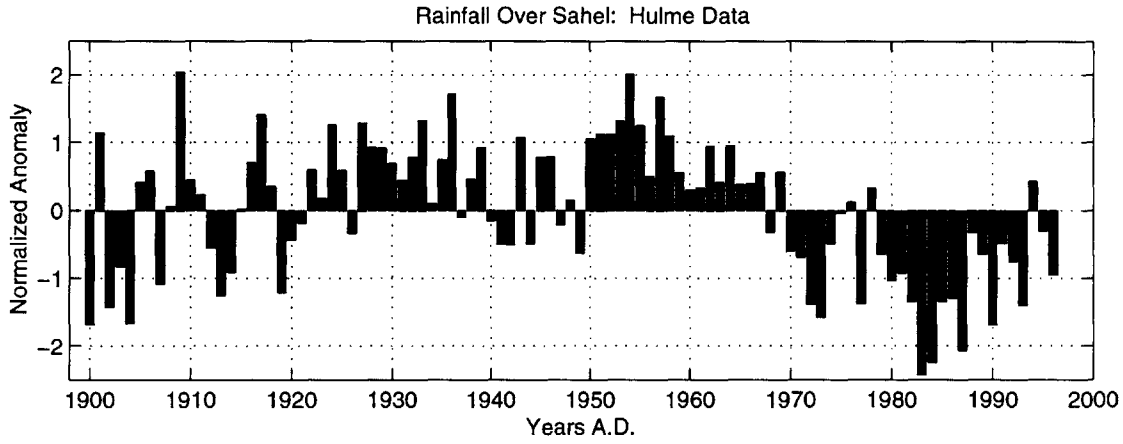

Figure 6-4: Time series of the normalized rainfall anomaly averaged over the region 15°W-15°E, 10°N-17.5°N, based on the Hulme data (Hulme *et al.*, 1998). The climatology is based on the whole time series (1900-1996).

major differences between the simulation and observations are identified: the model simulates a wet episode during the first two decades of the century in the Sahel region, while average to dry conditions were observed; a persistent Sahel drought was observed in the past three decades, while the model simulates a drought interrupted by a wet spell in 1970s. The simulated wet event early in the century is associated with the extremely low SST in the Atlantic Ocean probably related to the "Little Ice Age" whose broad impact is not included in our model. At the same time, it may also have to do with the initial conditions of the simulation. As will be demonstrated

in the next section, when starting with an arid condition, the model does simulate a dry episode in the beginning of the century. For the "not-so-dry" 1970s, the lack of human-induced vegetation degradation may play a role. It is encouraging to note that the simulation captures the wet event in 1950s. Moreover, the simulated wet event in 1970s, which breaks an otherwise continuous drought, takes place around a time when the severity of the observed drought was significantly alleviated (Figure 6-4). Most importantly, the model reproduces the low-frequency variability of the Sahel rainfall, a feature that was also observed in the past several centuries (see Figure 1-5) and is therefore independent of the omitted forcings. Analyses in the following focus on understanding the mechanisms of this low-frequency variability.

6.2.2 Role of Vegetation Dynamics

When vegetation dynamics is included, it takes the regional climate system years or longer to recover from certain vegetation perturbations (Figure 5-16). This may have significant implications regarding the mechanisms of low-frequency rainfall variability. Without the functioning of vegetation dynamics, a perturbation in atmospheric variables would be wiped out within weeks. The corresponding time scale for soil moisture changes would be in the order of months. This contrast in time scales makes vegetation dynamics more important than other factors as a source for low-frequency climate variability.

An experiment (*Stat-Exp*) is carried out to study the role of vegetation dynamics in the long-term rainfall variability over the Sahel region. *Stat-Exp* is similar to *Dyn-Control* but assuming static vegetation conditions, i.e., vegetation distribution during the period of 1898-1997 remains fixed at the same condition as the first year of the *Dyn-Control* simulation. Therefore, the rainfall variability simulated in *Stat-Exp* merely reflects the response of the atmospheric climate to SST forcings, while the rainfall variability simulated in *Dyn-Control* results from both SST forcings and the impact of vegetation dynamics.

In the same scale as Figure 6-3a, Figure 6-5 shows the time series of the rainfall anomaly over the Sahel region based on *Stat-Exp*. It is readily noticeable that the

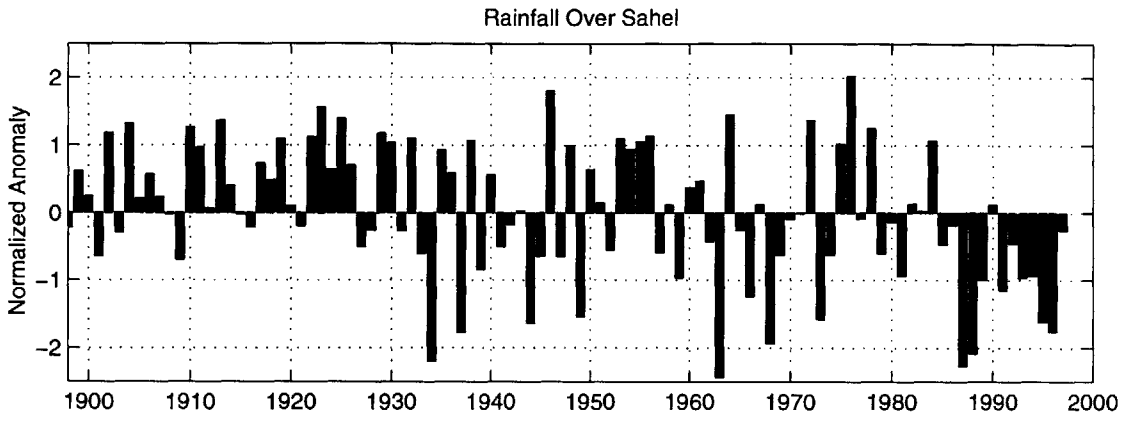

Figure 6-5: Time series of the normalized rainfall anomaly averaged over the Sahel region, simulated in *Stat-Exp*. The climatology for each region is based on the whole time series (1898-1997).

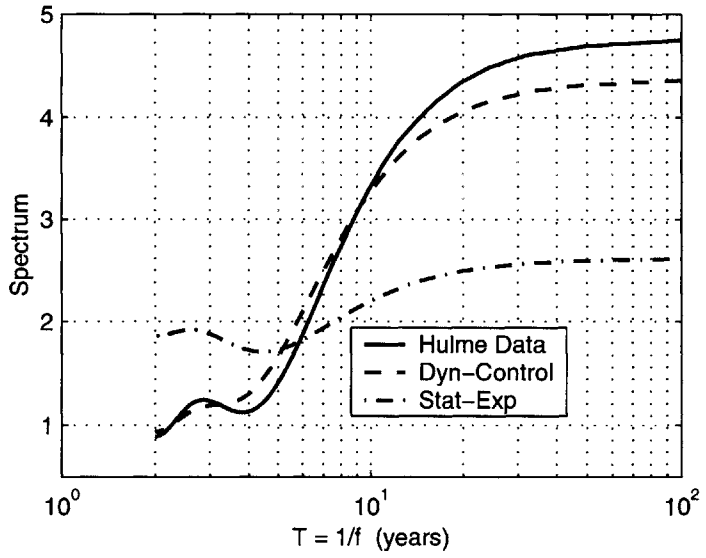

Figure 6-6: Spectra of the simulated rainfall in *Dyn-Control* (dash line) and *Stat-Exp* (dash-dot line), compared with the spectrum of the observed rainfall (solid line) based on the Hulme data (Hulme *et al.*, 1998).

rainfall variability in the *Dyn-Control* simulation contains more low-frequency components than the *Stat-Exp* simulation. As a quantitative measure, Figure 6-6 shows the spectrum of the annual rainfall based on the *Dyn-Control* and *Stat-Exp* simulations, compared with the spectrum based on the Hulme data. The simulation with dynamic vegetation (*Dyn-Control*) not only captures the dominance of low-frequency components in the rainfall variability, but also reproduces the full spectrum of the rainfall variability with reasonable accuracy. In contrary, the rainfall variability in the simulation with static vegetation (*Stat-Exp*) demonstrates no clear dominance of low-frequency components. Figure 6-6 suggests that vegetation dynamics enhances the low-frequency variability and suppresses the high-frequency variability of the climate over Sahel. The response of the regional climate system to forcings such as the regional or global SST variations is significantly regulated by vegetation dynamics, without which the low-frequency climate variability over the Sahel region is unlikely to be as significant as observed. Studies on the climate variability of this region should take into consideration the role of vegetation dynamics.

6.3 Sensitivity to Initial Conditions

6.3.1 Multiple Climate Equilibria

The century-long simulations in the previous section start from the equilibrium "A" of the coupled biosphere-atmosphere system (Chapter 5). The assumption that the climate system in 1898 was at this specific equilibrium may not be justifiable. First, it is uncertain whether the biosphere and the atmosphere in 1898 were at equilibrium. Secondly, even if the biosphere-atmosphere system was anywhere close to an equilibrium, it is hard to identify that equilibrium due to the multiple-equilibrium nature of the climate system. To address the issue of uncertainty associated with initial conditions, we carry out a group of sensitivity experiments using dynamic vegetation, each with a different degree of initial vegetation perturbation in the grassland region where the coupled biosphere-atmosphere system is highly sensitive to vegetation changes.

Four experiments, *Dyn-Pert1, 2, 3,* and *4,* will be presented in this study. With respect to the initial condition in the *Dyn-Control* simulation, *Dyn-Pert1* features a 25% increase of grass density, while *Dyn-Pert2, 3,* and *4* feature a grass removal of 25%, 60%, and 80%, respectively.

Figure 6-7(a, b), using the annual rainfall and growing-season LAI at the grid point near 16°N as examples, presents the sensitivity of the climate system to initial conditions. Despite an initial vegetation difference of +25%, -25%, and -60% over the grassland region in *Dyn-Pert1, Dyn-Pert2,* and *Dyn-Pert3* respectively, simulations in these three experiments converge to the *Dyn-Control* simulation within several years. After the first convergence, although some local differences of small magnitudes do exist, a very good agreement between different simulations is observed. For convenience, in the following we refer to this climate regime as the "wet regime". In *Dyn-Pert4*, with a grass removal of 80%, a significantly drier climate (referred to as the "dry regime") results, which features desert condition at 16°N where the "wet regime" features short grass. Experiments with 70% and 75% grass removal (not shown here) all converge to the "dry regime". Further experiments failed to introduce a third climate regime.

Figure 6-8(a,b) presents the latitudinal distribution of the net primary productivity (NPP) for both the "dry regime" (*Dyn-Pert4*) and the "wet regime" (using *Dyn-Control* as an example) during the period 1898-1997, with the approximate desert border marked by the isohyets of the 200-mm annual rainfall. Significant differences exist between the two distinct climate regimes. The "dry regime" is in general less productive than the "wet regime", and features a southward expansion of the Sahara desert.

The sensitivity of the long-term climate simulation to initial vegetation conditions reflects the response of the coupled biosphere-atmosphere system to vegetation perturbations in the scenario of varying SSTs. Therefore, results of the sensitivity experiments shown in Figure 6-7 can be analyzed in comparison with the multiple climate equilibria ("A", "B", and "C") in Figure 5-16. Comparison between these two figures shows that the "wet regime" is in fact a reflection of the wet equilibrium

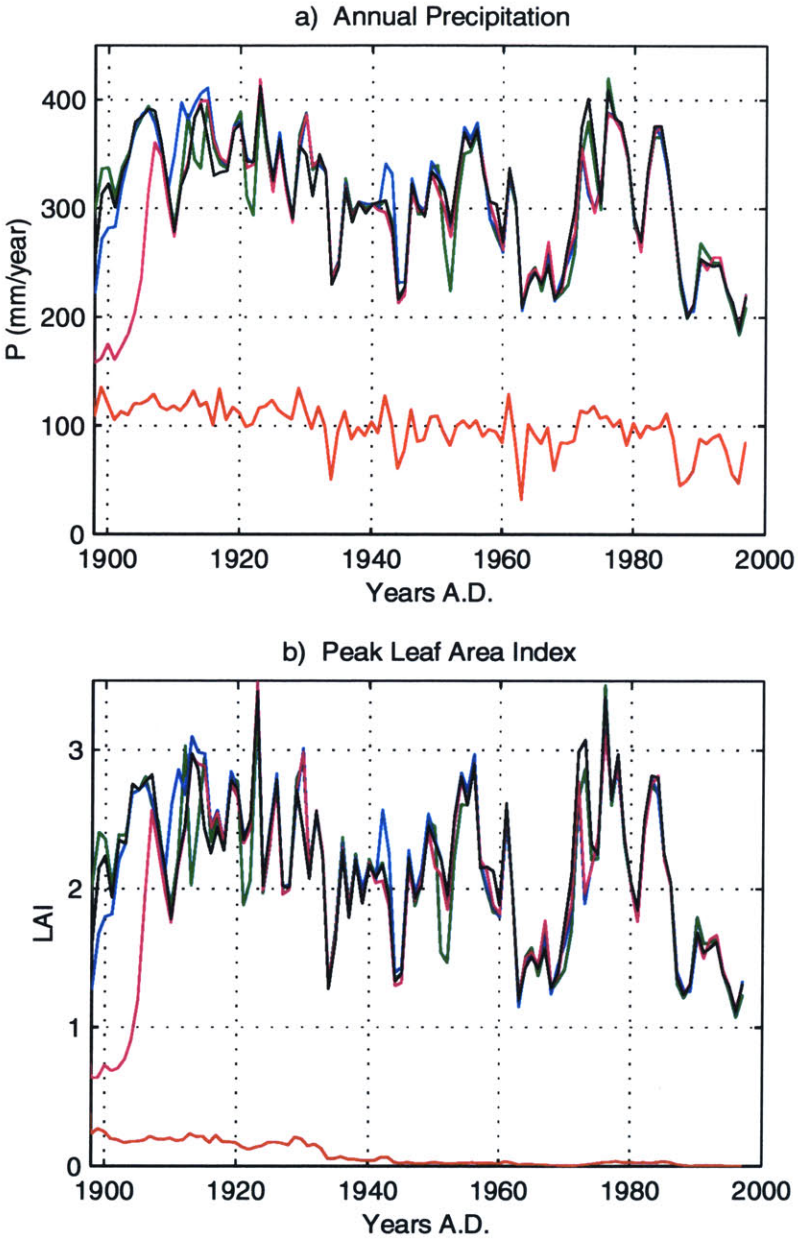

Figure 6-7: Time series of (a) the annual rainfall and (b) the growing-season LAI at the grid point near 16°N, in the control simulation *Dyn-Control* (black) and sensitivity experiments *Dyn-Pert1* (green), *Dyn-Pert2* (blue), *Dyn-Pert3* (magenta), and *Dyn-Pert4* (red).

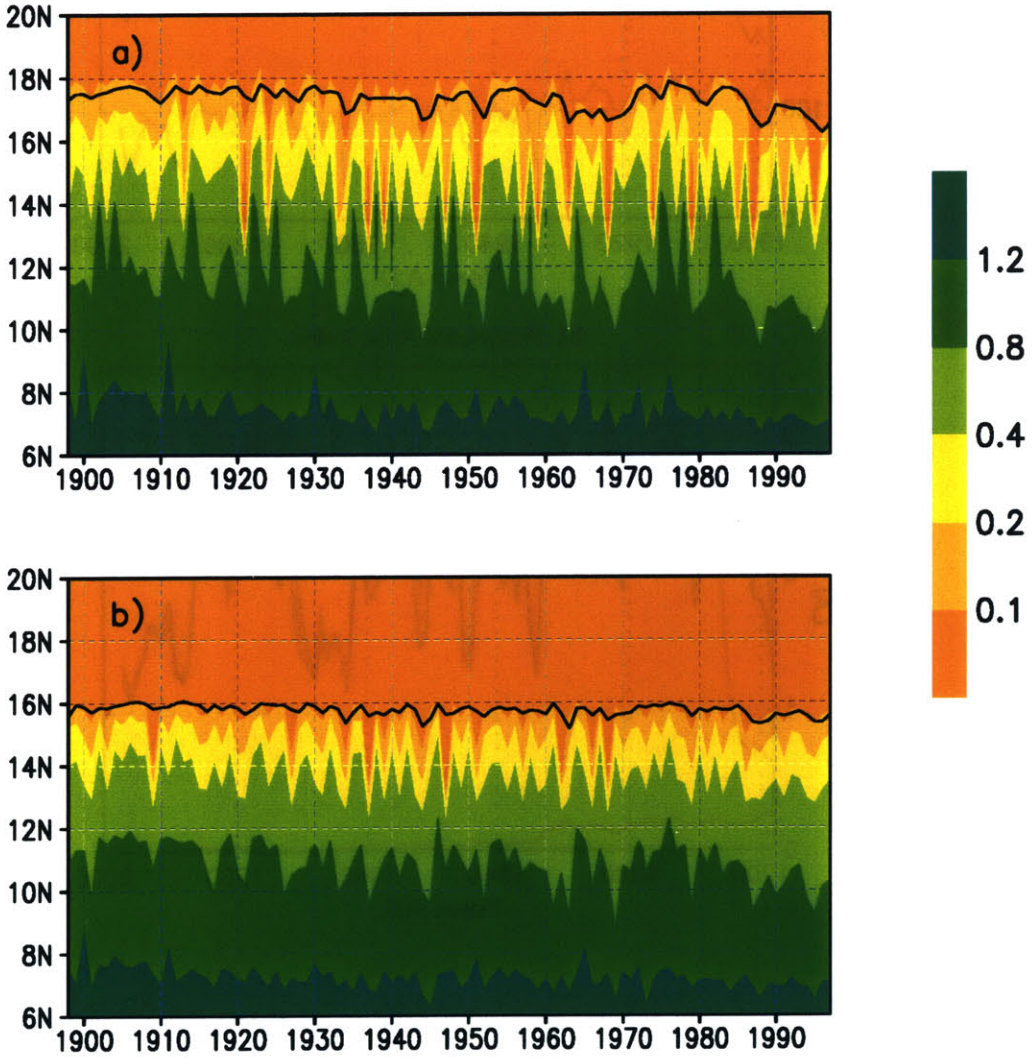

Figure 6-8: Net primary productivity (in $kgC/m^2/year$) distribution for the simulation period 1898-1997: a) *Dyn-Control* (wet regime); b) *Dyn-Pert4* (dry regime). The black lines are the isohyets of the 200-mm annual rainfall.

"A" in the scenario of varying SSTs, while the "dry regime" is a reflection of the dry equilibrium "C". The lack of a climate regime that resembles equilibrium "B" may have to do with the stability of equilibrium "B" under the influence of varying SSTs. This point is also supported by the observation that the climate during the driest periods of the "wet regime" is wetter than equilibrium "B", while the climate during the wettest periods of the "dry regime" is drier than equilibrium "B". To address this issue, we carry out a group of experiments by restarting the coupled model from equilibrium "B" at different times. In Figure 6-9, the red and green lines show the annual

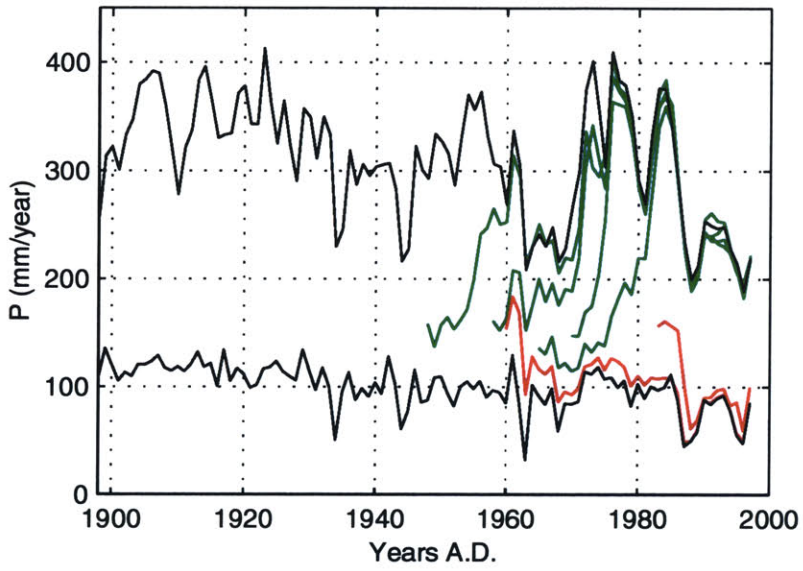

Figure 6-9: Time series of the annual rainfall at the grid point near 16°N. Green and red lines stand for the experiments that begin from different years with the initial condition at the model's medium equilibrium "B"; black lines plot the wet regime (*Dyn-Control*) and the dry regime (*Dyn-Pert4*) for references.

rainfall of these experiments at the grid point near 16°N, while black lines plot the annual rainfall of the "wet regime" (*Dyn-Control*) and "dry regime" (*Dyn-Pert4*) for references. LAI and other variables evolve in a similar way. The climate system in the model, although initialized with the medium equilibrium "B", eventually converges to either the "wet regime" or the "dry regime" depending on when the simulation starts. This suggests that the medium equilibrium "B", which is stable under fixed SST forcings, becomes unstable under varying SSTs. Only two equilibria (the wet

one "A" and the dry one "C") are viable when the inter-annual variability of SST forcings is included.

6.3.2 Climate Transitions

It can be observed from Figure 6-7 that there is no intersection between the "wet regime" and the "dry regime", which suggests that the observed SST variability over the Atlantic Ocean alone is not large enough to cause transitions between the two climate regimes, or equivalently, between equilibria "A" and "C". In reality, such transitions may take place due to other large-scale forcings, for example, SST variations over the Pacific and the Indian oceans which also have a significant impact on the Sahel rainfall (Palmer, 1986). However, due to its zonal symmetry, our model cannot represent the global-scale SST forcings. To better understand the behavior of the climate system under the influence of larger external forcings, here we perform two experiments (*Wet2* and *Dry2*) on the system's response to the artificially increased SST forcings over the Atlantic Ocean. Here the *Wet2* and *Dry2* experiments have the same initial conditions as *Dyn-Control* and *Dyn-Pert4*, respectively, but with the magnitude of SST anomalies being doubled.

Figure 6-10 presents the annual rainfall at the grid point near 16°N for *Wet2* (green line) and *Dry2* (blue line) experiments. Interestingly, *Dry2* converges to *Wet2* before the end of the decades-long wet event simulated in the early stage of the century. As mentioned earlier, the cold SST in the first several decades of the 20th century causes a long wet period, which is favorable enough to allow the climate system to develop from an arid equilibrium into a humid one. The impact of this wet event is obviously enhanced due to the doubling of SST forcings. To avoid this wet event, we start the *Dry2* experiment from 1938, 40 years later than 1898. Result of this experiment is also presented in Figure 6-10 (red line), which introduces a climate regime much drier than the one in *Wet2*. During most of the time in the 100 years of simulation, the climate of the *Wet2* experiment is similar to the "wet regime" explored with observed SST forcings (shown in Figure 6-7a), which is the reflection of the wet equilibrium "A" (in Figure 5-16). When starting from 1938, climate of the *Dry2* experiment is close to the

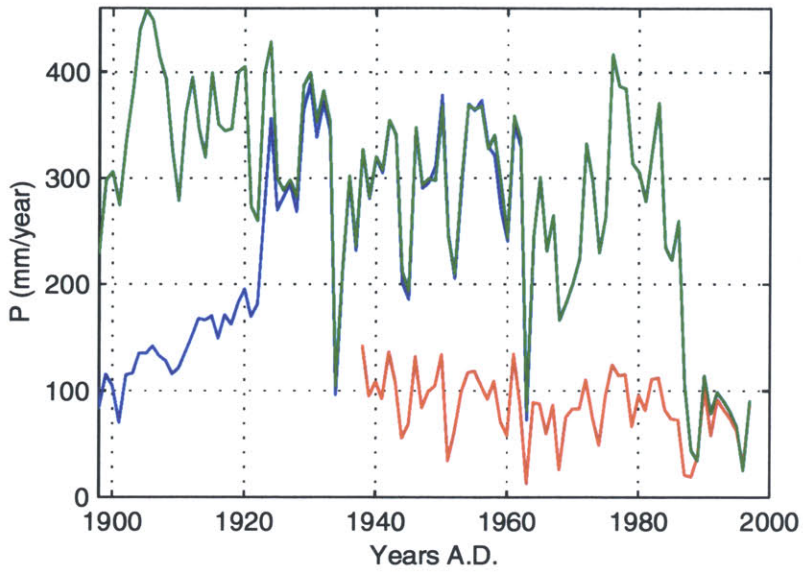

Figure 6-10: Time series of the annual rainfall at the grid point near 16°N, in the *Wet2* experiment (green) and the *Dry2* experiments starting from 1898 (blue) and 1938 (red).

"dry regime" and the dry equilibrium "C". As demonstrated clearly in Figure 6-10, under the influence of enhanced SST forcings, climate transitions between different regimes take place at various moments. For example, a climate transition from the "dry regime" to the "wet regime" is simulated in the early stage of the 20th century (around the 1920s), and a reverse transition takes place towards the end of the 20th century (in the 1980s). Climate transitions from the "wet regime" towards the "dry regime" are triggered around 1934 and 1963, which are interrupted and reversed by subsequent forcings.

The Sahel region during several earlier centuries experienced major rainfall fluctuations of large amplitude (Malay, 1973,1981; Nicholson, 1981b; Farmer and Wigley, 1985), which may have to do with transitions of the regional climate system between different equilibria as demonstrated in Figure 6-10. For example, historical lake level records in the Sahel region (see Figure 1-5) indicate three major events of rainfall fluctuation since the 19th century: a change from wet conditions to dry conditions late in the 19th century, a change from dry conditions to wet conditions early in the 20th

century, and a rapid desiccation later in the 20th century. This makes the arid initial condition for 1898 used in *Dry2* a better reflection of reality than the initial condition used in *Wet2* and *Dyn-Control*. When starting from 1898, the *Dry2* experiment produces a dry episode of almost two decades at the beginning of the 20th century, followed by a climate transition from the "dry regime" to the "wet regime", which agrees well with the general trend in Figure 1-5. The rapid climate transition from the "wet regime" to the "dry regime" in the 1980s simulated in the *Dry2* experiment may reflect the occurrence of the current Sahel drought with some time shift.

The above results and analyses suggest that climate persistence at one equilibrium and climate transitions between different equilibria can act as an important mechanism for climate fluctuations of large amplitude at the time scale of decades to centuries.

6.4 Discussion and Conclusions

This chapter investigates the mechanisms behind the low-frequency variability of the Sahel rainfall using the coupled biosphere-atmosphere model ZonalBAM. Climate simulations for the past 100 years have been carried out using SST in the tropical Atlantic Ocean as the driving forcing. Analyses on simulations with and without vegetation dynamics lead to a conclusion that vegetation dynamics enhances the low-frequency variability of rainfall over the Sahel. Large scale factors including SST variations in the Atlantic Ocean may act as the driving forcings for the climate variability in the Sahel region. However, the response of the regional climate system to these forcings is significantly regulated by vegetation dynamics. Without the role of vegetation dynamics, the low-frequency rainfall variability would be less significant than observed. Studies on the long-term rainfall variability over the Sahel region should take into consideration this impact of vegetation dynamics.

The multiple-equilibrium behavior of the regional climate system under the influence of varying SSTs is also examined. Although three equilibria (wet, medium, and dry) are documented when the model is forced with the climatology of SST seasonal

cycle, only two climate regimes (wet and dry) are viable when the inter-annual variability of SST is included. The observed SST forcings in the Atlantic Ocean alone are not large enough to cause a climate transition between different regimes. However, climate transitions do take place when SST forcings over the Atlantic are artificially doubled, which suggests the potential for climate transitions under the impact of global-scale SST forcings. Such climate transitions may be of close relevance to the climate fluctuations observed in the past several centuries, and is likely to be another important mechanism (in addition to vegetation dynamics) contributing to the low-frequency variability of the Sahel rainfall.

The time scale of the system's recovery from vegetation perturbations, which is in the order of years or even longer, may be the key for understanding the role of vegetation dynamics in enhancing the low-frequency rainfall variability. When SST or any other forcing causes a significantly wetter-than-normal (drier-than-normal) event, vegetation develops denser (thinner) than normal, especially if this event spans several years. When the external forcing ceases to operate, the biosphere-atmosphere system still has a denser-than-normal (thinner-than-normal) vegetation, which is equivalent to the situation after vegetation perturbations. In the next several years following the termination of the original event, the biosphere-atmosphere system will be in a status of recovering from the vegetation anomaly, which favors wetter-than-normal (drier-than-normal) conditions before the full recovery, assuming that a recovery is possible. As a result, the original event gets amplified by vegetation dynamics. This mechanism applies to our simulation using observed SST variations. In occasions when a recovery is not possible, climate transitions will take place. As a result, the original event will be not only amplified, but also sustained and perpetuated. Several periods in our simulations with doubled SST forcing can be described by this mechanism. Both mechanisms, the enhancement of anomalies through vegetation dynamics and the occurrence of climate transitions, favor the dominance of the low-frequency variability in the regional climate.

The decadal variability in the inter-hemispheric gradient of the global SST, which is statistically related to the low-frequency variability of the Sahel rainfall (Ward,

1998), cannot be represented in our zonally symmetric model. However, it is likely that vegetation dynamics would play a significant role in shaping the response of the regional climate system to such global forcings.

Vegetation in West Africa has experienced intense anthropogenic perturbations since the 1950s (Gornitz and NASA, 1985; Fairhead and Leach, 1998), which is likely to have contributed to the severe persistent drought in Sahel. So far, we have focused on the natural biosphere-atmosphere system without considering the impact of recurrent or permanent land cover changes. The possibility that changes in land use may have altered the climate in the past several decades will be investigated in the next Chapter.

Chapter 7

Ecosystem Dynamics and the Sahel Drought

7.1 Introduction

As reviewed in Chapter 1, despite of the considerable research effort in the past two decades, the cause of the current Sahel drought and the mechanism of its persistence remain a topic of inconclusive debate. In Chapter 6, we demonstrate that, under the influence of SST interannual variability, the natural climate system in West Africa has two stable climate equilibria/regimes with reversible transitions between them. Droughts can take place as a result of a climate transition from the wet regime to the dry regime which can be triggered by large-scale forcings. Such climate transitions may be a convincing explanation for the historical occurrence of the Sahel droughts, before the emergence of human activities as an important factor modifying the regional climate. However, the cause of the current Sahel drought is complicated by the extensive anthropogenic disturbances which have effectively reshaped the regional landscape (Bourliere and Hadley, 1983; Sprugal, 1991).

This Chapter investigates both the possibility of drought initiation by human activities and that by large-scale forcings. Using the coupled biosphere-atmosphere model ZonalBAM, we perform climate simulations by driving the model with SST variations during 1950-1997 over the tropical Atlantic ocean. Experiments are carried

out to study the impact of patchy land cover changes and the impact of large scale SST forcings. We show that, no matter what initiated the 20th century drought, the feedback associated with the natural vegetation dynamics may have played the dominant role in the dynamics of this drought.

7.2 New Feature of the Model

Over the ocean (south of 6°N), the model setup is the same as in Chapter 6, with SST prescribed but varying with time as observed (Parker *et al.*, 1995; Rayner *et al.*, 1996). However, over land, the model used in this chapter features a new development on the description of the terrestrial ecosystem.

Each grid cell over land is divided into two parts: vegetation is static over the area of fraction f and is dynamic over the area of fraction *(1-f)*. The fraction f with static vegetation represents the managed landscape where vegetation structure is prescribed according to permanent land use conditions; the fraction *(1-f)* with dynamic vegetation represents the natural landscape where vegetation structure is updated every year based on the carbon budget and allocation. Therefore, the model features a mosaic combination between natural ecosystem and managed ecosystem for each grid cell. Here the division of the grid cell is only limited to the surface, and we assume that the two portions are subjected to the same meteorological forcings (e.g., precipitation, temperature, humidity, wind, and incoming radiative fluxes). Fluxes from the land surface to the atmosphere (e.g., outgoing radiative fluxes, sensible and latent heat fluxes, and evapotranspiration) are the area-weighted averages between the two parts.

In the southern region of West Africa where the natural ecosystem features forest and woodland, vegetation for the managed fraction of each grid cell is prescribed as dense herbaceous plants which characterize the agriculture and pasture land use; in the north, where the natural ecosystem features grassland, the managed fraction of each grid cell is prescribed as bare soil which reflects the impact of man-made desertification. The fraction of managed landscape (f) may increase with time to

simulate the progressive impact of human activities.

7.3 Drought Initiation by Human Activities

The climatic impact of land cover changes such as desertification, though a topic of decades-long modeling studies, is not fully resolved. Due to the lack of the representation of vegetation dynamics, previous studies did not include the response of vegetation to the induced climate change. This is insufficient in the case of non-permanent vegetation perturbation where succession is active, as demonstrated in Chapter 5. Even in the case of permanent land use pattern, the lack of representation of vegetation dynamics still poses a severe problem. Land cover changes often occur to only a certain fraction of the region or the grid cell, and vegetation elsewhere still responds to climate changes induced by the fractional permanent land cover changes. Such feedback mechanism may significantly modify the sensitivity of a climate model to land cover changes. In this section we address this topic through a study on the drought initiation by human-induced vegetation changes.

7.3.1 Scenario of Land Cover Changes

Vegetation distribution in West Africa has experienced significant modifications due to human activities in the twentieth century, which include deforestation near the coast and desertification in the north. Here we define the most likely scenarios of land cover changes that will be investigated in this chapter.

Deforestation occurs as people clear up the forest for agricultural land use or pasture land. Selective logging of short return period may also cause destruction of the forest stand. It is widely accepted that deforestation in West Africa has been intense and extensive, but different sources disagree on the quantitative measures. A recent study by Fairhead and Leach (1998), based on careful examination and interpretation of ecological data, claimed that deforestation in West Africa has been largely exaggerated. For example, in Ivory Coast which hosts about half of the rain forest over West Africa, early studies (FAO, 1981; Myers, 1980-1994; Thulet, 1981;

Bertrand, 1983; Gornitz and NASA, 1985) estimated that more than 10 *Mha* of humid forest has been lost since 1900, while the estimate by Fairhead and Leach (1998) is less than 5 *Mha*. All studies agree on the extent of the remaining forest. The main difference lies in the estimation of how much forest did exist in the beginning of the twentieth century. Instead of using the absolute values of the forest cover, we normalize each estimate by the forest cover in 1900 from the same source. The envelop of these results are plotted in Figure 7-1(a), which presents the area of forest loss as a fraction of the total forest area in 1900. Based on Figure 7-1(a), deforestation did not become significant until the 1950s. Therefore we concentrate on the period from 1950 on. Since the deforestation record during the 1990s is not available, we assume that there is no further forest loss after 1990.

Shifting agriculture is one major cause of deforestation in West Africa. Only part of the area where forest is destroyed will be used for cultivation. The rest is left as fallow land. According to Gornitz and NASA (1985), between the 1950s and the present, the ratio of cultivated to fallow land is about 1:3 to 1:4. Over the fallow land, vegetation succession is active. In part of the fallow land, the fallow period may be long enough for tree saplings to establish. As reported by Golley *et al.* (1975), leaf production of woody plants is extremely high during the early stage of succession, which causes the LAI of young trees to be almost as high as LAI of mature trees. Therefore, despite the small statue and low level of carbon biomass, the vegetation in part of the fallow land may function in terms of evapotranspiration (dependent on LAI) in a way closer to forest than to grassland. Therefore, in our study, we assume that vegetation functions in the same way as herbaceous plants in only half of the deforested region, and as trees in the other half.

Desertification takes place as a result of overgrazing, soil erosion, and other similar processes. Despite numerous claims for the existence of desertification in the Sahel region, there is very little quantitative documentation on land cover changes. This problem is further complicated by the fact that land cover changes similar to that caused by desertification can also result from a severe drought. For the land cover changes during the past several decades, it is hard to distinguish how much is man-

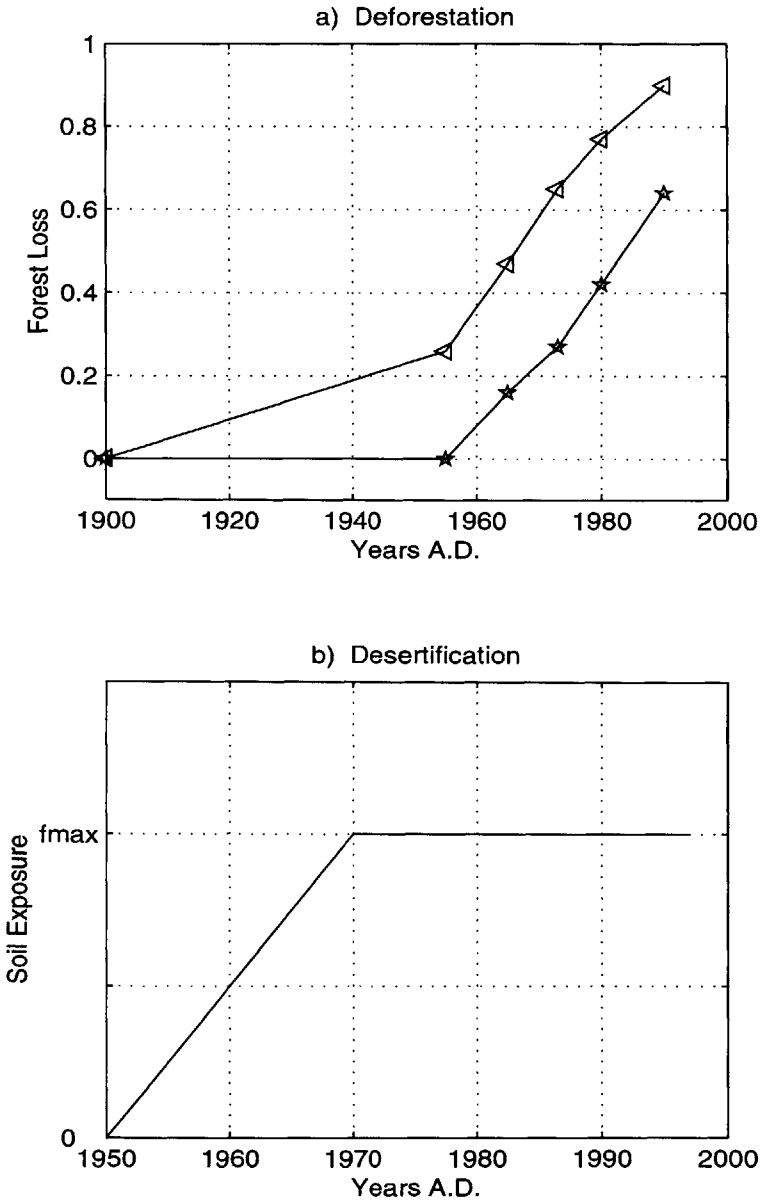

Figure 7-1: Scenarios of land cover changes: a) Minimum (line with pentagram, *Scenario A*) and maximum (line with triangle, *Scenario B*) estimation for the area of deforestation as a fraction of the total forest cover in 1900; b) Fractional exposure of the bare soil due to man-made desertification.

made and how much is induced by the drought. Since the main cause of desertification in West Africa is overgrazing, we can gain some insight about desertification processes based on the dynamics of herbivore population. Over many parts of the Sahel region, the herbivore population increased during the 1950s and 1960s, probably as a result of the rainfall surplus; following the onset of the drought, a large fraction of the livestocks perished, and its population afterwards stayed stable or even decreased due to the lack of forage (Warren,1996). Therefore, it is a conceivable scenario that the extent of man-made desertification may increase from 1950s to the late 1960s and becomes stable shortly after the drought onset. Here we assume that the fraction of bare soil exposed by anthropogenic activities over the Sahelian grassland linearly increases from zero in 1950 to the value f_{max} in 1970, and remains at that level afterwards, as shown in Figure 7-1(b). No progressive man-induced desertification is considered after the drought onset, which is consistent with observations (Nicholson, 1998). The value of f_{max} can be used as the variable for sensitivity experiments.

7.3.2 Experiments Design

Our study on the impact of land cover change is based on climate simulations for the period 1950-1997. SST variations over the Atlantic ocean during the same period are used as the driving forcing. All simulations start from the wettest equilibrium state of the biosphere-atmosphere model which is close to the observed condition in West Africa (see Chapter 3 and Chapter 5). This equilibrium is derived by running the coupled biosphere-atmosphere model for 40 years, starting from a vegetation distribution close to observations, with SST fixed at its climatology and dynamic vegetation within the tropics. The vegetation distribution of this equilibrium can be found in Figure 3-21, with forest near the coast, woodland reaching about 12°N, and grassland in the north bordering the desert around 17.5°N. Here we use the equilibrium state of the biosphere-atmosphere system as the initial condition in order to avoid the unrealistic climate trend imposed by the system's development towards an equilibrium. The choice for the wettest equilibrium is justified by the observation that wet conditions prevailed over the Sahel region around 1950 and lasted for more

than one decade.

The control simulation, *Dyn-Control*, features natural dynamic vegetation during the whole simulation period. No human-induced land cover changes are included. Therefore, it only simulates the response of the natural biosphere-atmosphere system in West Africa to SST forcings over the Atlantic Ocean.

The first group of experiments include *Dyn-Def1* and *Dyn-Def2*, which account for deforestation of scenario A and B in Figure 7-1, respectively. Deforestation takes place between the coast and 12°N, in a region covered by forest and woodland at the natural equilibrium of the model. These experiments are designed to address whether the past deforestation in West Africa is large enough to initiate a drought in the Sahel region.

The second group of experiments concentrate on the impact of desertification on the regional climate. Desertification is considered here in addition to deforestation. Land cover changes in each experiment include deforestation of scenario A in the south and desertification in the north with f_{max} varying between experiments. Therefore, the *Dyn-Def1* experiment can be used as the control for desertification experiments. Here we only present one desertification experiment *Dyn-Des1*, which has a f_{max} value of 20%. This experiment is chosen because 20% is approximately the threshold value upon which desertification starts to significantly impact the biosphere-atmosphere system in the Sahel region.

The third group of experiments are designed to demonstrate the role of natural vegetation dynamics in the response of the regional climate system to desertification, which include experiments *Stat-Des0* and *Stat-Des1*. *Stat-Des0* and *Dyn-Def1* are identical except that *Stat-Des0* does not include vegetation dynamics. Similarly, *Stat-Des1* and *Dyn-Des1* are identical except that *Stat-Des1* does not include vegetation dynamics. Therefore, over the unperturbed fraction of each grid cell in the third group of experiments, instead of responding to the subsequent climate changes, vegetation after 1950 is fixed at the initial vegetation condition.

The characteristics of all the experiments are listed in Table-1.

Table 1: Experiments Design

Experiments ID	Vegetation Over Unperturbed Region	Maintained Perturbation	
		Deforestation	Desertification
Dyn-Control	Dynamic	no	no
Dyn-Def1	Dynamic	scenario A	no
Dyn-Def2	Dynamic	scenario B	no
Dyn-Des1	Dynamic	scenario A	f_{max}=0.20
Stat-Des0	Static	scenario A	no
Stat-Des1	Static	scenario A	f_{max}=0.20

7.3.3 Impact of Land Cover Changes on the Sahel Rainfall

In the following we present the results on how the human-induced land cover changes might have altered the rainfall trend in the Sahel region during the past several decades. As demonstrated in Chapter 6, when the model is driven by the SST variations in the Atlantic Ocean, the interannual variability of the simulated rainfall demonstrates significant spatial coherency within the Sahel region (10°N-17.5°N) as well as in the region of Guinea coast (south of 10°N). Such spatial coherency is also evident in observational data (Nicholson and Entekhabi, 1986). Therefore, the areal average of rainfall over each of the two regions can be used for further analysis.

Figure 7-2(a,b) presents the time series of the Sahel rainfall and rainfall over the Guinea coast, simulated in *Dyn-Control* (solid line), *Dyn-Def1* (dash-dot line), and *Dyn-Def2* (dot line). Deforestation causes significant reduction in rainfall over the Guinea Coast. From 1950s to 1990s, a rainfall reduction of about 20% is simulated. However, the model shows no systematic impact of deforestation on the Sahel rainfall. Further experiments suggest that deforestation does not cause significant decrease of Sahel rainfall unless its extent and intensity reach a certain level, a level higher than that of the recorded deforestation in West Africa. This result seems inconsistent with the finding of previous studies such as Zheng and Eltahir (1998), who showed that deforestation causes rainfall decrease over the entire West Africa. However, in their

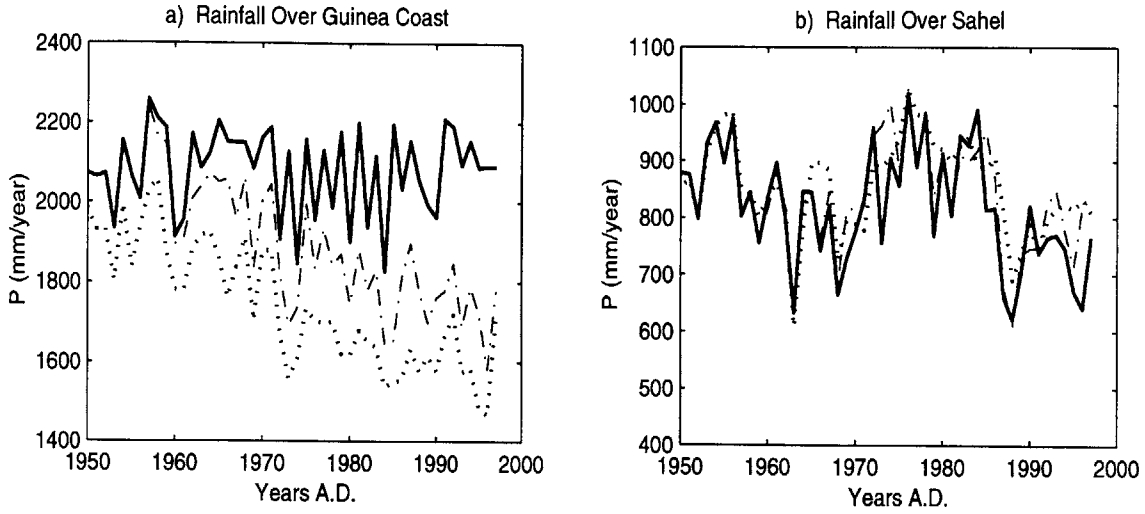

Figure 7-2: Rainfall time series for a) the Guinea coast region and b) the Sahel region, in experiments *Dyn-Control* (solid line), *Dyn-Def1* (dash-dot line), and *Dyn-Def2* (dot line).

study, deforestation was defined as a complete replacement of forest by grassland, which is the most severe scenario of forest loss. Our study takes a more realistic approach: deforestation is described as a gradual process of patchy land cover changes from forest to grassland; within the undisturbed area, forest still exists and is able to respond to the climate changes induced by forest loss elsewhere. When a complete replacement of forest by grassland is considered in our model, the decrease of rainfall takes place all over West Africa including the Sahel region, which is consistent with Zheng and Eltahir (1998).

The impact of desertification also tends to be concentrated in the perturbation zone. While desertification within a reasonable range causes negligible climate modification over the Guinea Coast, it can induce significant response of the climate system within the Sahel region. This is shown in Figure 7-3(a,b), where the light line stands for the *Dyn-Def1* experiment, and the heavy line stands for the *Dyn-Des1* experiment. Here the *Dyn-Def1* experiment is used as the control case for the desertification experiment. In addition to the deforestation process of scenario A considered in *Dyn-Def1*, land cover changes in *Dyn-Des1* also includes a desertification process (as shown in Figure 7-1) with f_{max} equal to 20%. Desertification of this scenario, i.e., the fraction

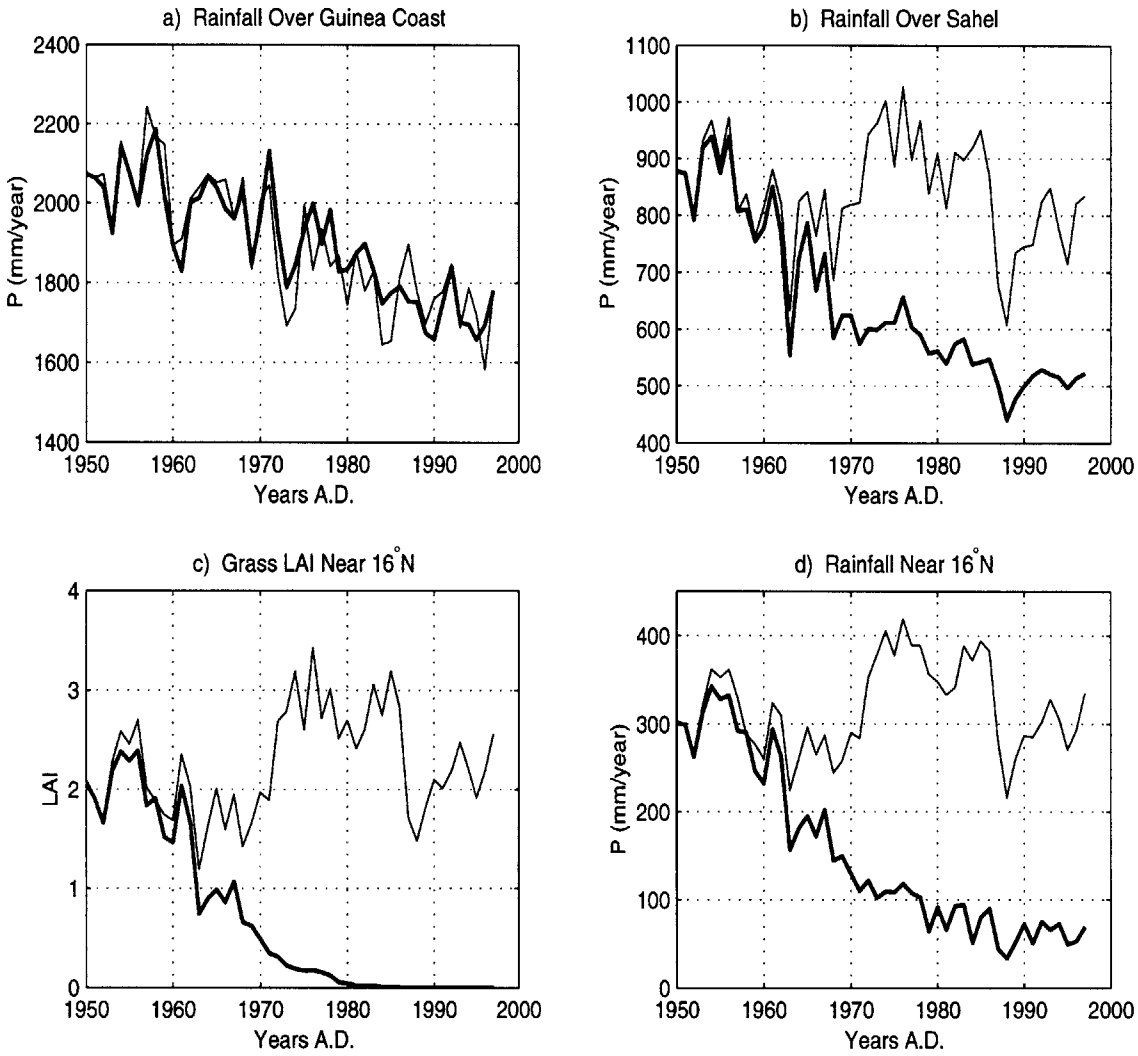

Figure 7-3: Comparison between the experiments *Dyn-Def1* (light line) and *Dyn-Des1* (heavy line): a) Rainfall average over the Guinea coast region; b) Rainfall average over the Sahel region; c) Growing-season leaf area index (LAI) at the grid point near 16°N; d) Rainfall at the grid point near 16°N.

of exposed bare soil increasing from zero in 1950 to 20% in 1970 and remaining constant afterwards, induces a large magnitude of rainfall reduction in the Sahel region during the second half of the 20th century: a severe Sahel drought is initiated in the late 1960s, and persists until the end of the simulation, in 1997. The rainfall amount averaged over the Sahel region after 1970 is only about 60-70% of that in the 1950s (Figure 7-3b), a decrease of more than 30%. This drought causes an expansion of the Sahara desert. As shown in Figure 7-3(c,d), the grassland near the desert border before the drought onset is transformed into desert, and the corresponding rainfall decrease is as large as 60% (compared with the wet 1950s). Figure 7-4 presents the spatial and temporal distribution of NPP in *Dyn-Des1*, with the approximate desert border marked by the black line. Comparing Figure 7-4 with Figure 6-8 suggests that

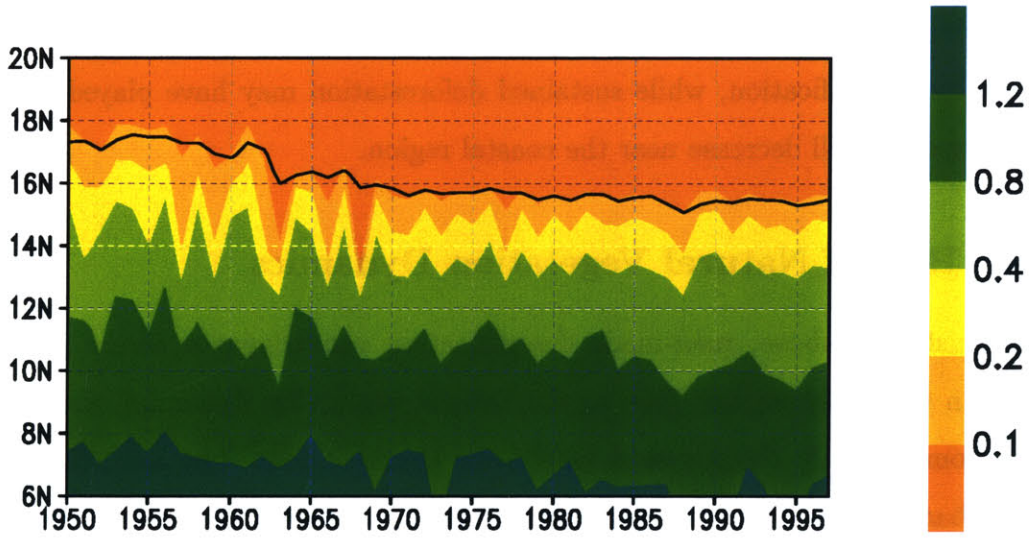

Figure 7-4: Net primary productivity (in $kgC/m^2/year$) distribution for the simulation period 1950-1997 in *Dyn-Des1*.

the simulated drought is associated with a transition of the regional climate system from its wet regime to its dry regime. It is worth noting that the magnitude of the desertification that causes such a climate transition is rather small: the desertification scenario with f_{max} equal to 20% represents a transformation of grassland into desert at a rate of only 1% per year during the period 1950-1970. The overall surface albedo

(i.e., the area-weighted albedo average between the portion of natural ecosystem and the portion of managed ecosystem) increases from the 1950s to the 1990s by less than 0.08, which is a conceivable amount based on observations (Nicholson et al., 1998).

Interestingly, the drought initiation shows a strong nonlinearity. When a slightly smaller f_{max} is used (e.g., 15%), the model simulates very little rainfall reduction caused by desertification. This is due to the nonlinearity in the resilience of the coupled biosphere-atmosphere system as presented in Chapter 5.

Our results suggests that man-made desertification of a realistic magnitude is able to trigger a persistent Sahel drought, while the deforestation-induced reduction of rainfall occurs mainly near the coast. Observations show that the current drought is not limited to the Sahel region. Although not as dramatic as in the Sahel region, a trend of rainfall decrease is also observed over the Guinea Coast (e.g., Nicholson, 1994). If human activities are to blame, the persistent Sahel drought might have been initiated by desertification, while sustained deforestation may have played a role in the observed rainfall decrease near the coastal region.

7.3.4 Role of Natural Vegetation Dynamics

As demonstrated above, man-made desertification can trigger a severe persistent drought in the Sahel region. Due to the natural vegetation dynamics, the drought results from not only the imposed land cover changes alone, but also, the vegetation feedback induced by these changes. Here, to elucidate the role of vegetation dynamics in the simulated drought, we investigate how much of the rainfall decrease is attributed to the vegetation feedback and how much is due to the imposed land cover changes alone.

Figure 7-5 presents the comparison of the Sahel rainfall between experiments *Stat-Des0* and *Stat-Des1*, which is similar to Figure 7-3(b) but without vegetation dynamics. These are the kind of results that traditional studies on the climatic impact of desertification would get. When assuming static vegetation, the prescribed land cover changes of the same magnitude result in only a minor reduction of rainfall without causing any climate transition. Therefore, the simulated drought conditions

in the Sahel region (Figure 7-3b-d) are primarily caused by vegetation dynamics which involves the response of the natural ecosystem to the atmospheric climate changes induced by the imposed land cover changes. When the initial damage of the ecosystem due to desertification reaches a certain threshold, the response of the atmospheric climate becomes significant enough to deteriorate the otherwise undisturbed portion of the ecosystem, which then works in the same direction as the man-made desertification in causing a drier climate. Therefore, natural ecosystem dynamics act to amplify the impact of man-induced land cover changes. This response, together with the system's natural response to the observed oceanic forcing during the late 1960s and early 1970s, eventually cause a persistent drought in the following decades.

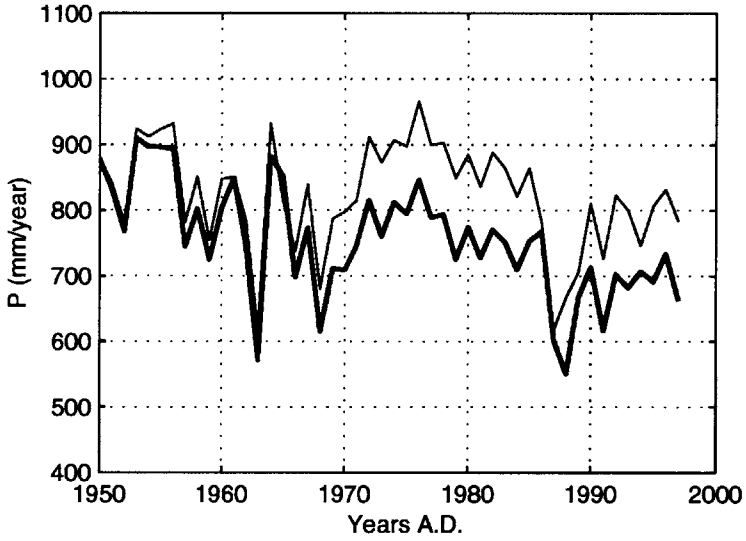

Figure 7-5: Comparison of the sahel rainfall between *Stat-Des0* (light line) and *Stat-Des1* (heavy line).

7.4 Drought Initiation by Large Scale Forcings

Although the man-made desertification can act as a triggering mechanism for the Sahel drought, it is not the only possible mechanism for drought initiation. Large scale forcings, e.g., the SST pattern in the Atlantic Ocean and over the globe, can also

cause the deterioration of the regional climate system by reducing the Sahel rainfall (e.g., Folland *et al.*, 1991; Ward, 1998). Due to its zonal symmetry, our model cannot represent the various global-scale forcings. Here, as a surrogate for those forcings, a warming perturbation in SST of the Atlantic ocean is imposed for a limited time to force a reduction of the Sahel rainfall (Eltahir and Gong, 1996) around the time of the drought onset. During the rest of the simulation period, the observed SST is used. The only difference between the *Dyn-Control* simulation in Section 7.3 and the SST perturbation experiments here is the imposed warming event. Therefore, *Dyn-Control* can be used as the control for the SST perturbation experiments.

Sensitivity experiments on different magnitudes and durations of the SST perturbation are carried out. The results suggest that a warming as small as 2.5°C, imposed uniformly for the four years 1968-1971, is sufficient to trigger a persistent Sahel drought which lasts for several decades. Figure 7-6 presents the temporal and spatial distribution of NPP in this SST experiment, where the isohyet of the 200-mm annual rainfall marks the approximate desert border. Comparing Figure 7-6 and Fig-

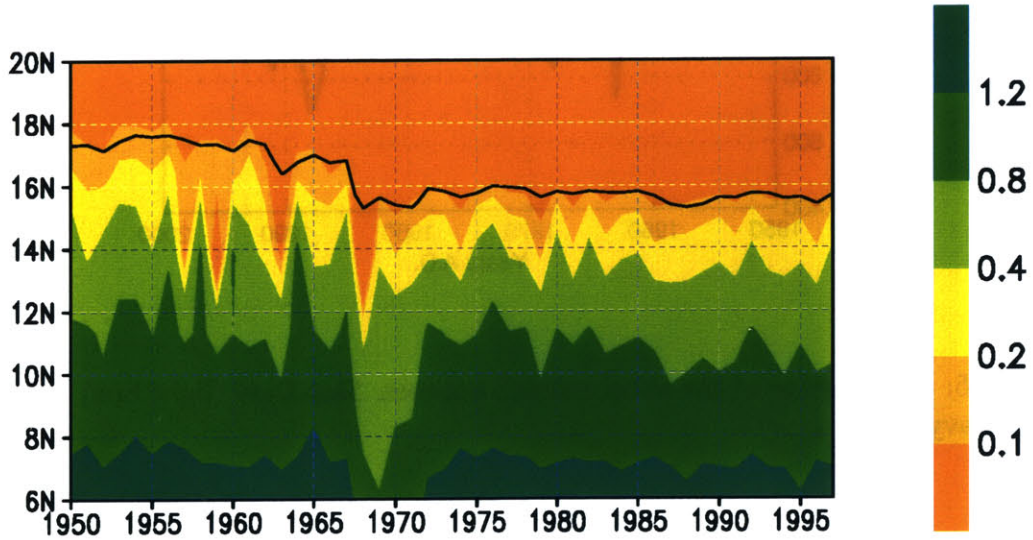

Figure 7-6: Net primary productivity (in $kgC/m^2/year$) distribution for the simulation period 1950-1997 in the experiment with a warming of four years (1969-1971) imposed over the Atlantic ocean.

ure 6-8 clearly indicates a climate transition from the wet regime to the dry regime

around the time of the drought onset. Rainfall time series for the Guinea coast and the Sahel region in this SST perturbation experiment are shown in Figure 7-7(a,b), compared with that of the control case. Similar results for the growing-season leaf

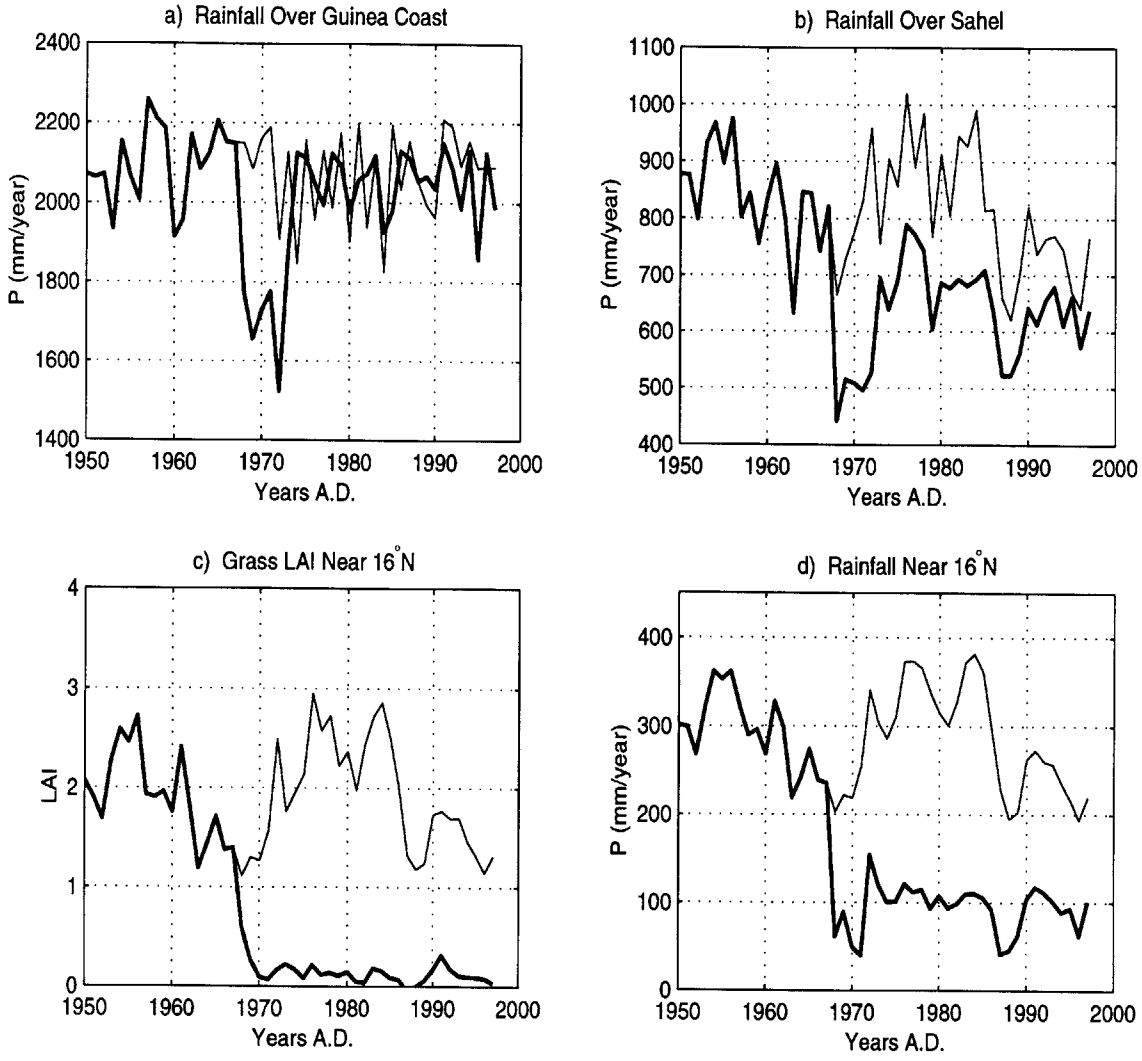

Figure 7-7: Comparison between *Dyn-Control* (light line) and the SST perturbation experiment (heavy line): a) Rainfall average over the Guinea coast region; b) Rainfall average over the Sahel region; c) Growing-season leaf area index (LAI) at the grid point near 16°N; d) Rainfall at the grid point near 16°N.

area index (LAI) and the annual rainfall at a grid point near 16°N are presented in Figure 7-7(c,d). Although no trend of rainfall decrease is observed over the Guinea coast, a significant drought occurs in the Sahel region. Figure 7-6 and 7-7 all suggest that the drought induced by large-scale forcings is also accompanied by an expan-

sion of the Sahara desert. Similar to the case of land cover changes, when the SST forcing reaches a certain threshold, the response of the atmospheric climate becomes significant enough to cause a change in the natural ecosystem, which then works in the same direction as the initial forcing in changing the regional climate.

For the case of drought initiation by anthropogenic desertification, albedo increases as a result of both desertification and the induced drought. Here, for the case of drought initiation by SST warming, as no human activity is involved, the changes of albedo merely reflect the response of the natural ecosystem. However, as shown in Figure 7-8, no readily identifiable difference between the two cases is observed in the

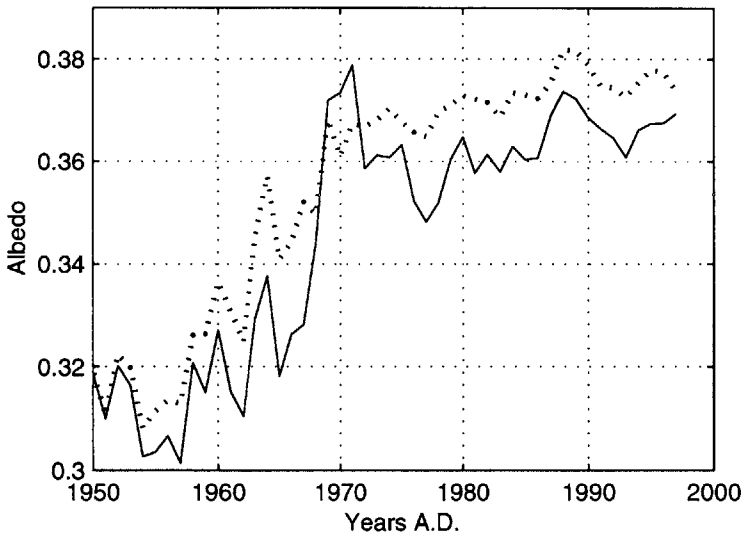

Figure 7-8: Annual variations of the overall surface albedo averaged over 12.5°N-17.5°N, in the desertification experiment (dot line) and the SST perturbation experiment (solid line).

pattern of the albedo evolution, and there is no significant difference between the two cases in the magnitude of the albedo change from the 1950s to the 1990s. Therefore, albedo increase derived from satellite data does not necessarily suggest the existence of man-induced vegetation degradation. Without more ecological data, it is hard to distinguish the land cover changes induced by human activities from those induced by a drought.

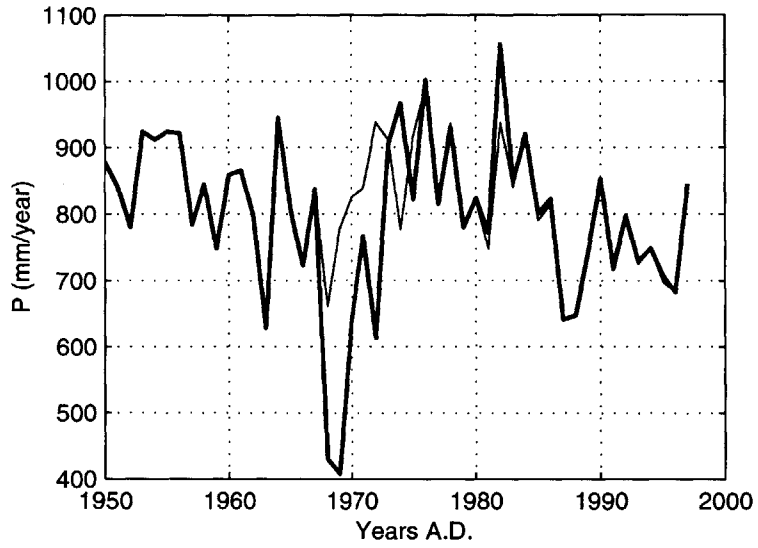

Figure 7-9: Similar to Figure 7-7b, but for experiments with static vegetation.

The role of vegetation dynamics in shaping the response of the climate system to SST perturbations is investigated in a similar way to the case of land cover changes. We perform two experiments which, except for the assumption of static vegetation, are exactly the same as the control and the SST perturbation experiment in Figure 7-7. The comparison between the control with static vegetation and the SST perturbation experiment with static vegetation is presented in Figure 7-9. Differences in the Sahel rainfall only exist during the perturbation period. After the termination of the SST perturbation, very little lasting impact on the Sahel rainfall is observed. Therefore, for a drought initiation by any large-scale forcing, the dynamic response of the biosphere plays a critical role. Without the functioning of ecosystem dynamics, the regional climate system will quickly recover from a non-persistent forcing.

7.5 Summary and Conclusions

This chapter investigates the potential triggering mechanisms for the Sahel drought using ZonalBAM. Long-term climate simulations are carried out by driving the model with SST variations during 1950-1997 over the tropical Atlantic ocean. By adding

different types of perturbations to the model, the possibility of drought initiation by anthropogenic activities and that by large-scale forcings are separately studied. Human activities considered include both deforestation and desertification of realistic magnitudes, which are described as a patchy, gradual change of the land cover. A uniform warming over the Atlantic ocean imposed for a certain period around the drought onset is used as the surrogate of the large-scale forcings that may cause a decrease of the Sahel rainfall. The role of ecosystem dynamics in shaping the response of the regional climate system to these external forcings is studied using experiments with and without vegetation dynamics.

Our results suggest that both human activities alone and large-scale forcings alone can trigger a persistent Sahel drought similar to what has been observed in the 20th century. However, no matter what the triggering mechanism is, ecosystem dynamics is the most significant process in maintaining the drought condition. The natural ecosystem deteriorates in response to changes of the atmospheric climate caused by the man-made vegetation degradation or the warming over the Atlantic ocean. This adds to the system an induced process of land cover degeneration which works to impact the regional climate system in the same direction as that of the initial forcing. As a result, the impact of the triggering forcing, whatever it is, gets amplified and perpetuated. When the initial forcing reaches a certain threshold, the feedback due to ecosystem dynamics becomes significant enough to result in a transition of the regional climate system from its wet regime to its dry regime. Such a transition features a persistent drought in the Sahel region which will last until a reverse transition takes place.

Due to the lack of reliable ecological data before the drought onset, it is hard to determine based on observations what triggered the recent Sahel drought. In the context of the model, when driven by the SST observations over the Atlantic ocean and subjected to no other external forcings (e.g., *Dyn-Control* experiment, solid line in Figure 7-2b), the regional climate system features a relatively dry condition over the Sahel region in the 1960s. This makes the climate system in the 1960s vulnerable to any external forcing which may further decrease the Sahel rainfall. The 1960s

happened to be a time when both the regional land cover changes (e.g., Warren, 1996) and the global SST pattern changes (e.g., Ward, 1998) favor a rainfall reduction in the Sahel region. The most likely scenario for the occurrence of the Sahel drought is that natural ecosystem dynamics has intensified and perpetuated an existing dry condition initiated by a combination of regional changes in land cover and changes in large-scale forcings such as the global SST pattern. We emphasize that, no matter what is the initial forcing, ecosystem dynamics plays the dominant role in sustaining the drought conditions.

Chapter 8

Summary and Conclusions

This chapter summarizes the main results and conclusions of this study, and suggests directions for future research.

8.1 Summary of the Results

8.1.1 Modeling the Biosphere-Atmosphere System

A zonally symmetric, synchronously coupled biosphere-atmosphere model ZonalBAM is developed to describe the climate system over West Africa. The coupled model combines a zonally symmetric atmospheric model and a fully dynamic biospheric model. It can simulate not only the transient climate but also the transient vegetation associated with the transient climate, i.e., the two-way biosphere-atmosphere interactions.

With the atmospheric forcings fixed at today's condition, the biospheric model is run in off-line mode to simulate the potential vegetation distribution; with the vegetation fixed at today's condition and the biospheric model functioning as a land surface scheme, the atmospheric model is used to simulate the current atmospheric climate. The model simulations compare well with various observational data over West Africa. Starting with an initial vegetation distribution close to today's observation and forced by the climatological SST, the fully coupled biosphere-atmosphere model produces an equilibrium state which is slightly greener and wetter than the

current climate (defined as the average during the entire twentieth century). One feature of this model equilibrium is the absence of savannah-type vegetation, for which the lack of a disturbance mechanism (e.g., fire and grazing) in the model is identified as a potential reason.

Taking West Africa as a case study, the importance of representing the rainfall sub-grid variability in climate modeling is demonstrated using ZonalBAM. When neglecting the sub-grid variability of rainfall, even if evapotranspiration is tuned to be consistent with observations, significant errors in surface hydrological processes and surface energy balance may result. These errors extend to the atmosphere via the low-level cloud feedback and impact a wide range of atmospheric processes. The same errors also propagate into the biosphere through vegetation dynamics, and can eventually lead to a significantly different biosphere-atmosphere equilibrium state. This case study provides a good example for the need to have physical realism in modeling the complex biosphere-atmosphere system.

8.1.2 Multiple Equilibrium States

Based on simple analyses on how the coupled biosphere-atmosphere system responds to vegetation perturbations (natural or anthropogenic) within the scope of a dynamic ecosystem, a hypothesis is proposed that the regional climate system may have multiple equilibrium states coexisting under the same precessional forcing. Following a vegetation perturbation, three possible types of response are predicted: a negative feedback leading to a full recovery; a positive feedback leading to perturbation enhancement and a new equilibrium; a negative feedback leading to a partial recovery and a new equilibrium.

The topic of multiple equilibria is first studied based on the sensitivity of the coupled biosphere-atmosphere model (ZonalBAM) to initial conditions. When starting from a forest-covered West Africa, the model evolves into an equilibrium which features trees over most of West Africa and grass over a narrow band in the north. When starting with a desert-covered West Africa, the model evolves into an equilibrium which features tall grass near the coast with short grass and desert in the north.

Other equilibria of the model fall in between these two extremes.

A further study on the multiple-equilibrium nature of the regional climate system using ZonalBAM is performed based on the resilience of the biosphere-atmosphere system at a "close-to-current" equilibrium. Perturbations considered here are non-permanent and include deforestation, desertification, and irrigation. When deforestation (up to a forest clearing) occurs, a negative feedback is always observed which eventually leads to the full recovery of the "pre-perturbation" equilibrium; when different degrees of desertification (in the form of a uniform grass thinning) are imposed, all the three predicted types of responses are observed. Following grass thinning of a small magnitude, the feedback is negative and leads to a full recovery; upon grass thinning of a large enough magnitude, a climate transition occurs through a positive feedback, or through a negative feedback leading to a partial recovery. Three different equilibria (wet, medium, and dry) are identified. While desertification can cause a climate transition from a wetter equilibrium to a drier one, irrigation can cause a climate transition from a drier equilibrium to a wetter one. In all the above experiments, the climatological SST is used.

8.1.3 Mechanisms of the Low-Frequency Rainfall Variability

Long-term climate simulations for the region of West Africa are performed using ZonalBAM forced with the observed SST in the tropical Atlantic Ocean from 1898 to 1997. Consistent with observations, the model rainfall over the Sahel region is dominated by low-frequency variability, and the model rainfall over the Guinea Coast features more high-frequency variability. However, when assuming static vegetation conditions (i.e., the vegetation dynamics is turned off), the model fails to reproduce the dominance of low-frequency variability in the Sahel rainfall.

Based on the sensitivity of the long-term climate simulations to initial vegetation conditions, the multiple-equilibrium behavior of the regional climate system under the influence of variable SST is examined. Although three equilibria (wet, medium, and dry) are documented when the model is forced with the climatology of SST seasonal cycle, only two climate regimes (wet and dry) are viable when the inter-

annual variability of SST is included. The observed SST forcings in the Atlantic Ocean alone are not large enough to cause transitions between different regimes. However, climate transitions take place when SST forcings over the Atlantic ocean are artificially doubled to surrogate the impact of global-scale forcings. Such transitions represent a potential mechanism for the low-frequency climate oscillation.

8.1.4 Ecosystem Dynamics and the Current Sahel Drought

The coupled model ZonalBAM with a mosaic representation of land surface is used to investigate the process of drought initiation by anthropogenically induced permanent land cover changes. The time period 1950-1997 is considered. When the extent of man-made desertification (i.e., changing a fraction of the grassland to desert) reaches a certain threshold, the induced changes in the atmospheric climate become significant enough to deteriorate the healthy sections of the local ecosystem which are not directly influenced by human activities. This response causes a climate transition towards a drier equilibrium in the late 1960s which takes place in the form of a severe persistent drought over the Sahel region. However, when vegetation dynamics is turned off, desertification of the same magnitude induces only a minor reduction of the Sahel rainfall.

A warming event of a limited time is imposed to the Atlantic ocean, as the surrogate for the global-scale SST variations that may cause a decrease of the Sahel rainfall, to study the process of a drought initiation by large-scale forcings. When the SST warming reaches a certain threshold, the rainfall reduction over the Sahel region becomes significant enough to cause the deterioration of the natural ecosystem, which then works in the same direction as the SST warming in causing dry conditions in the Sahel region. As a result, a climate transition to the drier regime takes place, leading to a persistent drought. In the case where vegetation dynamics is not considered, instead of developing into a persistent drought, the impact of the warming event disappears shortly after the termination of the warming.

8.2 General Conclusions

The coupled biosphere-atmosphere system over West Africa is intransitive. The regional climate system has multiple equilibrium states coexisting under the same precessional forcing, with reversible transitions between different equilibria. The climate system can remain around one equilibrium under the influence of small perturbations (i.e., climate persistence) until a large enough perturbation leads the system towards a different equilibrium (i.e., climate transition). Following a vegetation perturbation, climate persistence is observed when the feedback is negative which leads to a full recovery; climate transitions take place when the feedback is positive, or when a negative feedback only leads to a partial recovery.

Triggered by external perturbations (natural or man-made) and governed by the two-way biosphere-atmosphere feedback involving vegetation dynamics, the biosphere-atmosphere system can evolve from one equilibrium to another within a relatively short time (on the order of one decade). The short time scale of climate transitions between different equilibria suggests that the multiple-equilibrium behavior of the regional climate system is a relevant process for shaping the climate variability at historical time scales. Vegetation dynamics, the fundamental physical process that ensures the multiple-equilibrium behavior of the coupled biosphere-atmosphere system, is important for understanding the observed climate characteristics in West Africa.

Vegetation dynamics enhances the low-frequency variability of the Sahel rainfall. Large-scale factors including SST variations in the Atlantic Ocean may act as the driving forcing for the climate variability over the Sahel region. However, the response of the regional climate system to these forcings is significantly regulated by vegetation dynamics. Without the role of vegetation dynamics, the low-frequency rainfall variability would be less significant than observed. When the SST or any other forcing causes a significantly wetter-than-normal (drier-than-normal) event, vegetation develops denser (thinner) than normal, especially if this event spans several years. When the driving forcing ceases to operate, the biosphere-atmosphere system still

has a denser-than-normal (thinner-than-normal) vegetation, which is equivalent to the situation after a vegetation perturbation. In the next several years following the termination of the original event, the biosphere-atmosphere system will be in a status of recovering from a vegetation anomaly that favors wetter-than-normal (drier-than-normal) conditions, assuming that a recovery is possible. As a result, the original event gets amplified by vegetation dynamics, which directly contributes to the low-frequency climate variability.

The regional climate system over West Africa in the model has two "close-to-current" climate regimes (wet and dry) in the scenario of varying SST forcings. When external forcings such as changes in the global SST pattern cause an unrecoverable anomaly, climate transition takes place. As a result, the impact of the original forcing is not only amplified, but may also be sustained and perpetuated. Such climate transitions between the two different regimes act as another important mechanism contributing to the low-frequency rainfall variability in the Sahel region. Climate persistence at one regime and climate transitions towards the other collectively compose a special type of multi-decadal fluctuations. It is important to note that vegetation dynamics is the fundamental physical process regulating the climate transitions between different regimes.

Vegetation dynamics plays an important role in the development and persistence of the current Sahel drought. A likely scenario for the triggering mechanism of the Sahel drought would involve a combination of several processes including regional changes in land cover as well as changes in the patterns of global and regional SST distributions. However, regardless of what the triggering mechanism is, the response of the natural vegetation to the atmospheric changes induced by the initial external forcing is a critical process for explaining the severity and persistence of the observed drought. The natural response of the grass ecosystem near the desert border to the dry conditions of the late 1960s seems to have played a significant role in the dynamics of the drought.

In summary, vegetation dynamics is a significant physical process in causing the observed characteristics of the climate over West Africa, including the low-frequency

climate variability and the persistence of the Sahel drought. The multiple-equilibrium nature of the regional climate system provides the theoretical basis for the special role of vegetation dynamics in the climate variability.

8.3 Future Research

In this study we document the multiple-equilibrium behavior (i.e., intransitiveness) of the regional climate system over West Africa using a zonally symmetric model. It remains to be addressed how the limitation of a zonal model may influence the results of our study. In future research we plan to carry out a similar study by coupling IBIS to a general circulation model. More importantly, it is essential for future research to address whether the existence of multiple equilibria is a general feature of the global climate system or specific for the region of West Africa. The intransitive nature of the climate system suggests that climate prediction should be treated as an initial value problem instead of as a boundary layer problem which is the general traditional view. Therefore, the development of a new approach to studies on climate prediction (e.g., doubling CO_2 studies) is also a task of future research.

The decadal variability in the inter-hemispheric gradient of global SST, which is statistically related to the low-frequency variability of the Sahel rainfall, cannot be represented in a zonally symmetric model. It will be important for future research using a 3-D model to address whether the decadal variability of the global inter-hemispheric SST gradient does contribute to the low-frequency variability of the Sahel rainfall, and if so, how significant it is compared with the contribution from the two-way biosphere-atmosphere feedback.

In this study we focus on the role of two-way biosphere-atmosphere interactions. The two-way atmosphere-ocean interactions are not included. Without incorporating the oceanic feedback, it is impossible to address whether the biosphere-atmosphere feedback is the most significant mechanism in regulating the climate variability. The role of oceanic feedback remains to be a topic for future research.

The increase of CO_2 concentration has significant impact on the coupled biosphere-

atmosphere system. In addition to the well-documented warming impact, CO_2 abundance also fertilizes the vegetation growth and modifies the competition between C3 and C4 plants. However, in this study, the CO_2 concentration is fixed at its post-industrial level, which is about $350ppm$. Future studies should address the impact of CO_2 increase in the scenario of a synchronously coupled biosphere-atmosphere system.

Bibliography

[1] Arking, A., 1996: Absorption of solar energy in the atmosphere: discrepancy between model and observations. *Science*, 273, 779-782.

[2] Baker, M. B., 1997: Cloud microphysics and climate. *Science*, 276, 1072-1078

[3] Bishop, J. K. B., W. B. Rossow, and E. G. Dutton, 1997: Surface solar irradiance from the International Satellite Cloud Climatology Project 1983-1991. *J. Geophys. Res.*, 102, 6883-6910

[4] Bourliere, F., and M. Hadley, 1983: Present-day savannas: an overview, in F. Bourliere, eds. Ecosystem of the World – Tropical Savannas. Elsevier Science Publishing Company, New York

[5] Bryson, R. A., 1973: Drought in Sahelia: Who or what is to blame? *the Ecologist*, 3, 366-371

[6] Carson, D. J., 1986: Parameterization of land surface processes in Meteorological Office numerical weather predicting and climate models. *Dyn. Climatol. Tech. Note 37*, Meteorol. Off., Bracknell

[7] Cess R. D., M. H. Zhang, P. Minnis, L. Corsetti, E. G. Dutton, B. W. Forgon, D. P. Garber, W. L. Gates, J. J. Hack, E. F. Harrison, X. Jing, J. T. Kiehl, C. N. Long, J.-J. Morcrette, G. L. Pottoer, V. Ramanathan, B. Subasilar, C. H. Whitlock, D. F. Young, and Y. Zhou, 1995: Absorption of solar radiation by clouds: observations versus models. *Science*, 267, 496-499

[8] Charney, J. G, P. H. Stone, and W. J. Quirk, 1975: Drought in the Sahara: a biogeophysical feedback mechanism. *Science*, 187, 434-435

[9] Charney, J. G., 1975: Dynamics of deserts and drought in the Sahel. *Q. J. R. Meteorol. Soc.*, 101, 193-202

[10] Charney, J., W. J. Quirk, S. Chow, and J. Kornfield, 1977: A comparative study of the effects of albedo change on drought in semi-arid regions. *J. Atmos. Sci.*, 34, 1366-1385

[11] Chou, M-D, 1984: Broadband water vapor transmission functions for atmospheric IR flux computations. *J. of Atmos. Sci.*, 41, 1775-1778

[12] Chou, M-D, 1986: Atmospheric solar heating rate in the water vapor bands. *Journal of Climate and Applied Meteorology*, 25, 1532-1542

[13] Chou, M-D, 1992: A solar-radiation model for use in climate studies. *J. Atmos. Sci.*, 49, 762-772

[14] Chou, M-D, D. P. Kratz, W. Ridgway, 1991: Infrared radiation parameterizations in numerical climate models. *J. Clim.*, 4, 424-437

[15] Chou, M-D, 1990: Parameterizations for the absorption of solar-radiation by O_2 and CO_2 with application to climate studies. *J. Clim.*, 3, 209-217

[16] Chou M-D and L. Kouvaris, 1991: Calculations of transmission functions in the infrared CO_2 and O_3 bands. *J. Geophys. Res.*, 96(D5), 9003-9012

[17] Claussen, M., 1994: On coupling global biome models with climate models. *Climate Research*, 4, 203-221

[18] Claussen, M., 1997: Modeling bio-geophysical feedback in the African and Indian monsoon region. *Climate Dynamics*, 13, 247-257

[19] Claussen, M., 1998: On multiple solutions of the atmosphere-vegetation system in present-day climate. *Global Change Biology*, 4, 549-559

[20] Cunnington, W. M. and P. R. Rowntree, 1986: Simulations of the Saharan atmosphere-dependence on moisture and albedo. *Q. J. R. Meteorol. Soc.*, 112, 971-999

[21] Dansgaard, W., S. J. Johnsen, N. Reeh, N. Gundestrup, H. B. Clausen, and C. U. Hammer, 1975: Climatic changes, Norsemem and modern man. *Nature*, 255, 24-28

[22] Demaree, G. R., and C. Nicolis, 1990: Onset of Sahelian drought viewed as a fluctuation-induced transition. *Q. J. R. Meteorol. Soc.*, 116, 221-238

[23] Dickinson, R. E., and A. Henderson-Sellers, 1988: Modeling tropical deforestation: A study of GCM land-surface parameterizations. *Q. J. R. Meteorol. Soc.*, 114, 439-462

[24] Dickinson, R. E., A. Henderson-Sellers, and P. J. Kennedy, 1993: Biosphere-Atmsophere Transfer Scheme (BATS) Version 1e as Coupled to the NCAR Community Climate Model. *NCAR Technical Note NCAR/TN-387+STR*, 72pp

[25] Dolman, A. J., and D. Gregory, 1992: The parameterization of rainfall interception in GCMs. *Q. J. R. Meteorol. Soc.*, 118, 455-467

[26] Druyan, L. M., 1991: The sensitivity of sub-Saharan precipitation to Atlantic SST. *Climate Change*, 18, 17-36

[27] Druyan, L. M., and S. Hastenrath, 1991: Modelling the differential impact of 1984 and 1950 sea-surface temperatures on Sahel rainfall. *International Journal of Climatology*, 11, 367-380

[28] Eagleson, P. S., and R. I. Segarra, 1985: Water-limited equilibrium of savanna vegetation systems. *Water Resources Research*, 21, 1483-1493

[29] Eltahir, E. A. B., 1996: Role of vegetation in sustaining large-scale atmospheric circulations in the tropics. *J. Geophys. Res.*, 101 (D2), 4255-4268

[30] Eltahir, E. A. B., and R. L. Bras, 1993a: Estimation of the fractional coverage of rainfall in climate models. *J. Clim.*, 6, 639-644

[31] Eltahir, E. A. B., and R. L. Bras, 1993b: Description of rainfalll interception over large areas. *J. Clim.*, 6, 1002-1008

[32] Eltahir, E. A. B., and C. Gong, 1996: Dynamics of wet and dry years in West Africa. *J. Clim.*, 9, 1030-1042

[33] Emanuel, K., 1991: A scheme for representing cumulus convection in large-scale models. *J. Atmos. Sci.*, 48, 2313-2335

[34] Entekhabi, D., I. Rodriguez-Iturbe, and R. Bras, 1991: Variability in large-scale water balance with land surface-atmosphere interaction. *J. Clim.*, 5, 798-813

[35] Entekhabi, D., and P. S Eagleson, 1989: Land surface hydrology parameterization for atmospheric general circulation models indlucing subgrid scale spatial variability. *J. Clim.*, 2, 816-831

[36] Ewel, J., 1971: Biomass changes in early tropical succession. *Turrialba*, 21, 110-112

[37] Ewel, J., 1983: Succession. in "Ecosystems of the World 14A", pp. 217-223. (Eds. F. B. Golley, ELSEVIER scientific publishing company).

[38] Fairhead, J., and M. Leach, 1998: Reconsidering the extent of deforestation in twentieth century West Africa. *Unasylva 192*, 49, 38-46

[39] Farmer, G., and T. M. L. Wigley, 1985: Climatic Trends for Tropical Africa. Research Report, 136 pp. University of East Anglia, Norwich, UK

[40] Foley, J. A., J. E. Kutzbach, M. T. Coe, and S. Levis, 1994: Feedbacks between climate and the boreal forests during the Holocene epoch. *Nature*, 371, 52-54

[41] Foley, J. A., I. C. Prentice, N. Ramankutty, S. Levis, D. Pollard, S. Sitch, and A. Haxeltine, 1996: An integrated biosphere model of land surface processes, ter-

restrial carbon balance, and vegetation dynamics. *Global Biogeochemical Cycles*, 10, 603-628

[42] Foley, J. A., S. Levis, I. C. Prentice, D. Pollard, and S. L. Thompson, 1998: Coupling dynamic models of climate and vegetation. *Global Change Biology*, 4, 561-579

[43] Folland, C., J. Owen, M. N. Ward, and A. Colman, 1991: Prediction of seasonal rainfall in the sahel region using empirical and dynamical methods. *Journal of Forecasting*, 10, 21-56

[44] Folland, c., T. Palmer, and D. Parker, 1986: Sahel rainfall and worldwide sea temperatures, 1901-1985. *Nature*, 320, 602-607

[45] Ghan, S. J., J. C. Liljegren, W. J. Shaw, J. H. Hubbe, and J. C. Dorman, 1997: Influence of subgrid variability on surface hydrology. *J. Clim.*, 10, 3157-3166

[46] Giorgi, F., and R. Avissar, 1997: Representaion of heterogeneity effects in earth system modeling: experience from land surface modeling. *Rev. Geophys.*, 35, 413-438

[47] Giorgi, F., 1997: An approach for the representation of surface heterogeneity in land surface models. Part 1: Theoretical framework. *Mon. Weather Rev.*, 125, 1885-1899

[48] Golley, F.B., 1975: Productivity and mineral cycling in tropical forests. In: *Proceedings of a Symposium presented at the Fifth General Assembly of the special Committee for the I.B.P.* National Academy of Science, Washington, D. C., pp. 106-115.

[49] Gornitz, V., and NASA, 1985: A survey of anthropogenic vegetation changes in West Africa during the last century – climatic implications. *Climatic Change*, 7, 285-325

[50] Gupta, S. K., C. H. Whitlock, N. A. Ritchey, A. C. Wilber, W. L. Darnell and W. F. Staylor, 1997: A climatology of surface radiation budget derived from satellite data. IRS '96: Current Problems in Atmospheric Radiation, Eds., W. L. Smith and K. Stamnes, A. Deepak Publishing, Hampton, VA, 1067pp.

[51] Gutman, G., G. Ohring, and J. H. Joseph, 1984: Interaction between the geobotanic state and climate: a suggested approach and a test with a zonal model. *J. Atmos. Sci.*, 41, 2663-2678

[52] Gutman, G., 1984: Numerical experiments on land surface alterations with a zonal model allowing for interaction between the geobotanic state and climate. *J. Atmos. Sci.*, 41, 2680-2685

[53] Gutman, G., 1986: On modeling dynamics of geobotanic state - climate interaction. *J. Atmos. Sci.*, 43, 305-307

[54] Hastenrath, S. L., 1984: Interannual variability and annual cycle: mechanisms of circulation and climate in the tropical Atlantic sector. *Mon. Weather Rev.*, 112, 1097-1107

[55] Henderson-Sellers, A., R. E. Dickinson, T. B. Durbidge, P. J. Kennedy, K. McGuffie, and A. J. Pitman, 1993: Tropical deforestation: modeling local- to regional- scale climate change. *J. Geophys. Res.*, 98 (D4), 7289-7315

[56] Holtslag, A. A. M. and B. A. Boville, 1993: Local versus nonlocal boundary-layer diffusion in a global climate model. *J. Clim.*, 6, 1825-1842

[57] Hulme, M., Osborn, T. J., and T. C. Johns, 1998: Precipitation sensitivity to global warming: Comparison of observations with HadCM2 simulations. *Geophys. Res. Lett.*, 25, 3379-3382

[58] Hulme, M., 1995: Estimating global changes in precipitation. *Weather*, 50, 34-42

[59] Idso, S. B., 1977: Note on some recently proposed mechanisms of genesis of deserts. *Q. J. R. Meteorol. Soc.*, 103, 369-370

[60] Jackson, R. B., J. Canadell, J. R. Ehleringer, H. A. Mooney, O. E. Sala, and E. D. Schulze, 1996: A global analysis of root distributions for terrestrial biomes. *Oecologia*, 108, 389-411

[61] Janicot, S., V. Moron, and B. Fontaine, 1996: Sahel drought and ENSO dynamics. *Geophys. Res. Lett.*, 23, 515-518

[62] Janicot, S., 1992: Spatiotemporal variability of West African rainfall. Part I: Regionalizations and Typings. *J. Clim.*, 5, 489-498

[63] Johnson, K. D., D. Entekhabi, and P. S. Eagleson, 1991: The implementation and validation of improved landsurface hydrology in an atmospheric general circulation model. *Ralph. M. Parsons Laboratory Tech. Rep. No. 334*, M. I. T., 192 pp

[64] Koster, R. D., and M. J. Suarez, 1992: A comparative analysis of two land surface heterogeneity representations. *J. Clim.*, 5, 1379-1390

[65] Kutzbach, J. E., P. J. Bartlein, J. Foley, S. P. Harrison, S. W. Hostetler, Z. Liu, I. C. Prentice, and T. Webb III, 1996: Potential role of vegetation feedback in the climate sensitivity of high-latitude regions: A case study at 6000 years B.P.. *Global Biogeochemical Cycles*, 10, 727-736

[66] Kutzbach, J. E., G. Bonan, J. Foley, and S. P. Harrison, 1996: Vegetation and soil feedbacks on response of the African monsoon to orbital forcing in the early to middle Holocene. *Nature*, 384, 623-626

[67] Kvamsto, N. G., 1991: An investigation of diagnostic relations between stratiform fractional cloud cover and other meteorological parameters in numerical weather prediction models. *J. Appl. Meteor.*, 30, 200-216

[68] Lamb, P. J., 1978a: Case studies of tropical Atlantic surface circulation patterns during recent sub-Saharan weather anomalies: 1967 and 1968. *Mon. Weather Rev.*, 106, 482-491

[69] Lamb, P. J., 1978b: Large-scale tropical Atlantic surface circulation patterns associated with Sub-saharan weather anomalies. *Tellus*, 30, 240-251

[70] Lean, J., and D. A. Warrilow, 1989: Simulation of the regional climatic impact of Amazon deforestation. *Nature*, 342, 411-413

[71] Lean, J., and P. R. Rowntree, 1993: A GCM simulation of the impact of Amazonian deforestation on climate using an improved canopy respresentation. *Q. J. R. Meteorol. Soc.*, 119, 509-530

[72] Le Barbe, L., and T. Lebel, 1997: Rainfall climatology of the HAPEX-Sahel region during the years 1950-1990. *J. Hydro.*, 188-189, 43-73

[73] Lebel, T., J. D. Taupin, and N. D'Amato, 1997: Rainfall monitoring during HAPEX-Sahel. 1. General rainfall conditions and climatology. *J. Hydro.*, 188-189, 74-96

[74] Levis, S., J. A. Foley, and D. Pollard, 1999: Potential high-latitude vegetation feedbacks on CO2-induced climate change. *Geophys. Res. Lett.*, 26, 747-750

[75] Li, Z., H. W. Barker, and L. Moreau, 1995: The variable effect of clouds on atmospheric absorption of solar radiation. *Nature*, 376, 486-490

[76] Lloyd, C. R., 1990: The temporal distribution of Amazonian rainfall and its implications for forest interception. *Q. J. R. Meteorol. Soc.*, 116, 1487-1494

[77] London, J., 1952: The distribution of radiational temperature change in the Northern Hemisphere during March. *Journal of Meteorology*, 9, 145-151

[78] Lough, J. M., 1986: Tropical Atlantic sea-surface temperatures and rainfall variations in Sub-Saharan Africa. *Mon. Weather Rev.*, 114, 561-570

[79] Maley, J., 1973: Mecanisme des changements climatiques aux basses latitudes. *Palae. Paleo. Paleo.*, 14, 193-227

[80] Maley, J., 1981: Etudes palynologiques dans le bassin du Tchad et pal'eoclimatologie de l'Afrique nord-tropicale de 30 000 ans a l"epoque actuelle. Technical Report No. 129, l'ORSTOM, Paris, France

[81] Menaut, J.-C., 1983: African Savannas, in F. Bourliere, eds. Ecosystem of the World – Tropical Savannas. Elsevier Science Publishing Company, New York

[82] Mocko, D. M. and W. R. Cotton, 1995: Evaluation of fractional cloudiness parameterizations for use in a mesoscale model. *J. Atmos. Sci.*, 52, 2884-2901

[83] Murphy, P. G., 1975: Net primary productivity in tropical terrestrial ecosystems. In H. Lieth and R. H. Whittaker, Eds. Primary Productivity of the Biosphere, Springer-Verlag, New York

[84] Newell, R. E. and J. W. Kidson, 1984: African mean wind changes in Sahelian wet and dry periods. *Journal of Climatology*, 4, 1-7

[85] Nicholson, S. E., 1980: The nature of rainfall fluctuations in subtropical West Africa. *Mon. Weather Rev.*, 108, 473-487

[86] Nicholson, S. E., 1981a: Rainfall and atmospheric circulation during drought periods and wetter years in West Africa. *Mon. Weather Rev.*, 109, 2191-2208

[87] Nicholson, S. E., 1981b: The historical climatology of Africa. In T. M. L. Wigley, M. J. Ingram, and G. Farmer, Eds. Climate abd History, pp. 249-270, Cambridge University Press

[88] Nicholson, S. E., 1989: African drought: Characteristics, causal theories and global teleconnections. *Geophysical Monograph*, 52 (7), 79-100

[89] Nicholson, S. E., 1994: Recent rainfall fluctuations in Africa and their relationship to past conditions over the continent, *Holocene*, 4 (2), 121-131

[90] Nicholson, S. E., and D. Entekhabi, 1986: The quasi-periodic behavior of rainfall variability in Africa and its relationship to the Southern Oscillation. *Rach. Met. Geoph. Biocl. Ser.*, A 34, 311-348

[91] Nicholson, S. E. and I. M. Palao, 1993: A re-evaluation of rainfall variability in the Sahel. Part I. Characteristics of rainfall fluctuations. *International Journal of Climatology*, 13, 371-389

[92] Nicholson, S.E., C. J. Tucker, and M. B. Ba, 1998: Desertification, drought, and surface vegetation: an example from the West African Sahel. *Bull. American Meteor. Soc.*, 79(5), 815-829

[93] Nicolis, 1982: Stochastic aspects of climate transitions – response to a periodic forcing. *Tellus*, 34, 1-9

[94] Ohmura, A., and 14 others, 1998: Baseline surface radiation network (BSRN/WCRP): new precision radiometry for climate research. *Bull. American Meteor. Soc.*, 79, 2115-2135

[95] Palmer, T. N., 1986: The influence of the Atlantic, Pacific, and Indian Oceans on Sahel rainfall. *Nature*, 322, 251-253.

[96] Parker, D. E., and E. B. Horton, 1999: Global and regional climate in 1998. *Weather*, 54(6), 173-184

[97] Parker, D. E., M. Jackson, and E.B. Horton, 1995: The GISST2.2 Sea Surface Temperature and Sea-ice Climatolgy. *Climate Research Technical Note 63 (CRTN63)*, Meteorolgical Office, UK

[98] Pielke, R. A., 1998: Climate prediction as an initial value problem. *Bull. American Meteorol. Soc.*, 79, 2743-2746

[99] Pilewskie, P., and F. P. J. Valero, 1995: Direct observations of excess solar absorption by clouds, Response to "How much solar radiation do clouds absorb?". *Science*, 267, 1626-1629

[100] Pitman, A. J., A. Henderson-Sellers, and Z-L. Yang, 1990: Sensitivity of regional climates to localized precipitation in global models, *Nature*, 346, 734-737

[101] Plumb, R. A., and A. Y. Hou, 1992: The response of a zonally symmetric atmosphere to subtropical thermal forcing: threshold behaviour. *J. Atmos. Sci.*, 49, 1790-1799

[102] Pollard, D., and S. L. Thompson, 1995: Use of a land-surface-transfer scheme (LSX) in a global climate model: the response to doubling stomatal resistance. *Global and Planetary Change*, 10, 129-161

[103] Porter, S. C., 1986: Pattern and forcing of northern hemisphere glacier variations during the last millenium. *Quaternary Research*, 26, 27-48

[104] Prentice, I. C., W. Cramer, S. P. Harrison, R. Leemans, R. A. Monserud, A. M. Solomon, 1992: A global biome model based on plant physiology and dominance, soil properties and climate. *Journal Biogeog*, 19, 117-134

[105] Protopapas, A. L., and R. L. Bras, 1988: State-space dynamic hydrological modeling of soil-crop-climate interactions. *Water Resources Research*, 24, 1765-1779

[106] Ramanathan, V., B. Subasilar, G. J. Zhang, W. Conant, R. D. Cess, J. T. Kiehl, H. Grassl, and L. Shi, 1995: Warm pool heat budget and shortwave cloud forcing: a missing physics ? *Science*, 267, 499-502

[107] Rayner, N.A., E.B. Horton, D.E. Parker, C.K. Folland, and R.B. Hackett, 1996: Version 2.2 of the Global sea-ice and Sea Surface Temperature data set, 1903-1994. *Climate Research Technical Note 74 (CRTN74)*, Meteorolgical Office, UK

[108] Reynolds, R. W. and T. M. Smith, 1994: Improved global sea-surface temperature analysis using optimum interpolation. *J. Clim.*, 7, 927-948

[109] Reynolds, R. W. and T. M. Smith, 1995: A high-resolution global sea-surface temperature climatology. *J. Clim.*, 8, 1571-1583

[110] Rodriguez-Iturbe, I., D. Entekhabi, and R. L. Bras, 1991: Nonlinear dynamics of soil moisture at climate scales 1. Stochastic Analysis. *Water Resources Research*, 27, 1899-1906

[111] Rowell, D. P., C. K. Folland, K. Maskell, J. A. Owen, and M. N. Ward, 1992: Modeling the influence of global sea surface temperatures on the variability and predictability of seasonal Sahel rainfall. *Geophys. Res. Lett.*, 19, 905-908

[112] Rowell, D. P., C. K. Folland, K. Maskell, and M. N. Ward, 1995: Variability of summer rainfall over tropical north Africa (1906-92): Observations and modelling. *Q. J. R. Meteorol. Soc.*, 121, 669-704

[113] Seth, A., F. Giorgi, and R. E. Dickinson, 1994: Simulating fluxes from heterogeneous land surfaces: Explicit subgrid method employing the biosphere-atmosphere transfer scheme (BATS). *J. Geophys. Res.*, 99, 18651-18667

[114] Shukla, J., C. Nobre, P. J. Sellers, 1990: Amazon deforestation and climate change. *Sience*, 247, 1322-1325

[115] Shuttleworth, W. J., 1988: Evaporation from Amazonia rainforest. *Proc. Roy. Soc. (B)*, 233, 321-346

[116] Shuttleworth, W. J., 1988: Macrohydrology – the new challenge for process hydrology. *J. Hydro.*, 100, 31-56

[117] Sinclair, A. R. E., 1979: Dynamics of the Serengeti ecosystem. In A. R. E. Sinclair and M. Norton-Griffiths, eds. Serengeti–Dynamics of an Ecosystem. University of Chicago Press

[118] Slingo, J. M., 1980: Cloud parameterization scheme derived from GATE data for use with a numerical model. *Q. J. R. Meteorol. Soc.*, 106, 747-770

[119] Slingo, J. M., 1987: The development and verification of a cloud prediction scheme for the ECMWF model. *Q. J. R. Meteorol. Soc.*, 113, 899-927

[120] Sprugel, D. G., 1991: Disturbance, equilibrium, and environmental variability – what is natural vegetation in a changing environment. *Biological Conservation*, 58, 1-18

[121] Stephens, G. L., 1996: How much solar radiation do clouds absorb? *Science*, 271, 1131-1133

[122] Sud, Y. C., and A. Molod, 1988: A GCM simulation study of the influence of Saharan evapo-transpiration and surface-albedo anomalies on July circulation and rainfall. *Mon. Weather Rev.*, 116, 2388-2400

[123] Sud, Y. C., and W. E. Smith, 1985: Influence of surface roughness of deserts on the July circulation. *Boundary-Layer Meteorology*, 33, 15-49

[124] Sud, Y. C., G. K. Walker, J.-H. Kim, G. E. Liston, P. J. Sellers, and W. K.-M. Lau, 1996: Biogeophysical consequences of a tropical deforestation scenario: a GCM simulation study. *J. Clim.*, 9, 3225-3247

[125] Sundqvist, H., E. Berge and J. E. Kristjansson, 1989: Condensation and cloud paramerization studies with a mesoscale numerical weather prediction model. *Mon. Weather Rev.*, 117, 1641-1657

[126] Texier, D., N. De Noblet, S. P. Harrison, A. Haxeltine, D. Jolly, S. Joussaume, F. Laarif, I. C. Prentice, P. Tarasov, 1997: Quantifying the role of biosphere-atmosphere feedbacks in climate change: coupled model simulations for 6000 years BP and comparison with palaeodata for northern Eurasia and northern Africa. *Climate Dynamics*, 13, 865-882

[127] Walter, H., 1985: Vegetation of the earth and ecological systems of the geo-biosphere. 318 pp, Springer-Verlag.

[128] Ward, M. N., 1998: Diagnosis and short-lead time prediction of summer rainfall in tropical North Africa at interannual and multidecadal timescales. *J. Clim.*, 11, 3167-3191

[129] Warren, A., 1996: Desertification. In The Physical Geography of Africa, W. M. Adams, A. S. Goudie, and A. R. Orme, Eds., pp 343-355. Oxford Univ. Press, New York

[130] Xue, Y., 1997: Biosphere feedback on regional climate in tropical North Africa. *Q. J. R. Meteor. Soc.*, 123, 1483-1515

[131] Xue, Y., K. Liou, and A. Kasahara, 1990: Investigation of biogeophysical feedback on the African climate using a two-dimensional model. *J. Clim.*, 3, 337-352

[132] Xue, Y. and J. Shukla, 1993: The influence of land surface properties on Sahel clim ate. Part I: Desertification. *J. Clim.*, 6, 2232-2245

[133] Zhang, H. and A. Henderson-Sellers, 1996: Impacts of tropical deforestation. Part I: Process analysis of local climate change. *J. Clim.*, 9, 1497-1517

[134] Zheng, X., 1997: Moist Zonally-Symmetric Models and Their Applications to West African Monsoons. Ph.D. Thesis, 217 pp, MIT

[135] Zheng, X., 1998: The response of a moist zonally symmetric atmosphere to subtropical surface temperature perturbation. *Q. J. R. Meteorol. Soc.*, 125, 1209-1226

[136] Zheng, X., and E. A. B. Eltahir, 1997: The response to deforestation and desertification in a model of West African monsoons. *Geophys. Res. Lett.*, 24, 155-158

[137] Zheng, X., and E. A. B. Eltahir, 1998: The role of vegetation in the dynamics of West African monsoons. *J. Clim.*, 11, 2078-2096

[138] Zheng, X., E. A. B. Eltahir, and K. A. Emanuel, 1999: A mechanism relating tropical Atlantic spring sea surface temperature and west African rainfall. *Q. J. R. Meteorol. Soc.*, 125, 1129-1164

[139] Zobler, L., 1986: A world soil file for global climate modeling, *Technical Report*, NASA